NASA TECHNICAL NOTE

NASA TN D-2824

a 1

LOAN COPY: RETUR
AFWL (WLIL-2)
KIRTLAND AFB, N M

0079648

TECH LIBRARY KAFB, NM

NASA TN D-2824

LARGE-SCALE WIND-TUNNEL INVESTIGATION OF THE LOW-SPEED AERODYNAMIC CHARACTERISTICS OF A SUPERSONIC TRANSPORT MODEL HAVING VARIABLE-SWEEP WINGS

by Anthony M. Cook, Richard K. Greif, and Kiyoshi Aoyagi

Ames Research Center
Moffett Field, Calif.

NATIONAL AERONAUTICS AND SPACE ADMINISTRATION • WASHINGTON, [redacted] MAY 1965

NASA TN D-2824

TECH LIBRARY KAFB, NM

0079648

LARGE-SCALE WIND-TUNNEL INVESTIGATION OF THE LOW-SPEED AERODYNAMIC CHARACTERISTICS OF A SUPERSONIC TRANSPORT MODEL HAVING VARIABLE-SWEEP WINGS

By Anthony M. Cook, Richard K. Greif, and Kiyoshi Aoyagi

Ames Research Center
Moffett Field, Calif.

NATIONAL AERONAUTICS AND SPACE ADMINISTRATION

For sale by the Clearinghouse for Federal Scientific and Technical Information
Springfield, Virginia 22151 – Price $4.00

LARGE-SCALE WIND-TUNNEL INVESTIGATION OF THE LOW-SPEED AERODYNAMIC CHARACTERISTICS OF A SUPERSONIC TRANSPORT MODEL HAVING VARIABLE-SWEEP WINGS*

By Anthony M. Cook, Richard K. Greif, and Kiyoshi Aoyagi
Ames Research Center

SUMMARY

The results are presented as six-component aerodynamic force and moment data obtained at various angles of attack and sideslip. Data were obtained at a Reynolds number of 16 million, based upon the mean aerodynamic chord of the wing swept to 75°. The investigation included variations of wing sweepback and aspect ratio, leading-edge slat deflection and geometry, trailing-edge flap deflection, geometry, and span extent, and horizontal-tail geometry.

The results show that all configurations tested, except one, were longitudinally unstable at high lift. The configuration that was not unstable had a tail in a low horizontal position, a wing sweepback angle of 25° with a large portion of the fixed wing deflected as a leading-edge flap.

INTRODUCTION

The development of any supersonic aircraft involves combining aerodynamically incompatible high- and low-speed design requirements. The variable-sweep wing concept is one approach to this problem. One basic requirement in this approach is to provide acceptable stability characteristics by minimizing the aerodynamic center shift due to wing sweep.

Earlier concepts of variable-sweep wings (ref. 1) incorporated a longitudinal translation of the wing together with change in sweep angle to eliminate the aerodynamic center shift associated with changing sweep. Efforts to avoid the mechanical difficulties inherent with longitudinal translation of the wing resulted in the concept of the fixed outboard pivot and a fixed, highly swept, inboard wing section designed to minimize aerodynamic center shift (refs. 2 through 6). Small-scale results give evidence of longitudinal instability characteristics at the stall for the high-lift configurations of this design. The purpose of the tests reported herein was to investigate this longitudinal instability and the maximum lift characteristics of high-lift, variable-sweep configurations at high Reynolds numbers.

The scope of this investigation was limited to the first-order effects of the variables considered most important: wing sweep in low-speed cruise and

*Title, Unclassified.

high-lift configurations, wing aspect ratio, trailing-edge flap systems, leading-edge slats, horizontal-tail area and location, and fixed-wing leading-edge radius and flaps.

NOTATION

A	wing area (see Reduction of Data), sq ft
AR	aspect ratio, $\frac{b^2}{A}$
ac	aerodynamic center
b	wing span, ft
C_D	drag coefficient, $\frac{\text{drag}}{qA}$
C_L	lift coefficient, $\frac{\text{lift}}{qA}$
C_l	rolling-moment coefficient, $\frac{\text{rolling moment}}{qAb}$
C_m	pitching-moment coefficient, $\frac{\text{pitching moment}}{qA\bar{c}}$
C_n	yawing-moment coefficient, $\frac{\text{yawing moment}}{qAb}$
C_y	side-force coefficient, $\frac{\text{side force}}{qA}$
c	chord
$\bar{c}$	mean aerodynamic chord, $\frac{2}{A}\int_0^{b/2} c^2\,dy$, ft
FDS	flap, double slotted
FLE	fixed-wing leading-edge flap
FSS	flap, single slotted
g_S	gap of leading-edge slats, fraction of chord
i_T	horizontal-tail incidence (positive when trailing edge is down), deg
L/D	lift-drag ratio
LE	leading edge

l_T tail length, measured from wing pivot axis to the quarter chord of the horizontal-tail mean aerodynamic chord

q dynamic pressure, lb/sq ft

r_{FLE} radius, fixed-wing leading edge

$\bar{V}_T$ tail volume coefficient

x streamwise distance along airfoil chord, ft

y spanwise distance perpendicular to the plane of symmetry, ft

z perpendicular distance above the wing-chord plane, ft

α angle of attack of wing-chord plane, deg

β angle of sideslip of plane of symmetry, deg

δ angle of deflection of control surfaces, measured normal to hinge line, deg

ϵ_{av} average effective downwash, deg

η wing semispan station, $\frac{2y}{b}$

λ wing taper ratio

Λ_{FLE} angle of sweepback of fixed-wing leading edge, deg

Λ_{LE} angle of sweepback of tail leading edge, deg

Λ_{WLE} angle of sweepback of movable-wing leading edge, deg

Subscripts

l lower surface

S slat, leading edge

TW total wing, including both variable-sweep panel and fixed wing

u upper surface

W wing

WLE movable-wing leading edge

MODEL AND APPARATUS

Description of Model

The basic model consisted of a low-wing, variable-sweep transport configuration. Various wing leading-edge sweepback angles ranging from 13-1/2° to 75° were tested. Four configurations are shown installed in the wind tunnel in the photograph of figure 1: two high-aspect-ratio configurations, with low and high horizontal-tail positions (configurations A_1 and A_2, respectively); and two low-aspect-ratio configurations, with high and mid horizontal-tail positions (configurations B_1 and B_2).

The wing pivot was located at 36-percent semispan and 46-percent chord of the fully swept wing (based upon the low-aspect-ratio wing of configuration B). The fixed portion of the wing was provided with either 70° or 75° leading-edge sweep.

Planform Geometry

Geometric details of the high-aspect-ratio configuration (A) and the low-aspect-ratio configuration (B) can be found in tables I and II, respectively. A sketch including pertinent dimensions of the model is shown in figure 2.

The airfoil section for the movable wing had a flat lower surface and the thickness distribution of an NACA 65A006 airfoil section. See table III for wing airfoil coordinates.

The lower aspect ratio of configuration B was obtained by removing 3-1/2 feet of wing tip from configuration A.

Fixed-wing section geometry is detailed in figure 2(c) by cross sections at various fuselage stations. Planform details are given in figure 2(d). The basic leading edge was sharp along its entire length. However, an alternate, rounded leading edge shown in figure 2(e) was also tested. This rounded leading edge tapered from a radius of 3 inches at the fuselage juncture to 0.75 inch (wing leading-edge radius at movable-wing juncture).

The fuselage consisted of a blended wing-body section, as shown in figure 2(c), with an underslung, side-by-side engine nacelle with plugged, two-dimensional inlets faired to the rectangular aft fuselage shown in figure 1.

Horizontal Tail

The horizontal tail was tested in three positions (see fig. 2(b)): low, mid, and high. In the low position it was mounted on the fuselage at 10 percent $\bar{c}$ (of 25° sweep) below the wing-chord plane; in the mid position it was mounted on the vertical stabilizer at 10 percent $\bar{c}$ above the wing-chord plane; in the high position it was also mounted on the vertical stabilizer,

at 50 percent $\bar{c}$ above the wing-chord plane. Because of the sweepback of the vertical stabilizer, horizontal-tail length (l_T) varied for the three positions. Two horizontal-tail sizes were tested in the high position.

For all tests of configuration A_1, the low tail was at a negative dihedral of 10°.

High-Lift Devices

Fixed-wing high-lift devices.- Details of the plain flap of the fixed wing are shown in figure 2(d).

A simulated Krüger type flap was tested on the leading edge of the fixed wing, with both sharp and rounded fixed-wing leading edge (see fig. 2(e)).

Movable-wing trailing-edge double-slotted flap system.- The double-slotted flap geometry and a typical cross section are shown in figure 2(f). The vane was 7-1/2 percent of the wing chord, streamwise, with the wing at 25° sweep. The main flap comprised 25 percent of the wing chord. A slot of 2-percent wing chord was maintained at the vane. Flap deflections ranged from 30° to 60° in 10° increments. The slot geometry was modified to improve flap performance. The modification (fig. 2(f)) consisted of adding sheet metal extensions to the wing trailing-edge shroud and vane and was used for all tests of double-slotted flaps unless otherwise noted.

Movable-wing trailing-edge single-slotted flap system.- The single-slotted flap configuration was achieved by removal of the vane of the double-slotted flap and moving the flap forward into the wing. This reduced the wing chord by 4 percent and accounts for the difference in wing area and aspect ratio between the two flap systems. A slot of 2-percent wing chord was maintained at all flap deflections, and the range of flap deflection was from 0° to 30°, 40°, and 50°. The geometry and cross-section details of this flap system are given in figure 2(g).

Both flap systems were constructed in three sections, extending (as shown in fig. 2(a)) from 20 to 52 percent semispan, from 52 to 67 percent semispan, and from 67 to 98 percent semispan of the high-aspect-ratio wing. As a result, flap deflection notation is indicated in three parts:

δ = inboard deflection/middle deflection/outboard deflection

Movable-wing leading-edge slats.- The details of leading-edge slat size, deflection, and positioning are shown in figure 2(h). Two sized slats were tested, one having a length equal to 15-percent streamwise wing chord (at 25° sweep), and the other, 18-3/4-percent wing chord. The profile of the 0.15c slat was made to match the leading-edge profile of the wing. The 0.1875c slat incorporates the basic 0.15c slat with a rounded leading-edge extension to provide camber as shown in the figure. Slat deflection, δ_S, is given relative to its undeflected position as if it were "gloved" onto the

wing. Slat gap, g_S, was varied from 0- to 2-percent chord in 1/2-percent increments. Unless otherwise noted, all slat data reflect the use of the basic slat of 0.15c length.

TESTING AND PROCEDURE

Six-component force and moment data were obtained by conventional wind-tunnel testing methods through an angle-of-attack range from -4° to $+22^\circ$, and an angle of sideslip from -12° to $+4^\circ$. Free-stream dynamic pressure was 15 pounds per square foot, corresponding to a Reynolds number of 16 million, based upon mean aerodynamic chord at 75° wing sweep.

The majority of tests were directed toward the development of high-lift devices and the investigation of longitudinal stability characteristics for landing and take-off configurations.

REDUCTION OF DATA

Corrections

Standard corrections were applied to angle of attack to account for wind-tunnel wall effects. The corrections accounted for the variations in span due to wing sweep. Measured drag was corrected in accordance with the angle-of-attack correction. In addition, the following correction was added to drag measurements to account for strut tares:

$$\Delta C_D = 0.0036$$

No ΔC_m correction was made for tunnel-wall corrections for tail-on conditions due to the variable-sweep nature of the configuration.

Reference Dimensions

The computation of force and moment coefficients for all wing sweeps of a given configuration was based on the dimensions corresponding to the total wing area, including fixed wing, at the 75° sweep condition of that particular configuration.

Moment Center

The moment center for all configurations, regardless of wing sweep, was taken on the axis of the wing pivot, 2.875 inches above the wing-chord plane.

RESULTS

The acquisition of data for this investigation covered four testing periods and the several configurations previously mentioned. The results in figures 3 through 48 present longitudinal characteristics and selected cases include lateral-directional characteristics. These results are summarized in figures 49 through 56 and are discussed more completely in the Discussion section of this report. Table IV is a complete index to the figures.

DISCUSSION

General Characteristics

Aspect ratio.- Figure 49 presents a comparison of the test data for wings of aspect ratio 6.9 and 8.4 at 25° of wing leading-edge sweepback and with high-lift devices installed. At 12° angle of attack, for instance, there is an incremental loss of 6.5 percent C_L in reducing aspect ratio from 8.4 to 6.9, accompanied by a decrease in stability of 5-percent static margin. The reduction in aspect ratio causes a lower lift-curve slope, but it is shown that for this degree of wing sweepback, there is essentially no difference in $C_{L_{max}}$.

Wing sweep.- Figure 50 shows the effects of 13-1/2° and 25° wing sweep for both the flaps-up and flaps-down conditions. In the case of 40° flap deflection, it is seen that there is no appreciable benefit to be derived by a wing sweepback angle of less than 25°, in terms of a "usable" $C_{L_{max}}$, or that C_L at which pitch-up occurs. Changes in lift due to wing sweep for the flaps-up condition are also very small. Note that the aerodynamic-center shift due to wing sweep from 13-1/2° to 25° with flaps up amounts to 8-percent static margin and is essentially the same as the change in static margin due to 40° of flap deflection at 13-1/2° of wing sweep. (The static margin change due to flap deflection, however, is a result of the downwash flow at the particular horizontal-tail location, since no change is indicated in the tail-off data of figs. 36 and 37.)

Longitudinal Stability

As mentioned in the Introduction, variable-sweep configurations generally have unstable pitching-moment characteristics at high lift coefficients. The reason is that a wing-tip stall progressing inboard (based on tuft observations) is further aggravated by a vortex generated along the highly swept leading edge of the fixed wing delaying inboard stall. The size and sweep of the fixed-wing portion contribute to the strength of this vortex. Part of this investigation involved testing horizontal-tail positions in combination with various flow control devices in order to alleviate this problem.

Effect of fixed wing.- Figure 24 shows that reducing fixed-wing leading-edge sweepback from 75° to 70° increases longitudinal stability approximately 7 percent and correspondingly increases maximum lift coefficient by 7 percent.

Effect of horizontal tail.- Figure 51 summarizes the effects of horizontal-tail location and size on pitching moment. The only tail position that gave reasonably linear pitching moment up to high lift coefficients was the low position, located 10 percent of the 25° sweep $\bar{c}$ below the wing-chord plane. Placing the tail at a high position (50 percent $\bar{c}$ above the wing-chord plane) caused a severe pitch-up at lift coefficients of 1.4. The tail midway between the high and low positions was somewhat better than the high tail position, but the longitudinal characteristics were still unsatisfactory.

Figure 52 presents the control effectiveness ($\partial C_m/\partial i_T$), for two of the horizontal-tail configurations just discussed, and effective downwash angle (ϵ_{av}) and tail angle of attack (α_T) for the tail in the high position. These curves were obtained from cross plots of pitching moment versus angle of attack for various values of tail incidence. It is shown that, for both tail positions, the $\partial C_m/\partial i_T$ curve has virtually no change in slope up to 12° angle of attack, indicating no change in tail efficiency factor. However, above 12° angle of attack for the high tail, the changing downwash field causes the tail angle of attack (α_T) to fall back to zero at 16° wing angle of attack so that the stability contribution of the tail is lost. This effect is primarily due to the vortex generated by the fixed-wing leading edge. At the same time, above 12° wing angle of attack, there is a reduction in control power ($\partial C_m/\partial i_T$) for the high tail, indicating a reduction in dynamic pressure at the horizontal tail. On the other hand, the low tail is not adversely affected by the wing downwash field (as illustrated by increasing $\partial C_m/\partial i_T$) above 12° angle of attack.

Flow-control devices.- Reduced fixed-wing sweepback and certain flow-control devices on the fixed-wing leading edge were effective in alleviating the reduction of longitudinal stability at high angles of attack. Figure 53 shows the effects of these control devices on pitching moment. With the tail in the low position, deflecting a large portion of the fixed wing about a hinge line along the fuselage juncture (similar to a plain leading-edge flap) essentially eliminated the unstable pitching moment break at the stall. A Krüger flap used with a large leading-edge radius (see fig. 2(e)) improved the stability at the stall but, as shown in figure 53, not sufficiently to overcome the large destabilizing moment contribution of the horizontal tail in the high position.

The improvements in stability resulting from the use of these control devices confirm that the stability problems are associated with the vortex shed from the fixed-wing leading edge. These devices delay formation of this vortex and thus tend to alleviate the instability.

Maximum Lift

Trailing-edge flaps.- Figure 54 summarizes the effects of both single-slotted and double-slotted flap systems. The full-span double-slotted flap

had a 0.3 greater lift increment at zero angle of attack. For both full-span flaps $C_{L_{max}}$ was essentially the same, with the double-slotted flap achieving $C_{L_{max}}$ at 15° angle of attack, 3° earlier than the single-slotted flap. With part-span deflection (outboard flap undeflected) the 40° single-slotted flap achieved higher $C_{L_{max}}$ than the 50° double-slotted flap partly because of a higher lift-curve slope. Tuft observations indicated that double-slotted flap effectiveness was reduced at higher angles of attack by the fixed-wing vortex effect.

Figure 55 shows the effects of the amount of flap-span deflected. Deflection of the outboard flap sections produced an increase in lift through nearly the entire range of lift coefficients, including $C_{L_{max}}$. However, the additional nose-down moment produced by the outboard flaps resulted in a trim requirement which, for all practical purposes, cancelled the advantage in maximum lift coefficient.

Leading-edge slats.- A limited program to optimize wing leading-edge slat deflection and gap size was conducted with the low-tail, high-aspect-ratio configuration (A_1). Figure 56 presents a summary of the results at a wing sweepback of 13-1/2° with 50° full-span double-slotted flaps. The effects of these slat variables on maximum lift coefficient are shown and were used to tailor the slat geometry for subsequent testing.

Lateral-Directional Stability

No unusual lateral or directional stability characteristics were evident in any of the configurations tested (see figs. 10, 13, 36, and 41). The model had directional stability and positive effective dihedral up to the stall angle of attack.

SUMMARY OF RESULTS

1. The results show that all configurations tested, except one, were longitudinally unstable at high lift. The one configuration that essentially eliminated this instability at stall consisted of a drooped fixed-wing leading-edge with the high-aspect-ratio wing at 25° of wing sweepback, in conjunction with the low horizontal-tail position.

2. No solution to longitudinal instability was achieved with the horizontal tail in any other than the low position (10 percent of the 25° sweep $\bar{c}$ below the wing chord plane).

3. Results indicate that, for the low-speed configuration, reducing wing sweepback below 25° yielded no appreciable benefit in terms of a usable maximum lift coefficient (or that C_L at which longitudinal instability occurs).

Ames Research Center
National Aeronautics and Space Administration
Moffett Field, Calif., Jan. 27, 1965

REFERENCES

1. Kemp, William B., Jr.; Becht, Robert E.; and Few, Albert G., Jr.: Stability and Control Characteristics at Low Speed of a 1/4-Scale Bell X-5 Airplane Model. Longitudinal Stability and Control. NACA RM L9K08, 1950.

2. Alford, William J., Jr.; and Henderson, William P.: An Exploratory Investigation of the Low-Speed Aerodynamic Characteristics of Variable-Wing-Sweep Airplane Configurations. NASA TM X-142, 1959.

3. Spencer, Bernard, Jr.: Stability and Control Characteristics at Low Subsonic Speeds of an Airplane Configuration Having Two Types of Variable-Sweep Wings. NASA TM X-303, 1960.

4. Spencer, Bernard, Jr.: Low-Speed Longitudinal Aerodynamic Characteristics Associated With Variations in the Geometry of the Fixed Portion of a Variable-Wing-Sweep Airplane Configuration Having an Outboard Pivot. NASA TM X-625, 1962.

5. Alford, William J., Jr.; Luoma, Avro A.; and Henderson, William P.: Wind-Tunnel Studies at Subsonic and Transonic Speeds of a Multiple-Mission Variable-Wing-Sweep Airplane Configuration. NASA TM X-206, 1959.

6. Foster, Gerald V.; and Morris, Odell A.: Stability and Control Characteristics at a Mach Number of 1.97 of an Airplane Configuration Having Two Types of Variable-Sweep Wings. NASA TM X-323, 1960.

TABLE I.- MODEL GEOMETRY OF CONFIGURATION A

Wing: NACA 65A006 modified airfoil; 0° twist, incidence, and dihedral

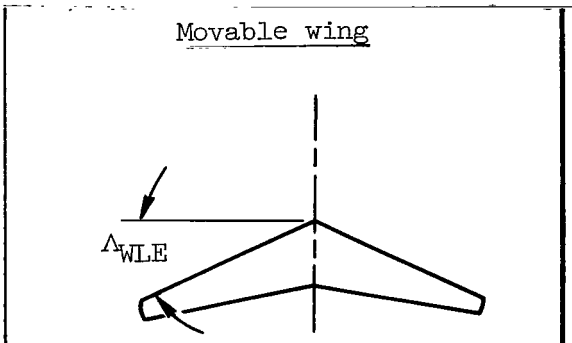

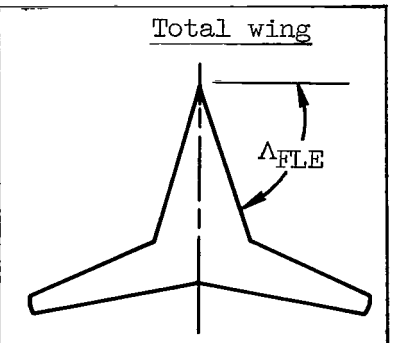

Λ_{WLE}	Span	Area	AR	λ	Λ_{FLE}	Area	AR	$\bar{c}$
High-aspect-ratio geometry, double-slotted flaps								
13-1/2°	56.7	369	8.7	0.343	70° 75°	491 540	6.6 6.0	12.75 15.80
25°	54.3	367	8.0	.337	70°	483	6.1	12.80
75°	26.6	462	1.5	.343	70°	462	1.5	19.44
75°	26.6	510	1.4	.470	75°	510	1.4	22.47
High-aspect-ratio geometry, single-slotted flaps								
13-1/2°	56.7	350	9.2	.344	70°	473	6.8	12.75
25°	54.3	350	8.4	.338	70°	466	6.3	12.95
55°	40.2	378	4.3	.344	70°	454	3.6	14.51
75°	26.6	486	1.5	.471	70°	437	1.6	19.83

	Λ_{LE}	Span	Area	AR	$\bar{c}$	l_T
Low horizontal tail (A_1)						
Total area	60°	19.4	169	2.2	10.0	15.8
Exposed area	60°	19.4	110	3.4	8.0	20.1
High horizontal tail (A_2)						
Large tail	60°	15.0	111	2.0	8.0	27.9
Small tail	60°	11.6	67	2.0	6.8	27.9

TABLE II.- MODEL GEOMETRY OF CONFIGURATION B

Wing: NACA 65A006 modified airfoil; 0° twist, incidence, and dihedral

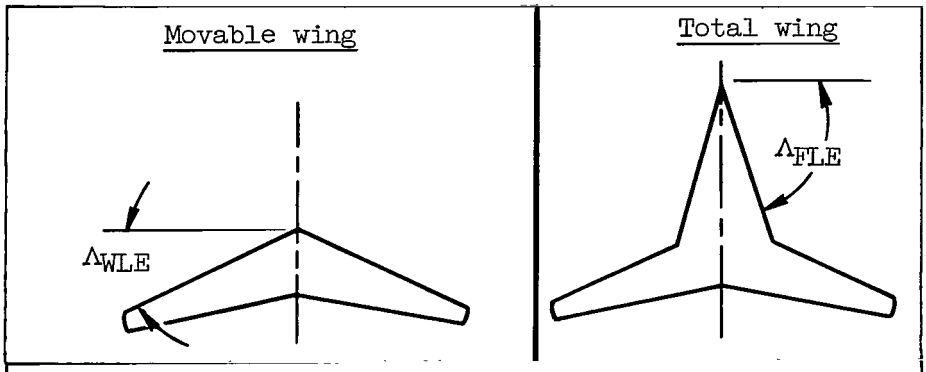

Low-aspect-ratio geometry, single-slotted flaps								
Λ_{WLE}	Span	Area	AR	λ	Λ_{FLE}	Area	AR	$\bar{c}$
13-1/2°	49.6	325	7.6	0.432	70°	447	5.5	13.35
18°	48.5	325	7.2	.429	70°	441	5.3	13.40
25°	47.4	324	6.9	.425	70°	440	5.1	13.50
32°	43.0	327	5.7	.430	70°	434	4.3	13.90
55°	34.9	352	3.5	.453	70°	428	2.8	15.20
75°	24.7	460	1.3	.590	70°	412	1.5	20.75

High horizontal tail (B_1)						
	Λ_{LE}	Span	Area	AR	$\bar{c}$	l_T
Total area	60°	15.0	111	2.0	8.0	27.9
Mid horizontal tail (B_2)						
Total area	60°	15.0	111	2.0	8.0	22.0

TABLE III.- WING AIRFOIL ORDINATES (MOVABLE SECTION); MODIFIED NACA 65A006; 0° TWIST, INCIDENCE, AND DIHEDRAL

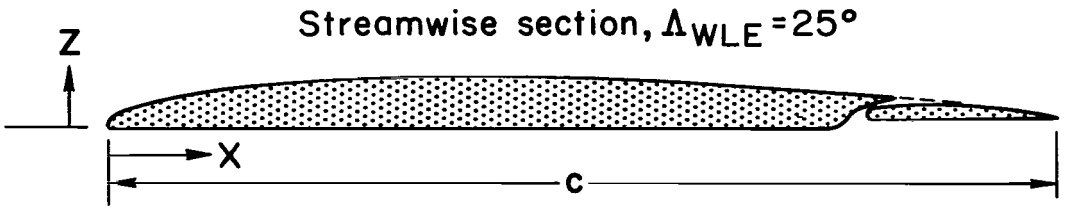

x/c	z_u/c	z_l/c
0	0.00727	0
.0073	.01498	0
.0086	.01533	0
.0130	.01672	0
.0260	.02044	0
.0500	.02667	0
.0780	.03315	0
.1000	.03729	0
.1500	.04479	0
.2000	.05052	0
.2500	.05500	0
.3000	.05844	0
.3500	.06083	0
.4000	.06219	0
.4500	.06240	0
.5000	.06167	0
.5500	.05969	0
.6000	.05625	0
.6500	.05208	0
.7000	.04688	0
.7500	.04104	.00604
.8000	.03458	.00604
.8500	.02750	.00604
.9000	.02052	.00604
.9500	.01333	.00604
1.0000	.00604	.00604

TABLE IV.- INDEX TO FIGURES

Effect of:	Wing sweep	Fixed-wing sweepback	Trailing-edge flaps		Figure number
Configuration A_1: high-aspect-ratio wing, low horizontal tail					
Clean configuration	13-1/2	70	0/0/0	FSS	3
Clean configuration	25	↓	↓	↓	4
Clean configuration	55				5
Clean configuration	75				6
Single-slotted trailing-edge flaps:	13-1/2	70	30/30/0	FSS	7
Part-span deflection	↓	↓	40/40/0	FSS	8
Full-span deflection			40/40/40	FSS	9
Part-span deflection	25		30/30/0	FSS	10
Part-span deflection	↓		40/40/0	FSS	11
Full-span deflection			30/30/30	FSS	12
Full-span deflection			40/40/40	FSS	13
Double-slotted trailing-edge flaps:	13-1/2		variable	FDS	14
Full-span deflection	13-1/2		50/50/50	FDS	15
Part-span deflection	25		30/30/0	FDS	16
Part-span deflection	↓		50/50/0	FDS	17
Full-span deflection			30/30/30	FDS	18
Full-span deflection			40/40/40	FDS	19
Full-span deflection			50/50/50	FDS	20
Full-span deflection	13-1/2	75	50/50/50	FDS	21
Leading-edge slat geometry	13-1/2	75	50/50/50	FDS	22
Leading-edge slat geometry	25	70	40/40/40	FSS	23
Fixed-wing sweepback	13-1/2	70,75	50/50/50	FDS	24
Fixed-wing leading-edge radius	↓	75	variable	FDS	25
Fixed-wing leading-edge flap deflection		75	50/50/50	FDS	26
Fixed-wing leading-edge flap deflection	25	70	40/40/40	FSS	27
Configuration A_2: high-aspect-ratio wing, high horizontal tail					
Fixed-wing leading-edge radius and flap deflection	25	70	40/40/0	FSS	28
Horizontal-tail size	25	70	40/40/0	FSS	29

TABLE IV.- INDEX TO FIGURES - Concluded

Effect of:	Wing sweep	Fixed-wing sweepback	Trailing-edge flaps	Figure number
Configuration B_1: low-aspect-ratio wing, high horizontal tail				
Clean configuration	18	70	0/0/0 FSS	30
Clean configuration	25	↓	↓ ↓	31
Clean configuration	32	↓	↓ ↓	32
Clean configuration	55	↓	↓ ↓	33
Clean configuration	75	↓	↓ ↓	34
High-lift configurations	18	↓	40/40/0 FSS	35
High-lift configurations	25	↓	40/40/0 FSS	36
High-lift configurations	25	↓	50/50/0 FSS	37
High-lift configurations	32	↓	40/40/0 FSS	38
Fixed-wing radius and Krüger flap	18	↓	40/40/0 FSS	39
Fixed-wing radius and Krüger flap	18	↓	40/40/40 FSS	40
Fixed-wing radius and Krüger flap	25	↓	40/40/0 FSS	41
Fixed-wing radius and Krüger flap	↓	↓	40/40/0 FSS	42
Fixed-wing radius and Krüger flap	↓	↓	40/40/40 FSS	43
Fixed-wing radius and Krüger flap	18	↓	40/40/0 FSS	44
Leading-edge slats and fixed-wing geometry	25	↓	40/40/0 FSS	45
Configuration B_2: low-aspect-ratio wing, mid horizontal tail				
Fixed-wing Krüger flap deflection	25	70	40/40/0 FSS	46
Fixed-wing Krüger flap deflection	↓	↓	↓ ↓	47
Fixed-wing Krüger flap deflection	↓	↓	↓ ↓	48
Summary plots				
Aspect ratio, tail off	25	70	40/40/0 FSS	49
Wing sweep, tail on	13-1/2,25	↓	variable FSS	50
Horizontal-tail location	25	↓	40/40/0 FSS	51
Horizontal-tail effectiveness	↓	↓	40/40/0 FSS	52
Fixed-wing leading-edge radius and flap deflection	↓	↓	variable FSS	53
Single-slotted and double-slotted flaps	↓	↓	variable FSS and FDS	54
Amount of flap span deflected	↓	↓	variable FSS	55
Leading-edge slat geometry	13-1/2	75	50/50/50 FDS	56

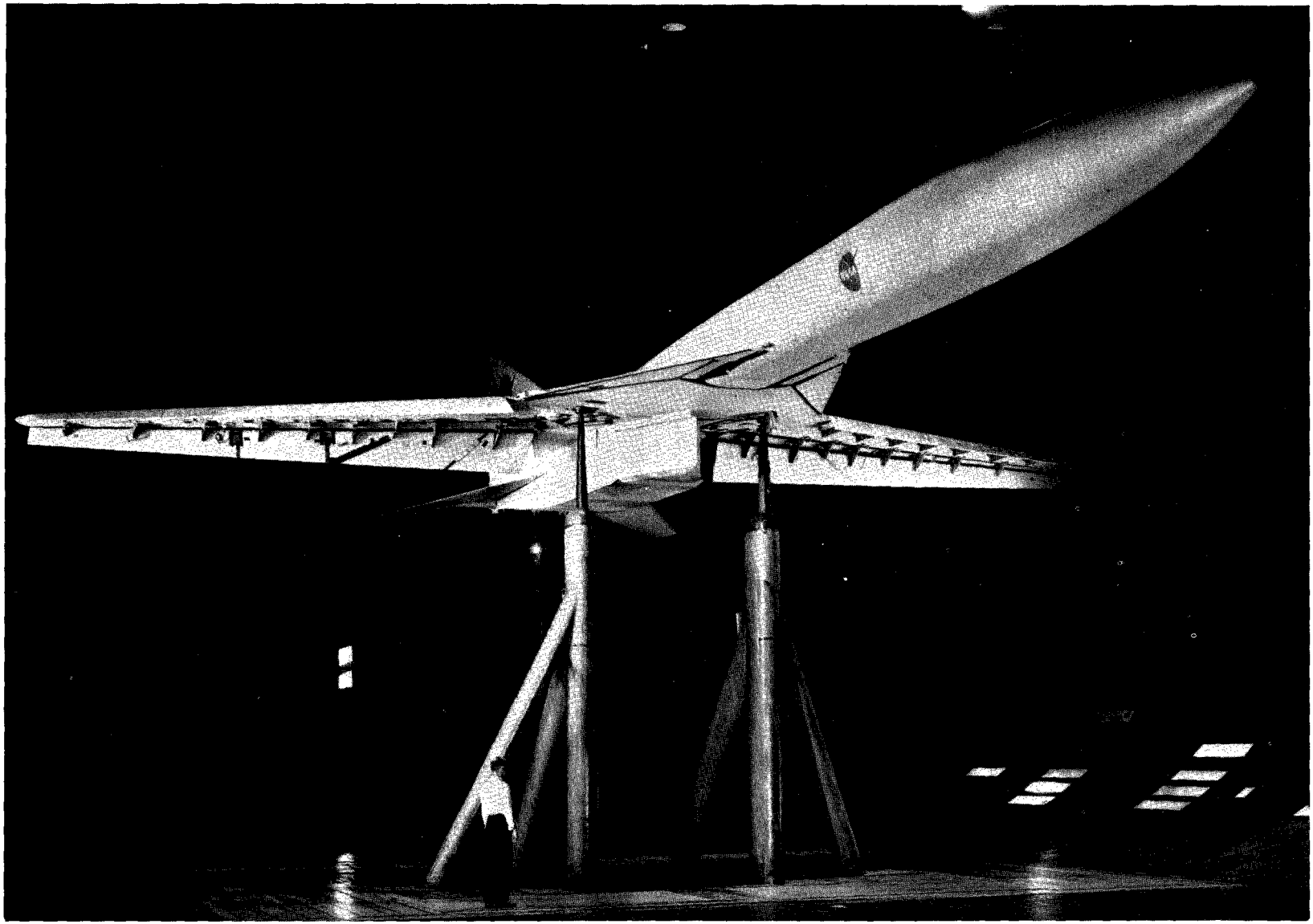

(a) Configuration A_1: low tail, aspect-ratio-8.4 wing. A-30876

Figure 1.- Photographs of the model mounted in the Ames 40- by 80-foot wind tunnel.

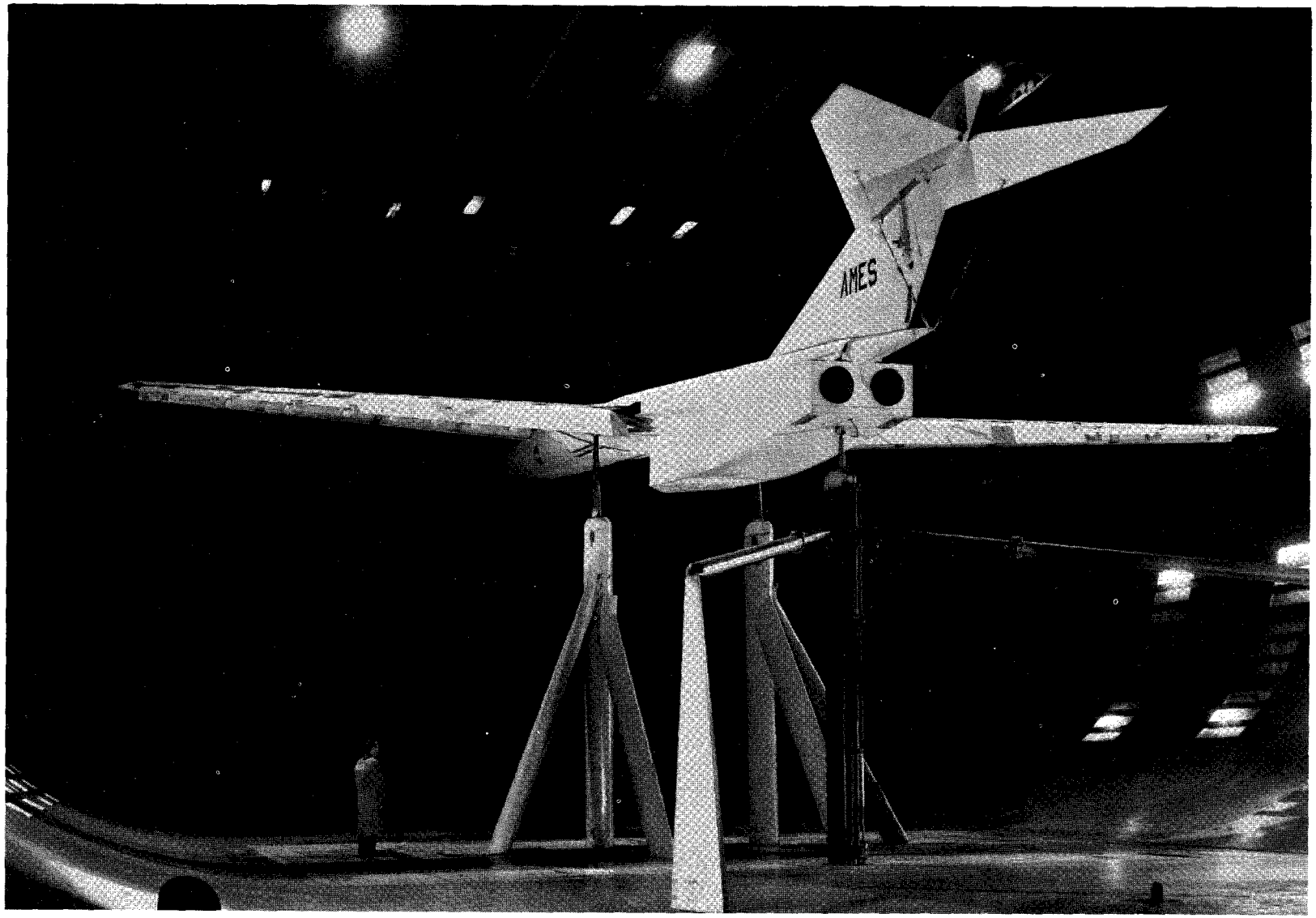

(b) Configuration A_2: high tail, aspect-ratio-8.4 wing. A-31298

Figure 1.- Continued.

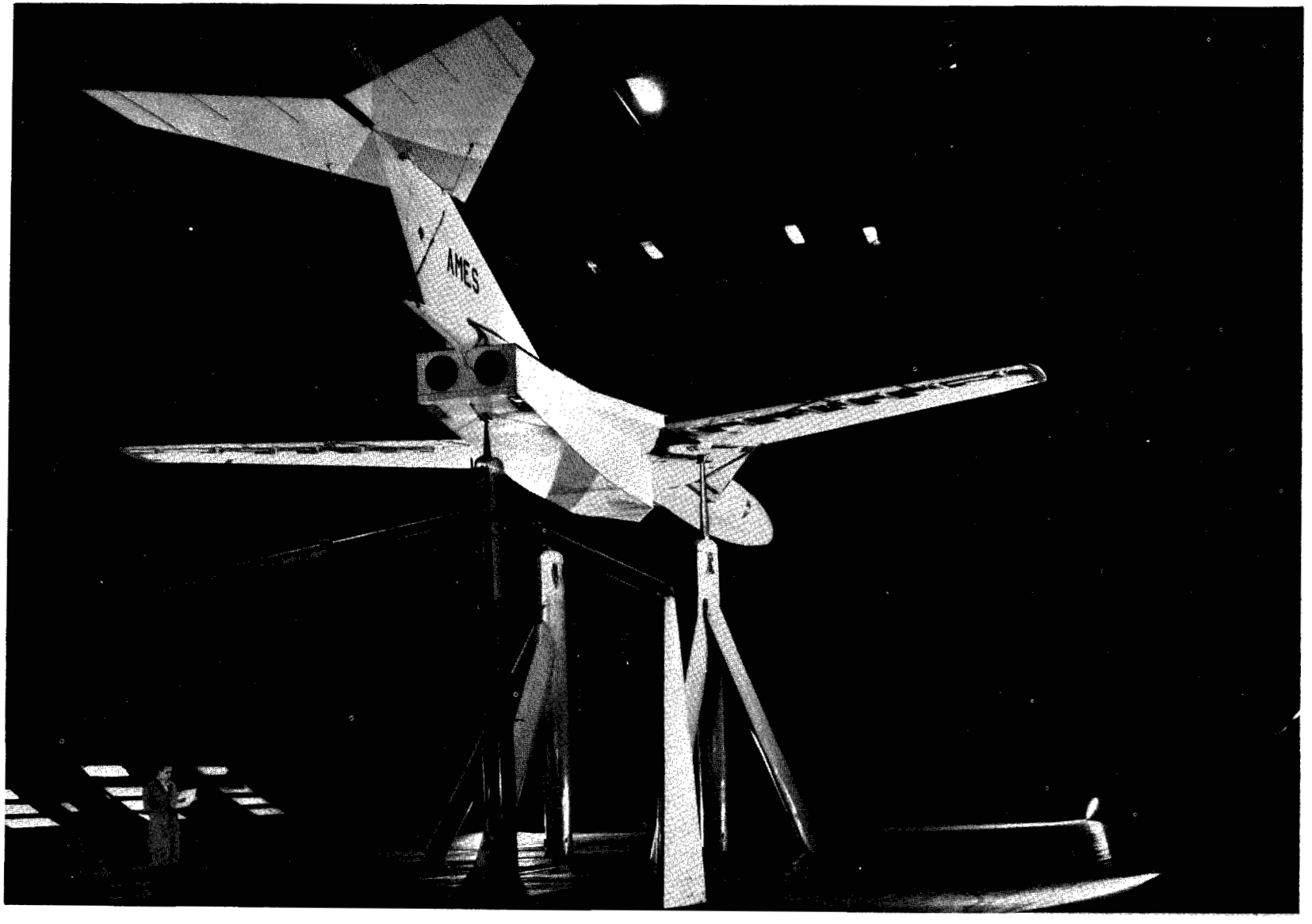

(c) Configuration B_1: high tail, aspect-ratio-6.9 wing. A-31299

Figure 1.- Continued.

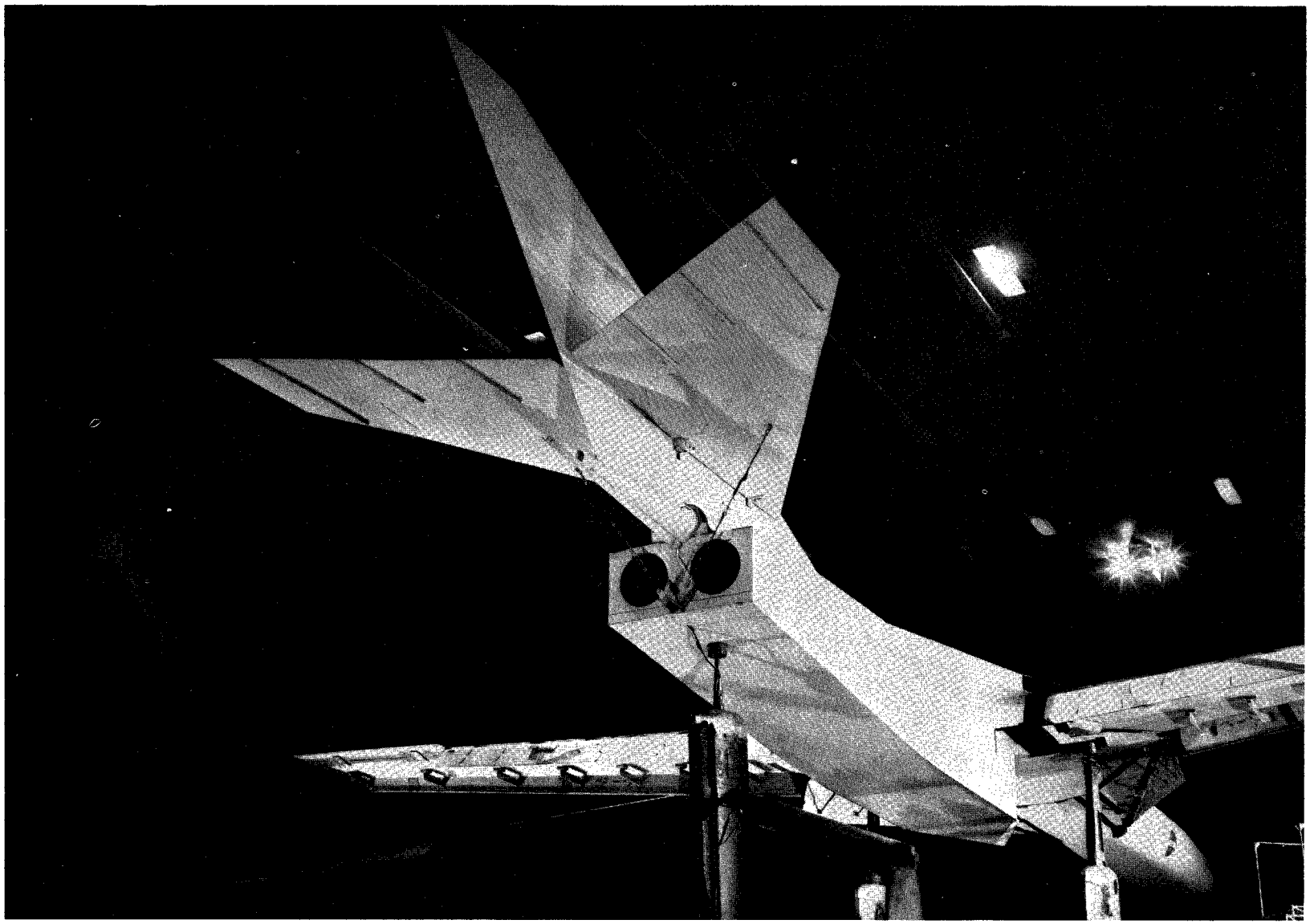

A-31705

(d) Configuration B_2: mid tail, aspect-ratio-6.9 wing.

Figure 1.- Concluded.

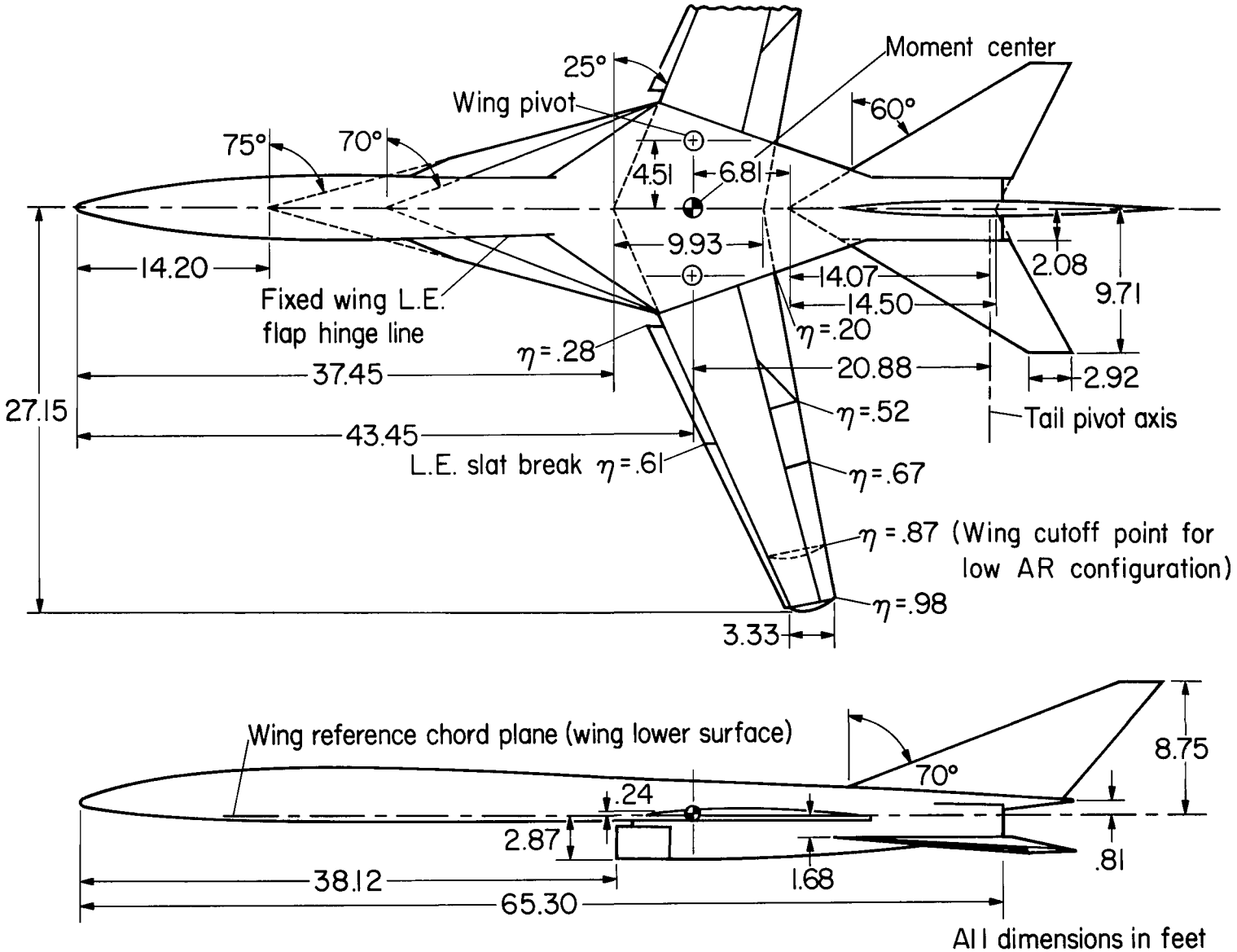

(a) General details of configuration A_1.

Figure 2.- Geometric details of the model.

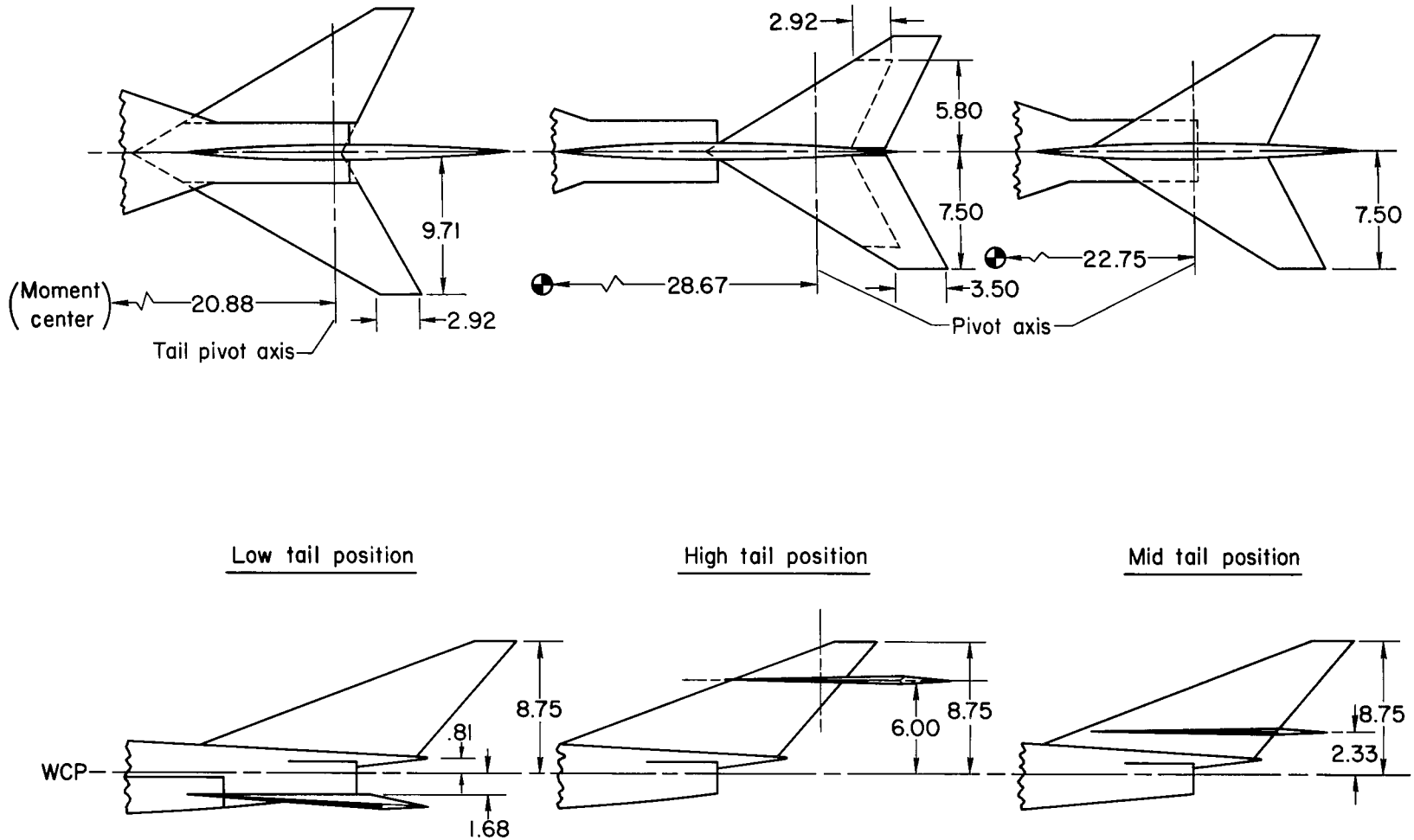

(b) Details of horizontal-tail locations.

Figure 2.- Continued.

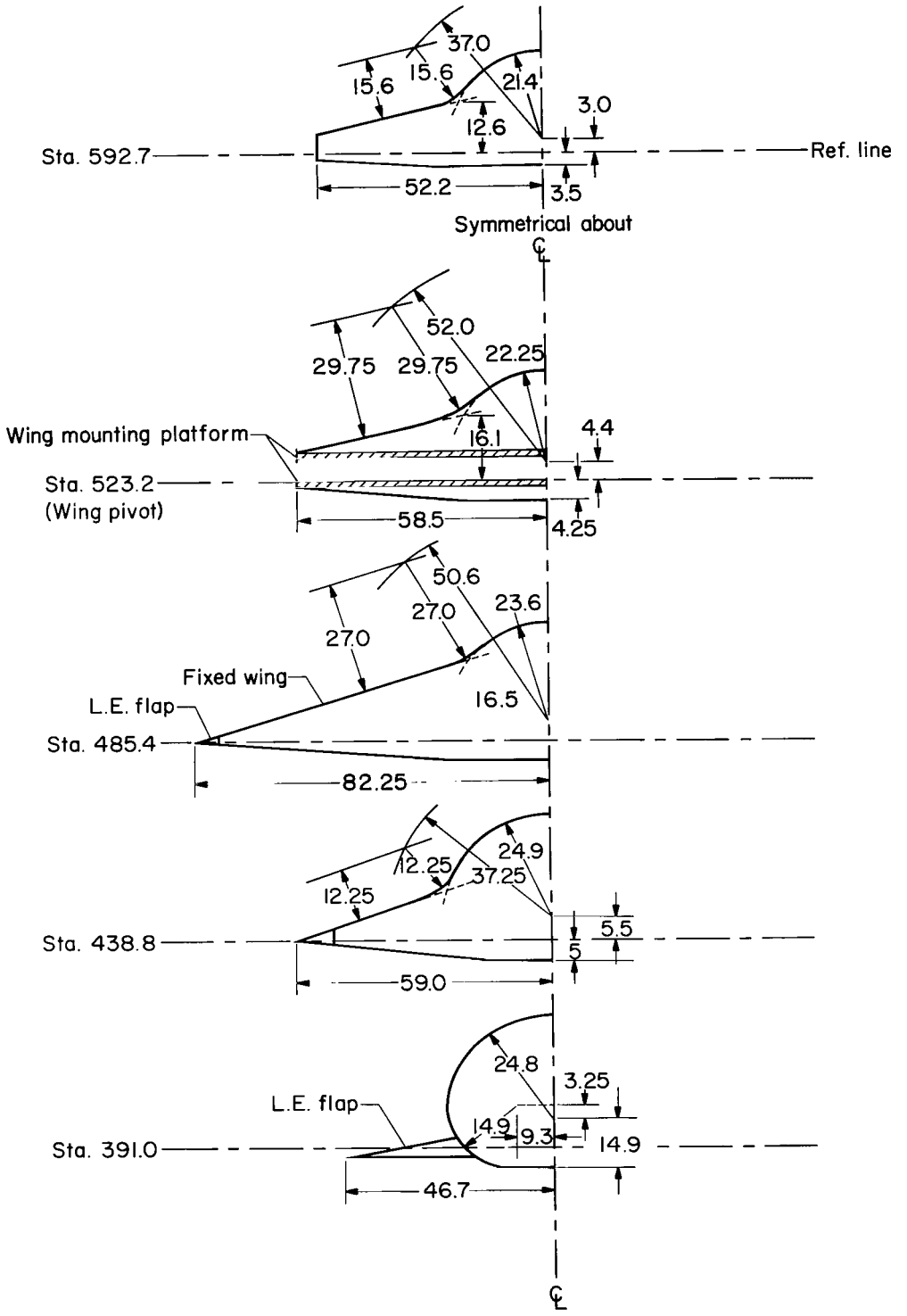

(c) Cross-section details of fixed wing.

Figure 2.- Continued.

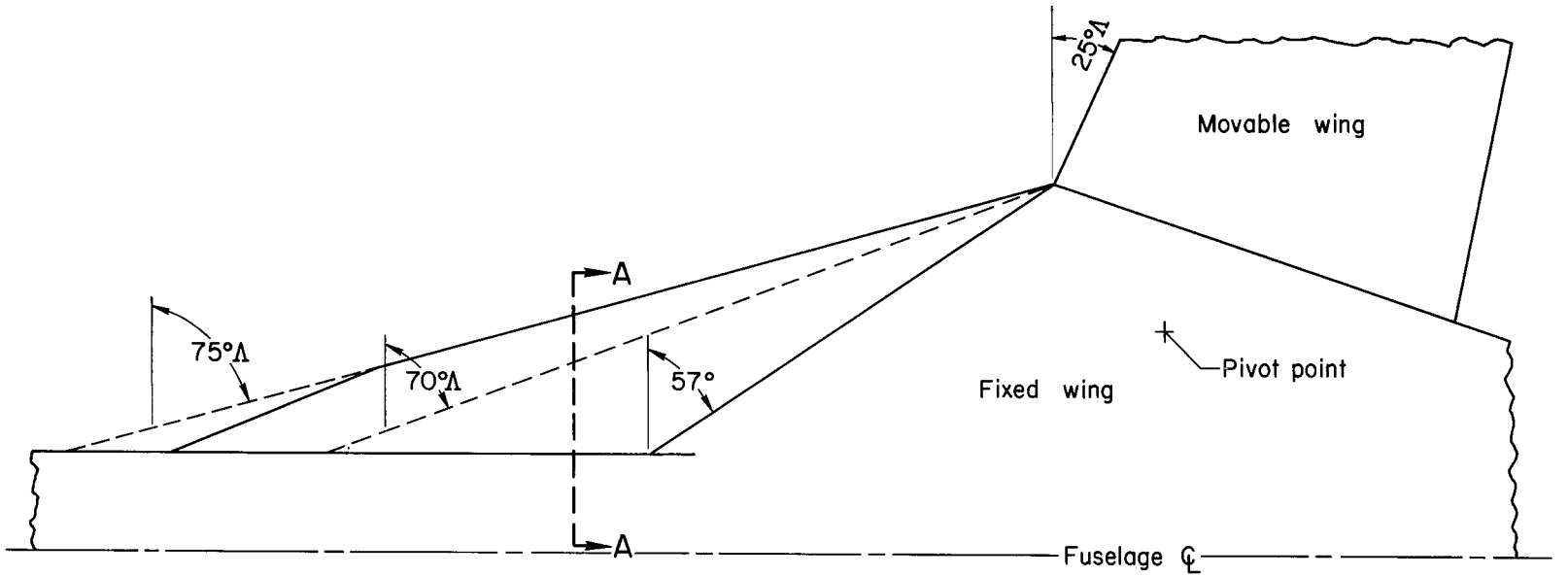

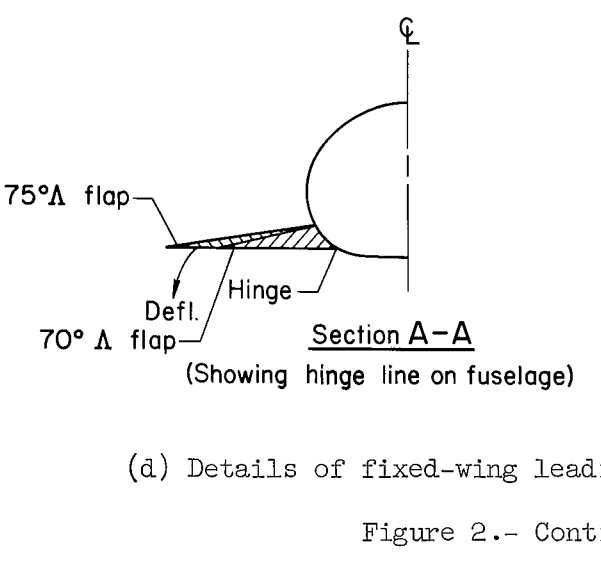

(d) Details of fixed-wing leading-edge plain flap.

Figure 2.- Continued.

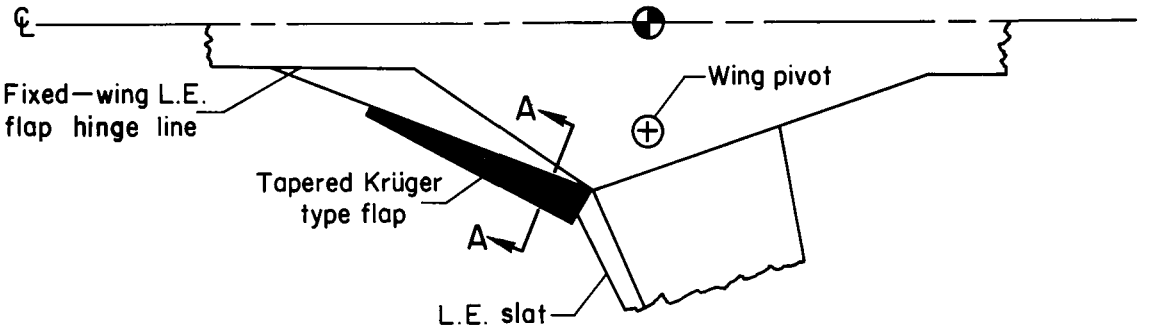

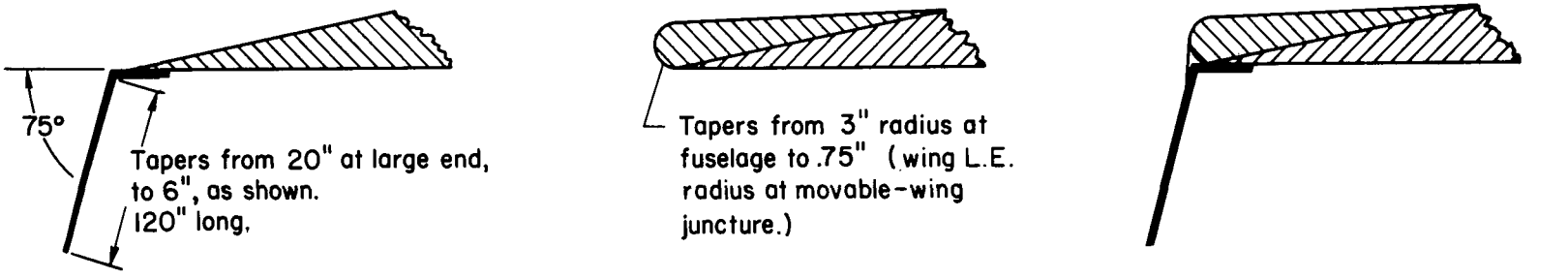

(e) Details of fixed-wing leading-edge radius and Krüger flap.

Figure 2.- Continued.

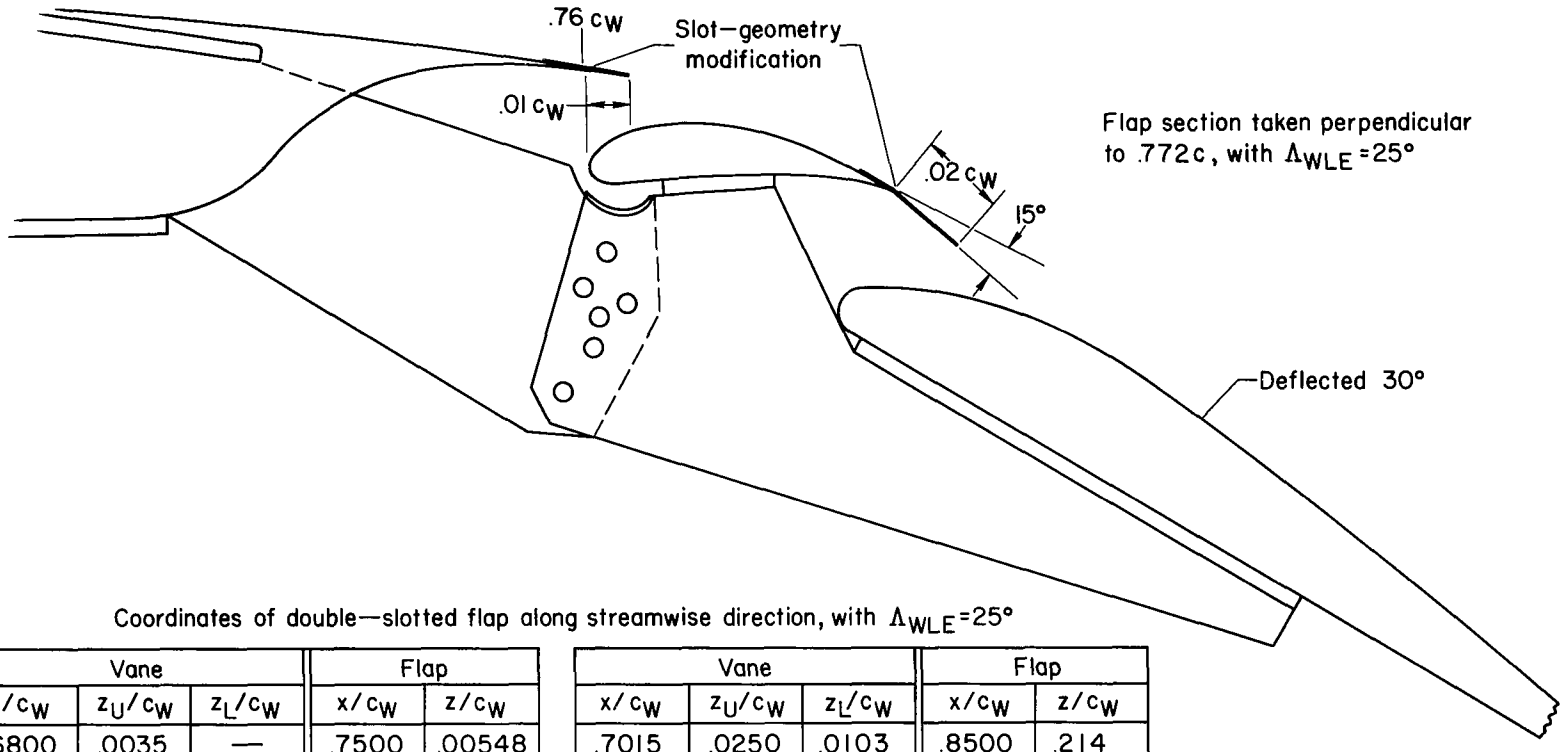

Coordinates of double—slotted flap along streamwise direction, with Λ_{WLE}=25°

Vane			Flap	
x/c_w	z_U/c_w	z_L/c_w	x/c_w	z/c_w
.6800	.0035	—	.7500	.00548
.6803	.0047	.0022	.7555	.0121
.6807	.0061	.0015	.7600	.0148
.6816	.0084	.0007	.7700	.0187
.6835	.0116	0	.7800	.0215
.6853	.0140	.0004	.7900	.0236
.6872	.0156	.0010	.8000	.0249
.6888	.0172	.0018	.8100	.0256
.6921	.0197	.0037	.8200	.0254
.6953	.0217	.0059	.8300	.0242

Vane			Flap	
x/c_w	z_U/c_w	z_L/c_w	x/c_w	z/c_w
.7015	.0250	.0103	.8500	.214
.7077	.0277	.0145	Straight line	
.7141	.0299	.0186	1.0000	.0016
.7207	.0312	.0225		
.7273	.0322	.0261	L.E. radius=.00548	
.7342	.0329	.0290		
.7414	.0334	.0314		
.7450	.0335	.0325		
.7486	.0332	.0332		

(f) Details of the double-slotted flap.

Figure 2.- Continued.

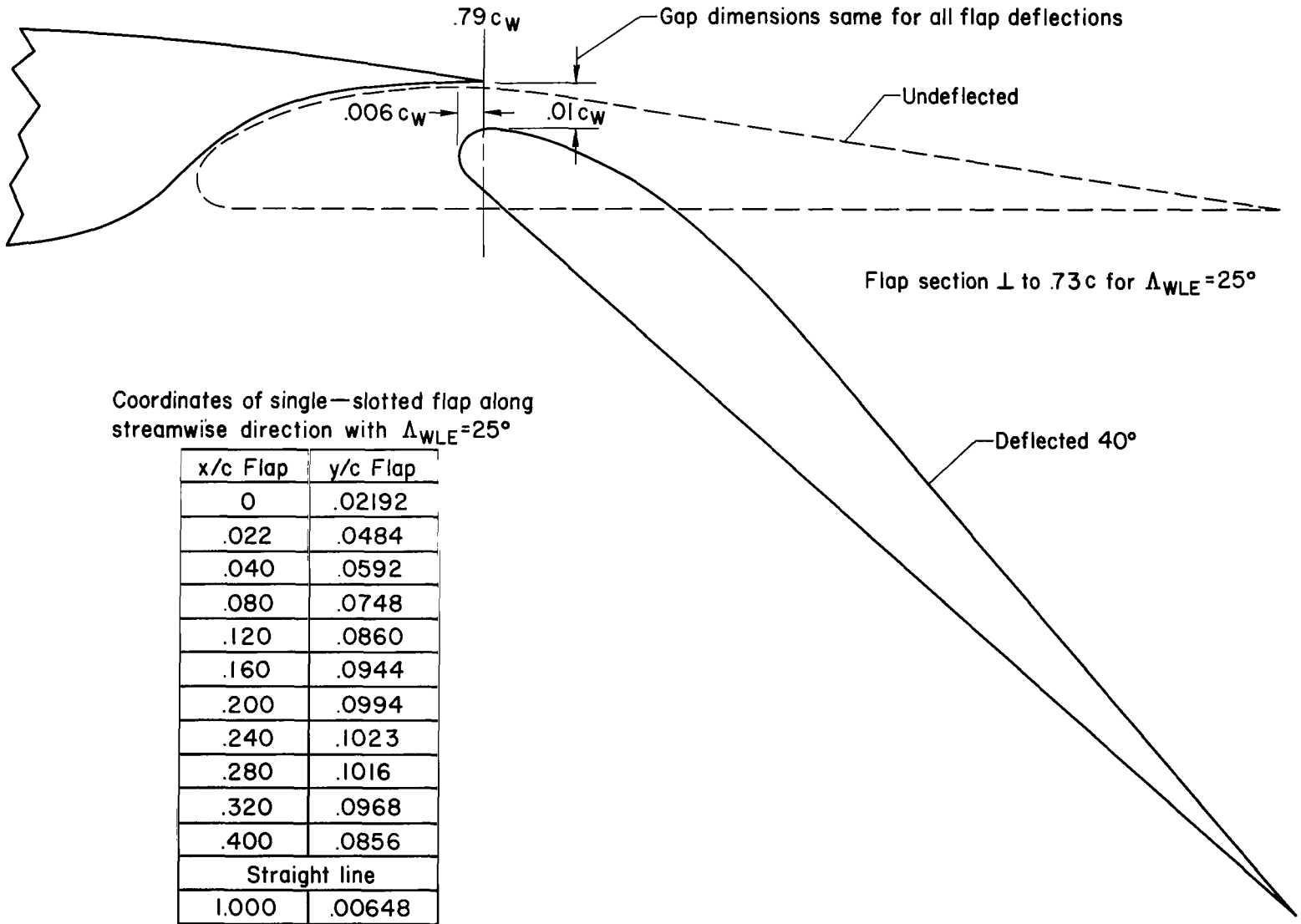

Coordinates of single—slotted flap along streamwise direction with Λ_{WLE}=25°

x/c Flap	y/c Flap
0	.02192
.022	.0484
.040	.0592
.080	.0748
.120	.0860
.160	.0944
.200	.0994
.240	.1023
.280	.1016
.320	.0968
.400	.0856
Straight line	
1.000	.00648
L.E. radius = .02192	

(g) Details of the single-slotted flap.

Figure 2.- Continued.

For gap (g_S) = 0.020c

δ_S = 10°, 20°, 30°; Slat T.E. was positioned to be ⊥ to a wing L.E. radius line as shown

δ_S = 25°, 35°; Slat was rotated with T.E. in same position as for δ_S=30°

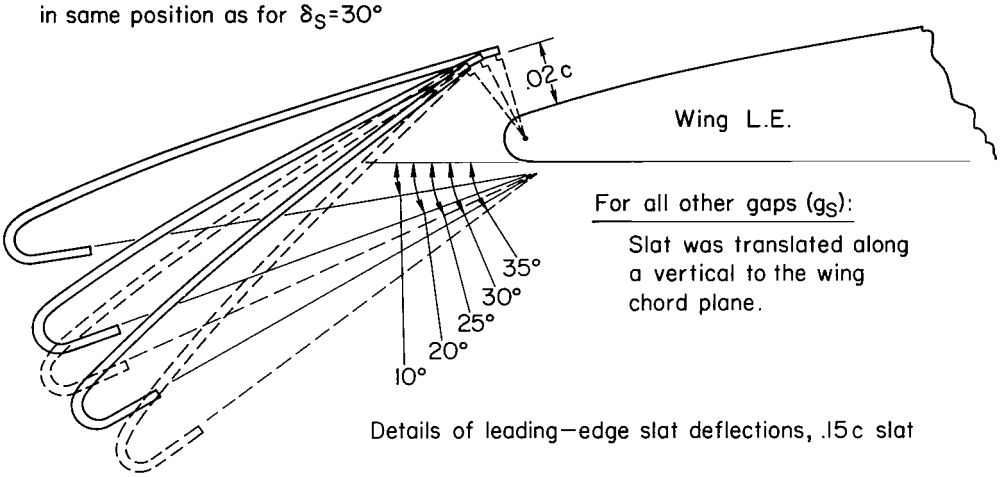

For all other gaps (g_S):

Slat was translated along a vertical to the wing chord plane.

Details of leading-edge slat deflections, .15c slat

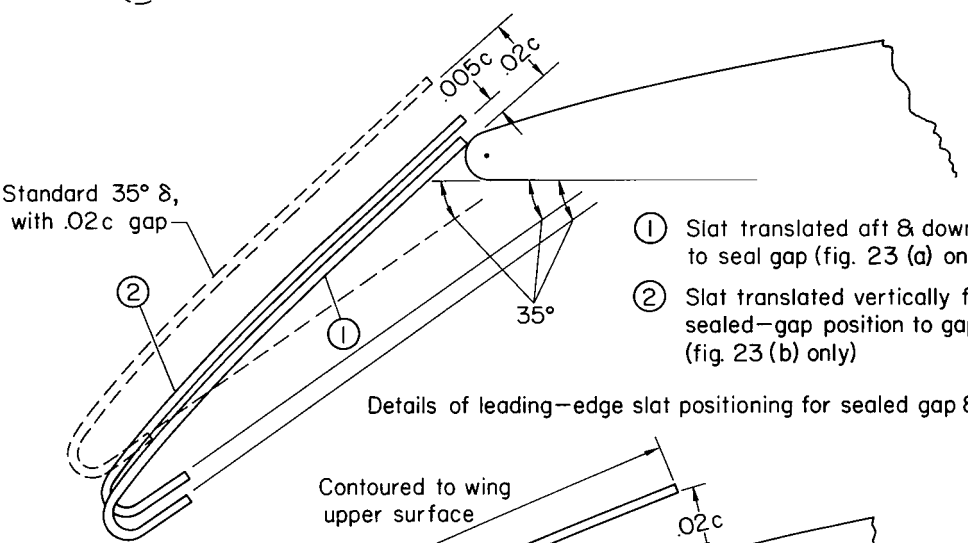

Details of leading-edge slat positioning for sealed gap & .005c gap

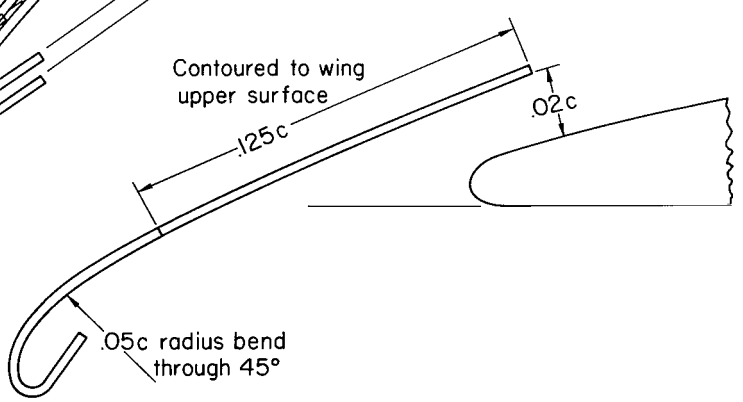

Details of .1875c slat

(h) Details of movable-wing leading-edge slats.

Figure 2.- Concluded.

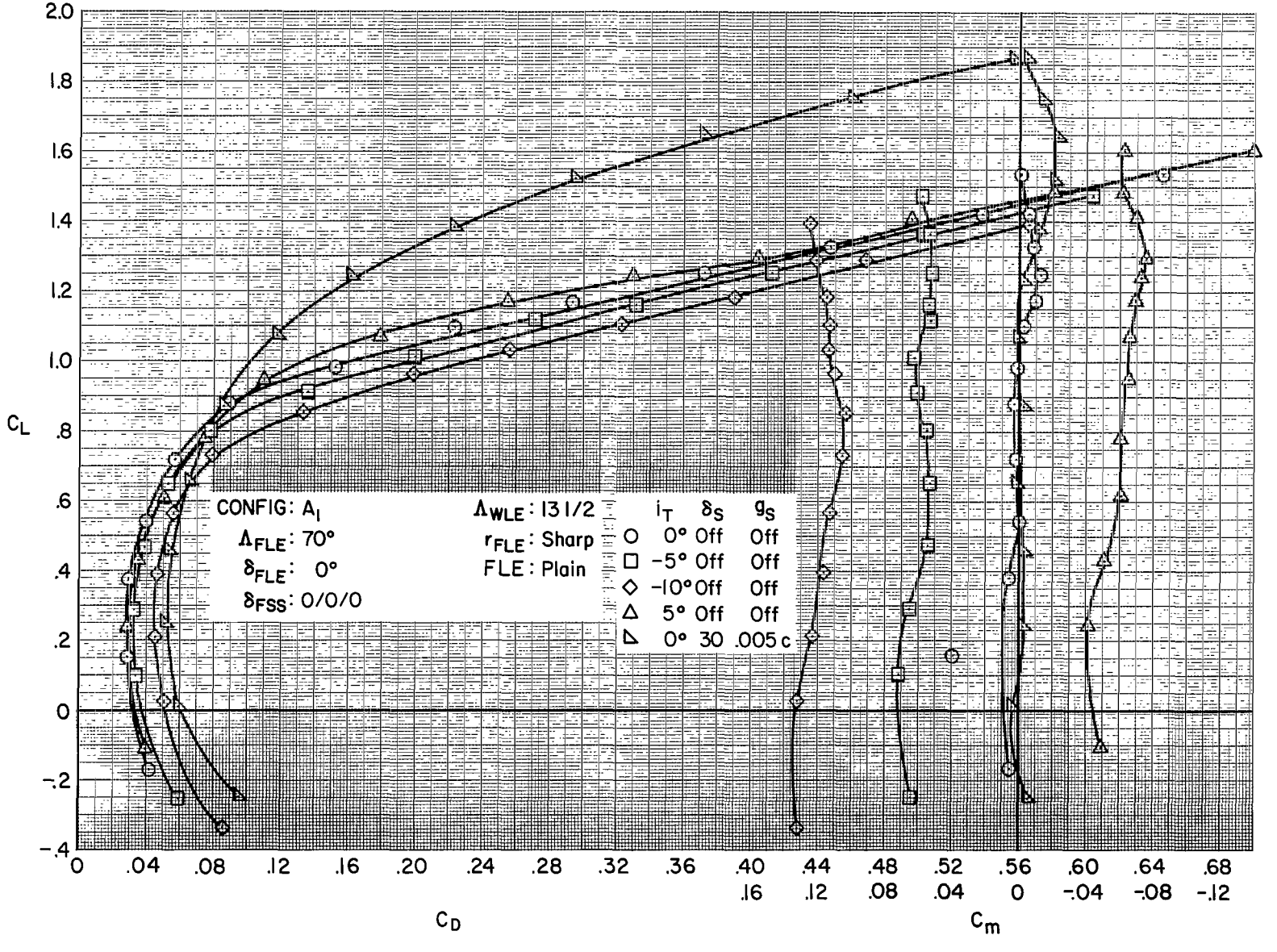

(a) Longitudinal characteristics with flaps up; slats on and off.

Figure 3.- Characteristics of cruise configuration at 13-1/2° sweep.

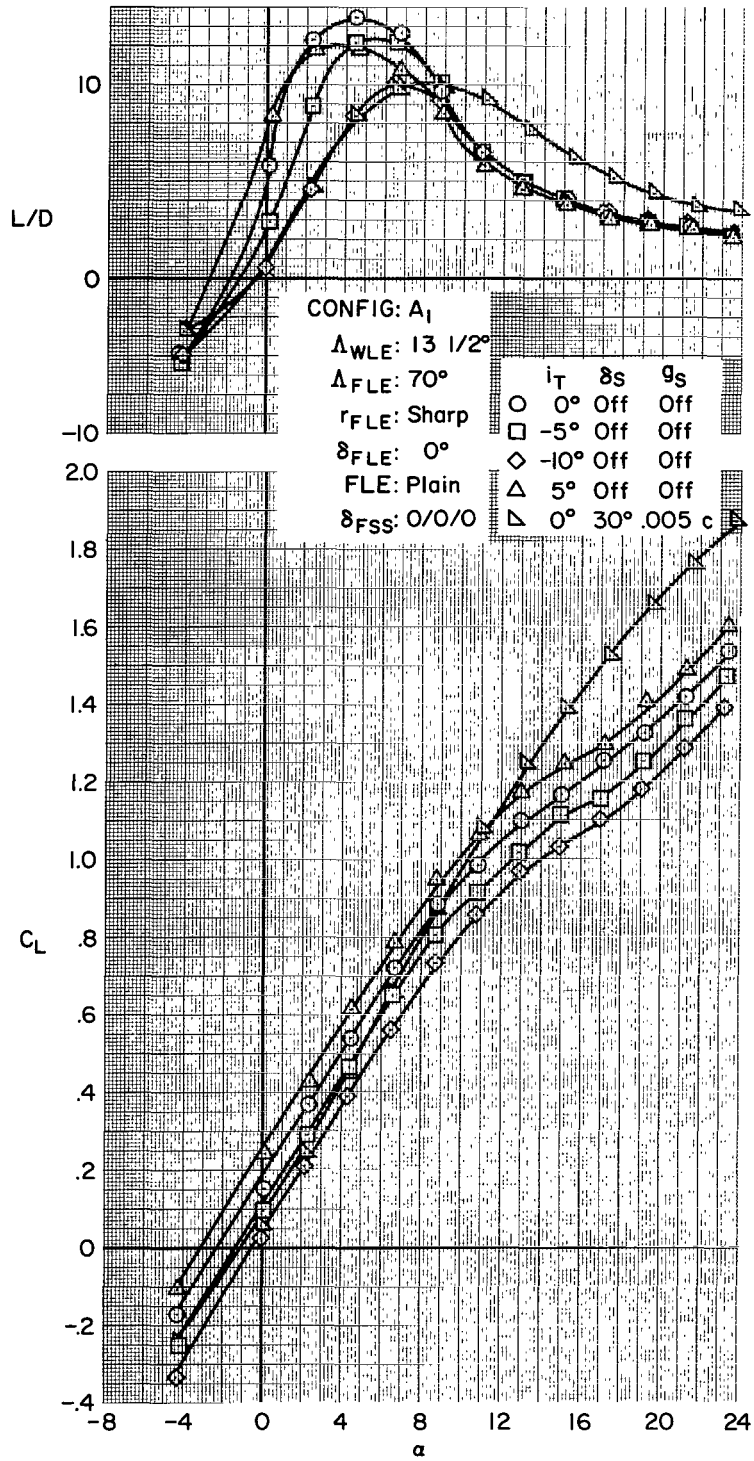

(b) Longitudinal characteristics including cruise lift-drag ratio.

Figure 3.- Concluded.

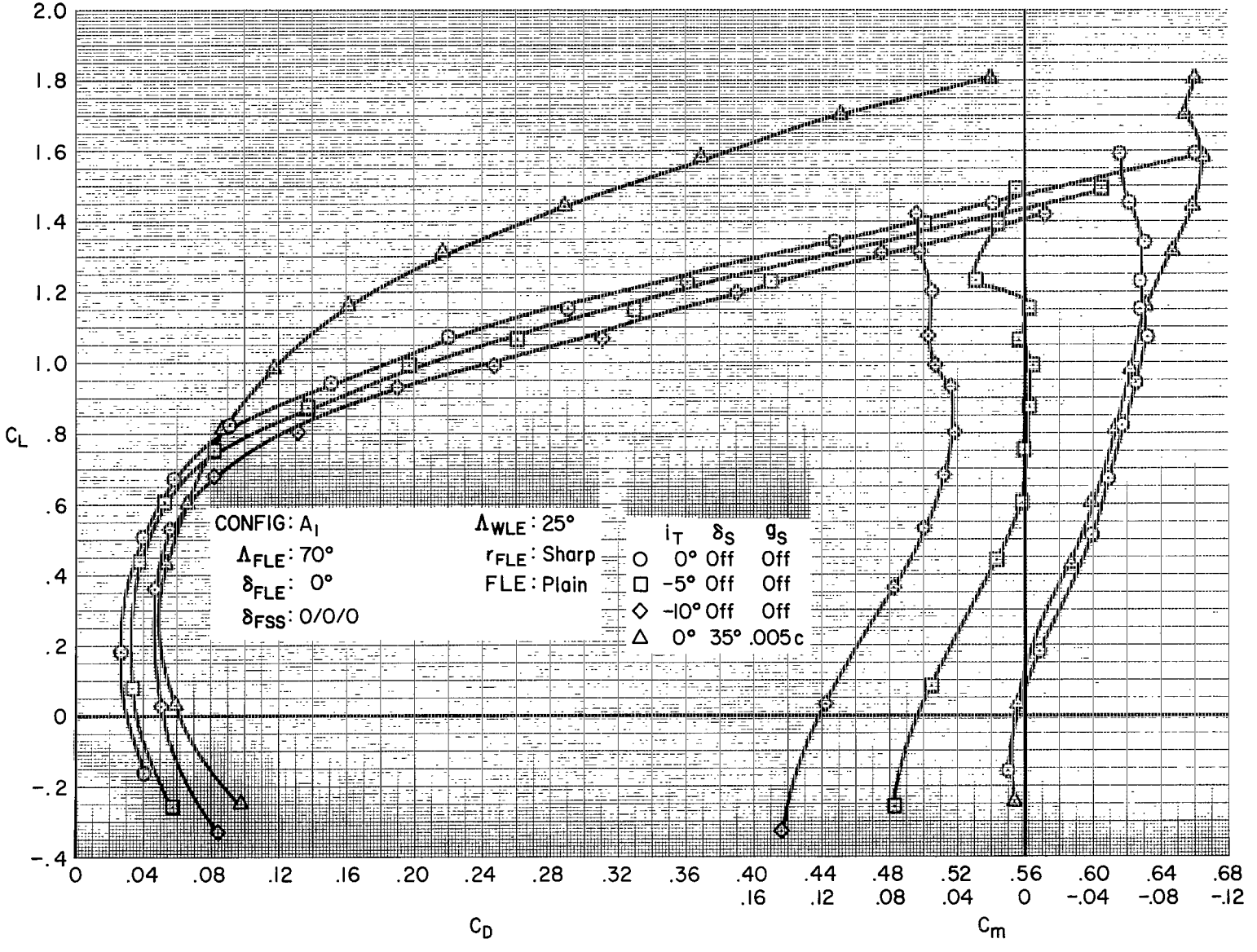

(a) Longitudinal characteristics with flaps up; slats on and off.

Figure 4.- Characteristics of cruise configuration at 25° sweep.

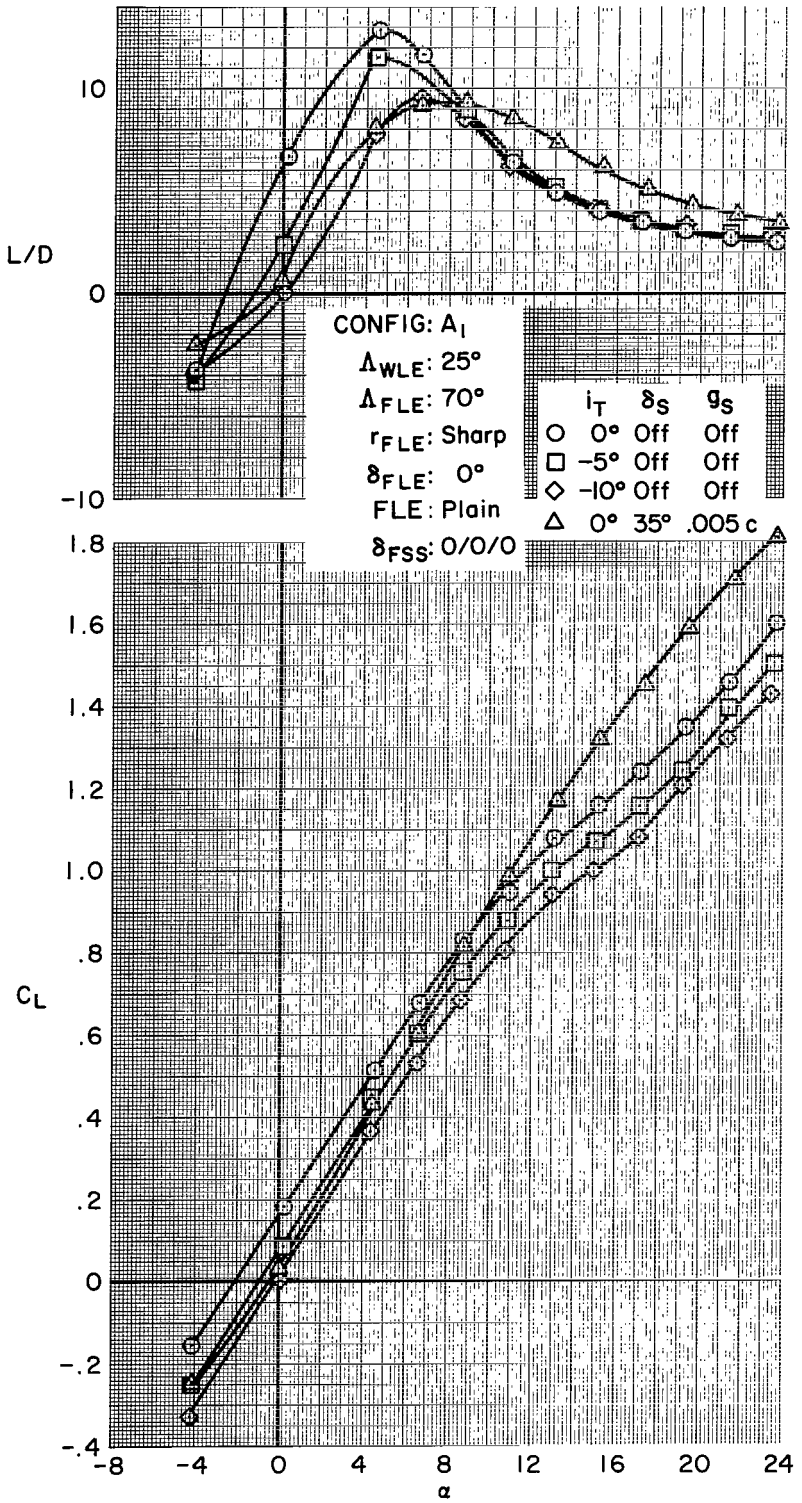

(b) Longitudinal characteristics including cruise lift-drag ratio.

Figure 4.- Concluded.

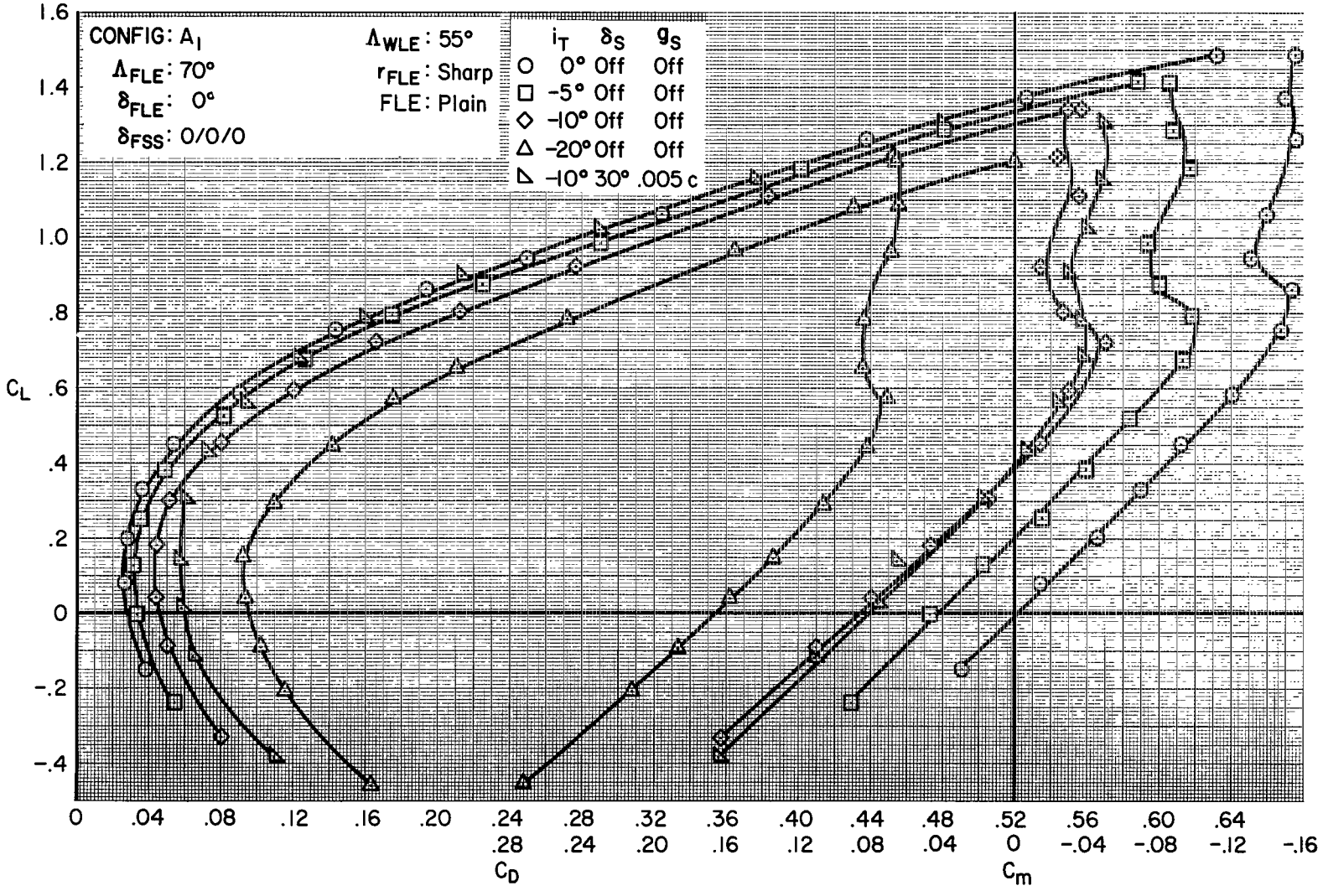

(a) Longitudinal characteristics with flaps up; slats on and off.

Figure 5.- Characteristics of cruise configuration at 55° sweep.

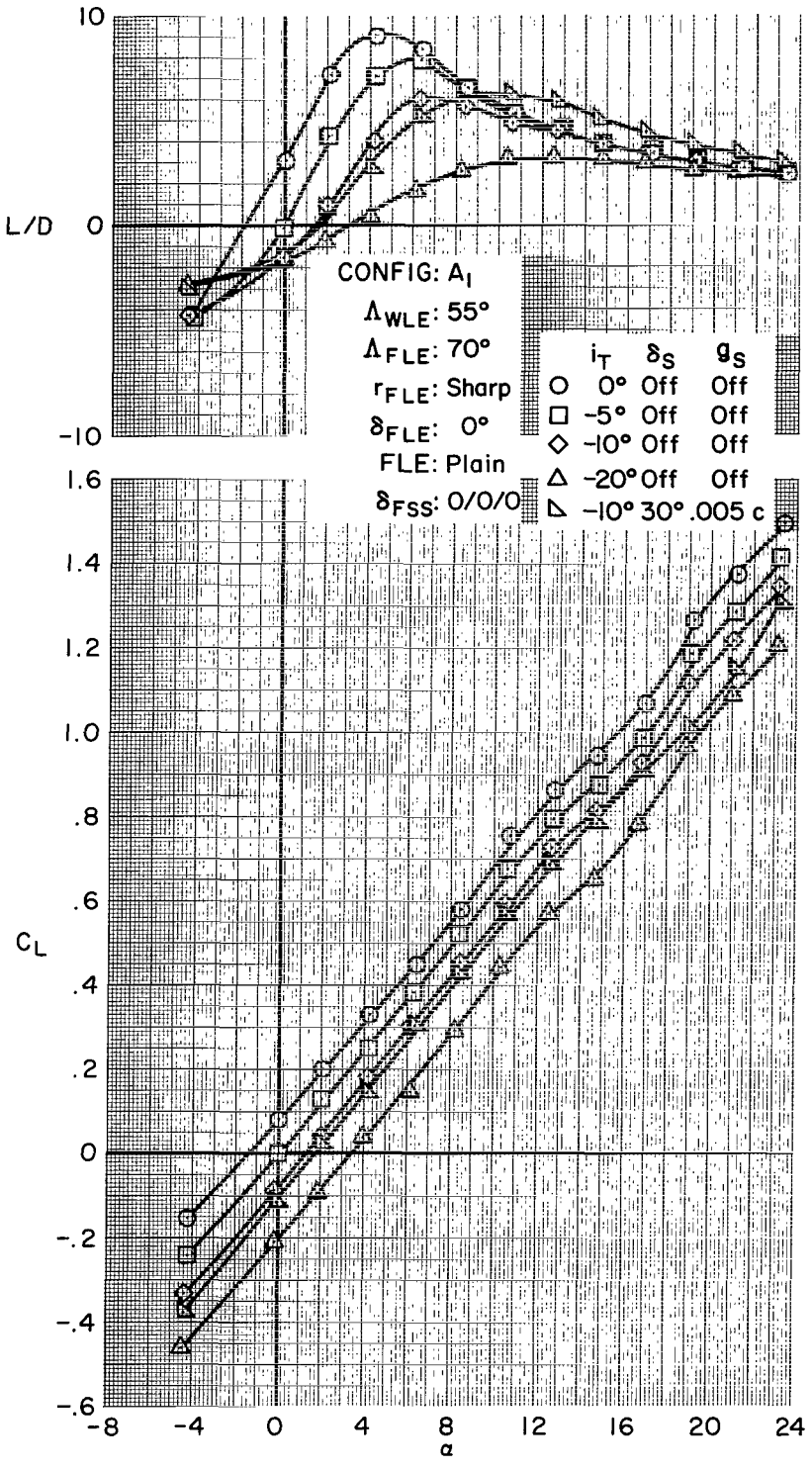

(b) Longitudinal characteristics including cruise lift-drag ratio.

Figure 5.- Concluded.

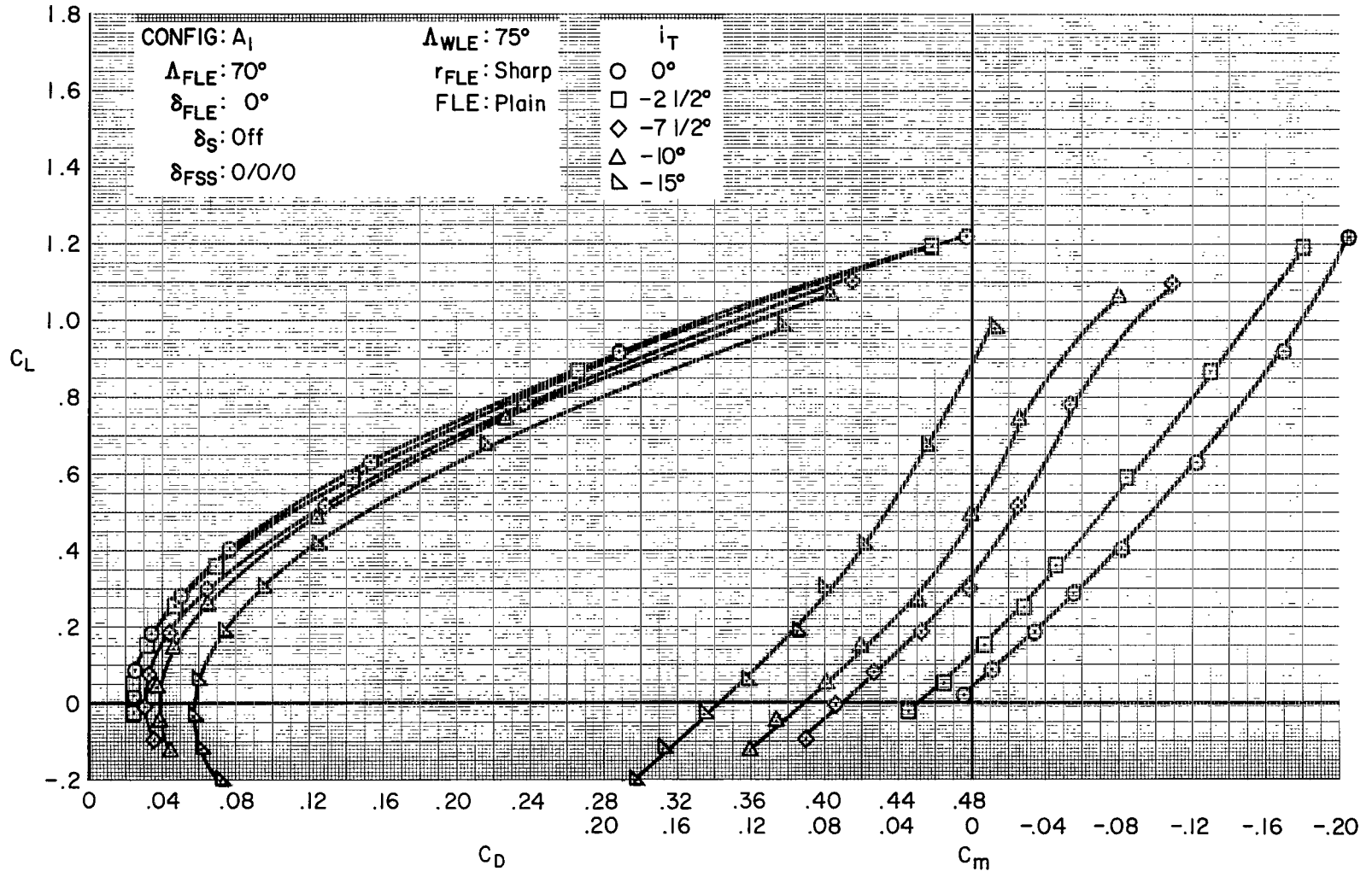

(a) Longitudinal characteristics with flaps up; slats off.

Figure 6.- Characteristics of cruise configuration at 75° sweep.

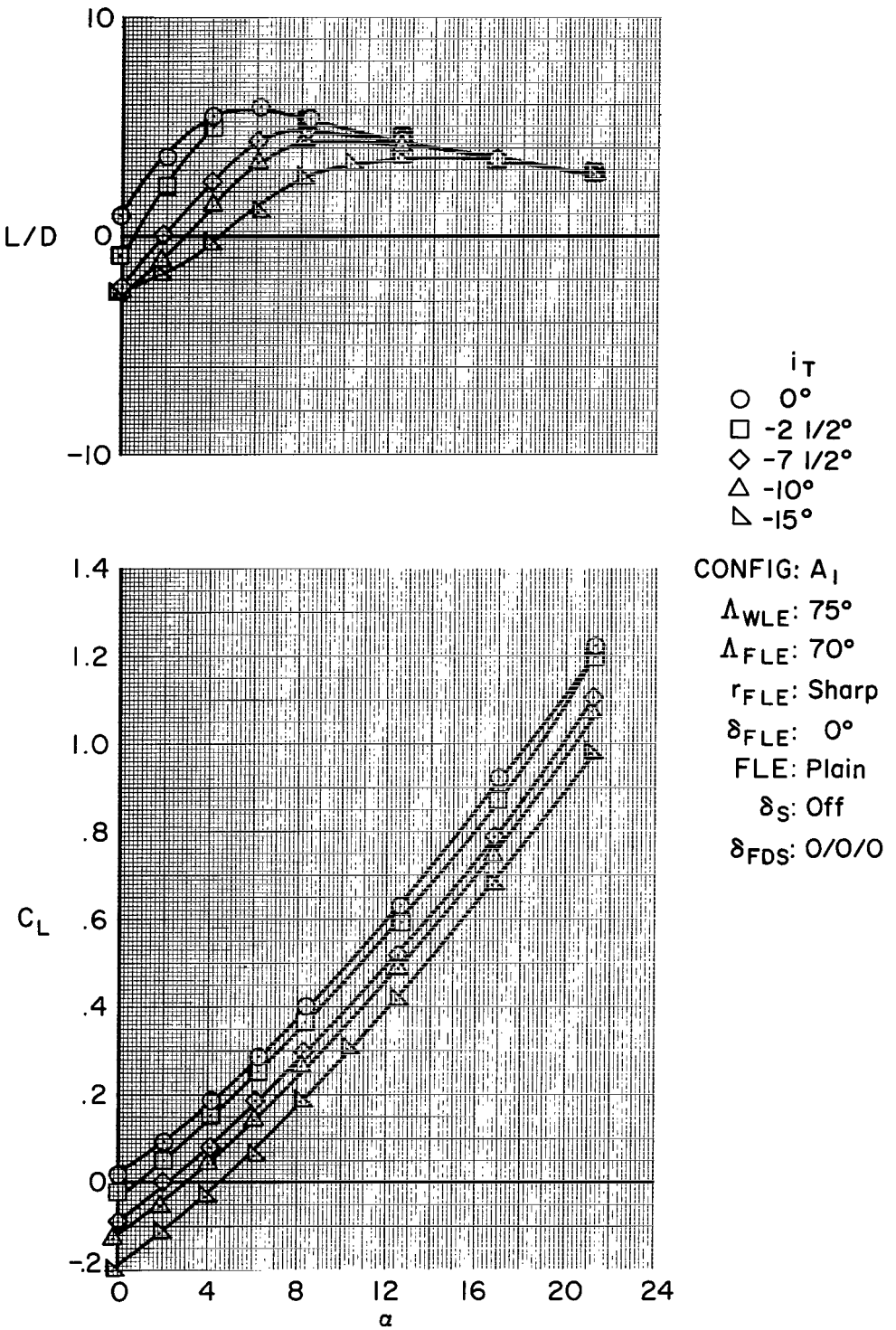

(b) Longitudinal characteristics including cruise lift-drag ratio.

Figure 6.- Concluded.

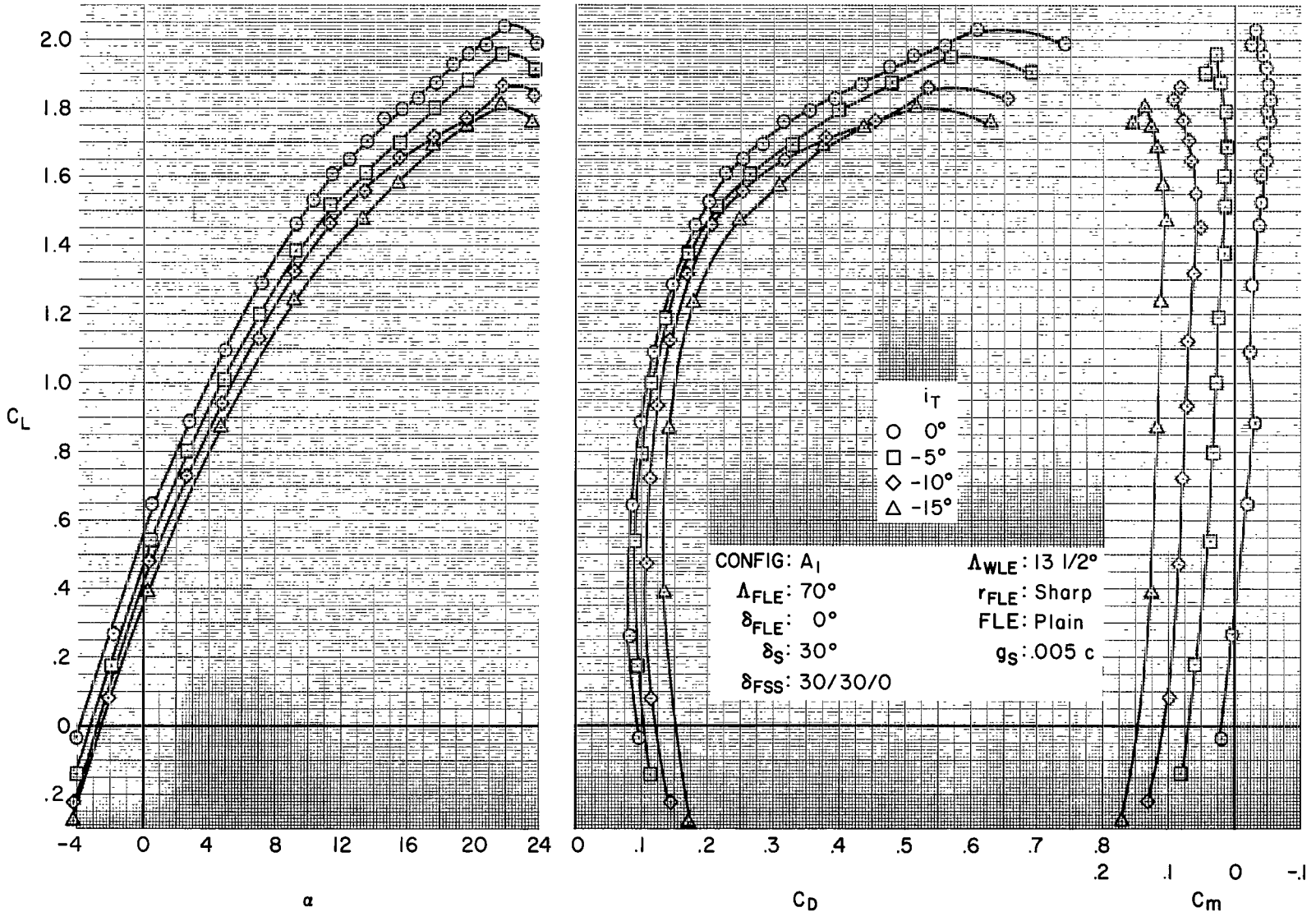

Figure 7.- Longitudinal characteristics of 30° partial-span single-slotted flaps at 13-1/2° sweep.

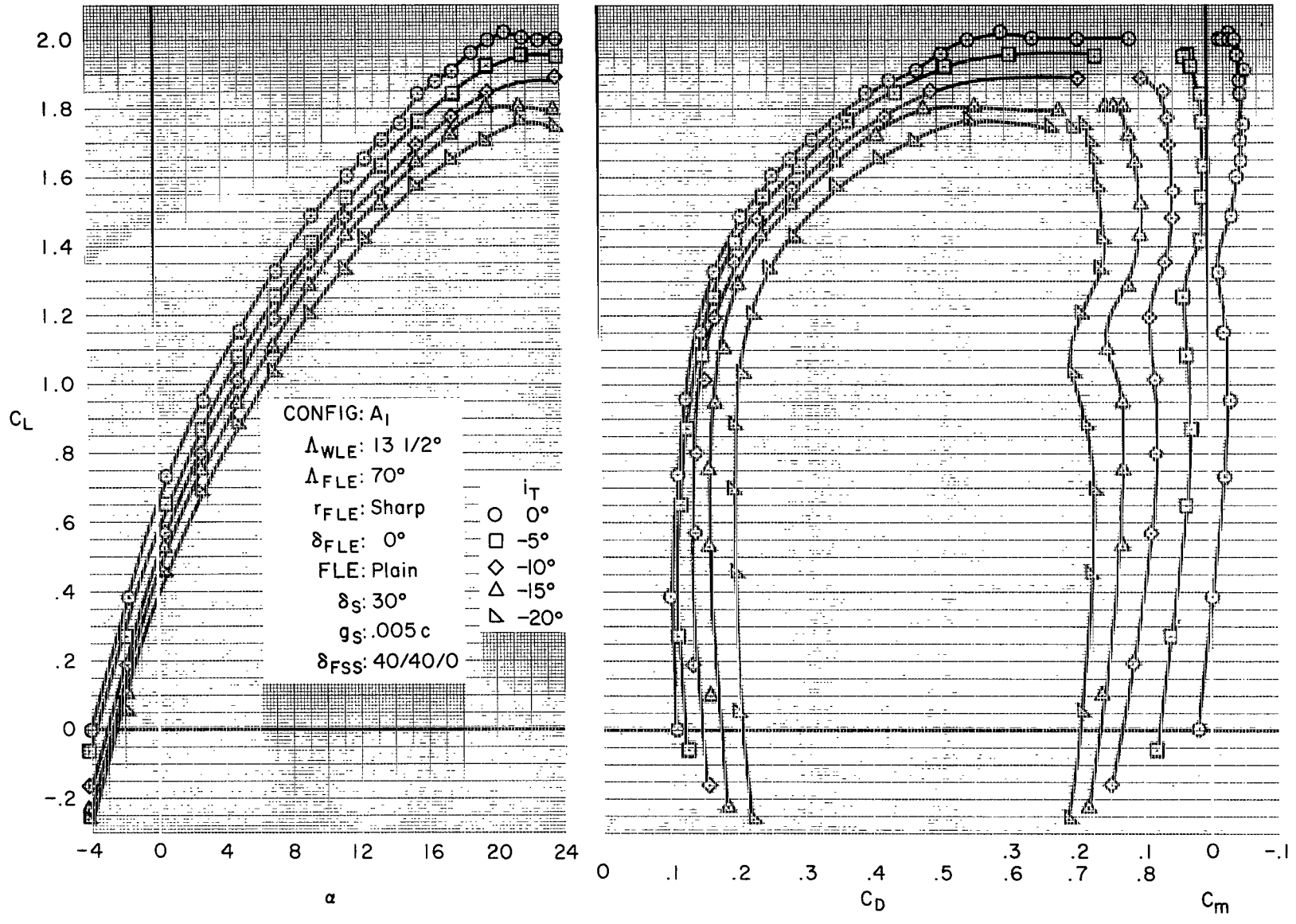

(a) Longitudinal characteristics with tail incidence.

Figure 8.- Characteristics of 40° partial-span single-slotted flaps at 13-1/2° sweep.

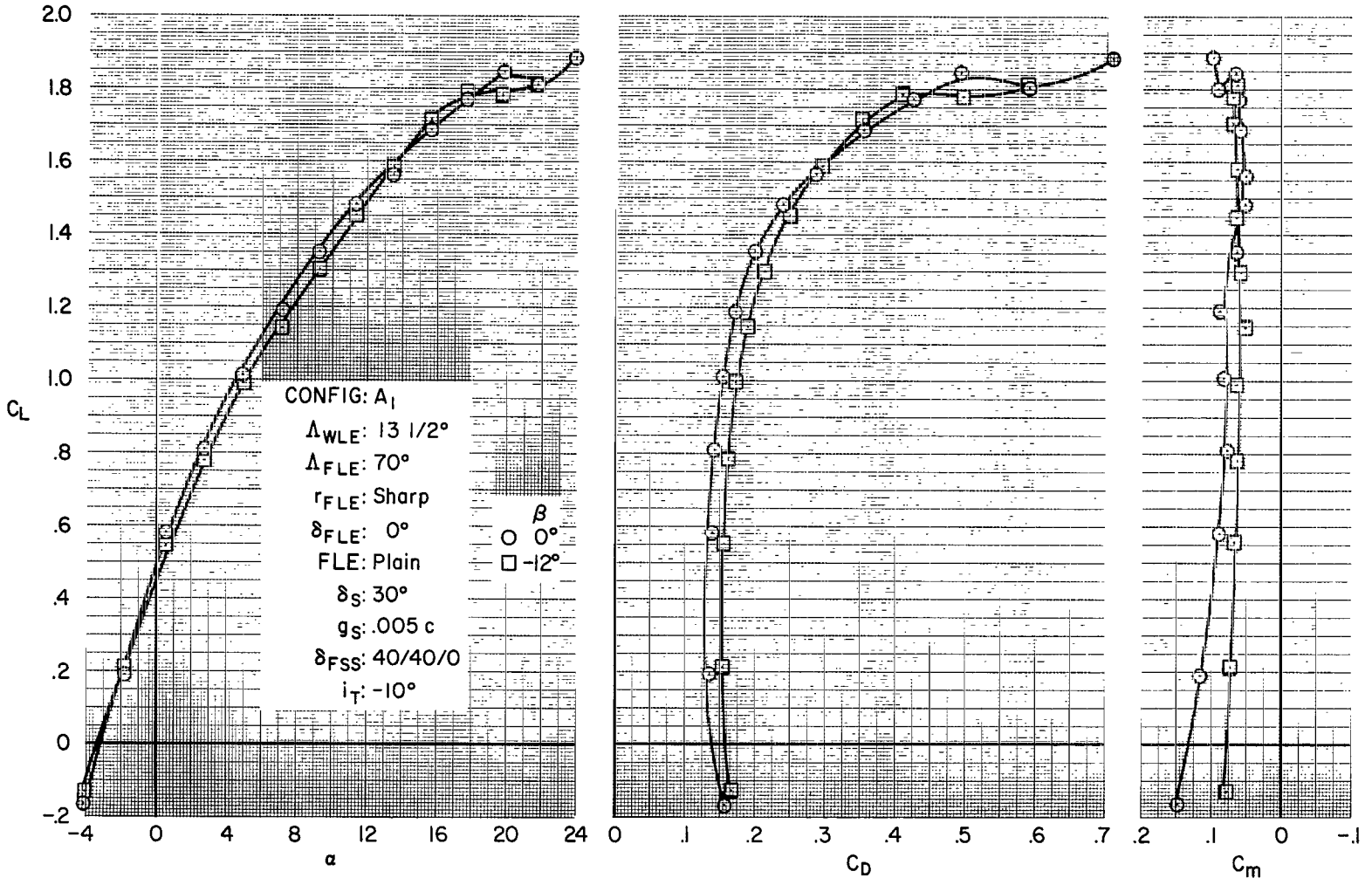

(b) Longitudinal characteristics at constant sideslip.

Figure 8.- Continued.

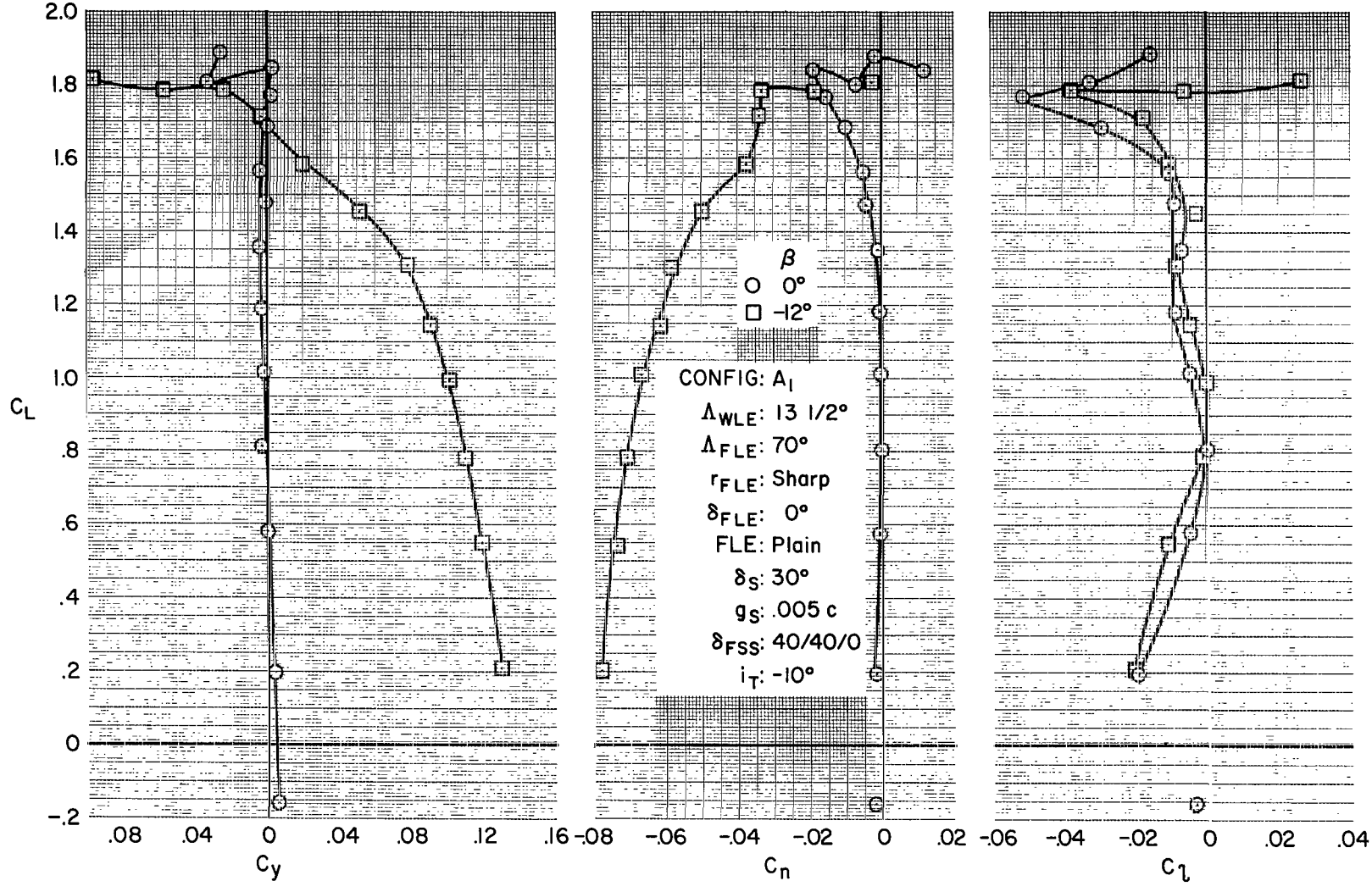

(c) Lateral characteristics at constant sideslip.

Figure 8.- Continued.

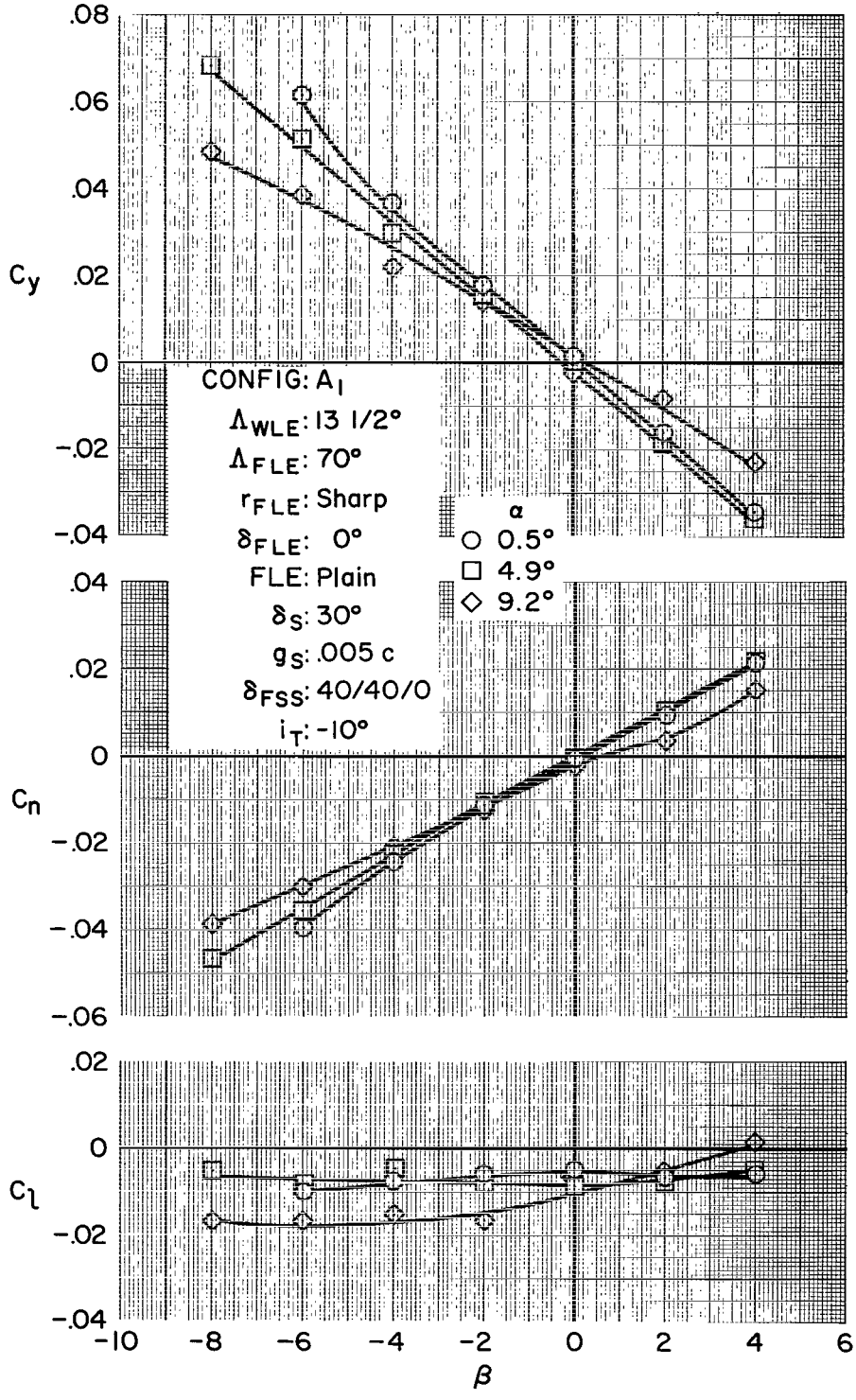

(d) Lateral characteristics at constant angle of attack.

Figure 8.- Concluded.

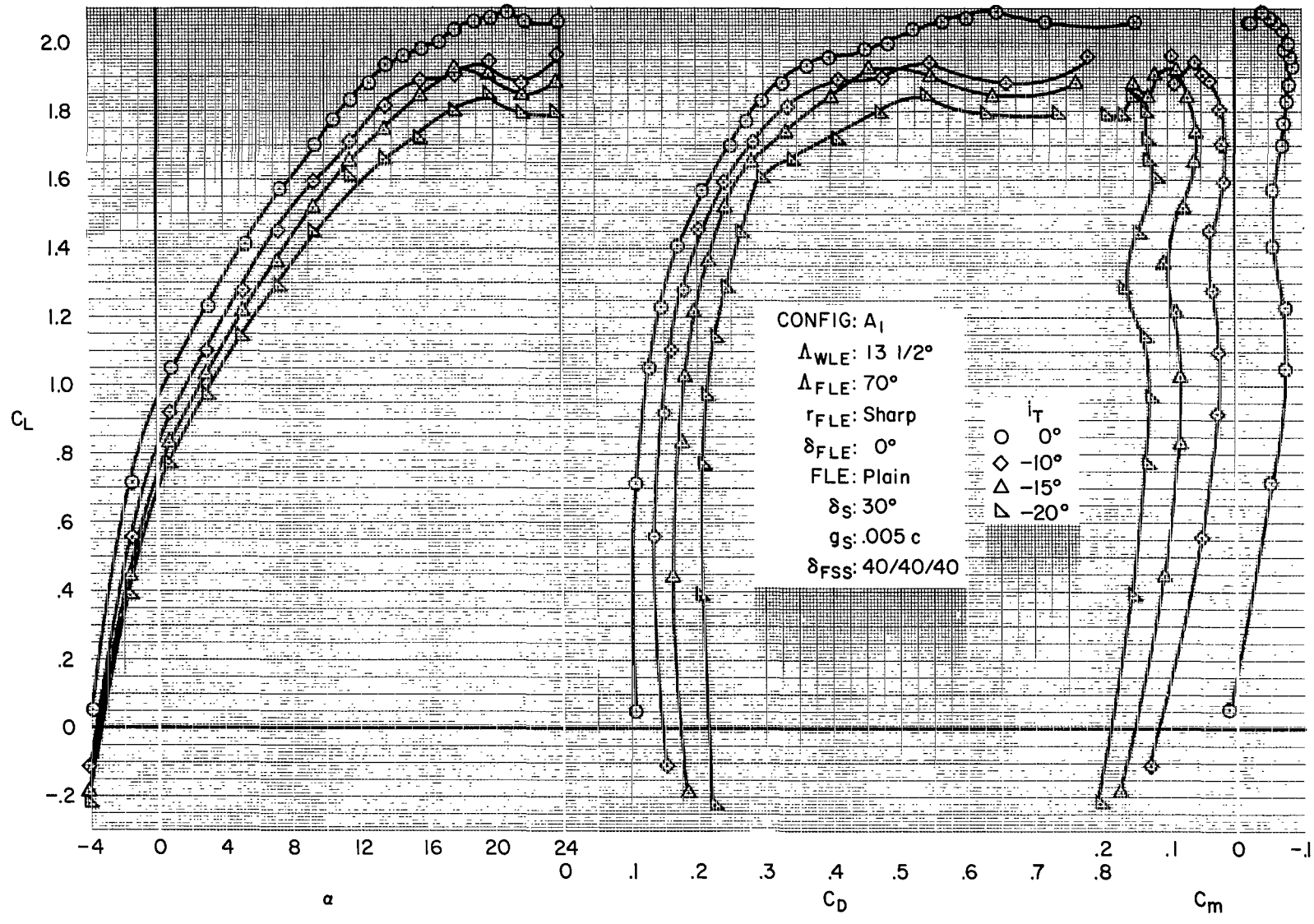

Figure 9.- Characteristics of 40° full-span single-slotted flaps at 13-1/2° sweep.

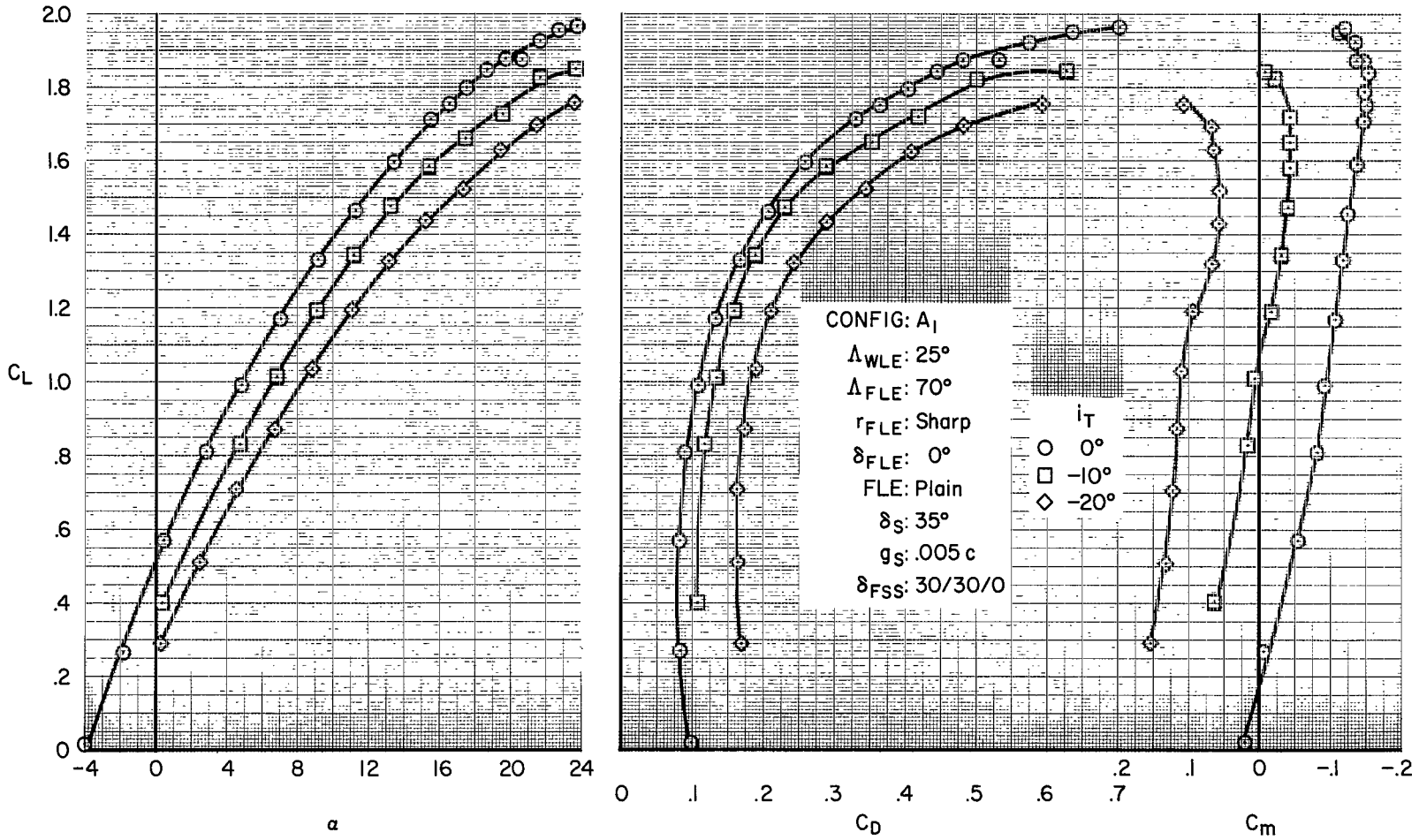

(a) Longitudinal characteristics with tail incidence.

Figure 10.- Characteristics of 30° partial-span single-slotted flaps at 25° sweep.

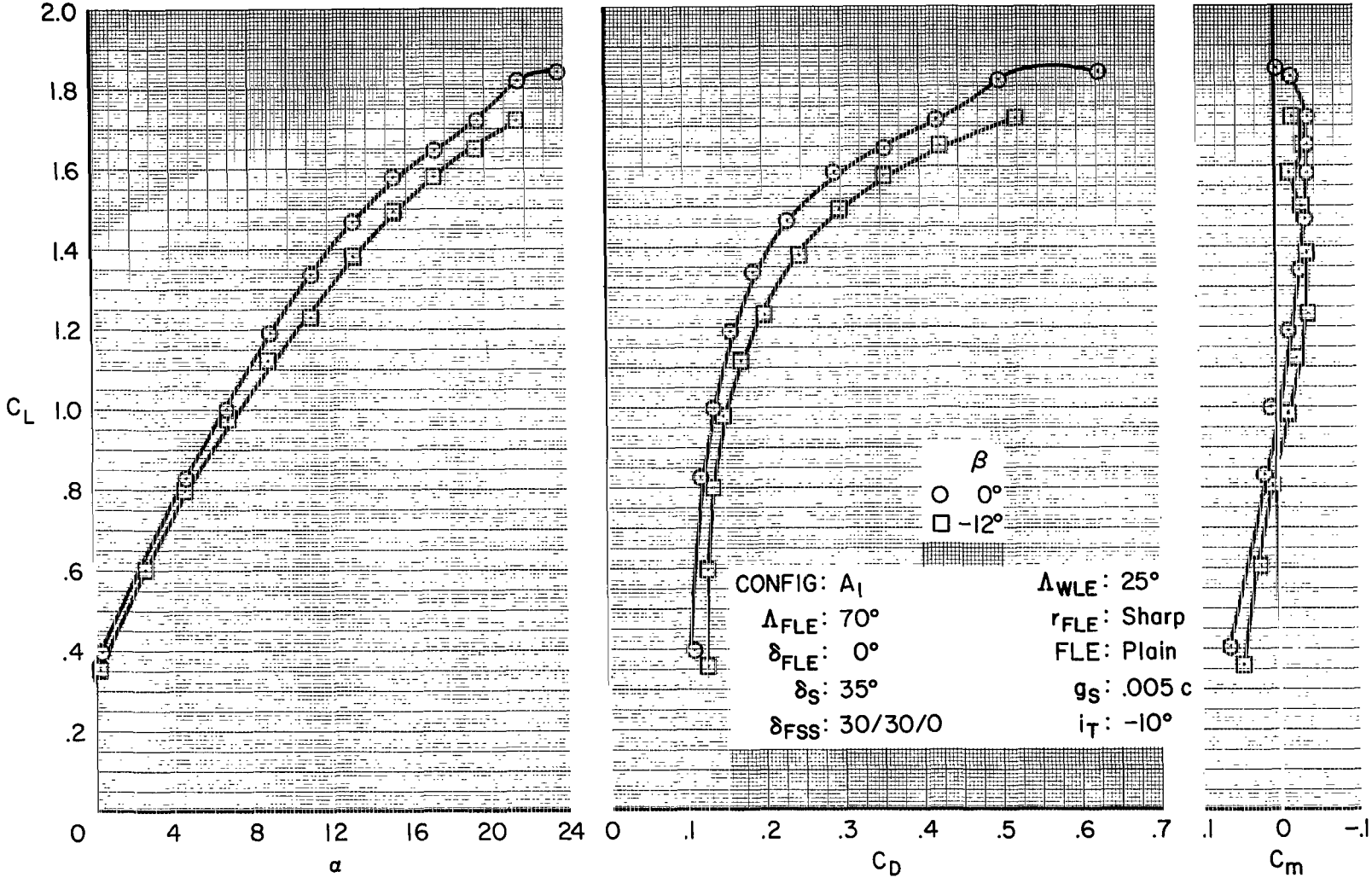

(b) Longitudinal characteristics at constant sideslip.

Figure 10.- Continued.

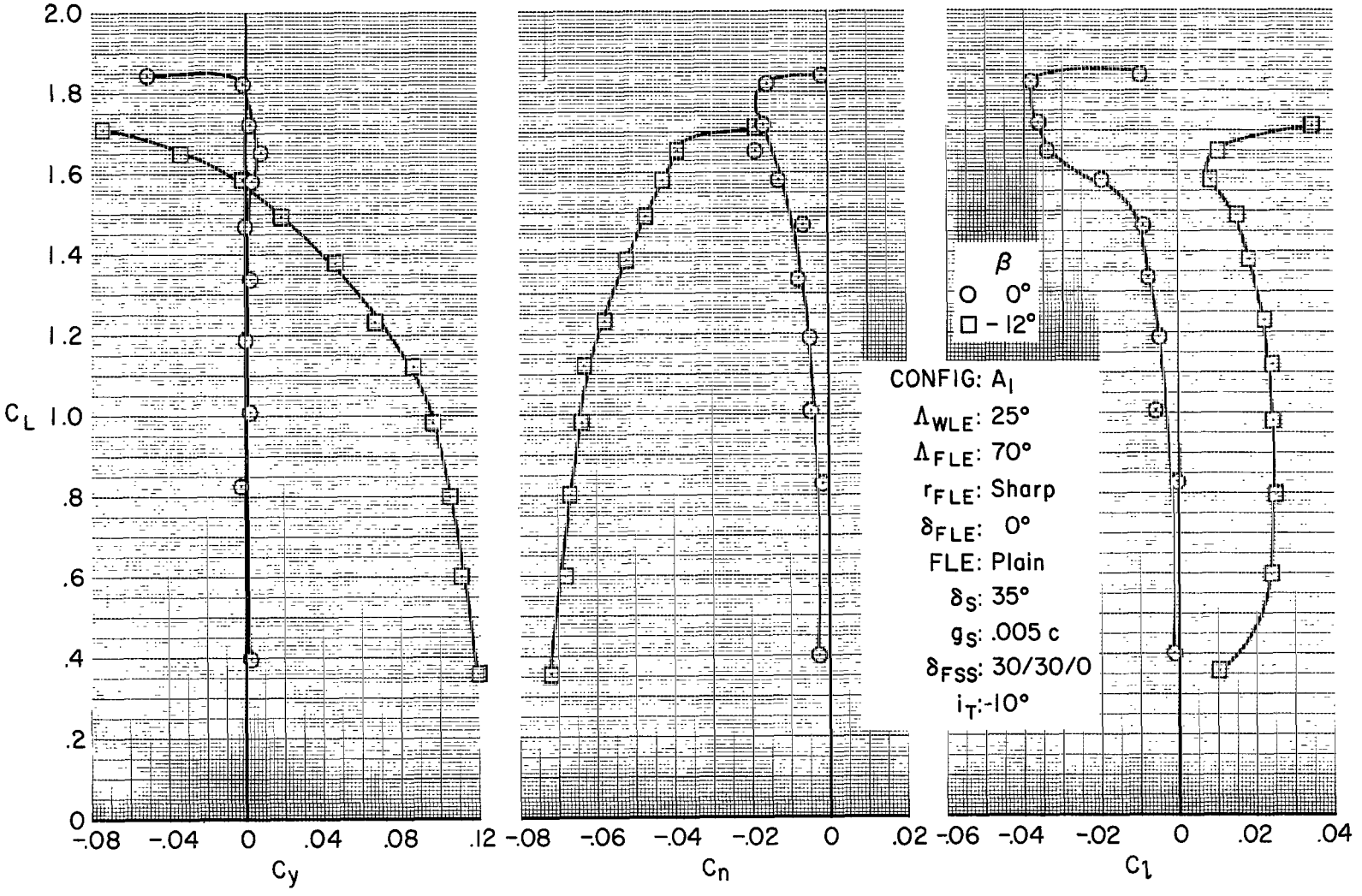

(c) Lateral characteristics at constant sideslip.

Figure 10.- Continued.

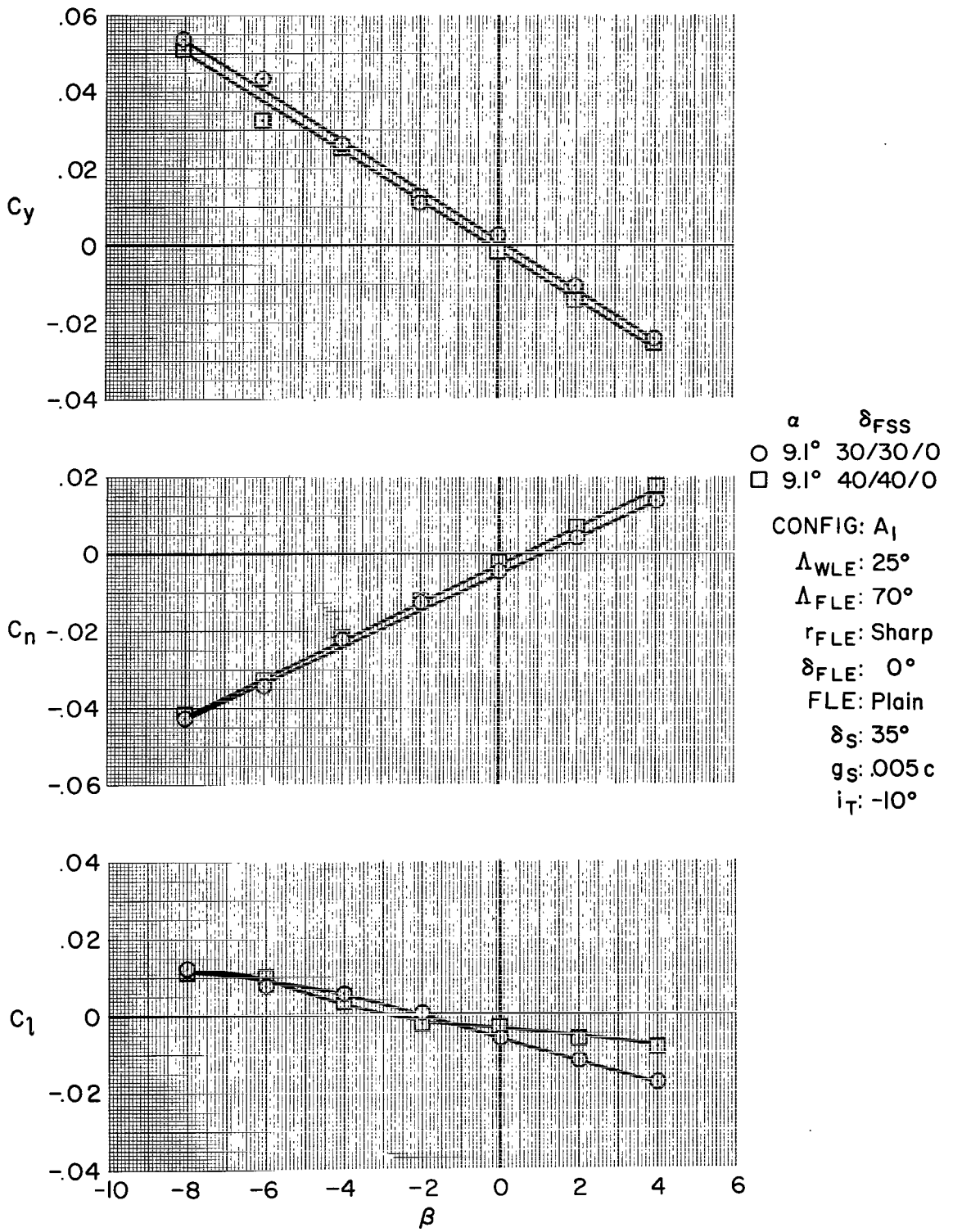

(d) Lateral characteristics at constant angle of attack.

Figure 10.- Concluded.

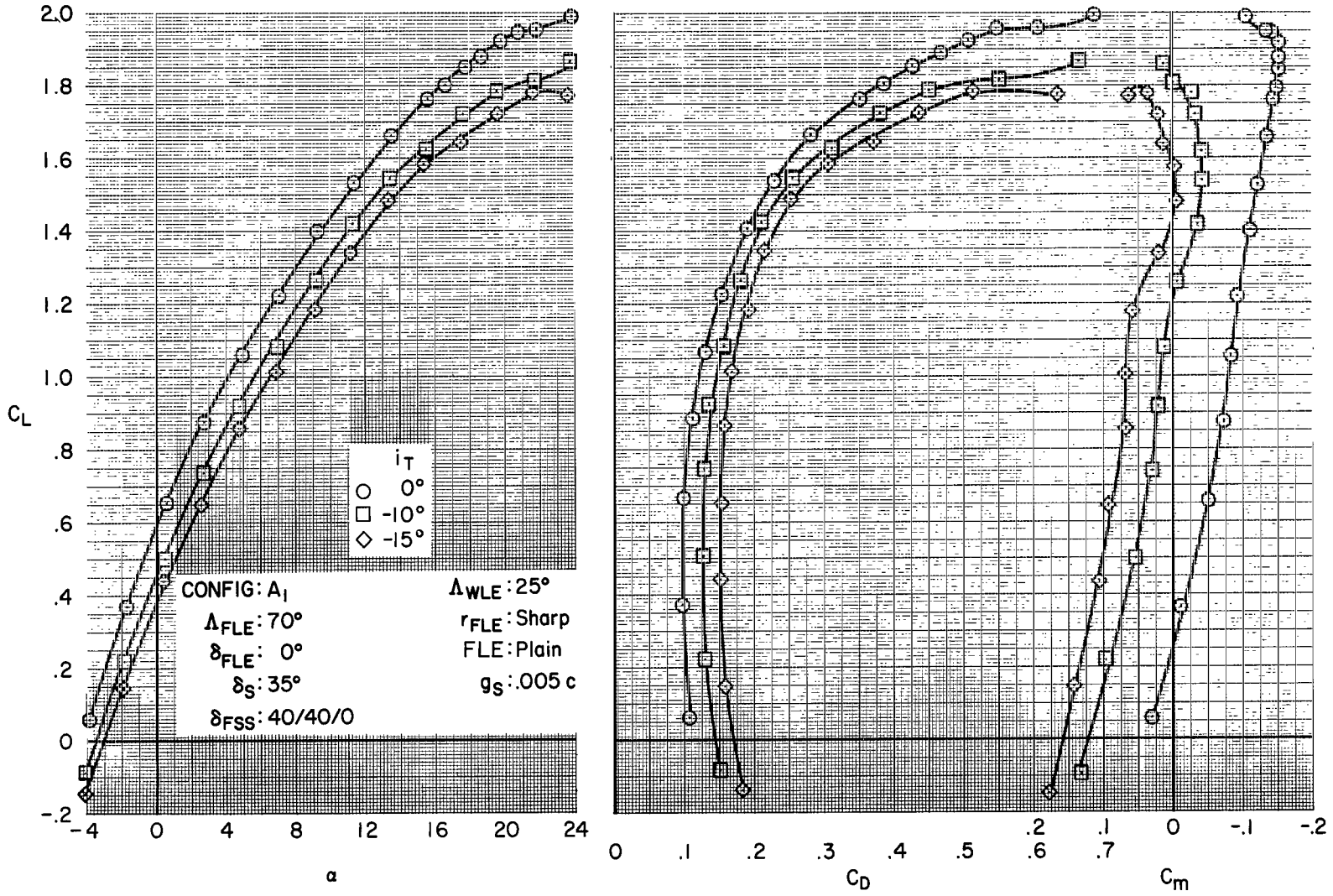

Figure 11.- Characteristics of 40° partial-span single-slotted flaps at 25° sweep.

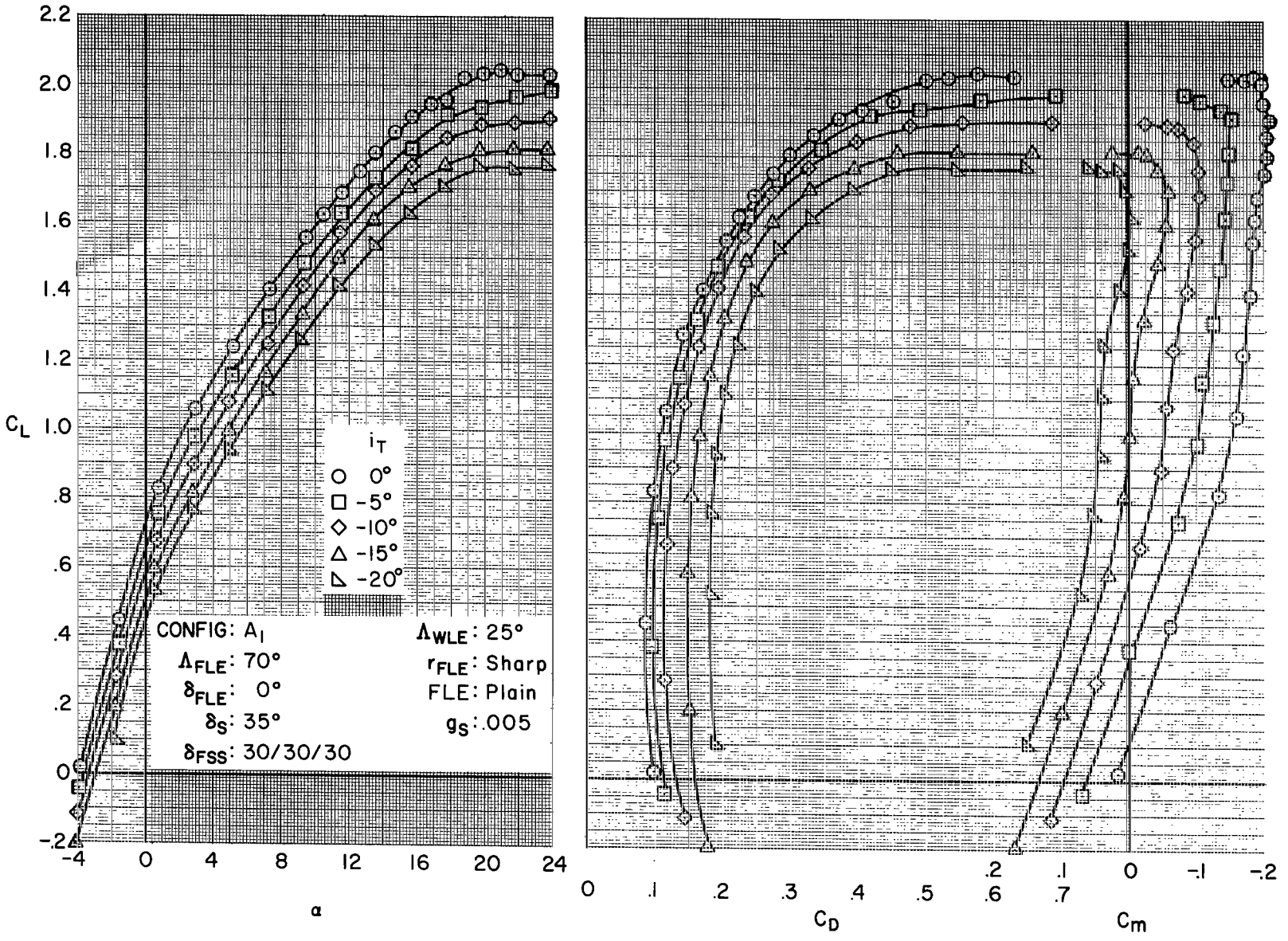

Figure 12.- Characteristics of 30° full-span single-slotted flaps at 25° sweep.

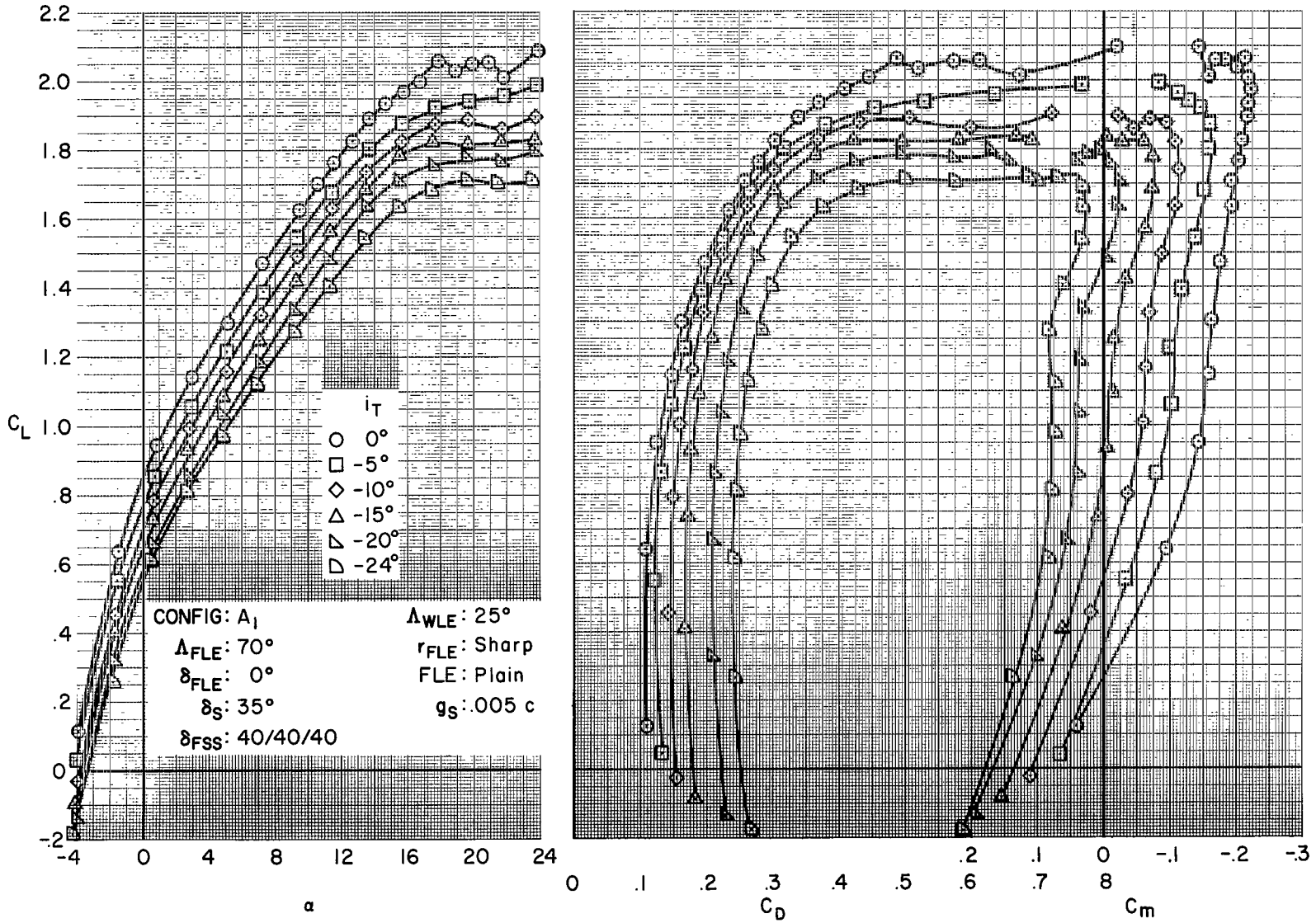

(a) Longitudinal characteristics with tail incidence.

Figure 13.- Characteristics of 40° full-span single-slotted flaps at 25° sweep.

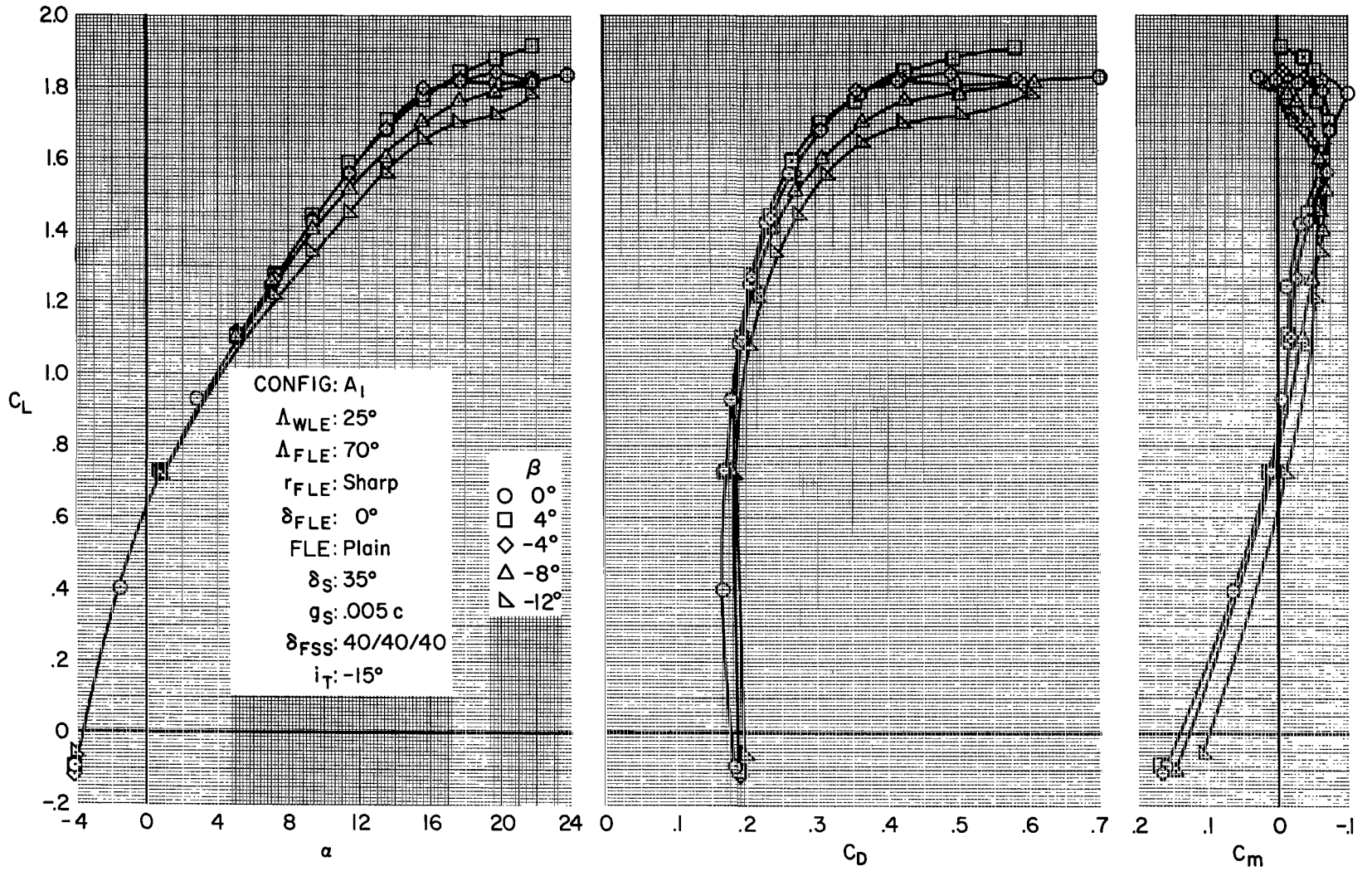

(b) Longitudinal characteristics at constant sideslip.

Figure 13.- Continued.

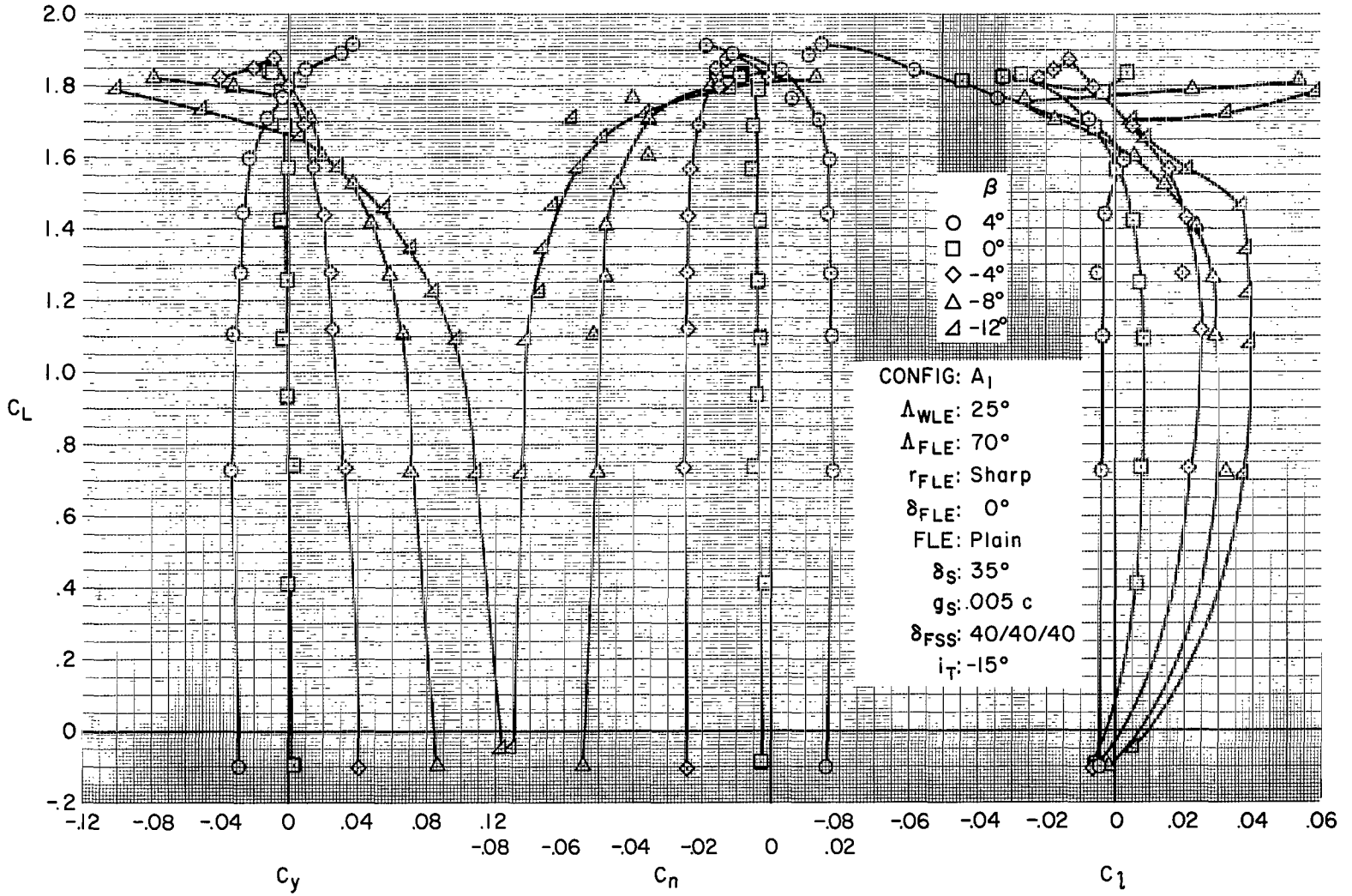

(c) Lateral characteristics at constant sideslip.

Figure 13.- Continued.

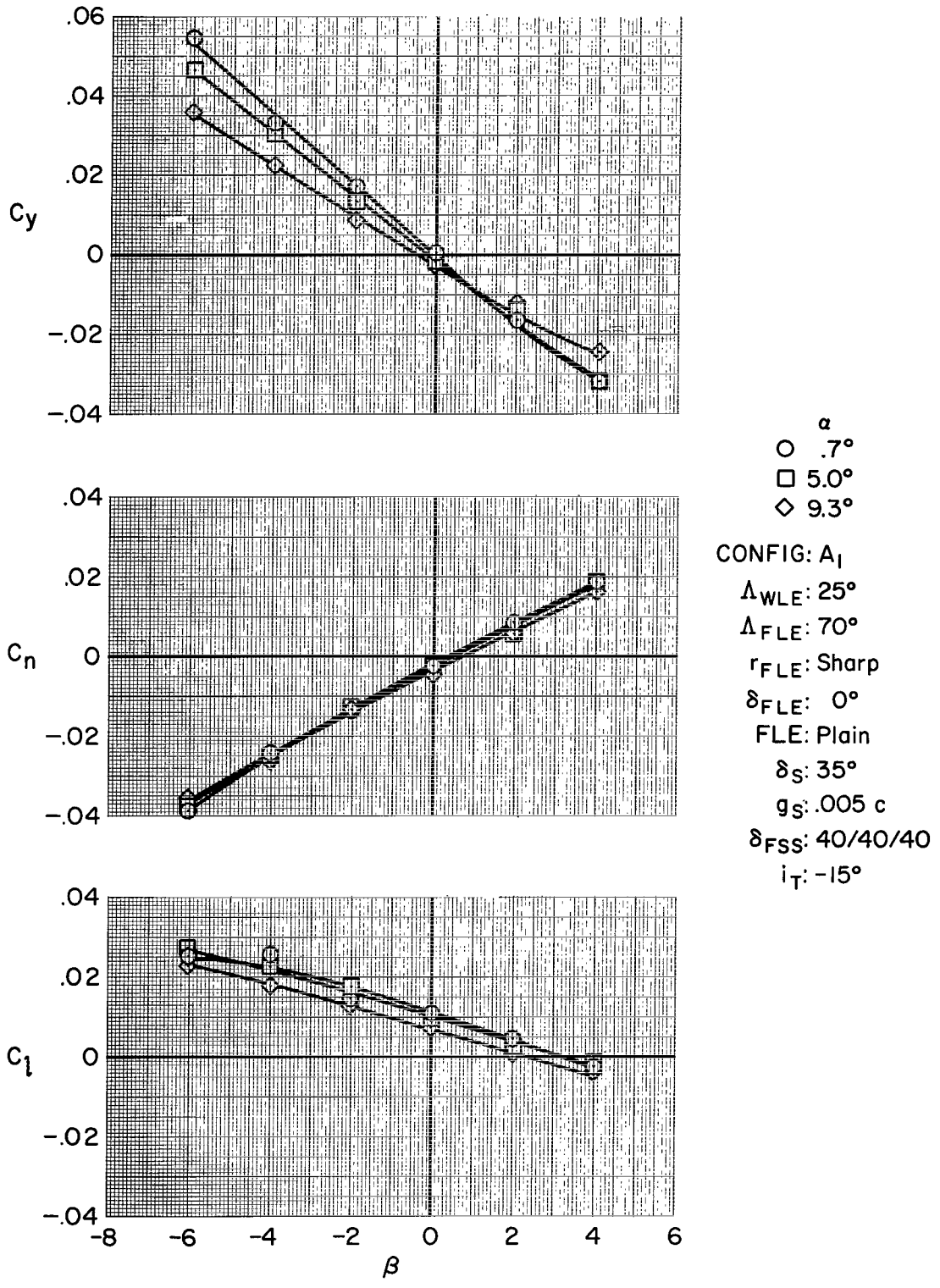

(d) Lateral characteristics at constant angle of attack.

Figure 13.- Concluded.

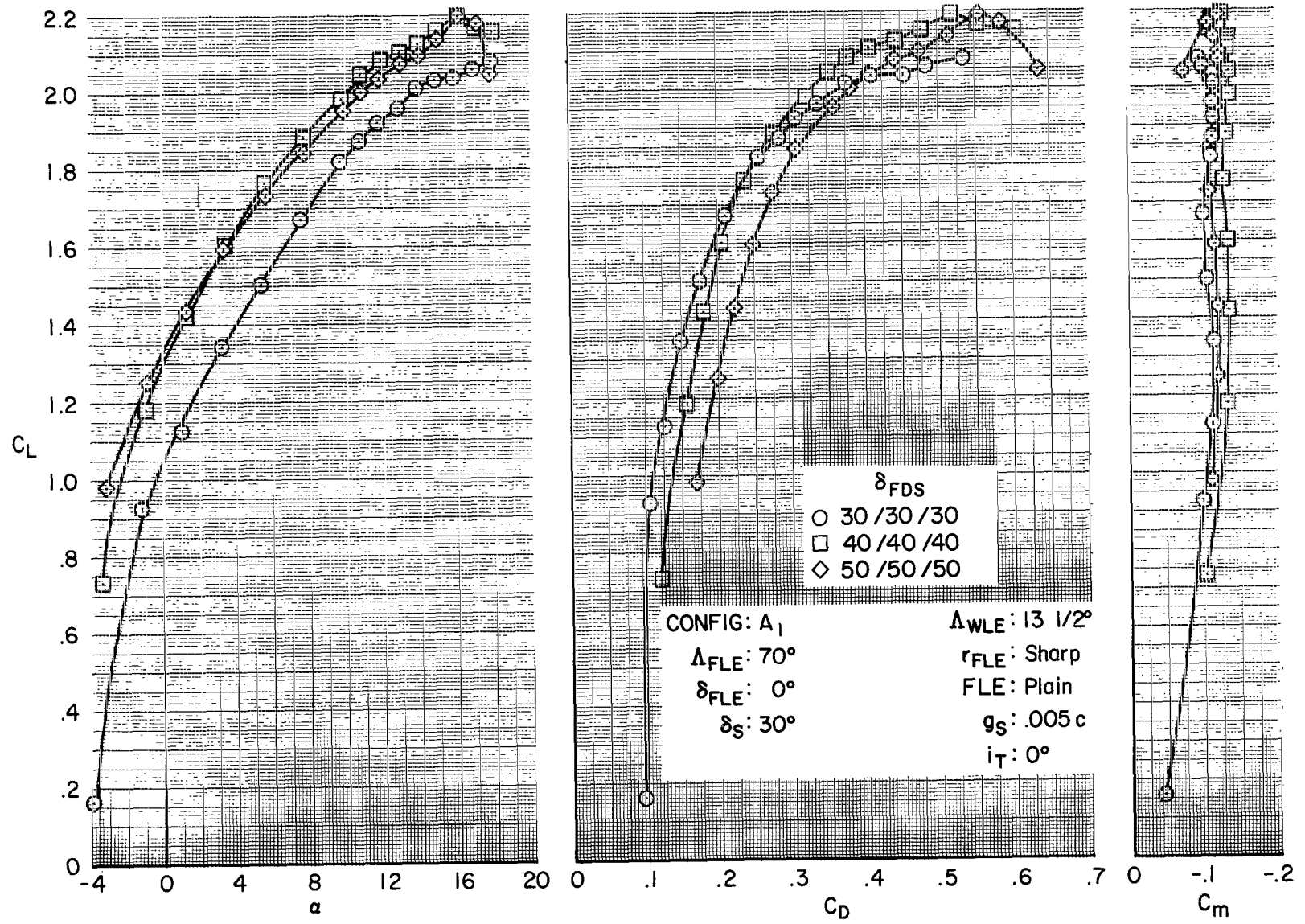

Figure 14.- Effect of double-slotted flap deflection at 13-1/2° sweep.

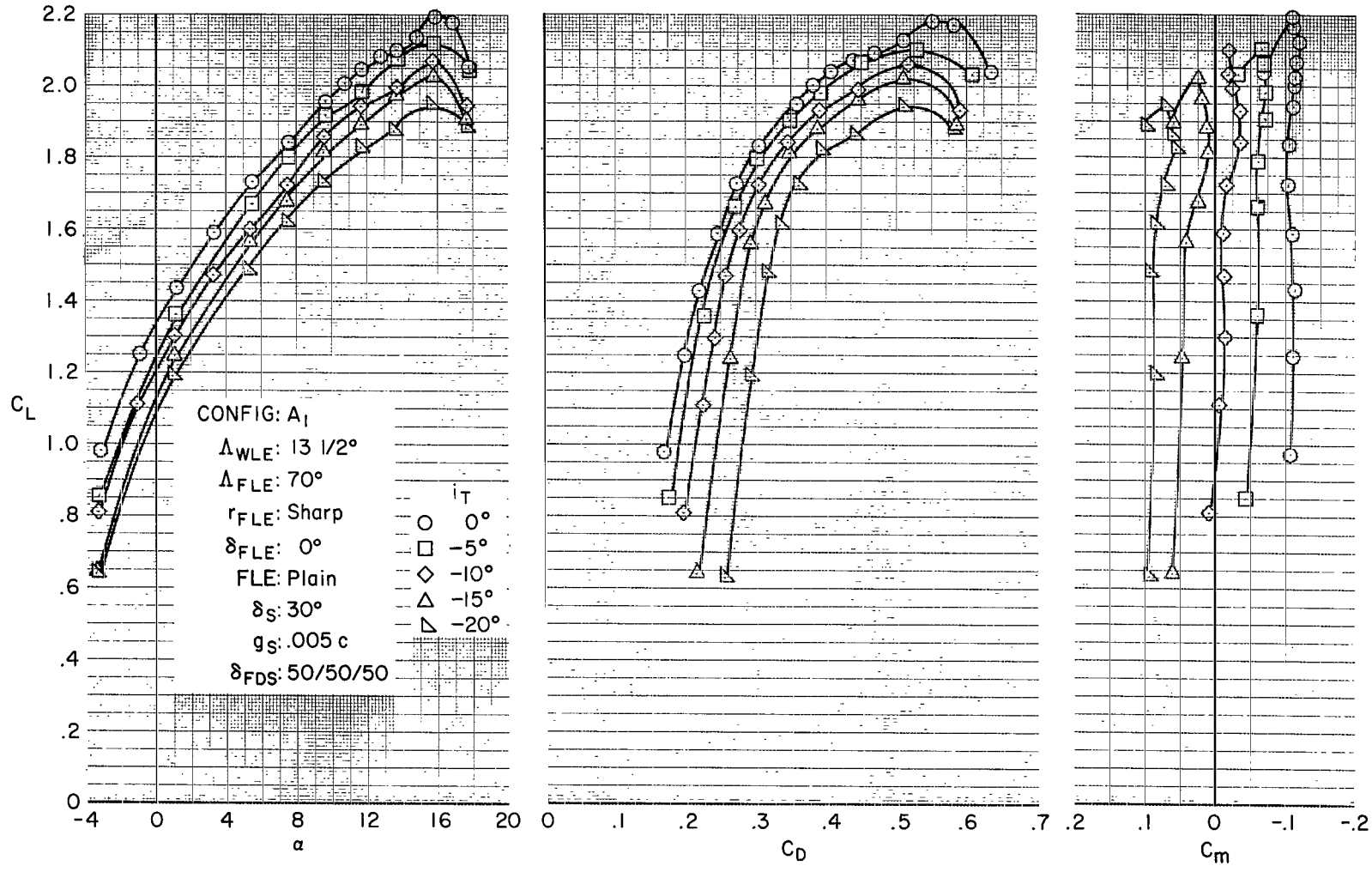

Figure 15.- Characteristics of 50° full-span double-slotted flaps at 13-1/2° sweep.

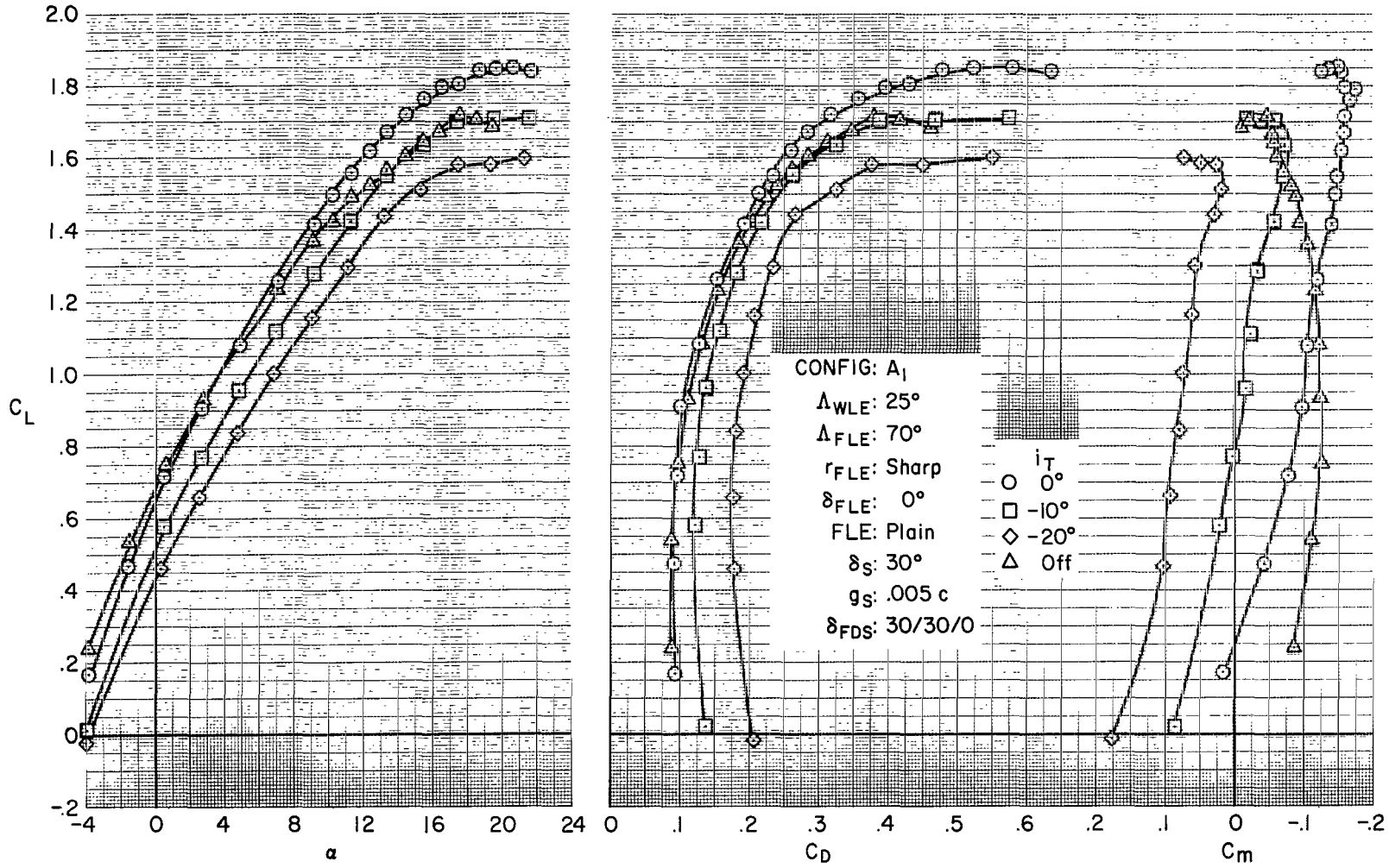

Figure 16.- Characteristics of 30° partial-span double-slotted flaps at 25° sweep.

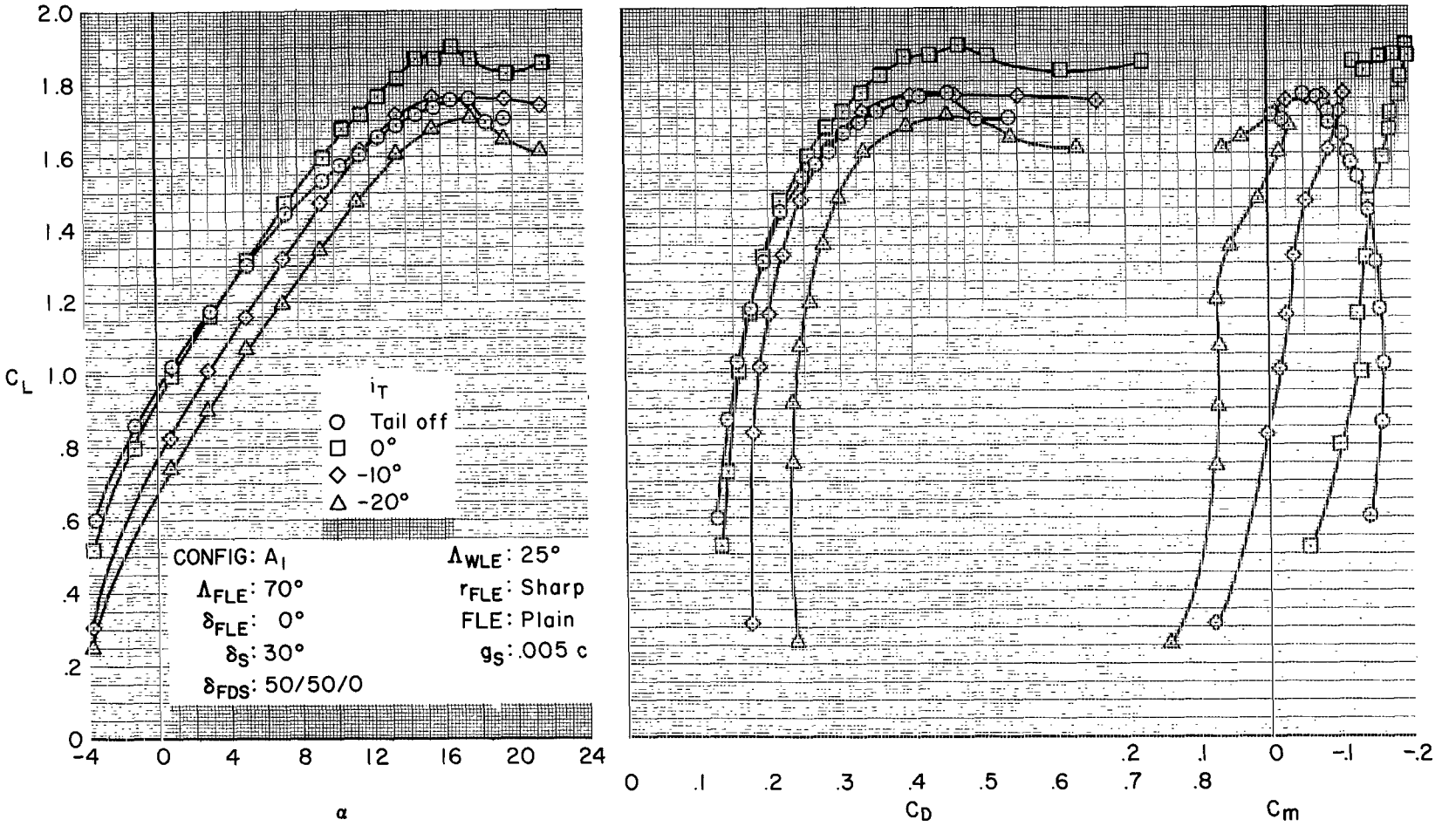

(a) Longitudinal characteristics with tail incidence.

Figure 17.- Characteristics of 50° partial-span double-slotted flaps at 25° sweep.

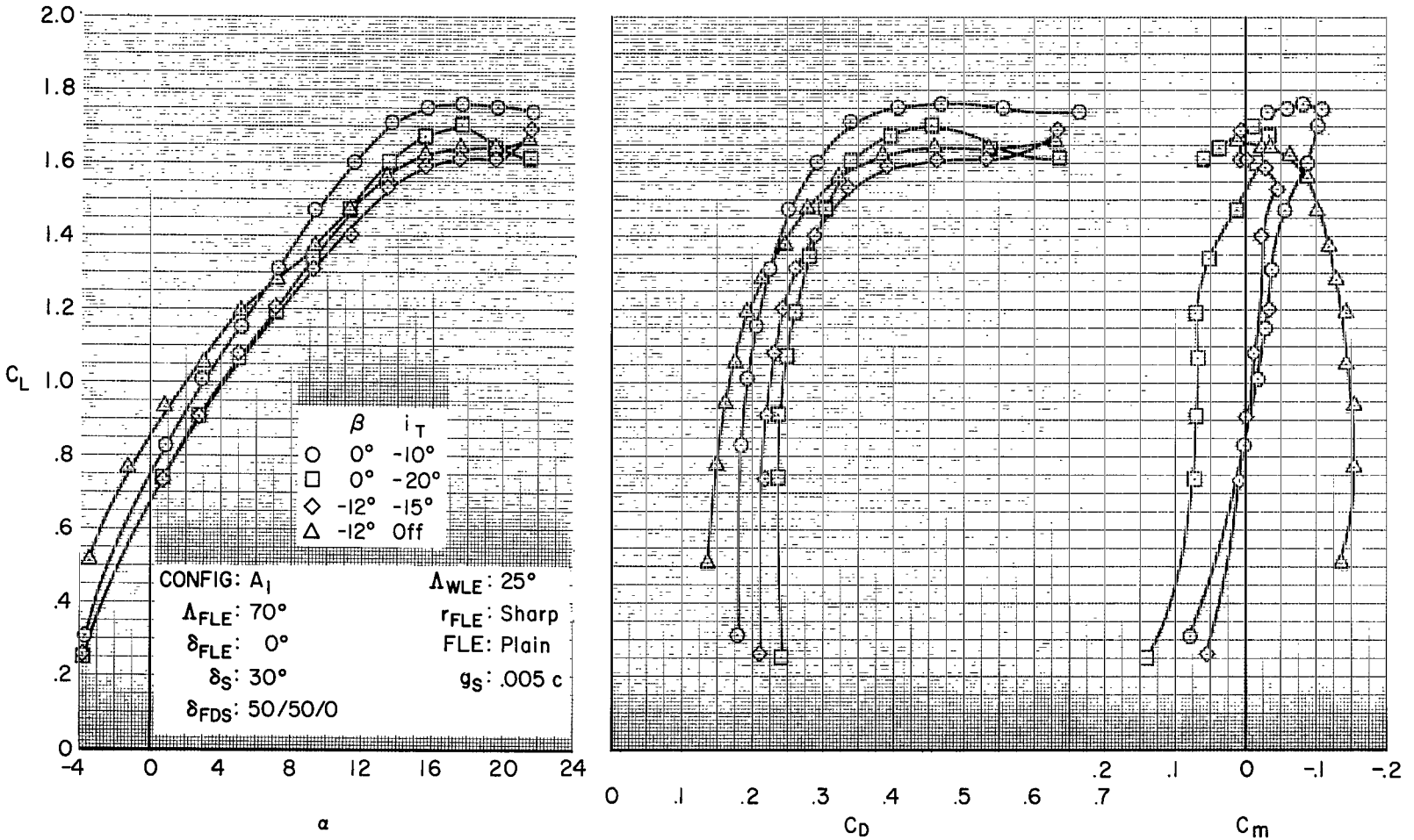

(b) Longitudinal characteristics at constant sideslip.

Figure 17.- Continued.

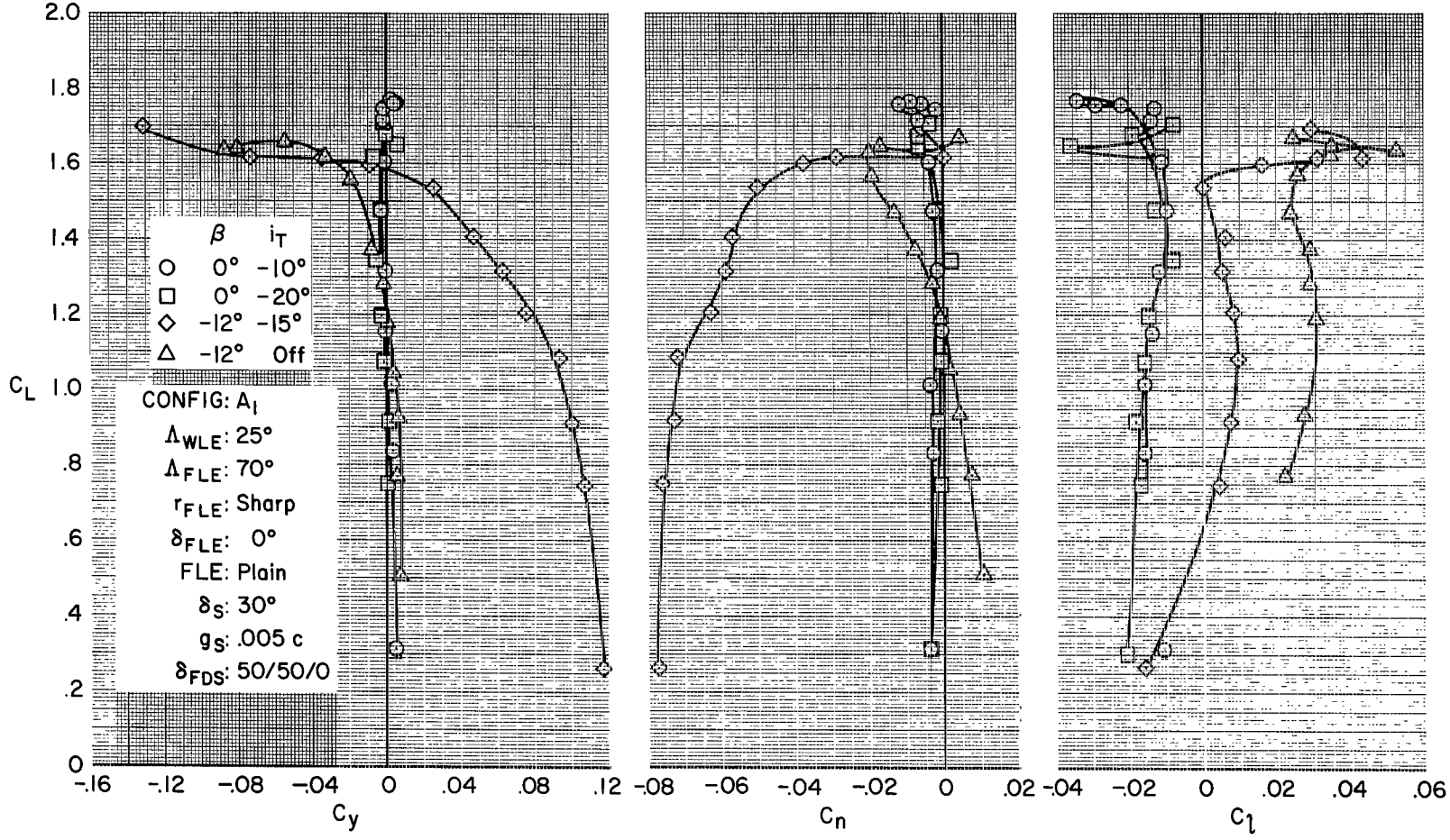

(c) Lateral characteristics at constant sideslip.

Figure 17.- Continued.

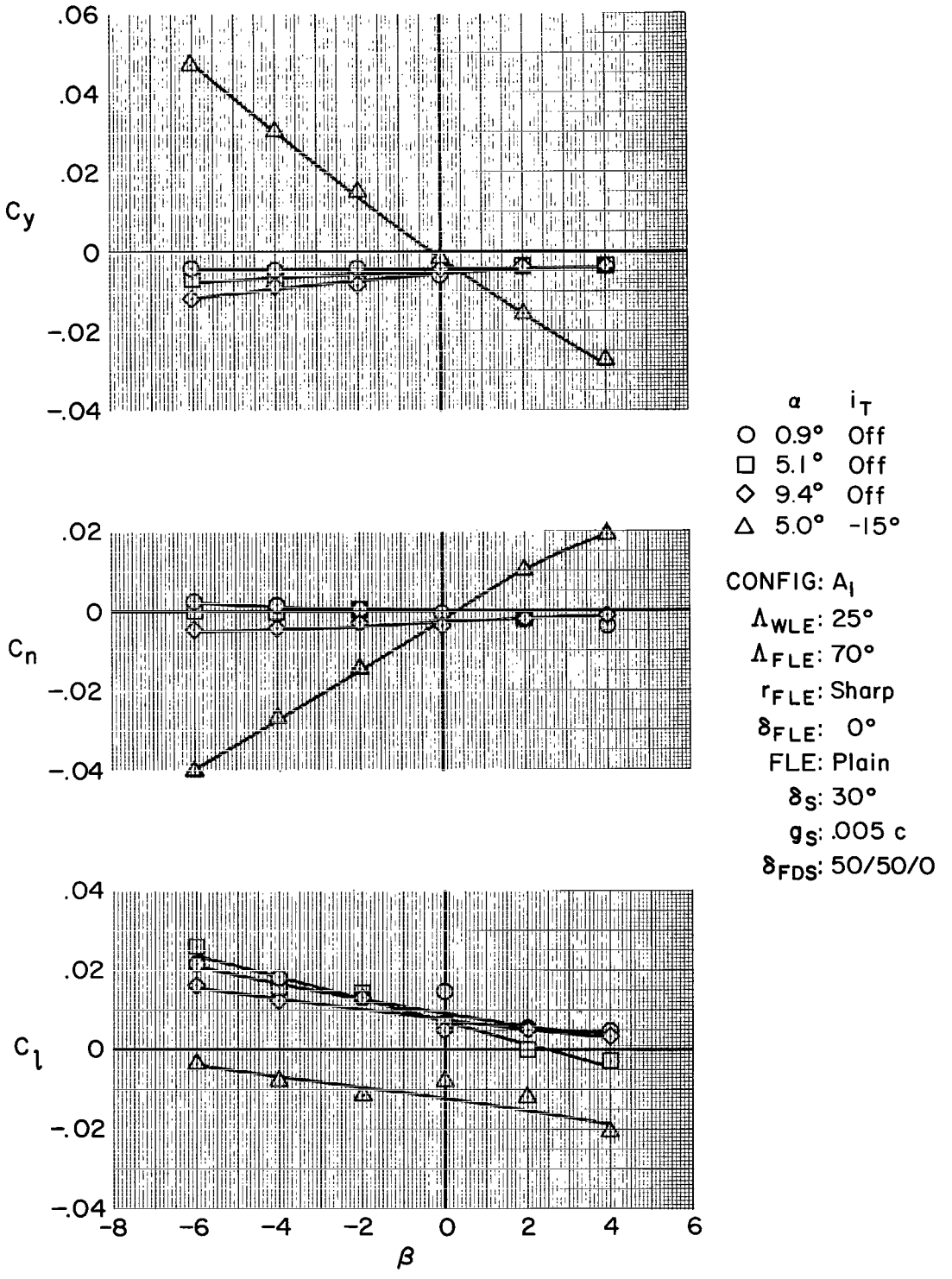

(d) Lateral characteristics at constant angle of attack.

Figure 17.- Concluded.

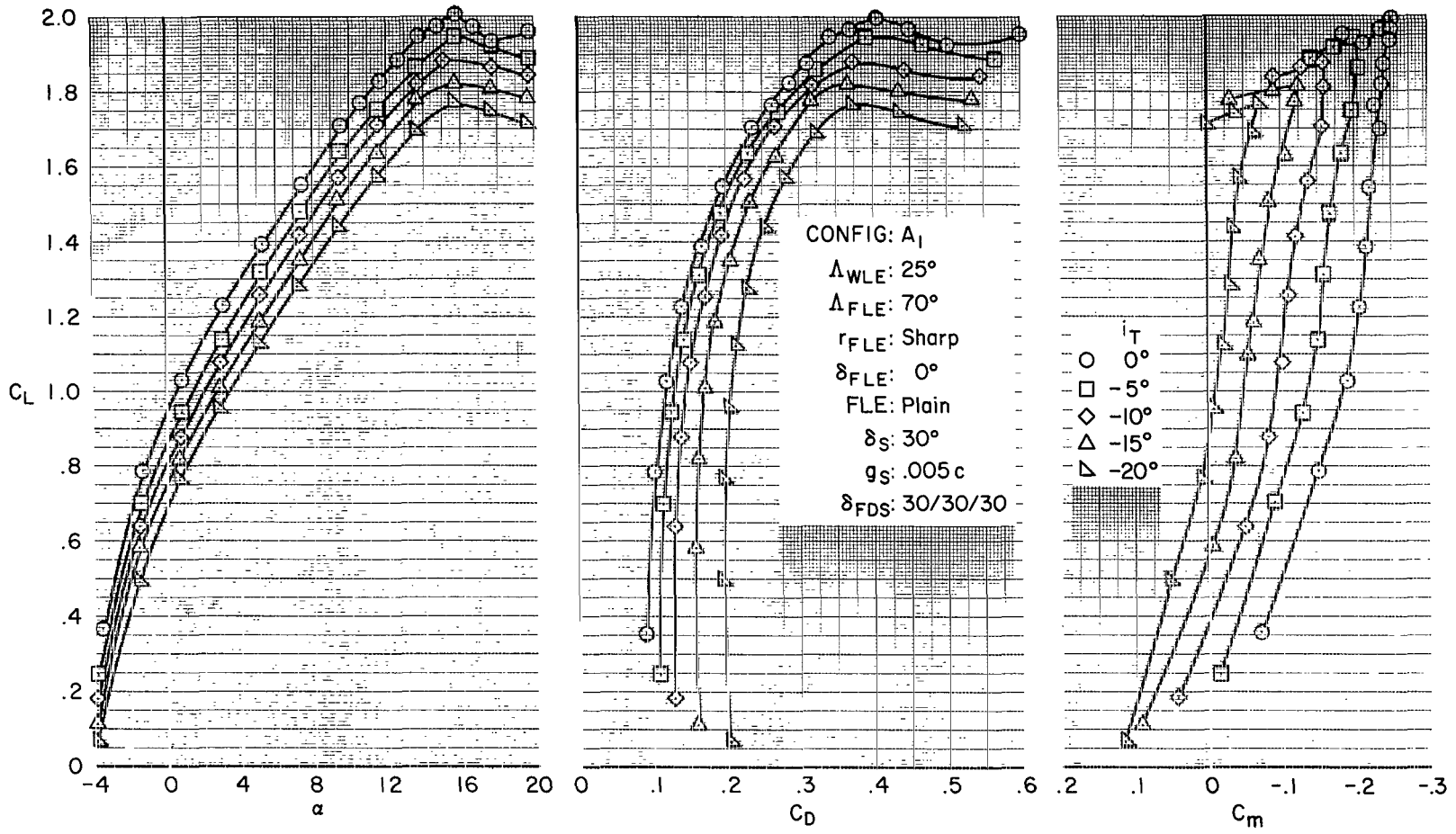

Figure 18.- Characteristics of 30° full-span double-slotted flaps at 25° sweep.

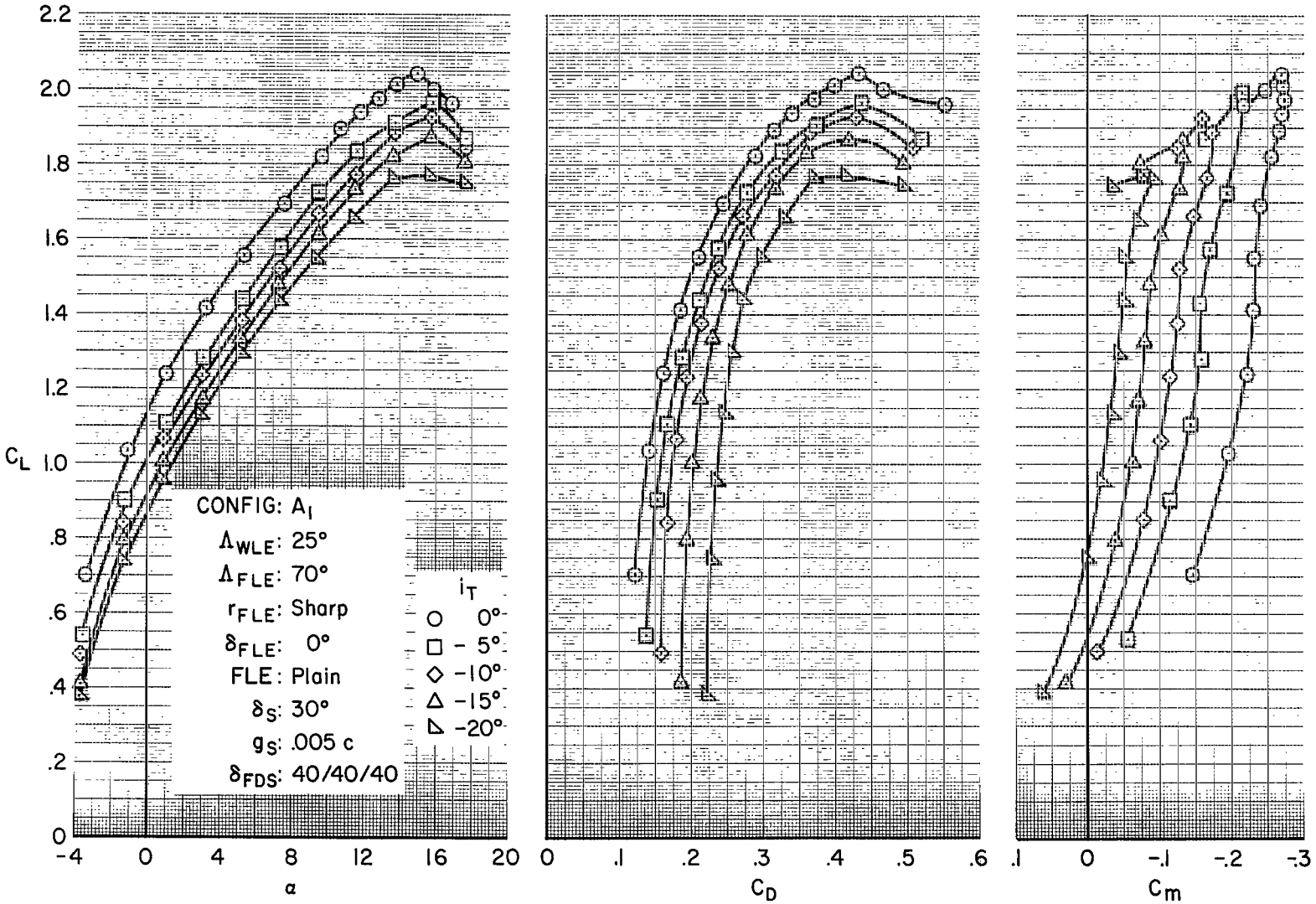

Figure 19.- Characteristics of 40° full-span double-slotted flaps at 25° sweep.

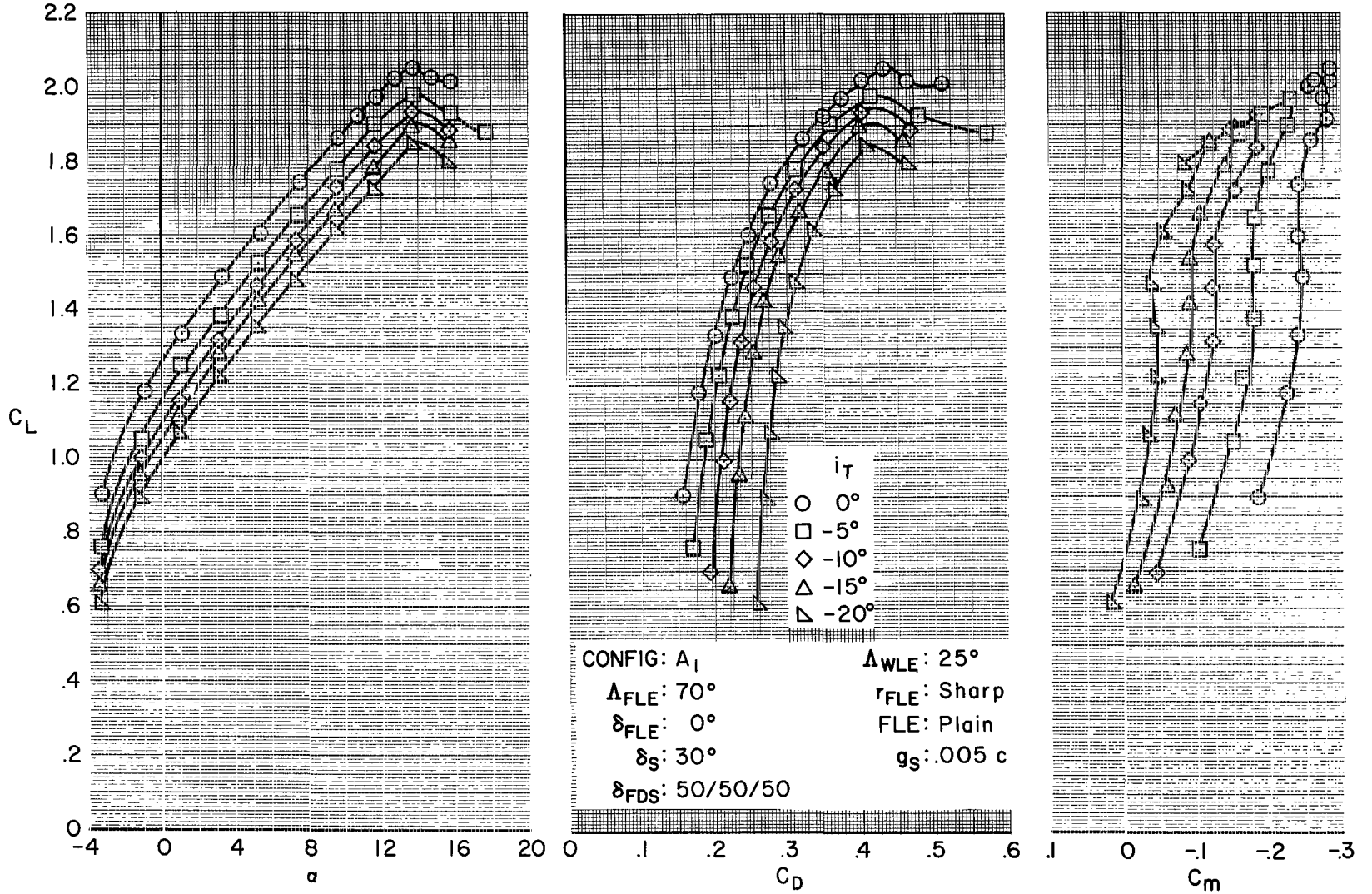

(a) Longitudinal characteristics with tail on.

Figure 20.- Characteristics of 50° full-span double-slotted flaps at 25° sweep.

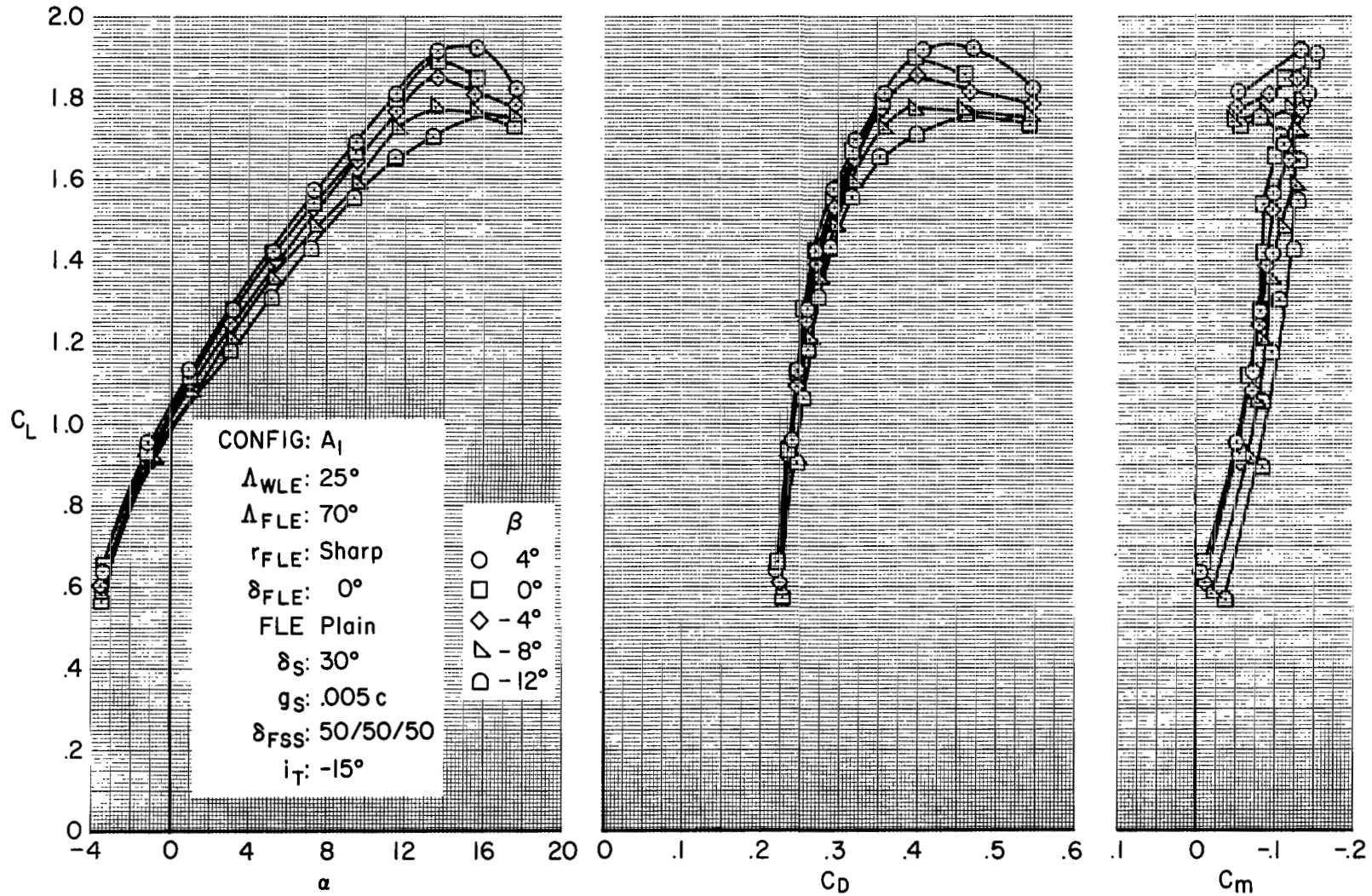

(b) Longitudinal characteristics at constant sideslip; tail on.

Figure 20.- Continued.

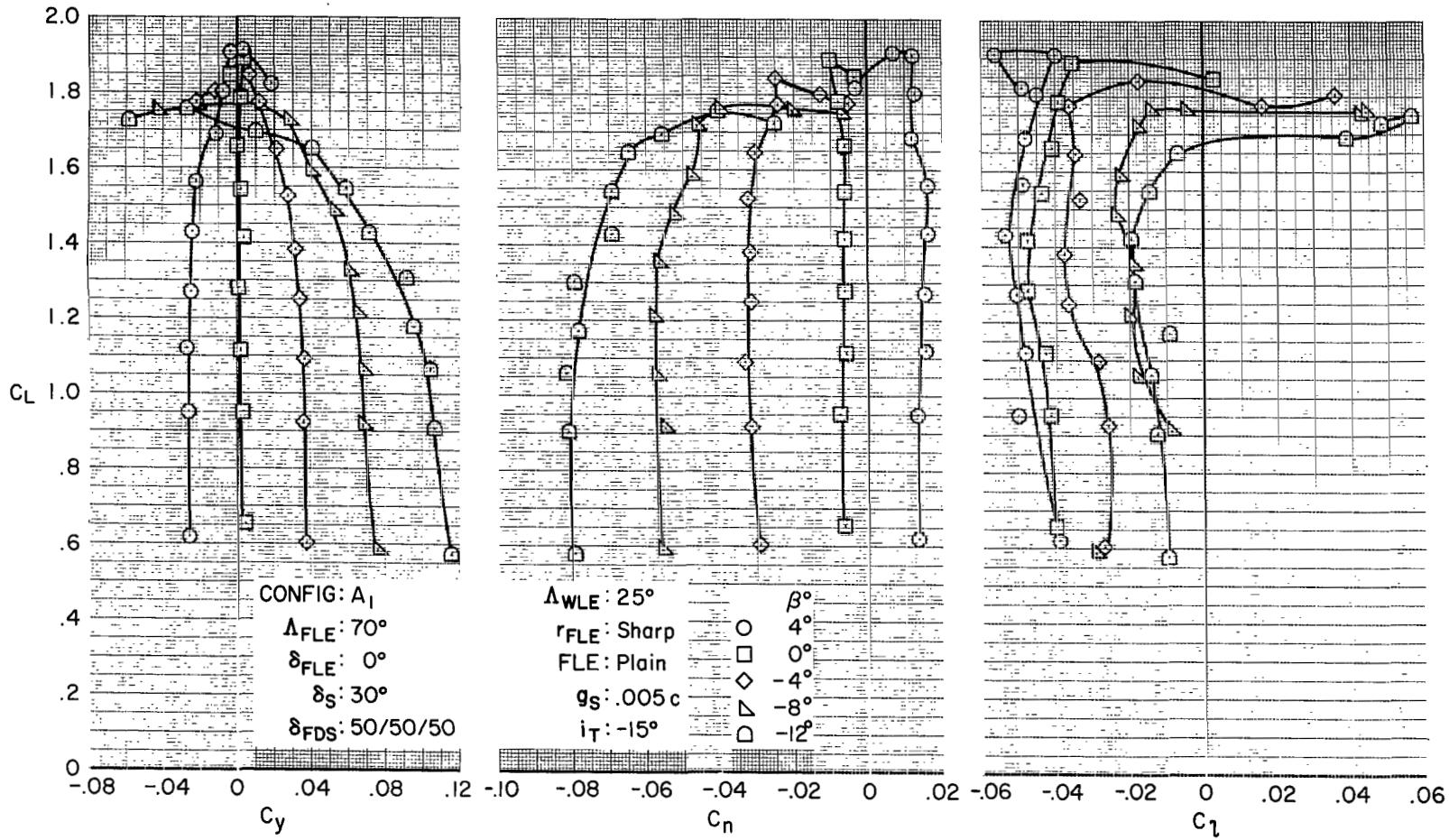

(c) Lateral characteristics at constant sideslip; tail on.

Figure 20.- Continued.

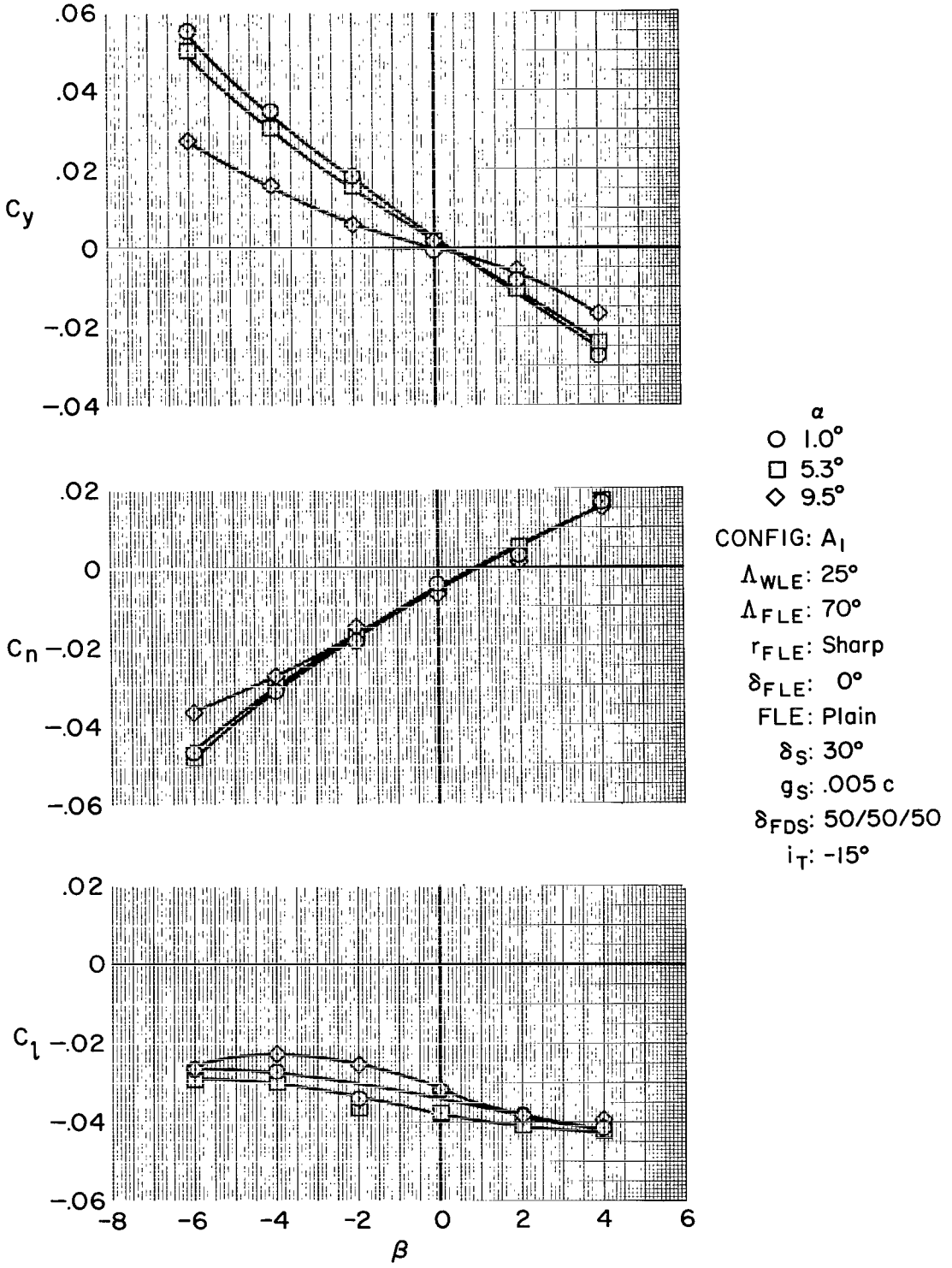

(d) Lateral characteristics at constant angle of attack; tail on.

Figure 20.- Continued.

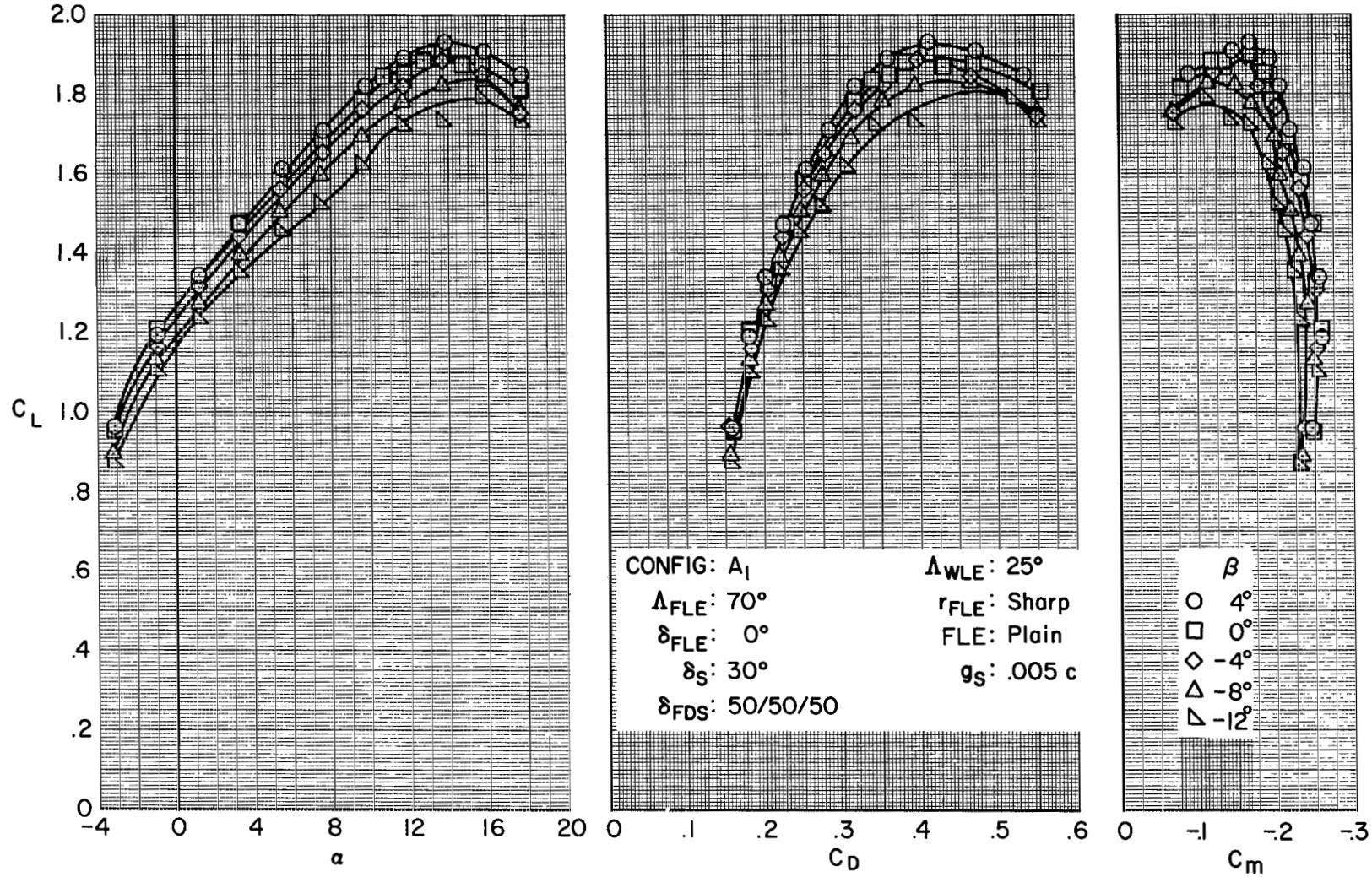

(e) Longitudinal characteristics at constant sideslip; tail off.

Figure 20.- Continued.

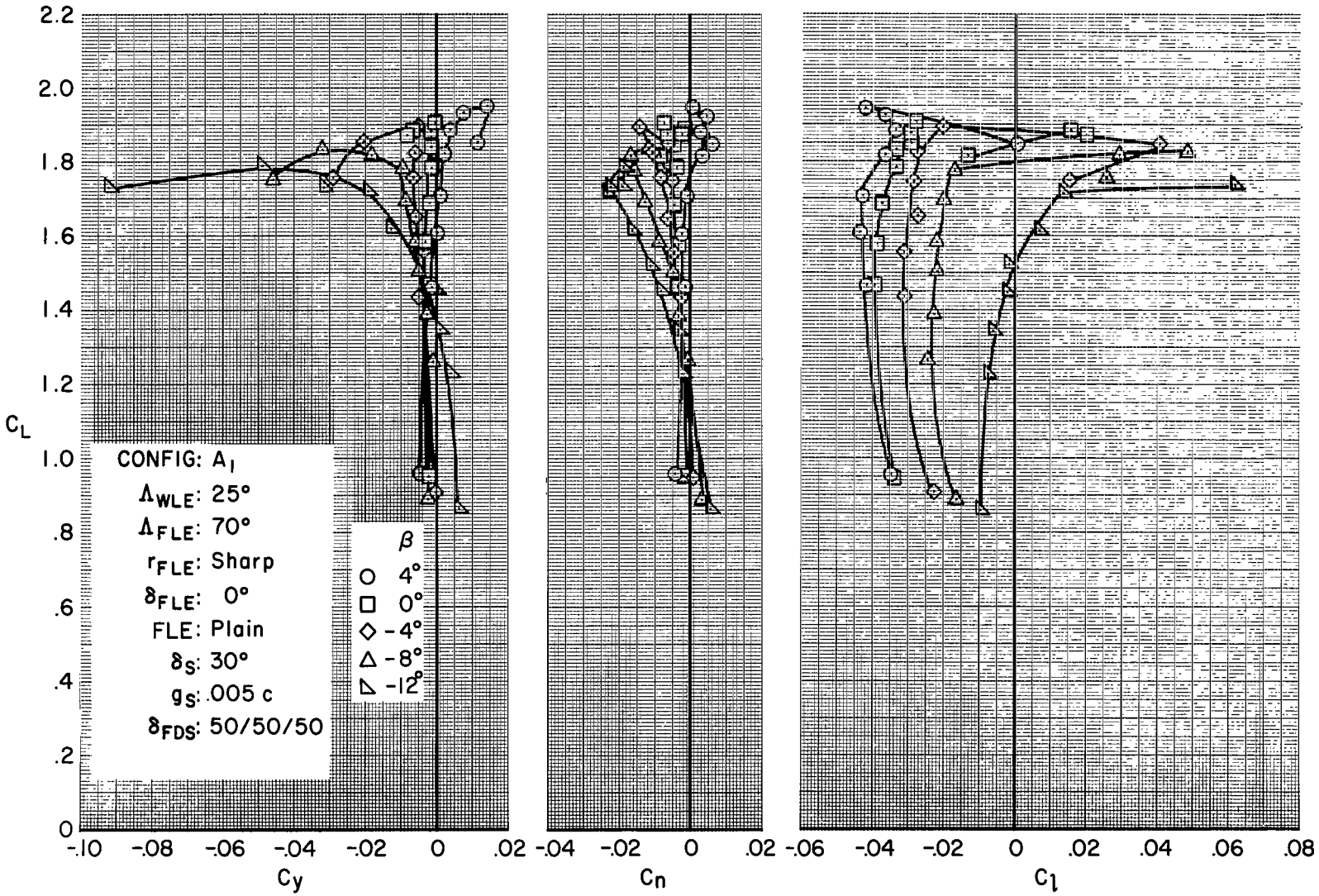

(f) Lateral characteristics at constant sideslip; tail off.

Figure 20.- Continued.

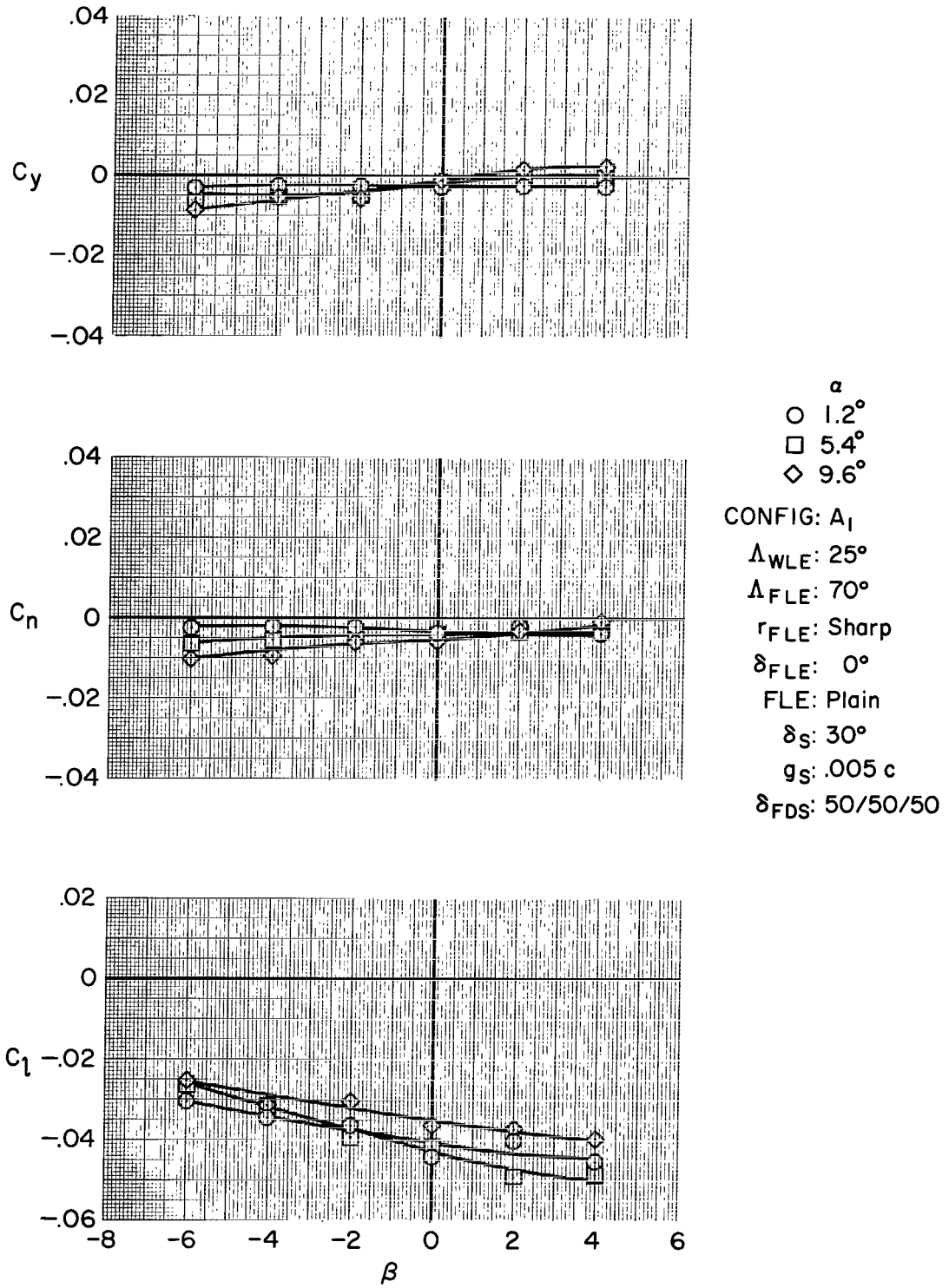

(g) Lateral characteristics at constant angle of attack; tail off.

Figure 20.- Concluded.

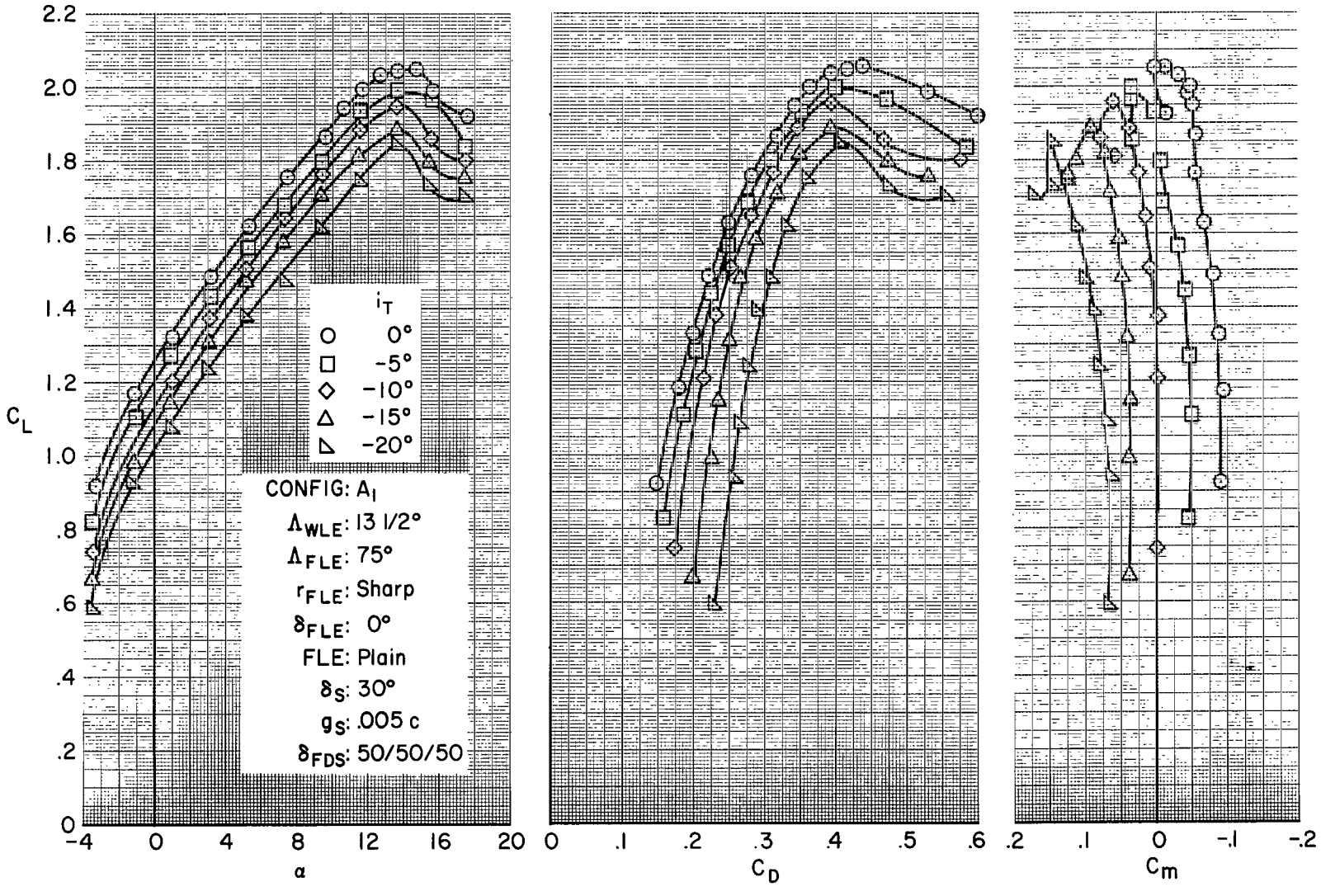

(a) Longitudinal characteristics with tail incidence.

Figure 21.- Characteristics of 50° full-span double-slotted flaps at 13-1/2° sweep and 75° fixed-wing sweep.

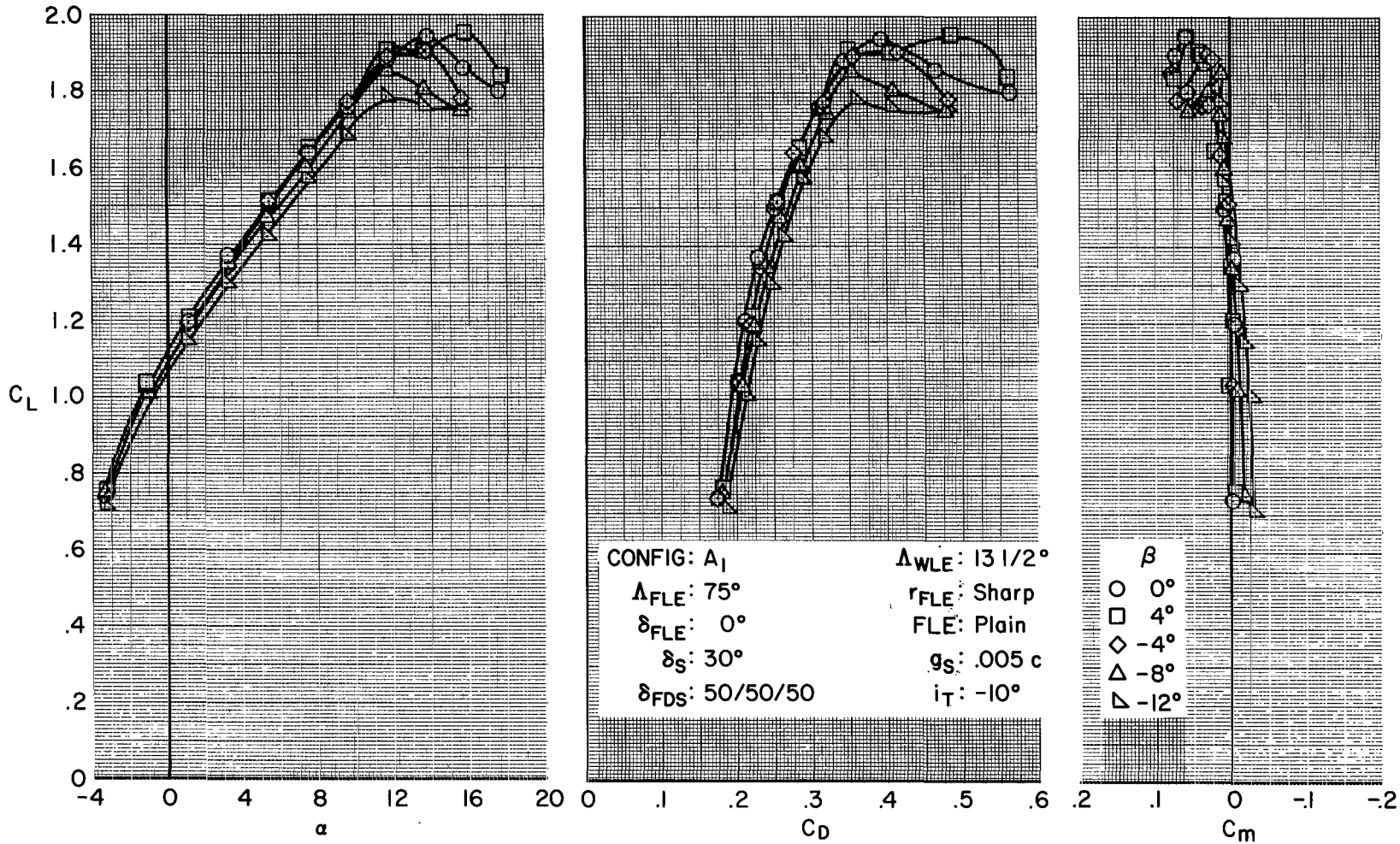

(b) Longitudinal characteristics at constant sideslip.

Figure 21.- Continued.

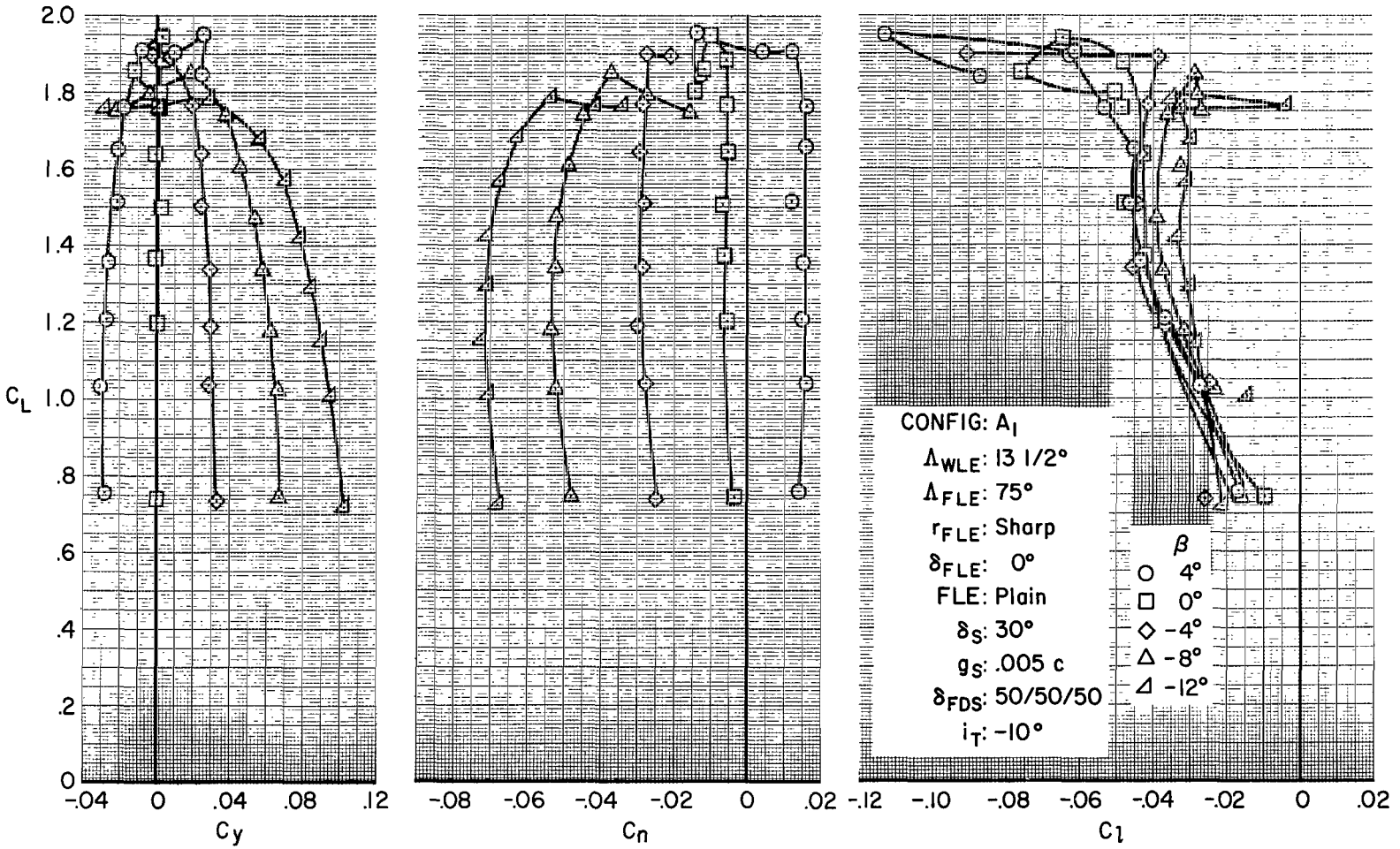

(c) Lateral characteristics at constant sideslip.

Figure 21.- Continued.

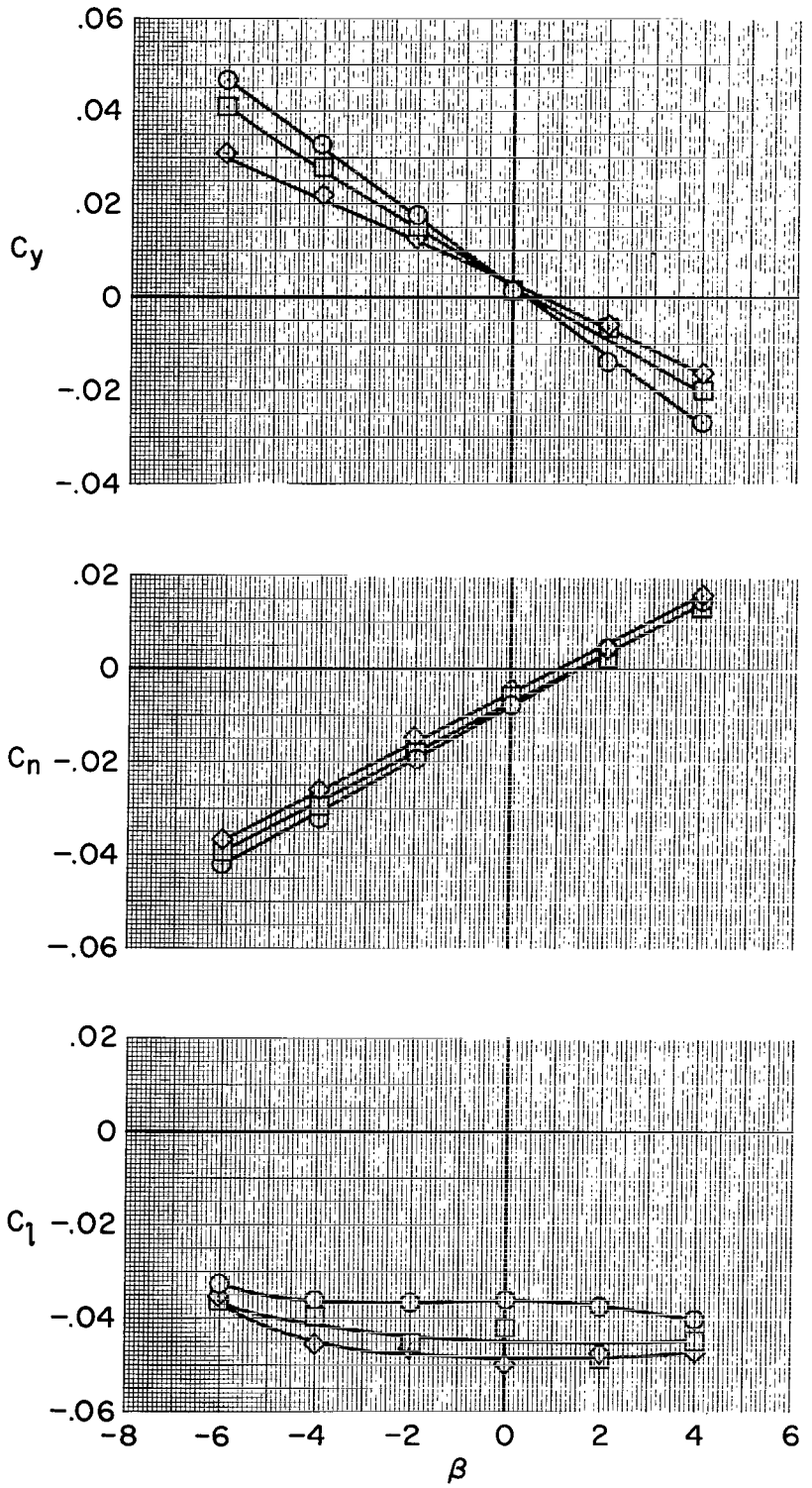

(d) Lateral characteristics at constant angle of attack.

Figure 21.- Concluded.

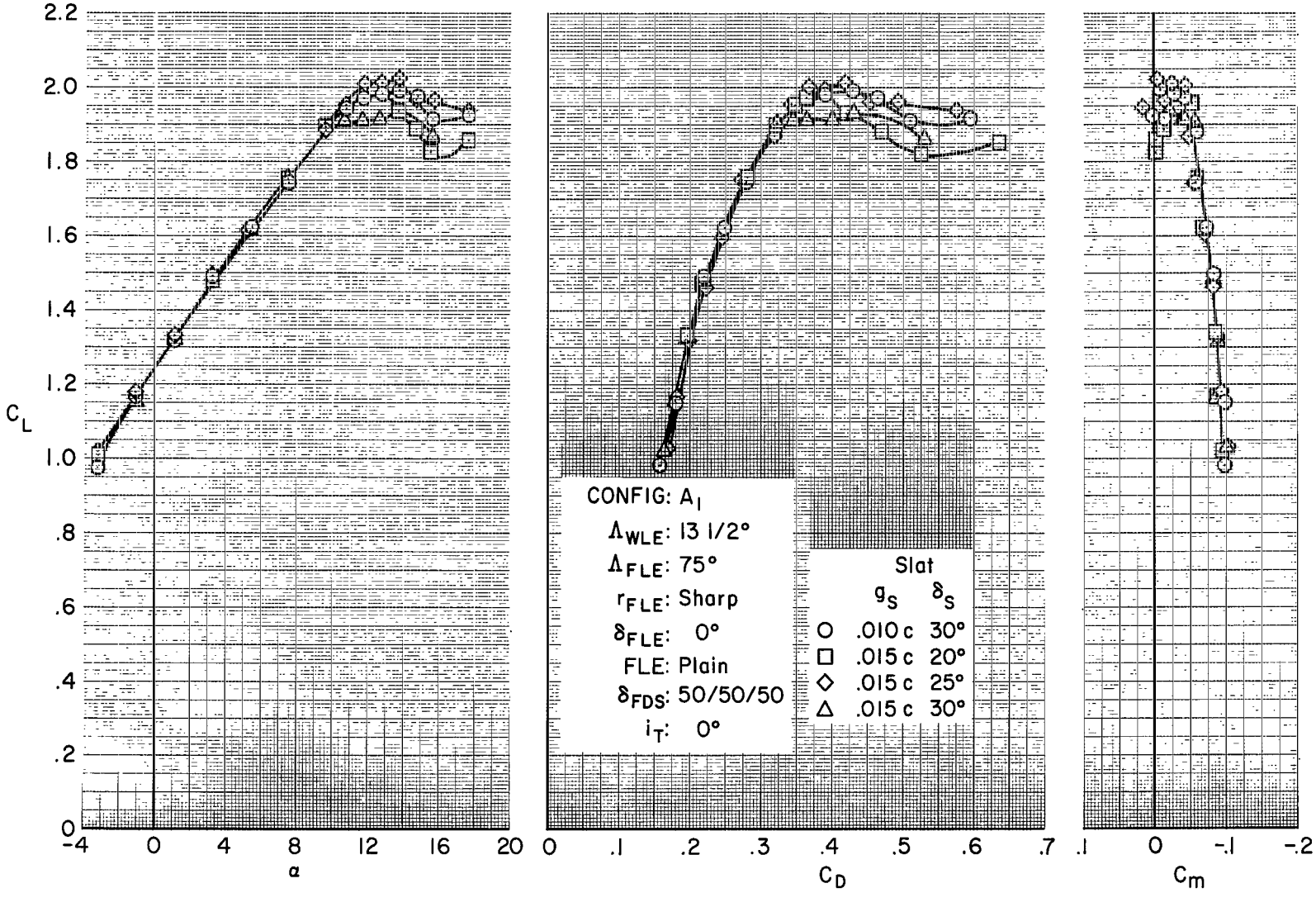

(a) Longitudinal characteristics for various slat positions.

Figure 22.- Leading-edge slat effects at 13-1/2° sweep with double-slotted flaps at 50° full-span.

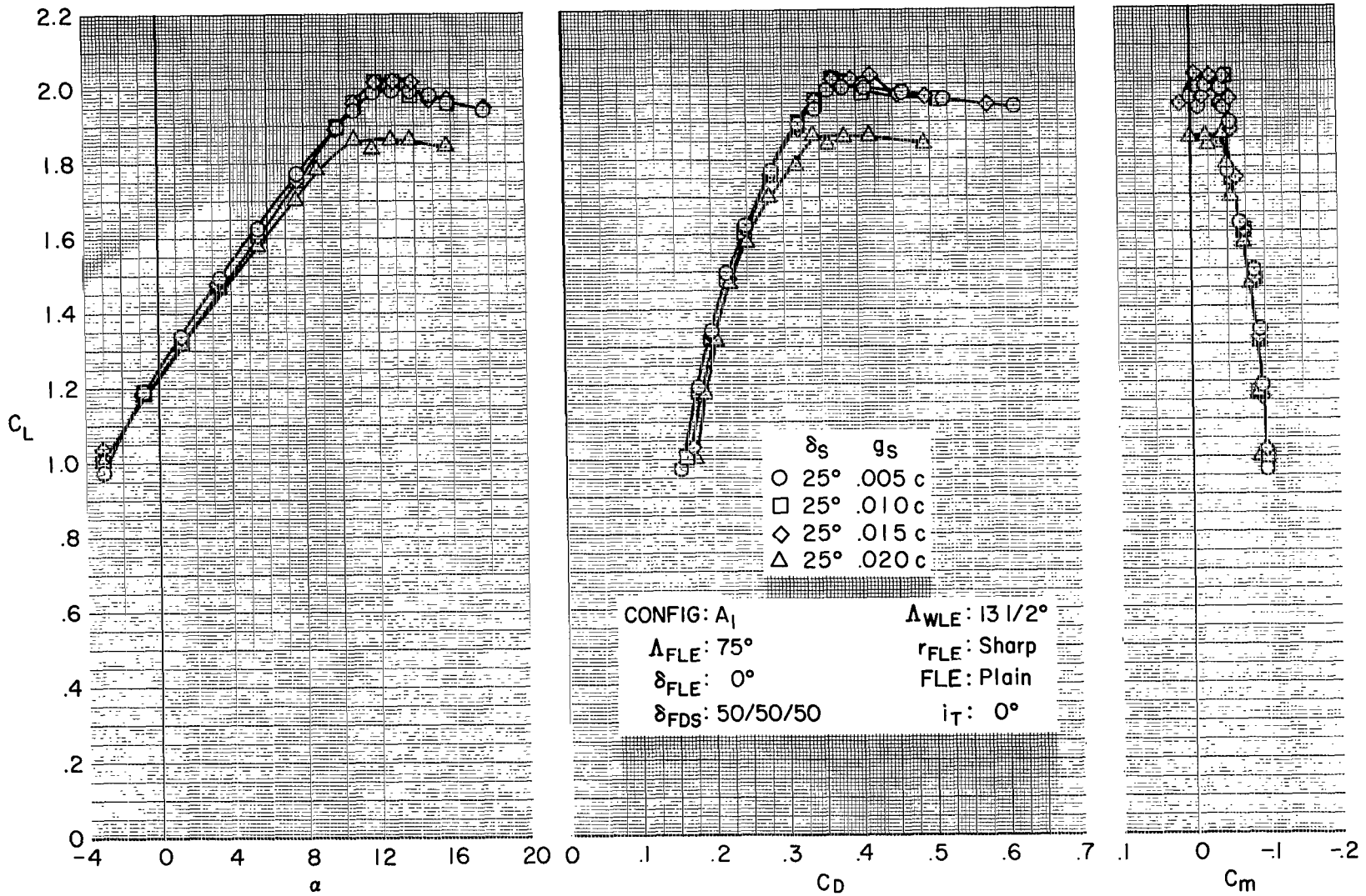

(b) Longitudinal characteristics for various slat gaps at constant deflection.

Figure 22.- Continued.

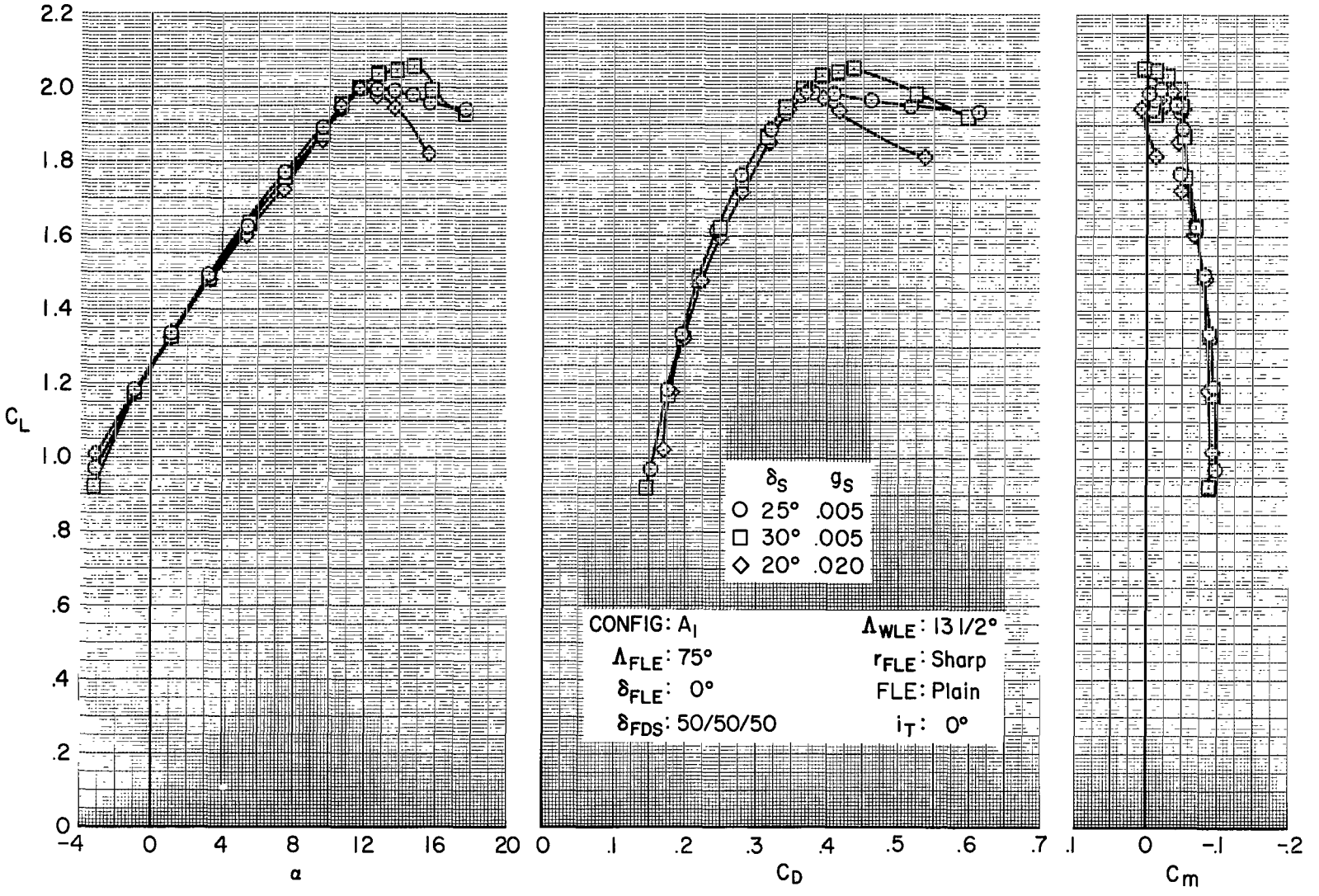

(c) Longitudinal characteristics for various slat positions.

Figure 22.- Concluded.

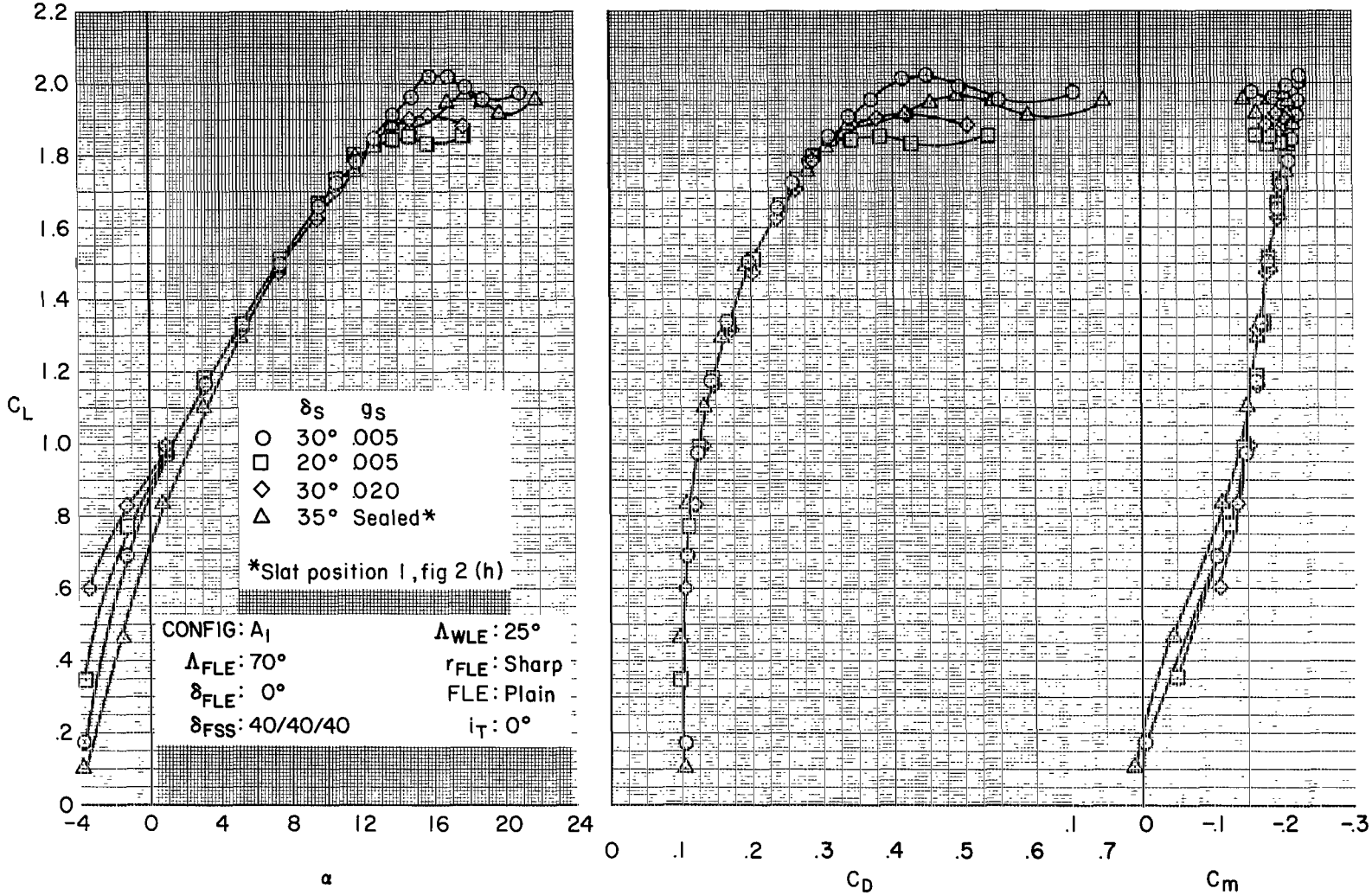

(a) Effect of slat geometry with 40° full-span flaps.

Figure 23.- Leading-edge slat effects at 25° sweep with single-slotted flaps.

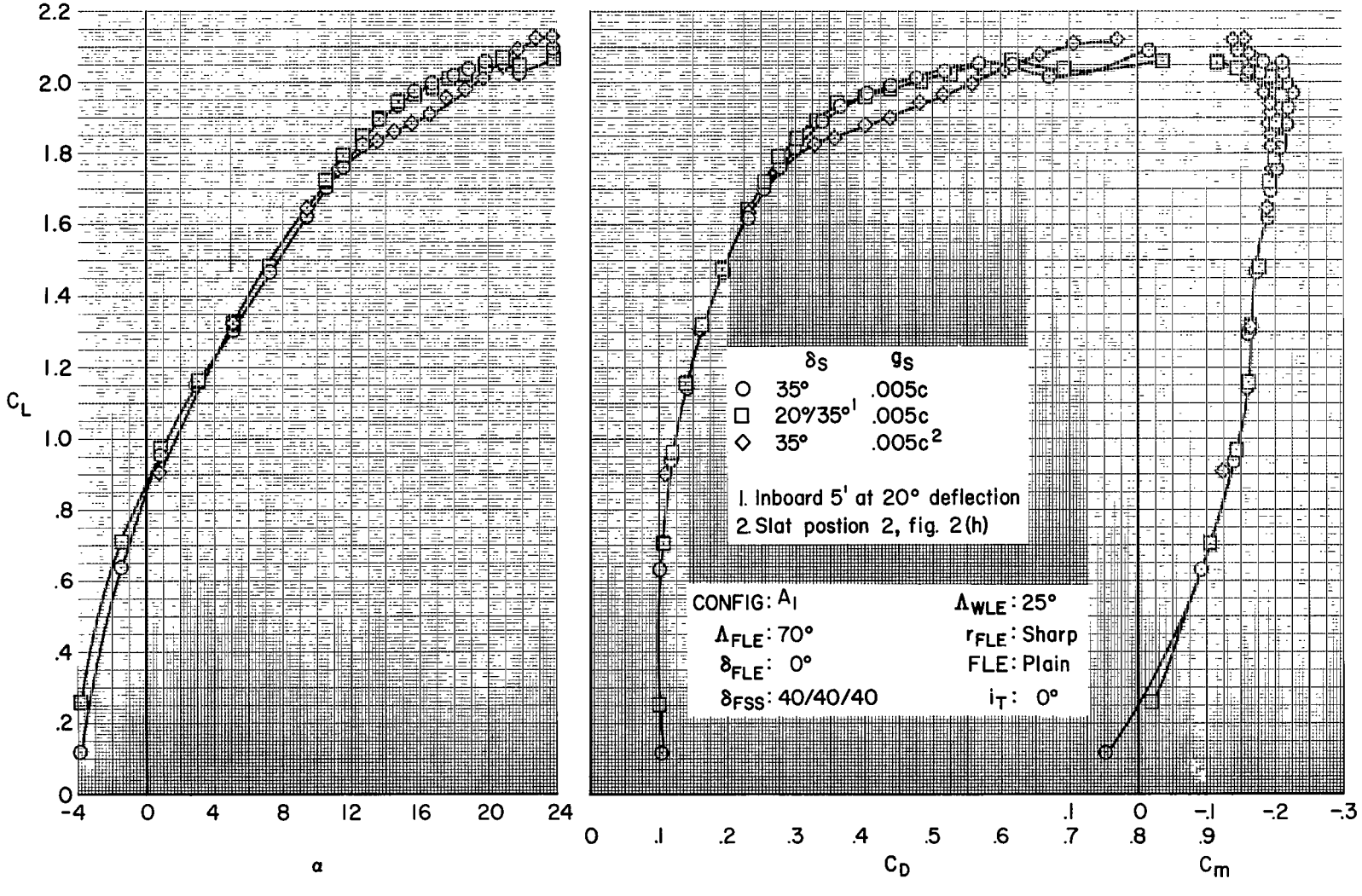

(b) Effect of slat geometry alterations with 40° full-span flaps.

Figure 23.- Continued.

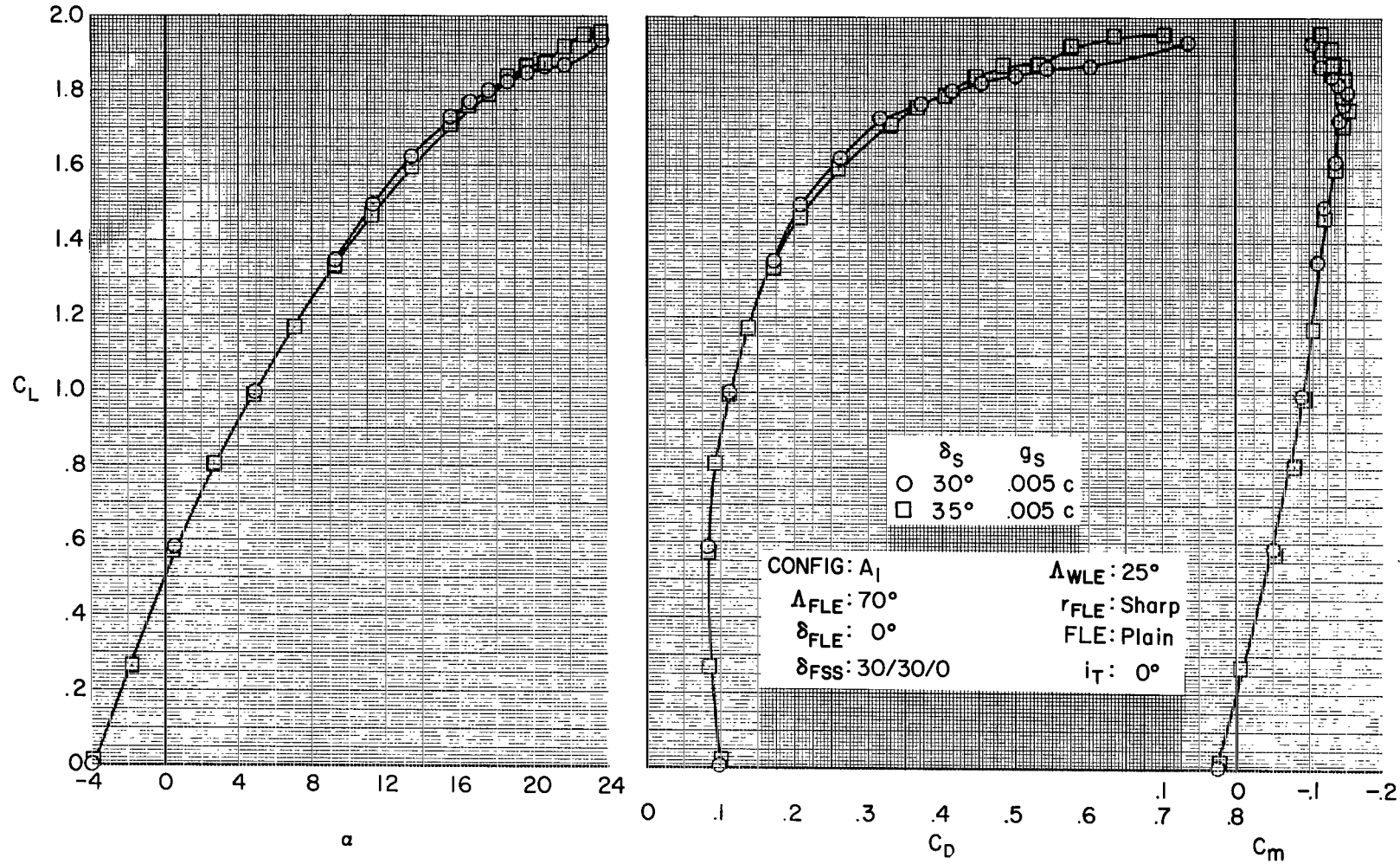

(c) Effect of slat deflections with 30° partial-span flaps.

Figure 23.- Concluded.

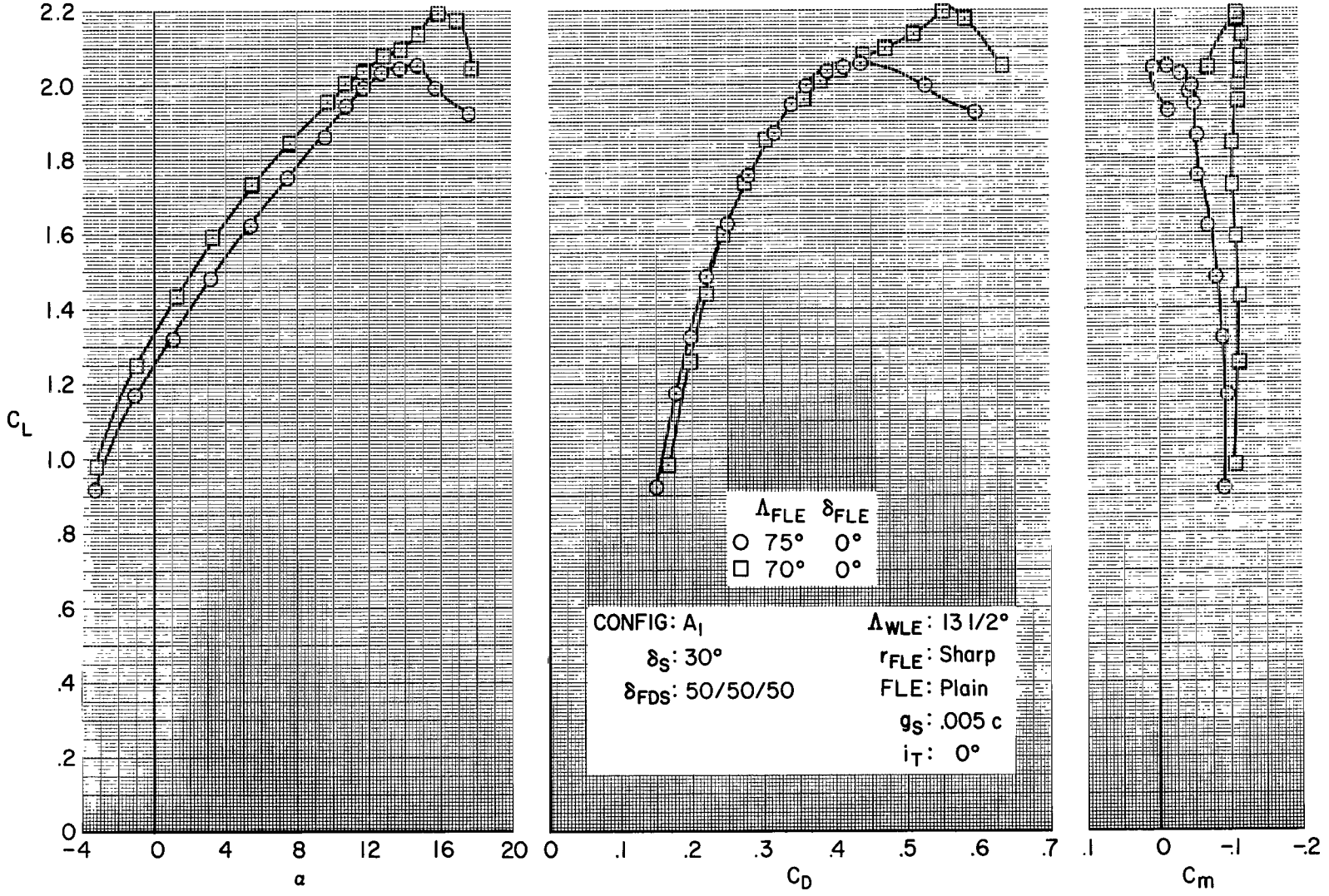

Figure 24.- Effect of fixed-wing leading-edge sweep with movable wing at 13-1/2° sweep.

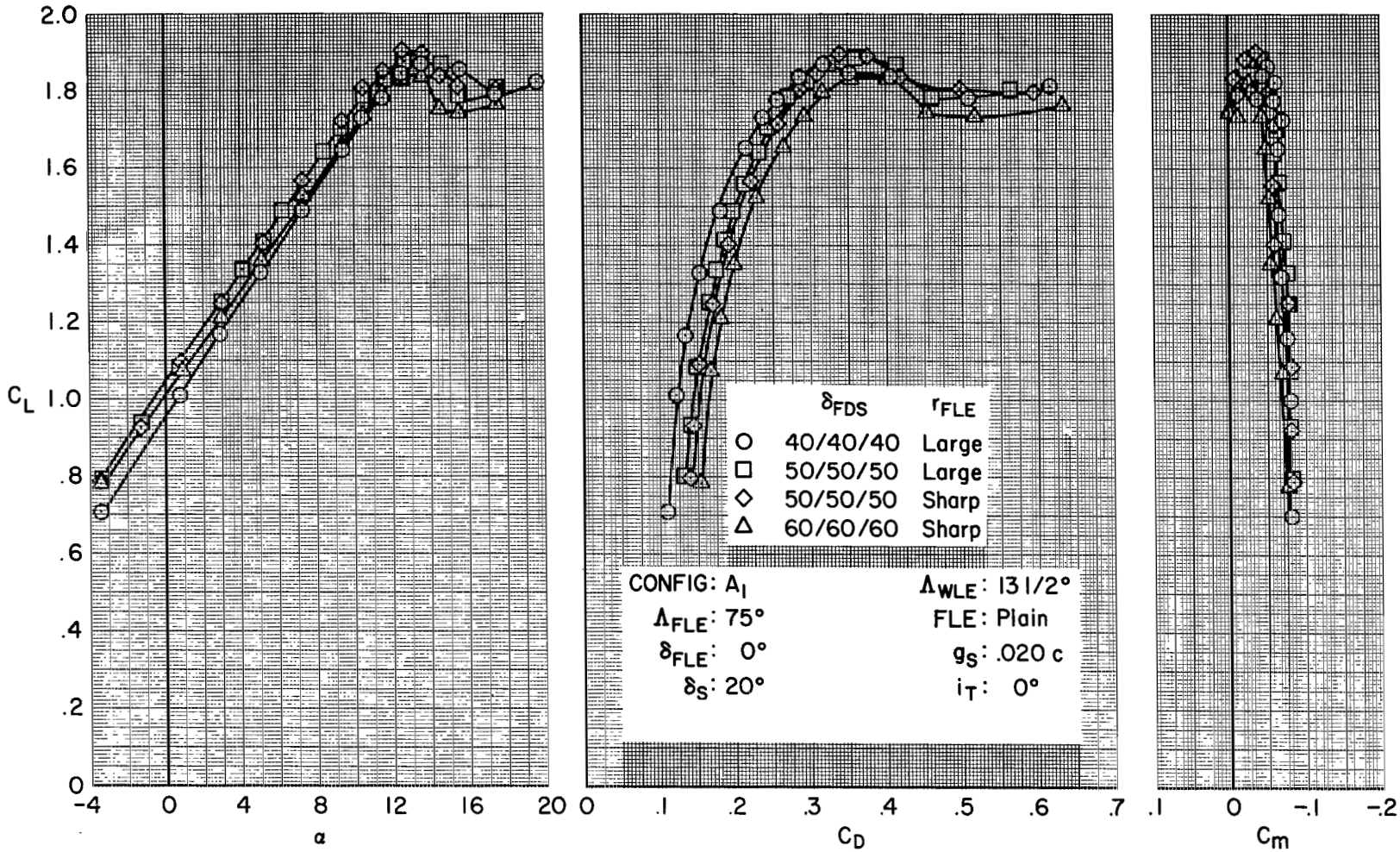

Figure 25.- Effect of fixed-wing leading-edge radius, with movable wing at 13-1/2° sweep, unmodified flap slot.

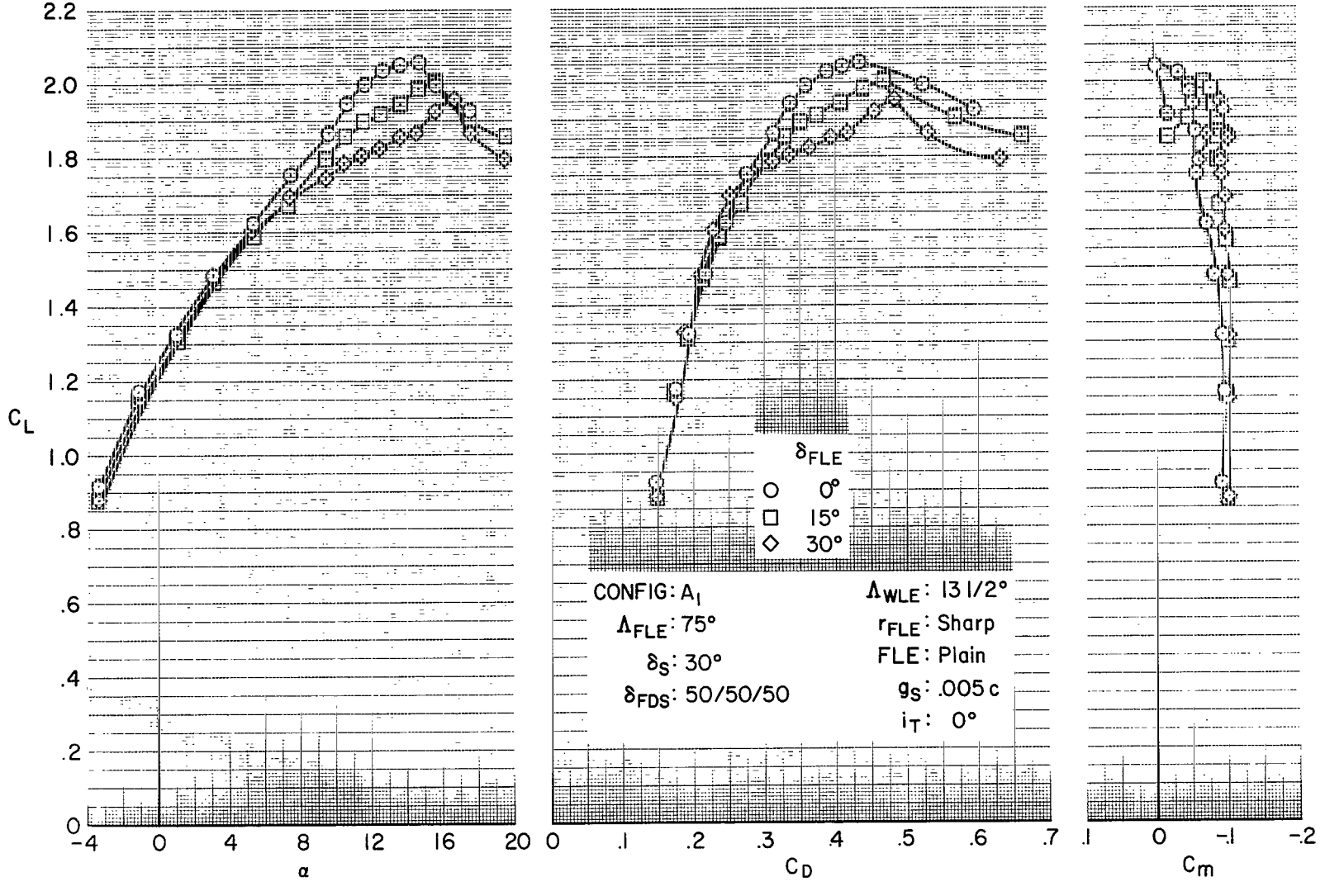

Figure 26.- Effect of fixed-wing leading-edge flap deflection, with 50° double-slotted trailing-edge flaps, 13-1/2° wing sweep.

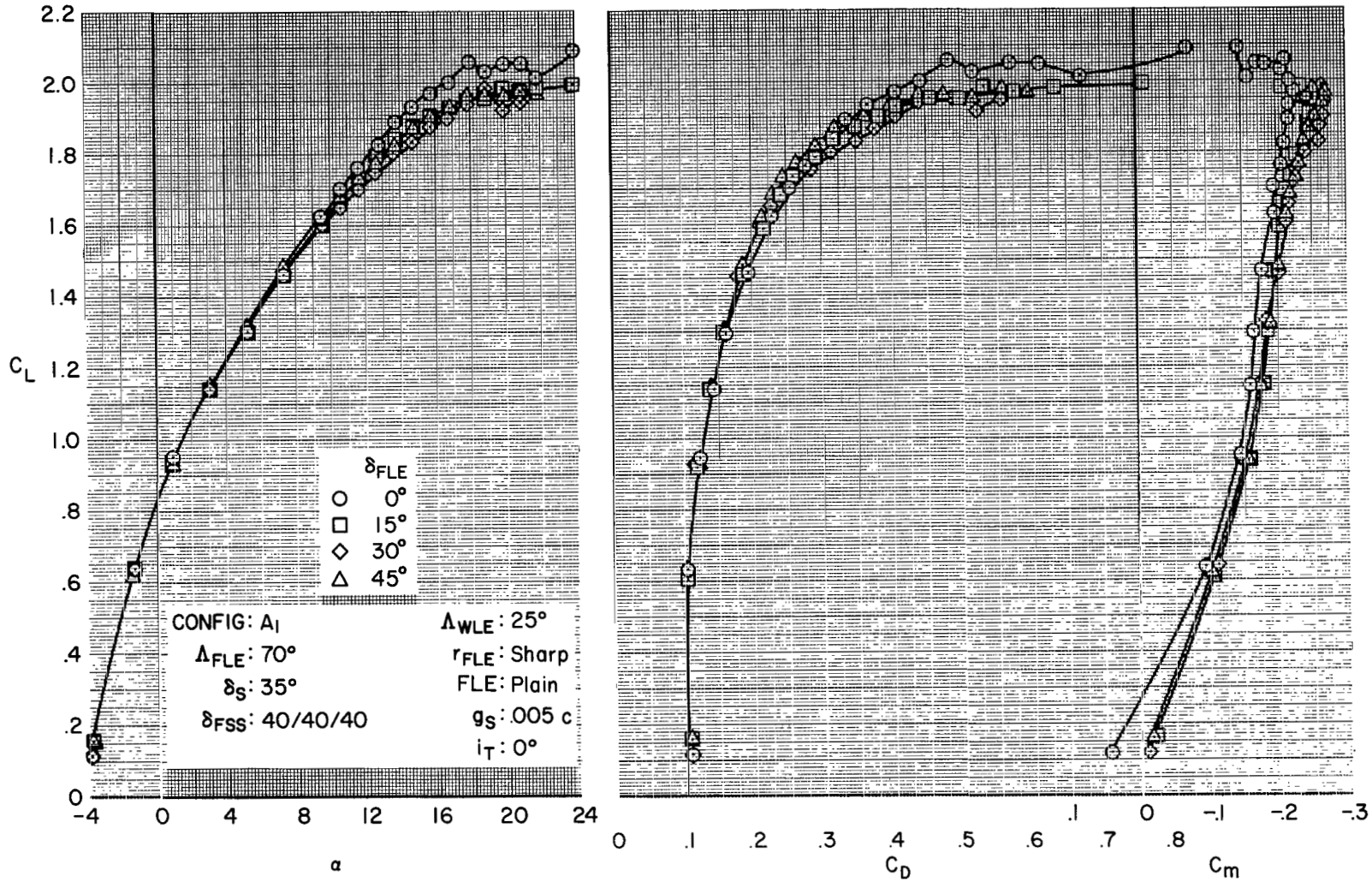

Figure 27.- Effect of fixed-wing leading-edge plain flap deflection, at 25° wing sweep and 70° fixed-wing sweep.

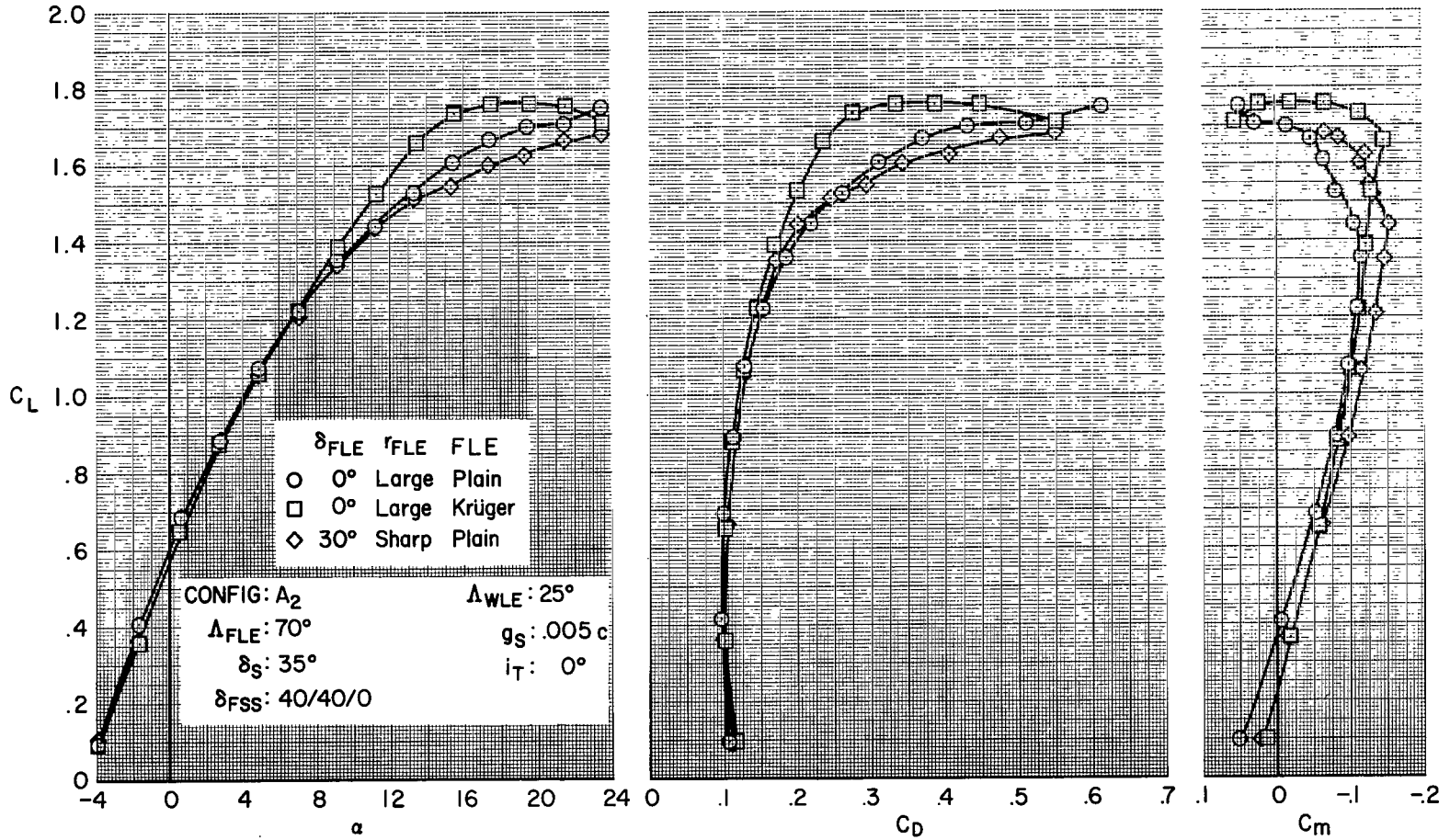

Figure 28.- Effect of fixed-wing leading-edge radius and Krüger flap, 40° partial-span flaps, 25° wing sweep.

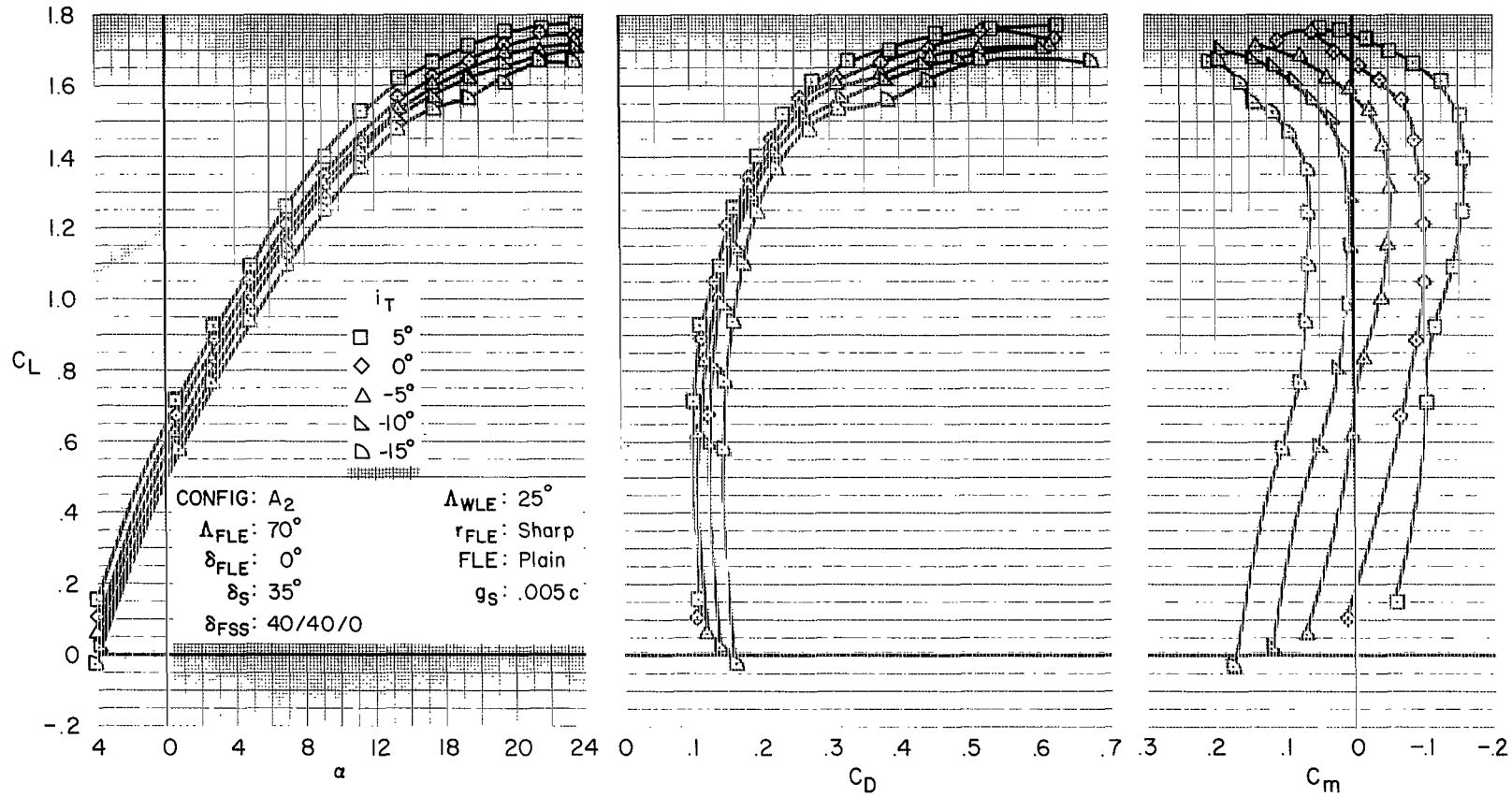

(a) Small horizontal tail.

Figure 29.- Effect of horizontal-tail size on longitudinal characteristics at 25° wing sweep, 40° partial-span single-slotted flaps.

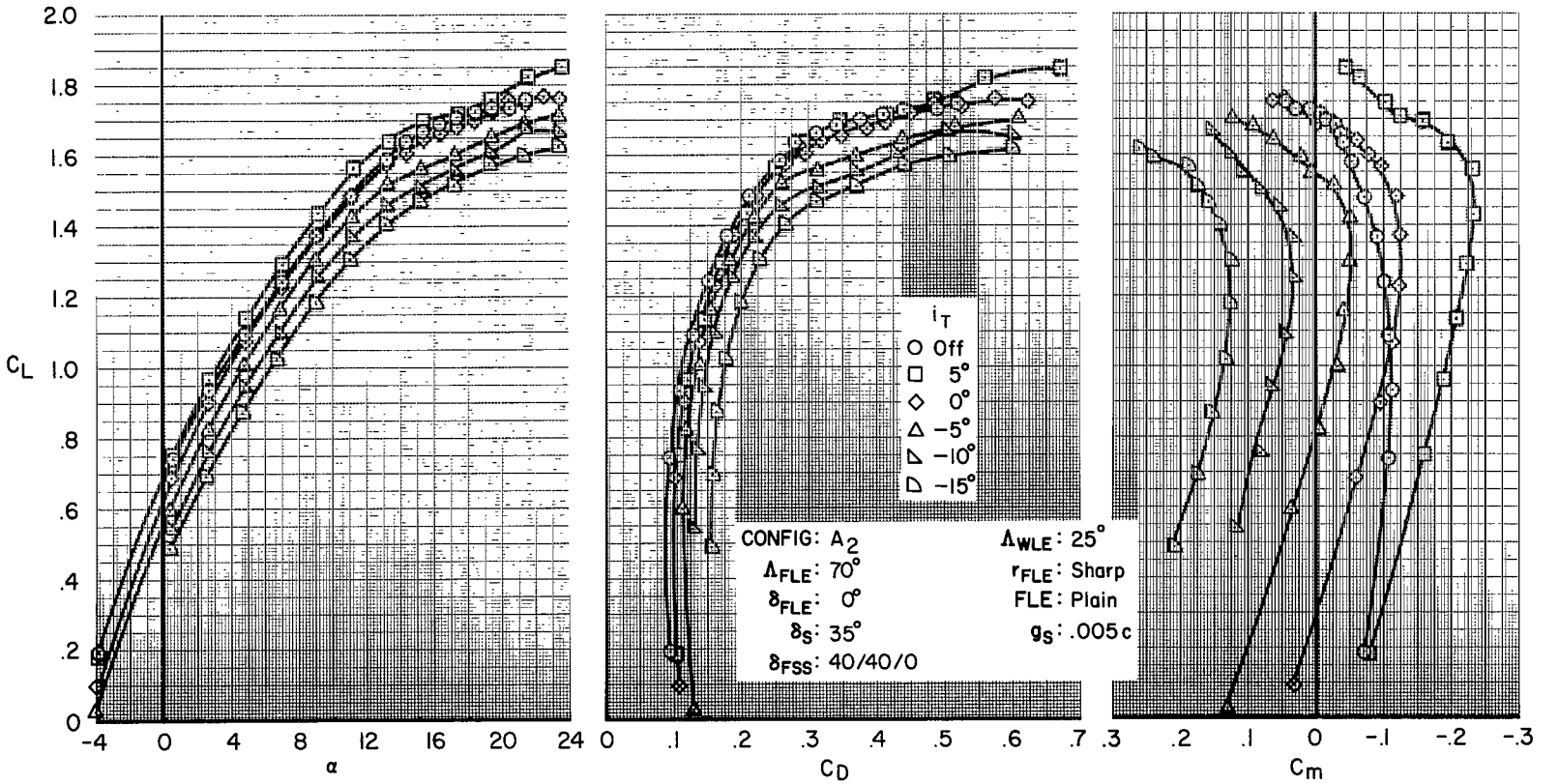

(b) Large (basic) horizontal tail.

Figure 29.- Concluded.

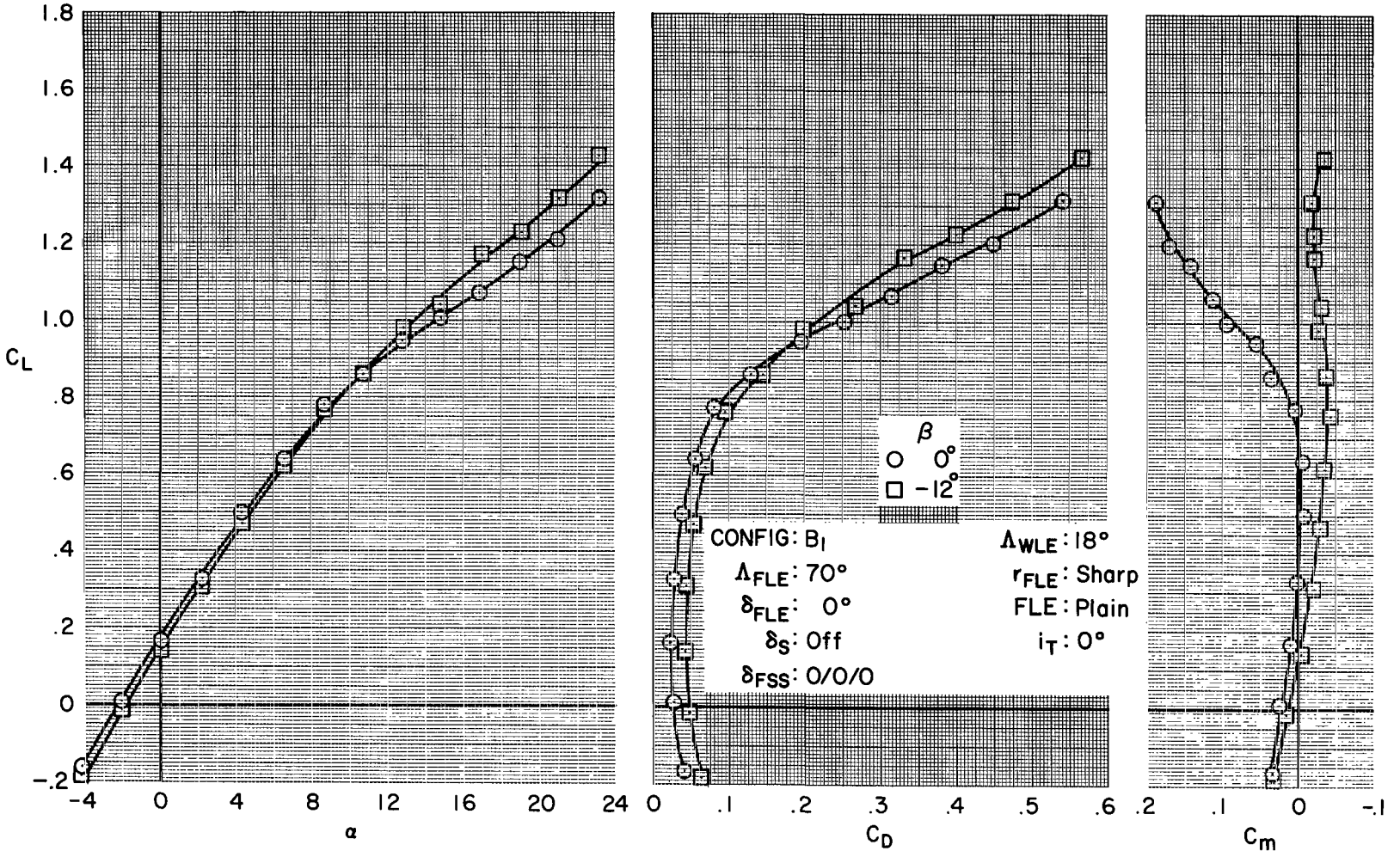

Figure 30.- Longitudinal characteristics, low-aspect-ratio wing, 18° wing sweep, flaps up, slats off.

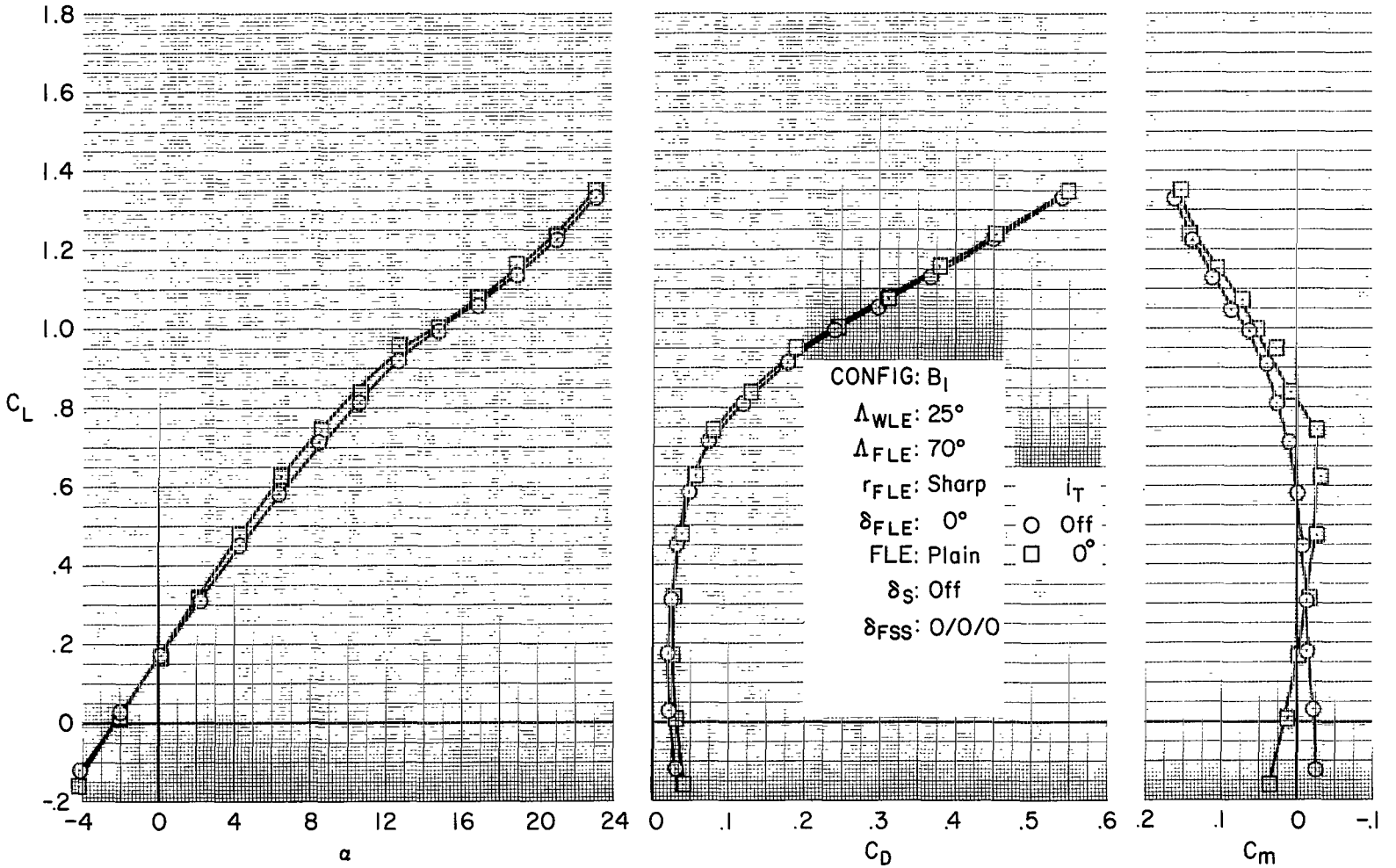

Figure 31.- Longitudinal characteristics, low-aspect-ratio wing, 25° wing sweep, flaps up, slats off.

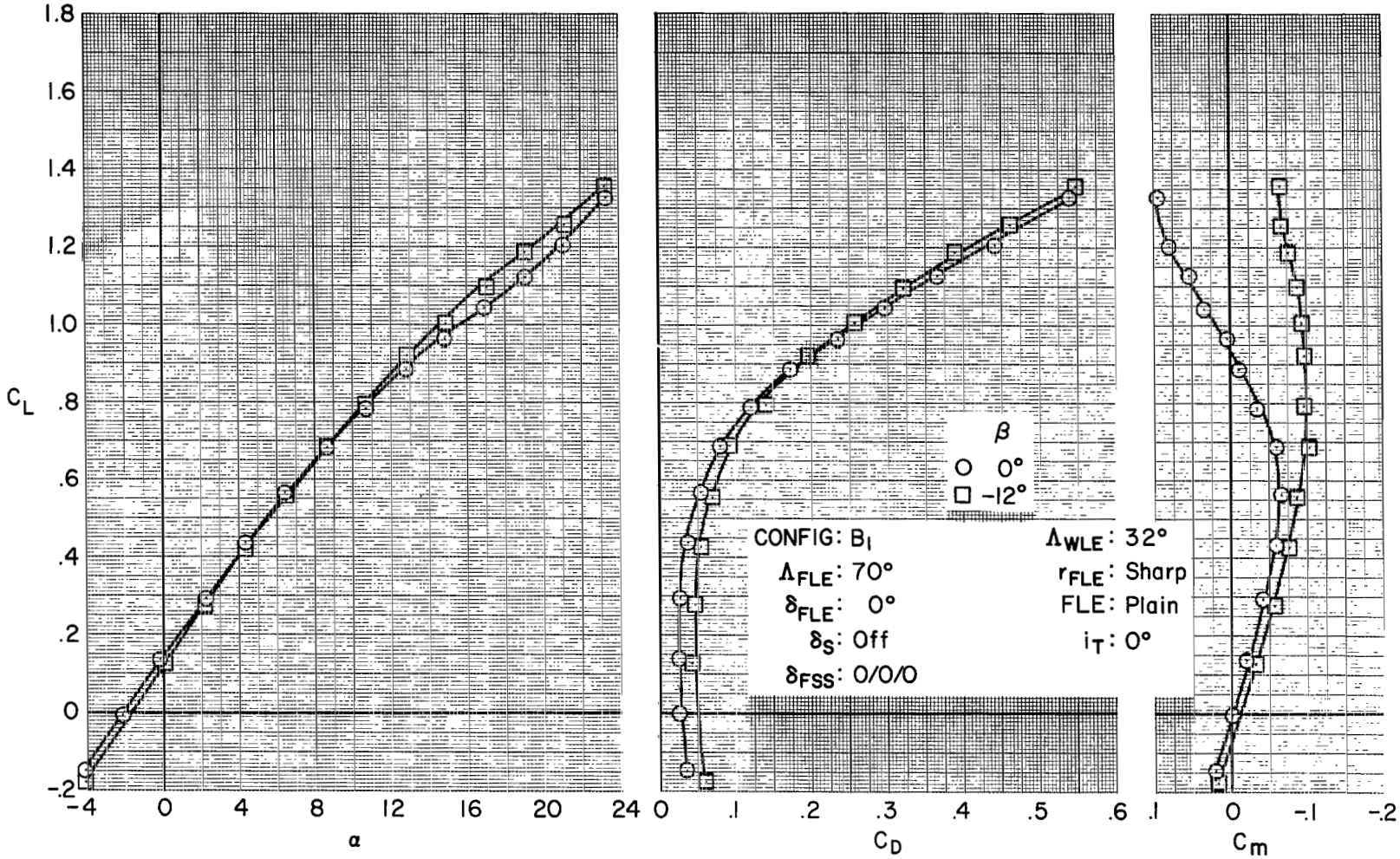

Figure 32.- Longitudinal characteristics, low-aspect-ratio wing, 32° wing sweep, flaps up, slats off.

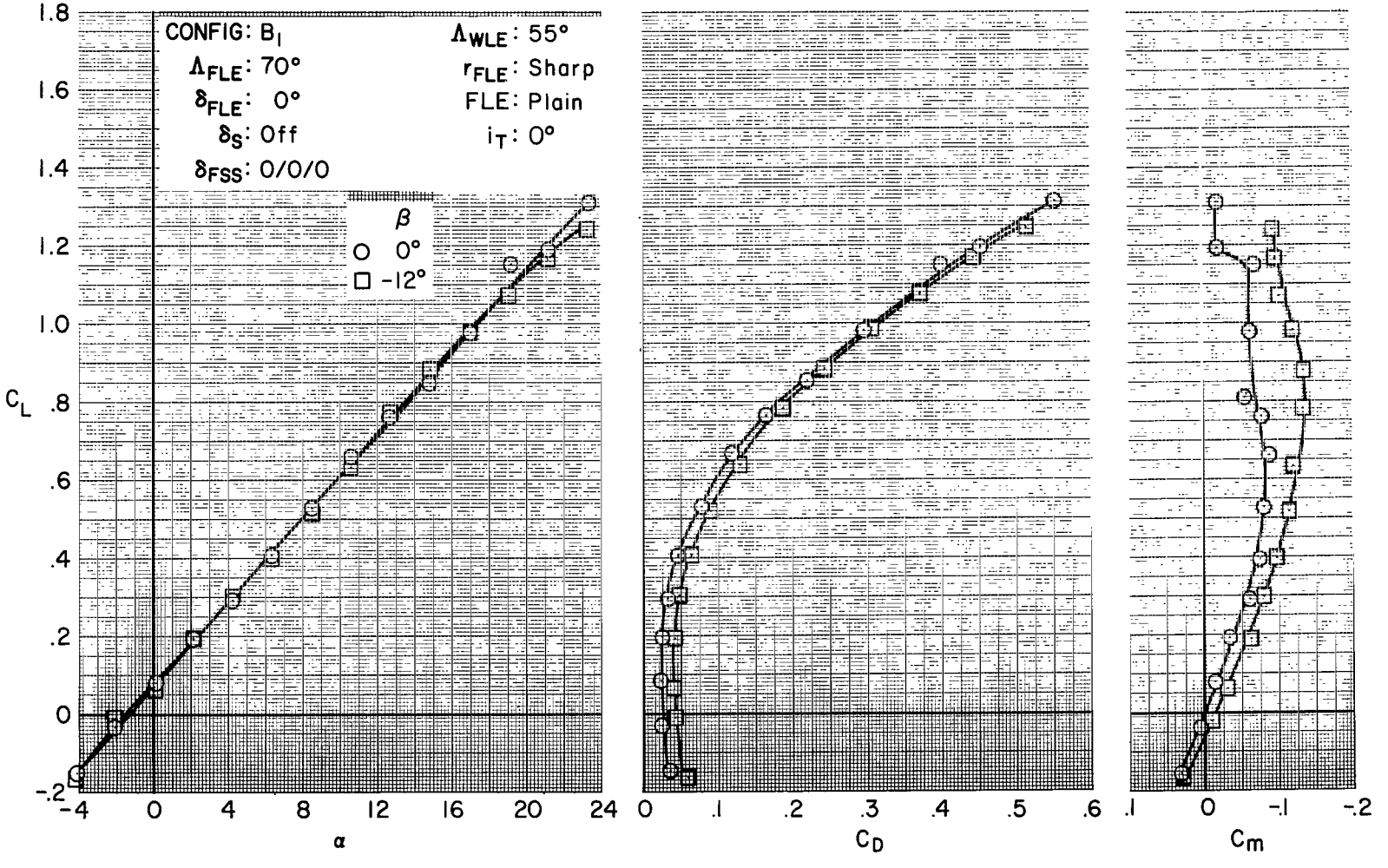

Figure 33.- Longitudinal characteristics, low-aspect-ratio wing, 55° wing sweep, flaps up, slats off.

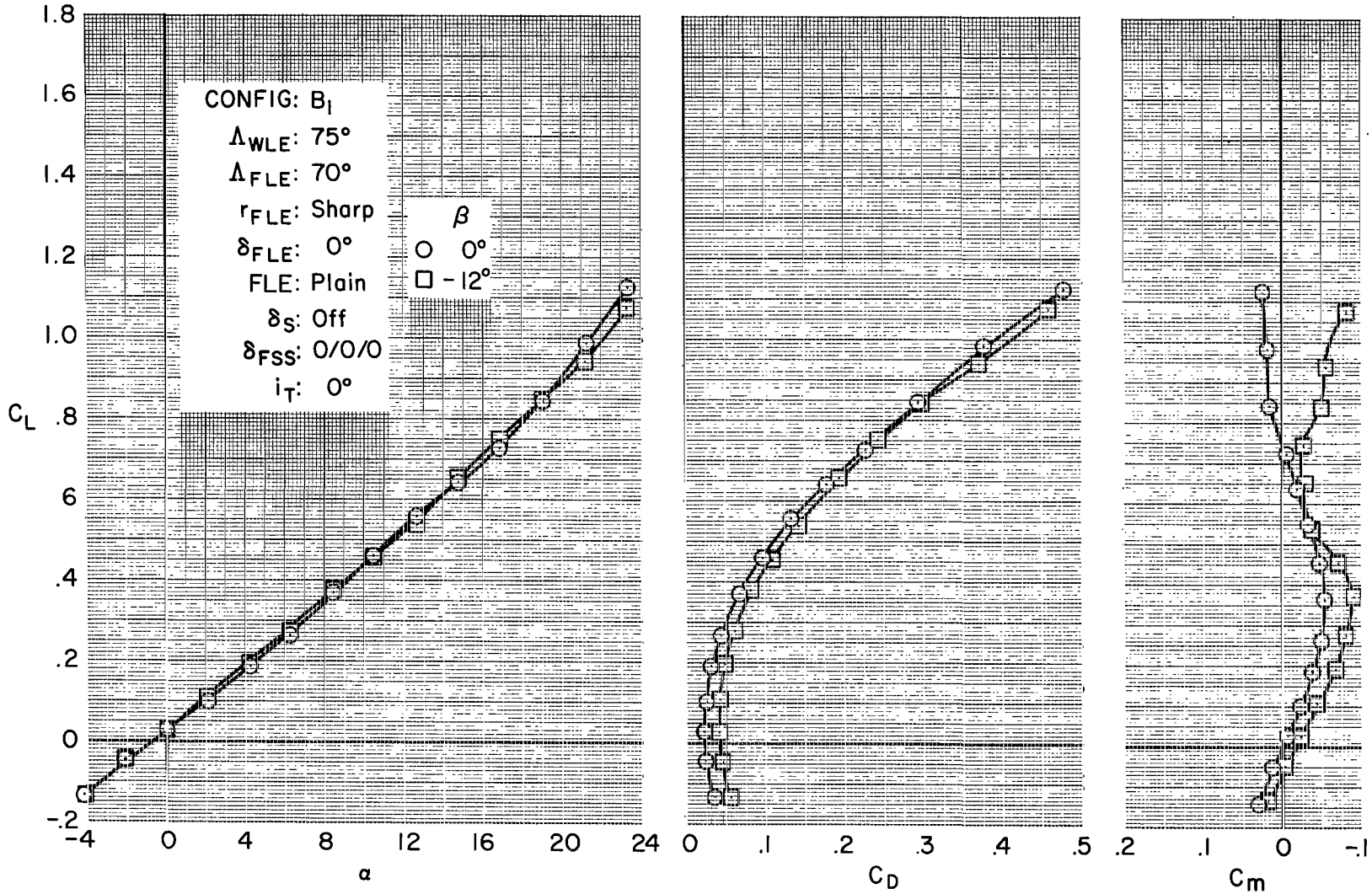

Figure 34.- Longitudinal characteristics, low-aspect-ratio wing, 75° wing sweep, flaps up, slats off.

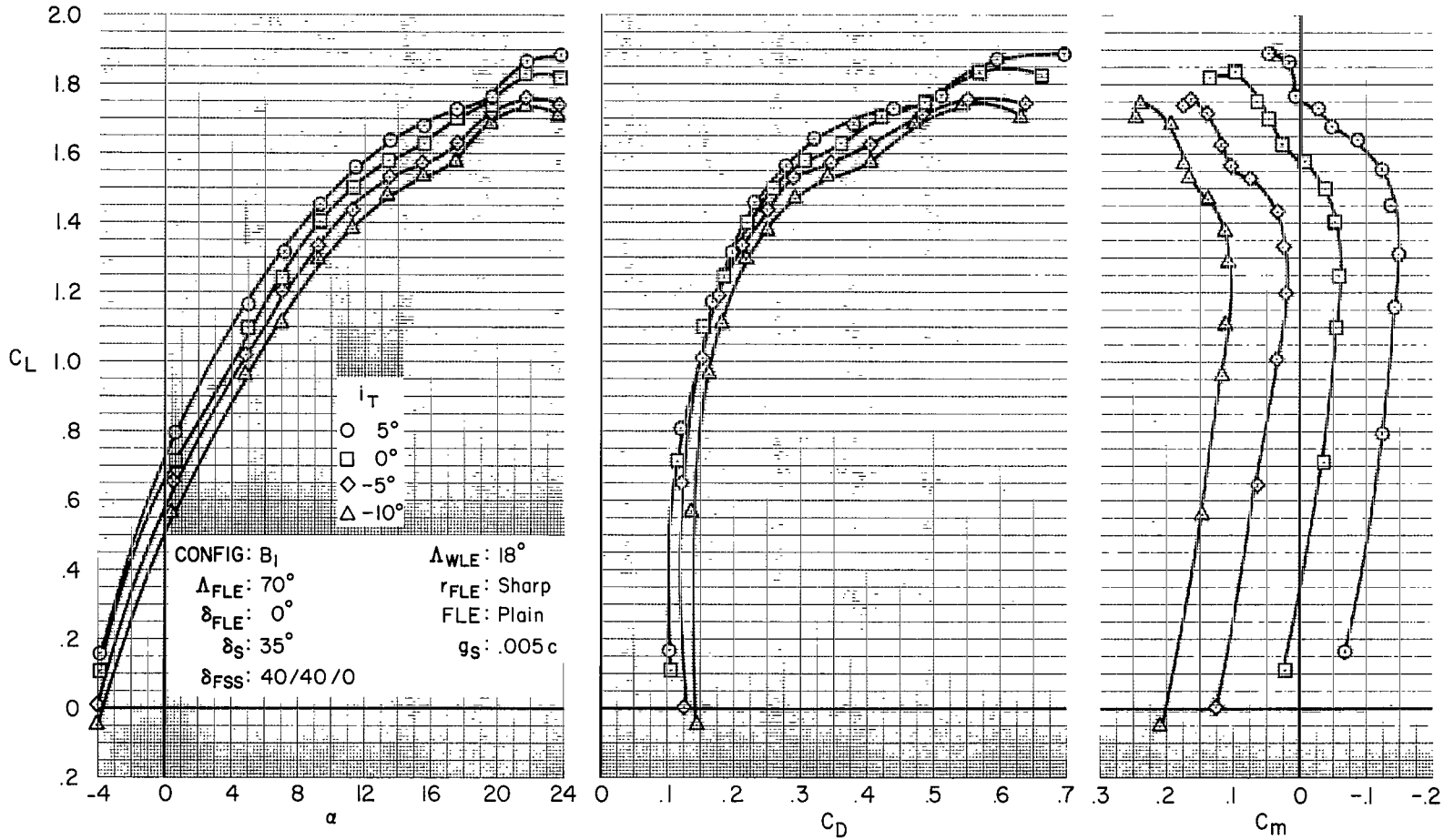

Figure 35.- Effect of 40° partial-span single-slotted flaps on low-aspect-ratio wing at 18° sweep.

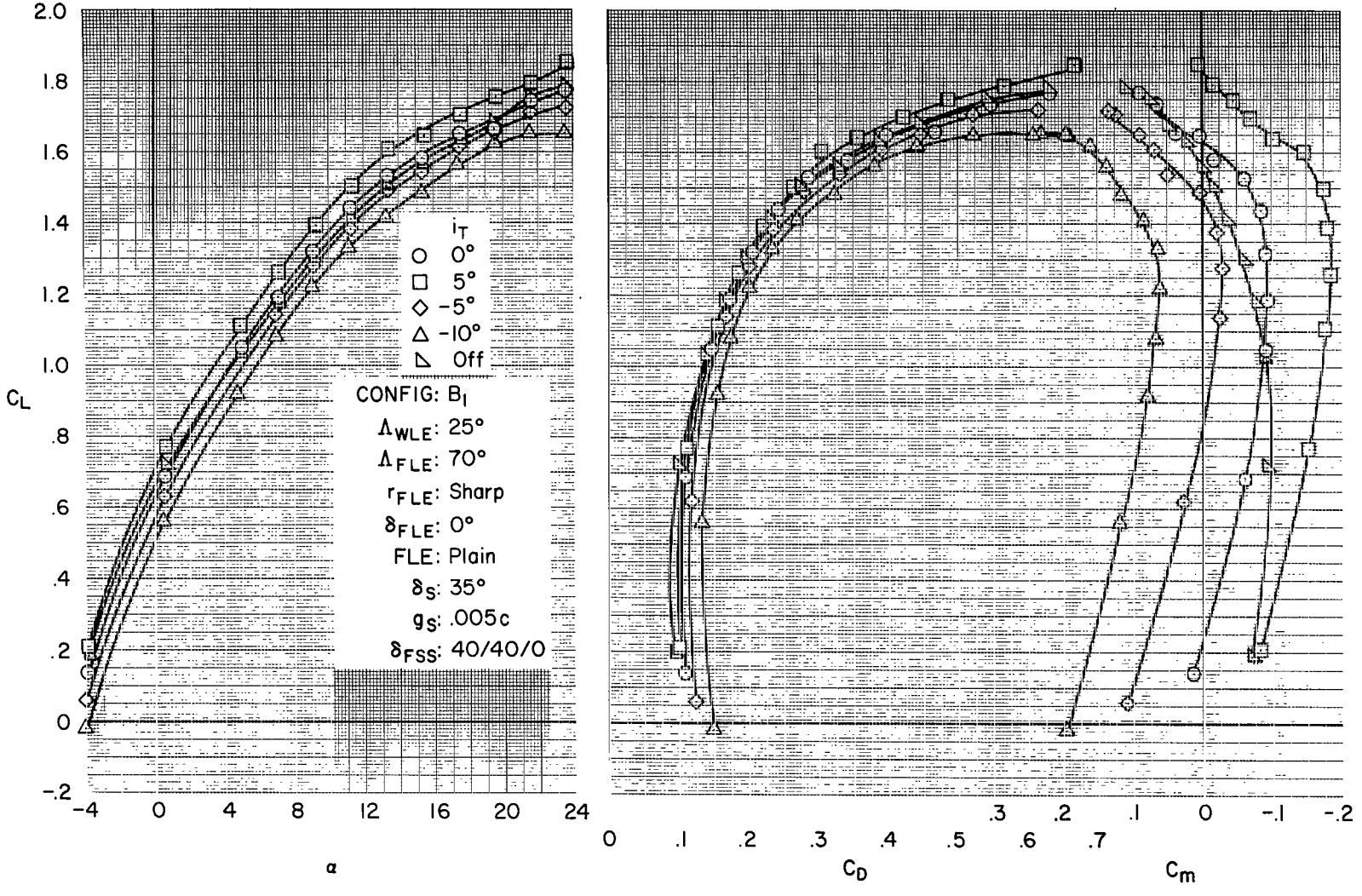

(a) Longitudinal characteristics with tail incidence.

Figure 36.- Characteristics of low-aspect-ratio wing at 25° sweep, 40° partial-span flaps, horizontal and vertical tail on and off.

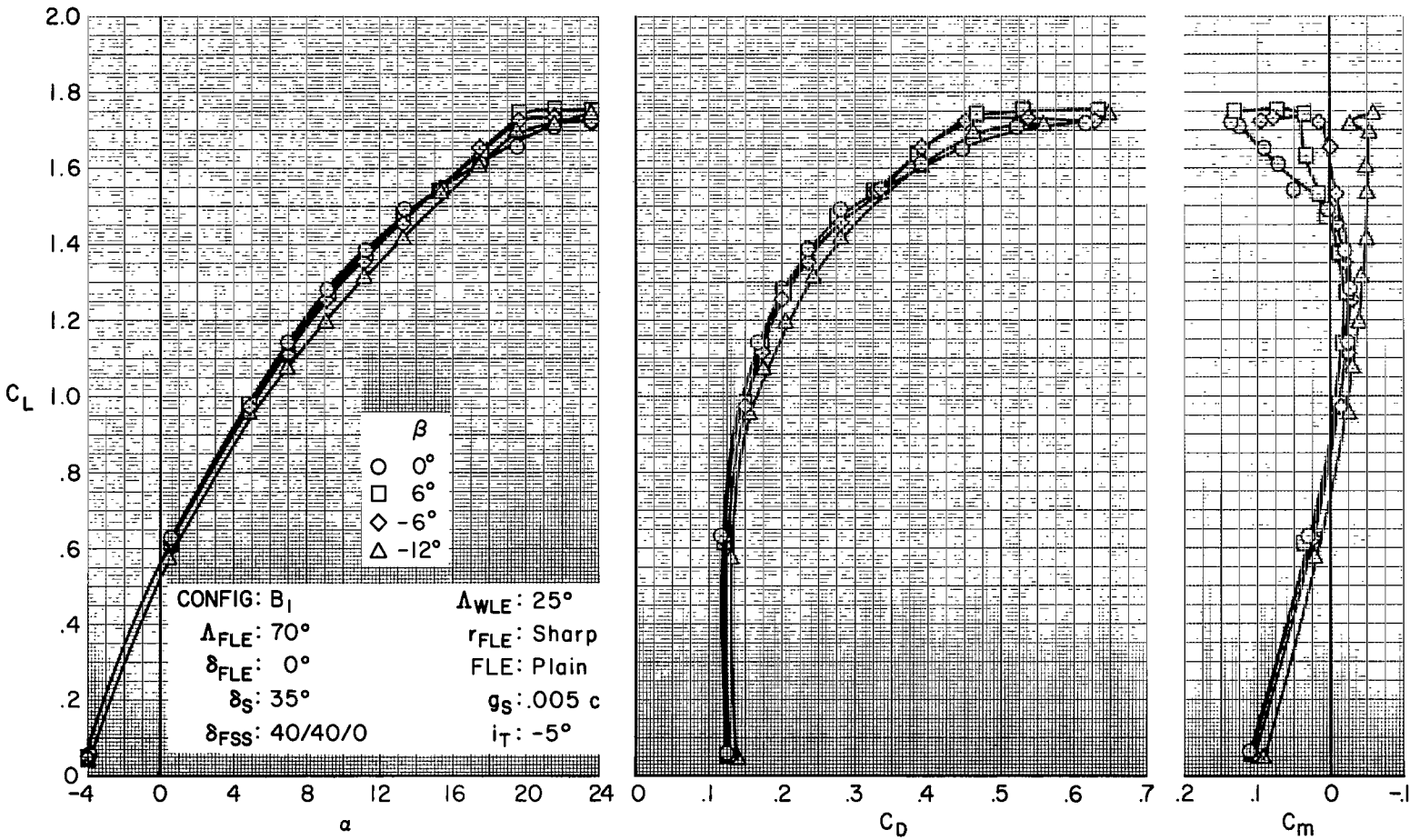

(b) Longitudinal characteristics at constant sideslip; tail on.

Figure 36.- Continued.

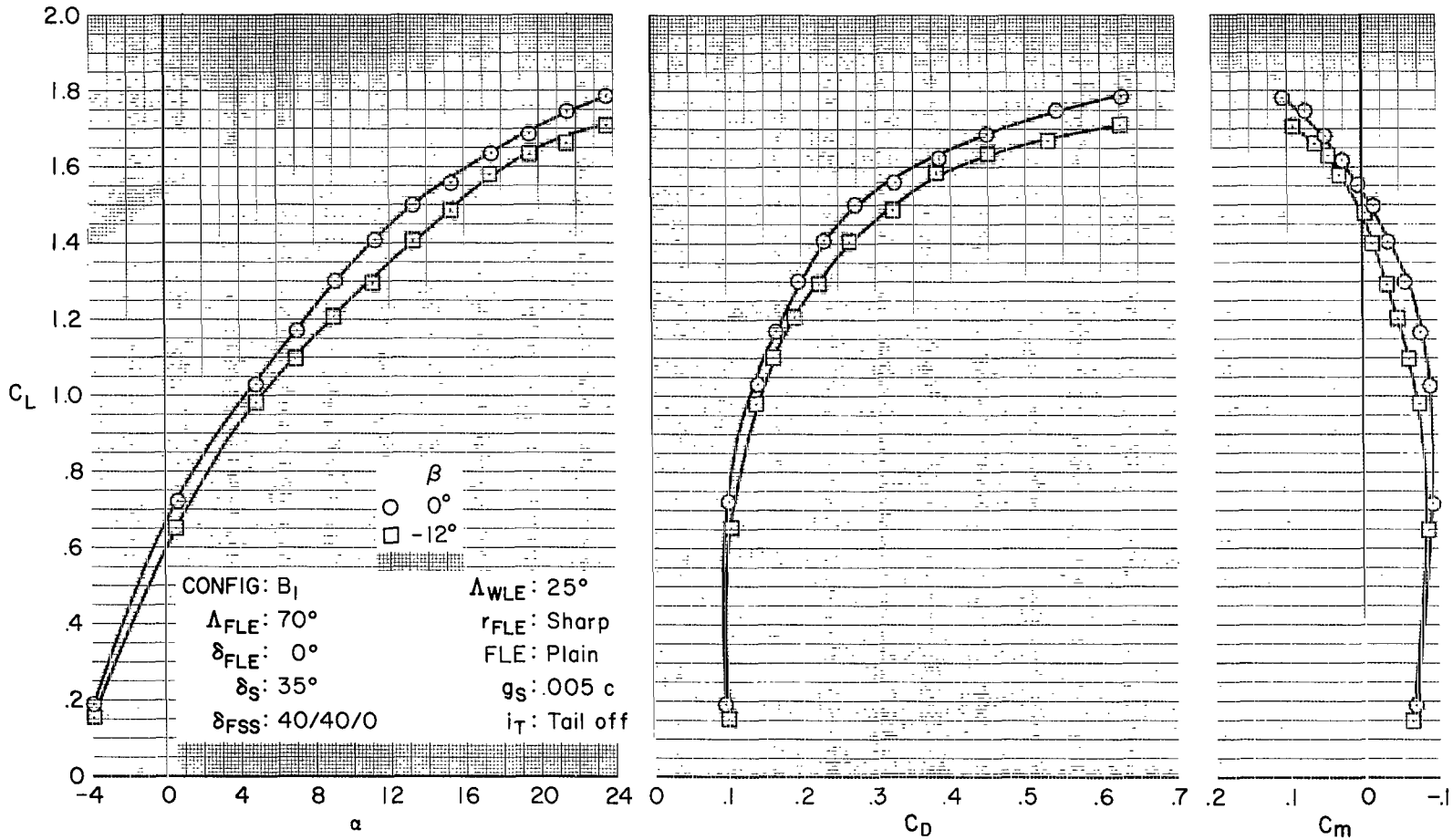

(c) Longitudinal characteristics at constant sideslip; tail off.

Figure 36.- Continued.

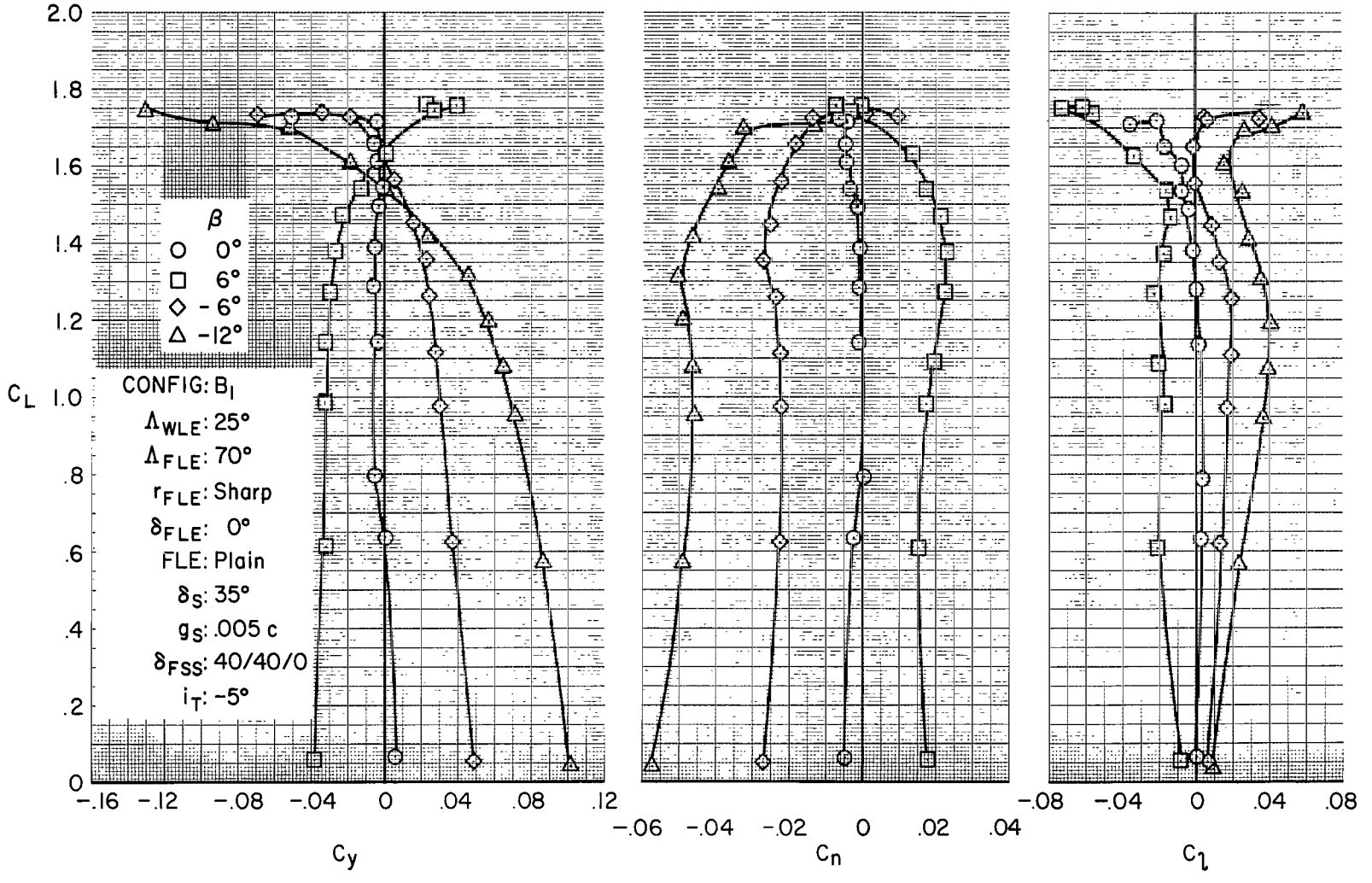

(d) Lateral characteristics at constant sideslip; tail on.

Figure 36.- Continued.

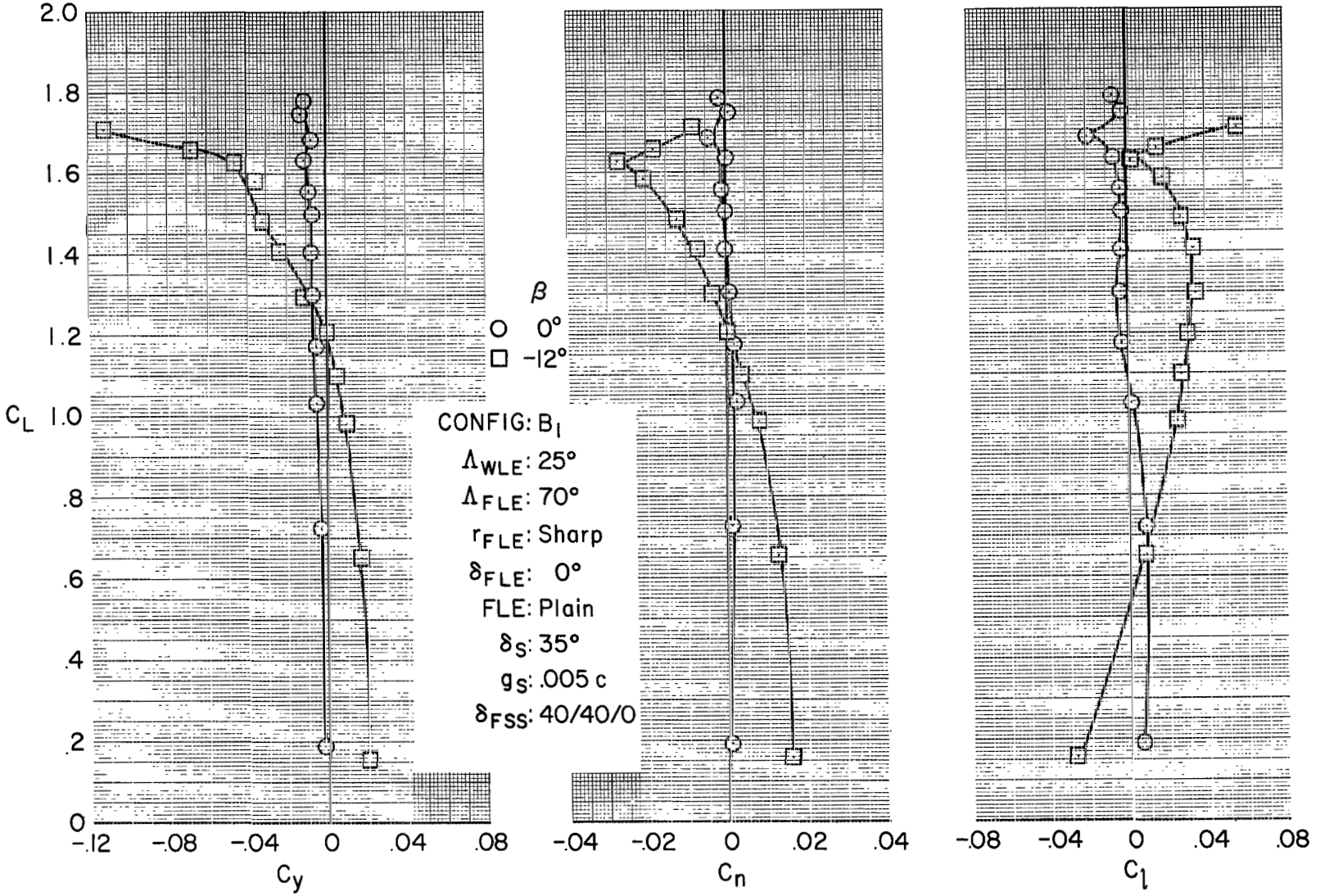

(e) Lateral characteristics at constant sideslip; tail off.

Figure 36.- Continued.

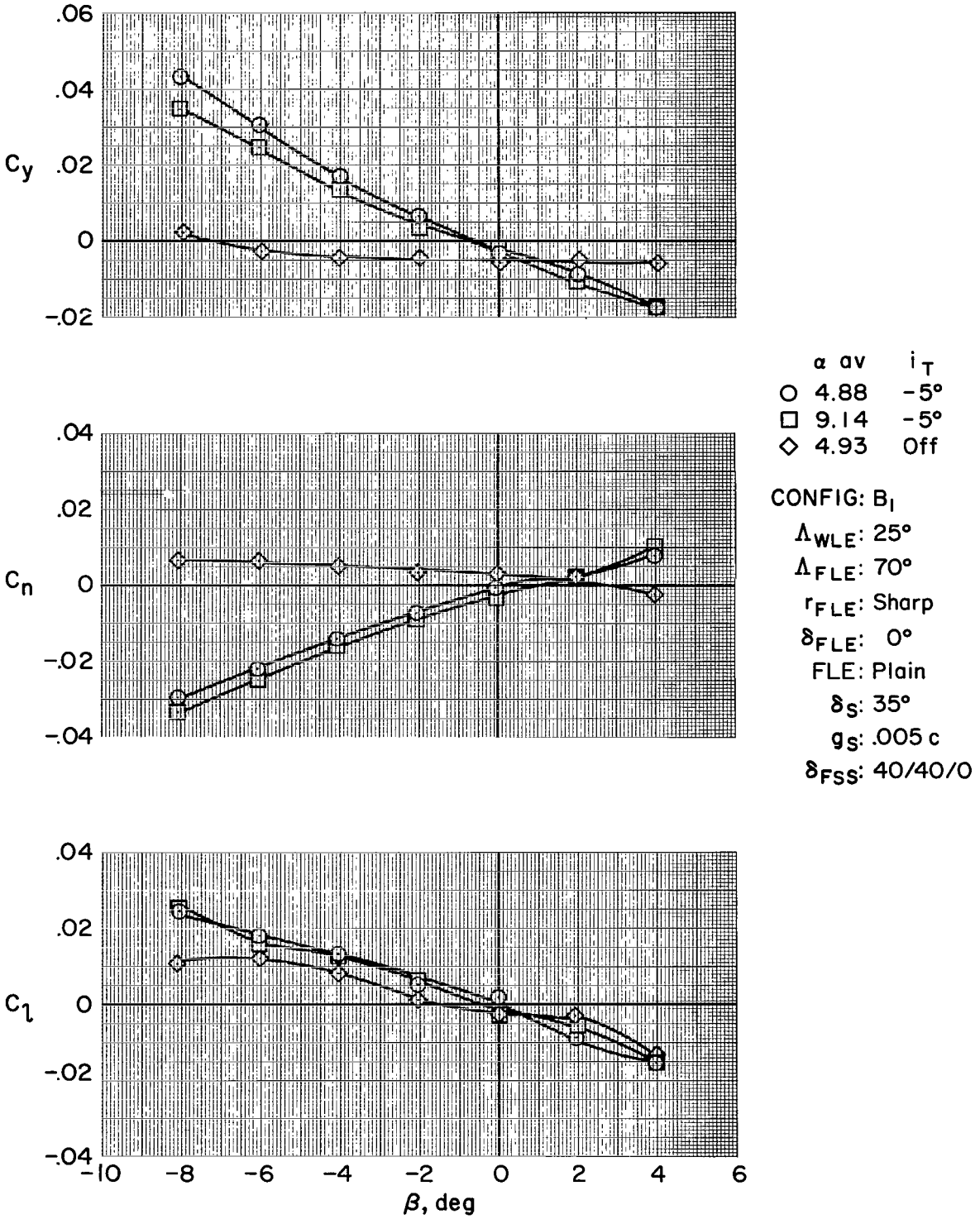

(f) Lateral characteristics at constant angle of attack.

Figure 36.- Concluded.

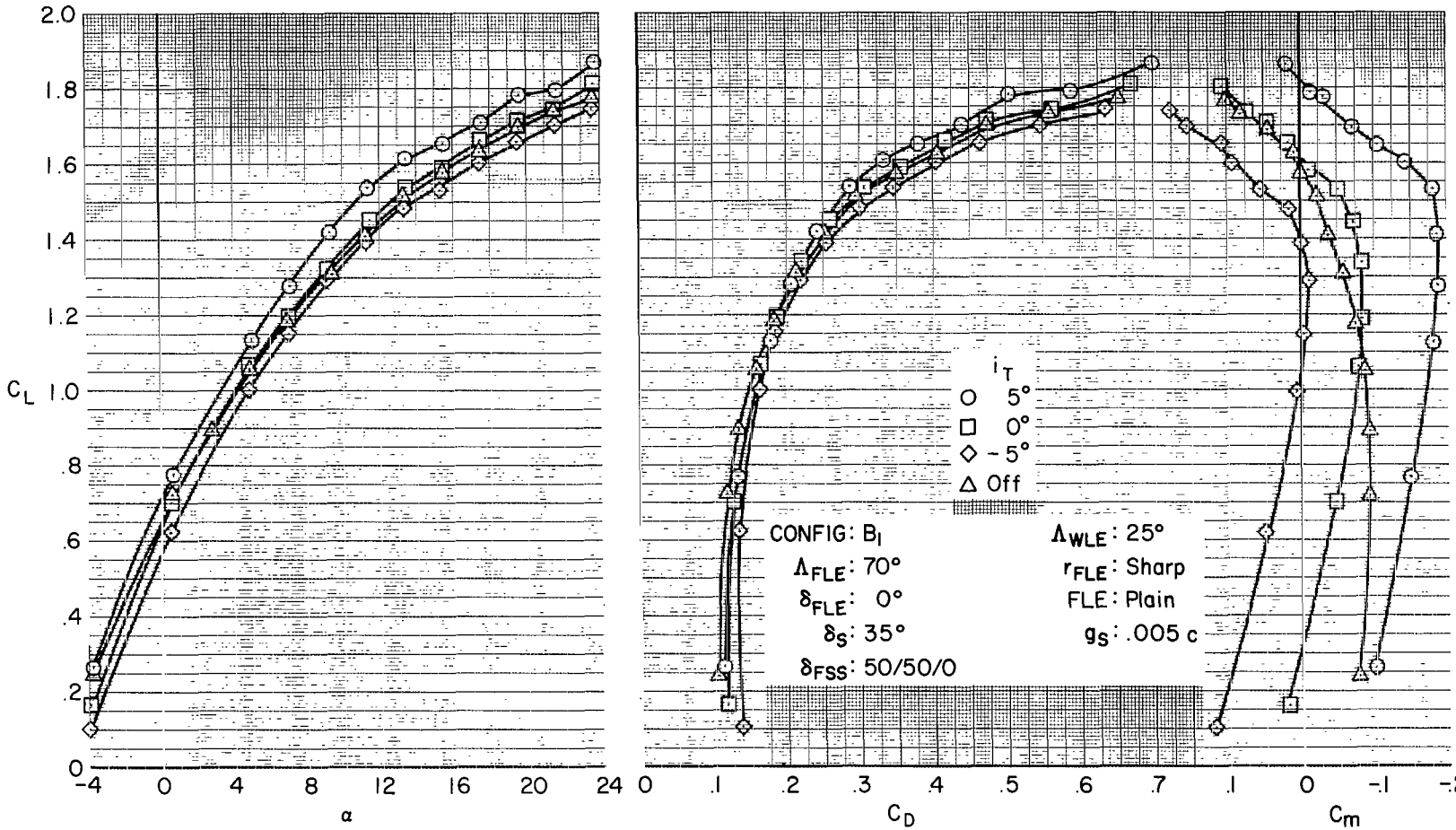

Figure 37.- Longitudinal characteristics, low-aspect-ratio wing at 25° sweep, 50° partial-span flaps.

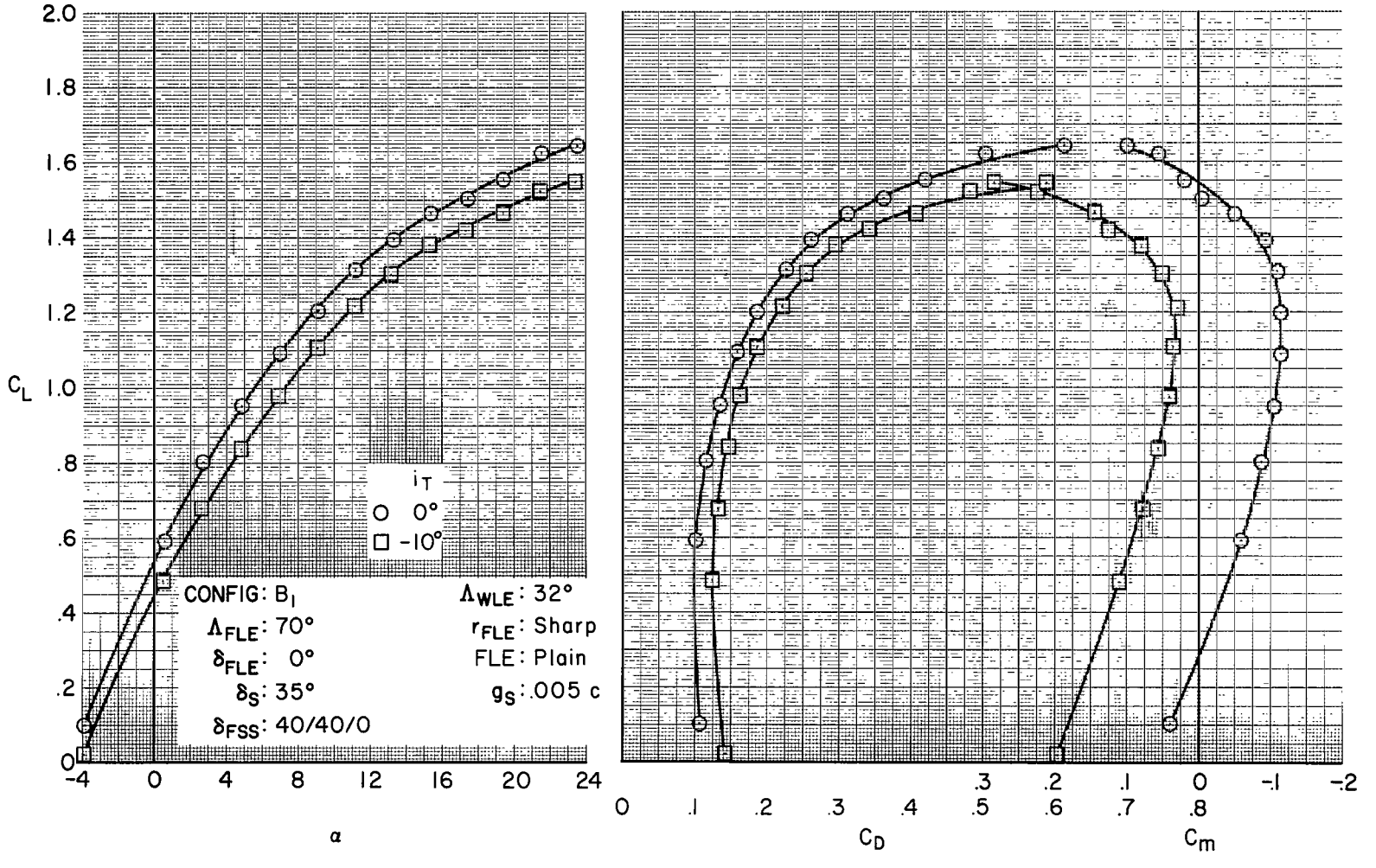

Figure 38.- Longitudinal characteristics, low-aspect-ratio wing, 32° sweep, 40° partial-span flaps.

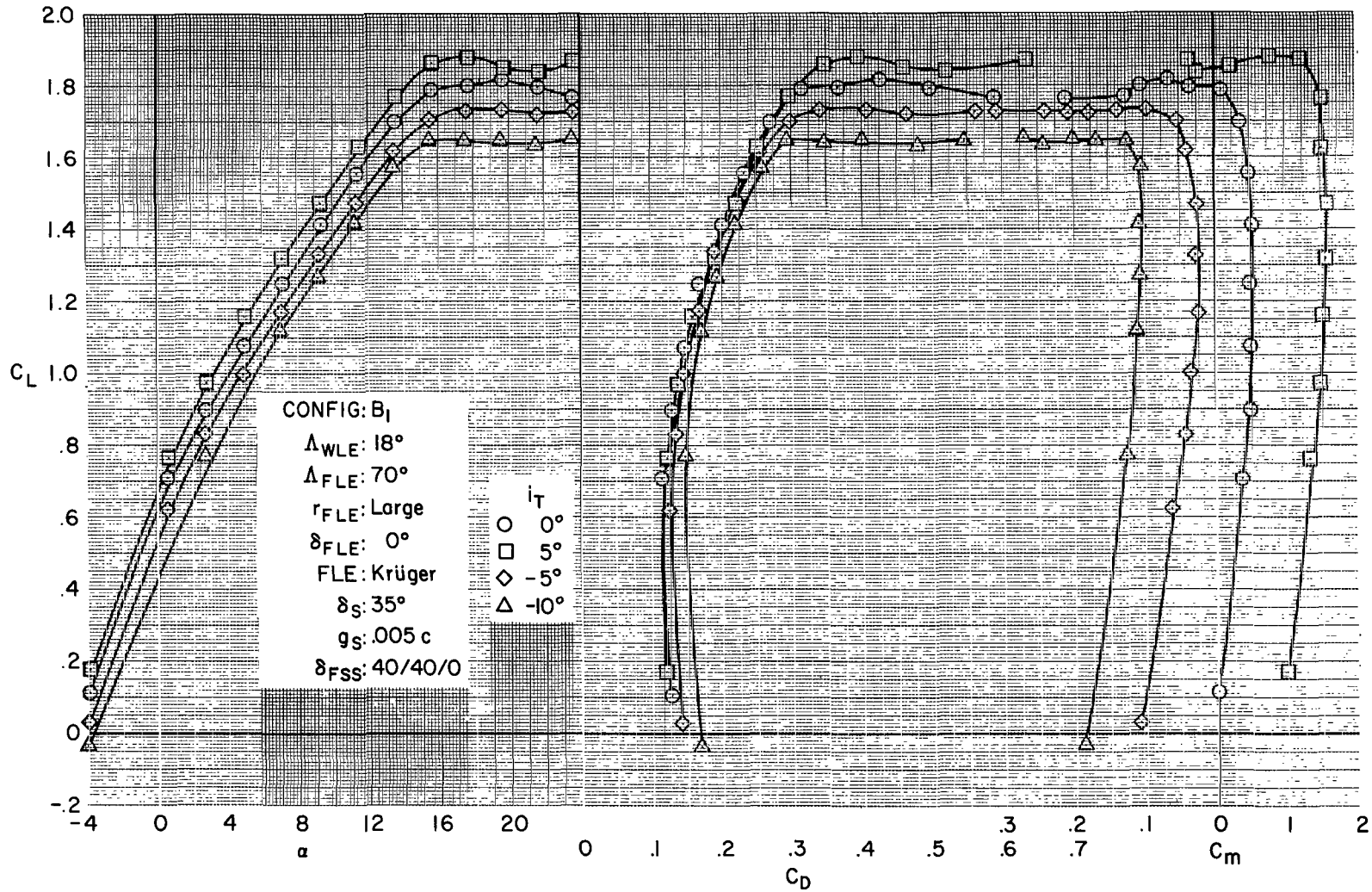

Figure 39.- Longitudinal characteristics, low-aspect-ratio wing, 18° sweep, with large fixed-wing leading-edge radius and Krüger-type flap.

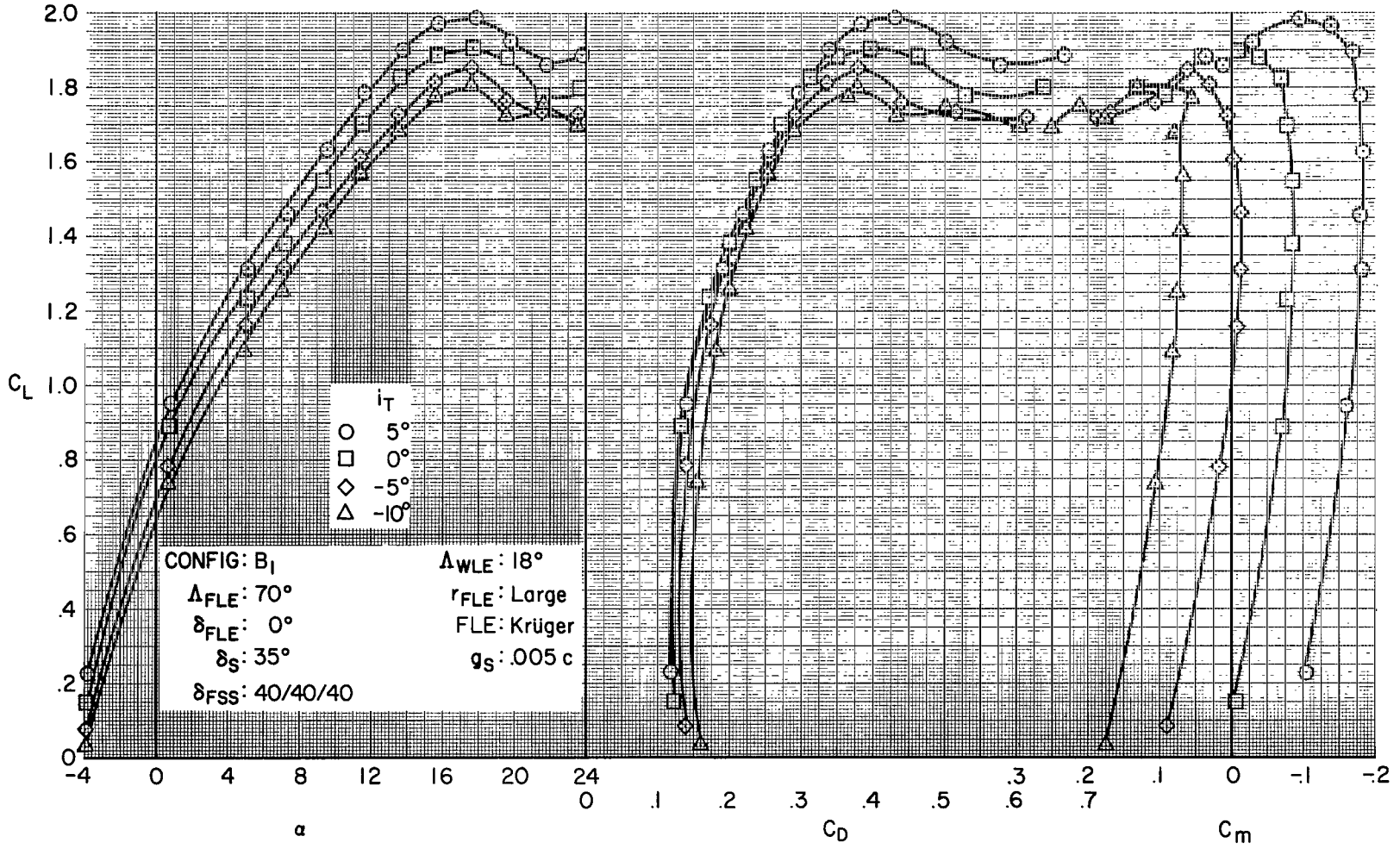

Figure 40.- Longitudinal characteristics, low-aspect-ratio wing at 18° sweep, 40° full-span flaps, large fixed-wing leading-edge radius and Krüger-type flap.

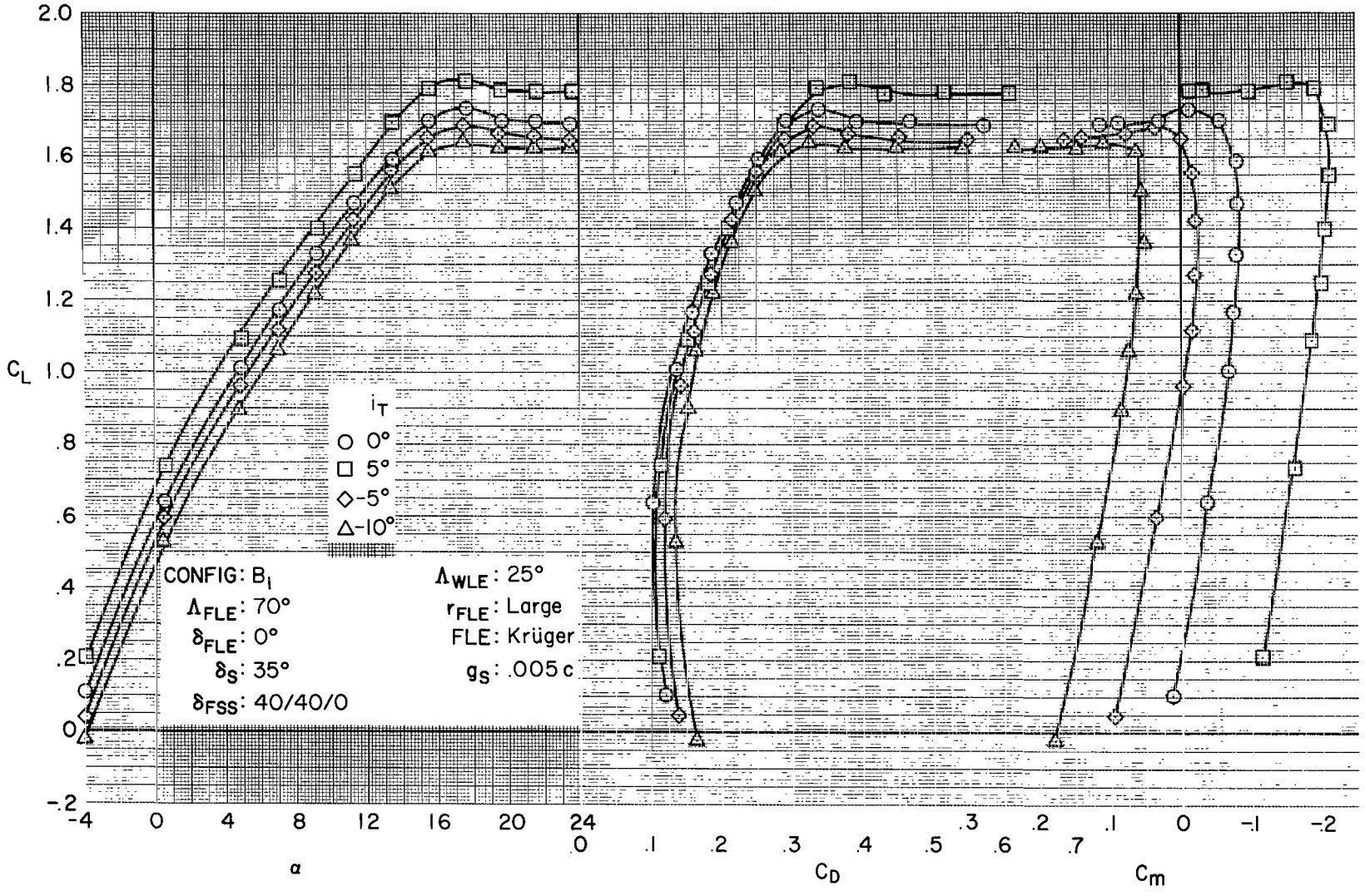

(a) Longitudinal characteristics with tail incidence.

Figure 41.- Characteristics of low-aspect-ratio wing at 25° sweep, with large fixed-wing leading-edge radius and Krüger-type flap.

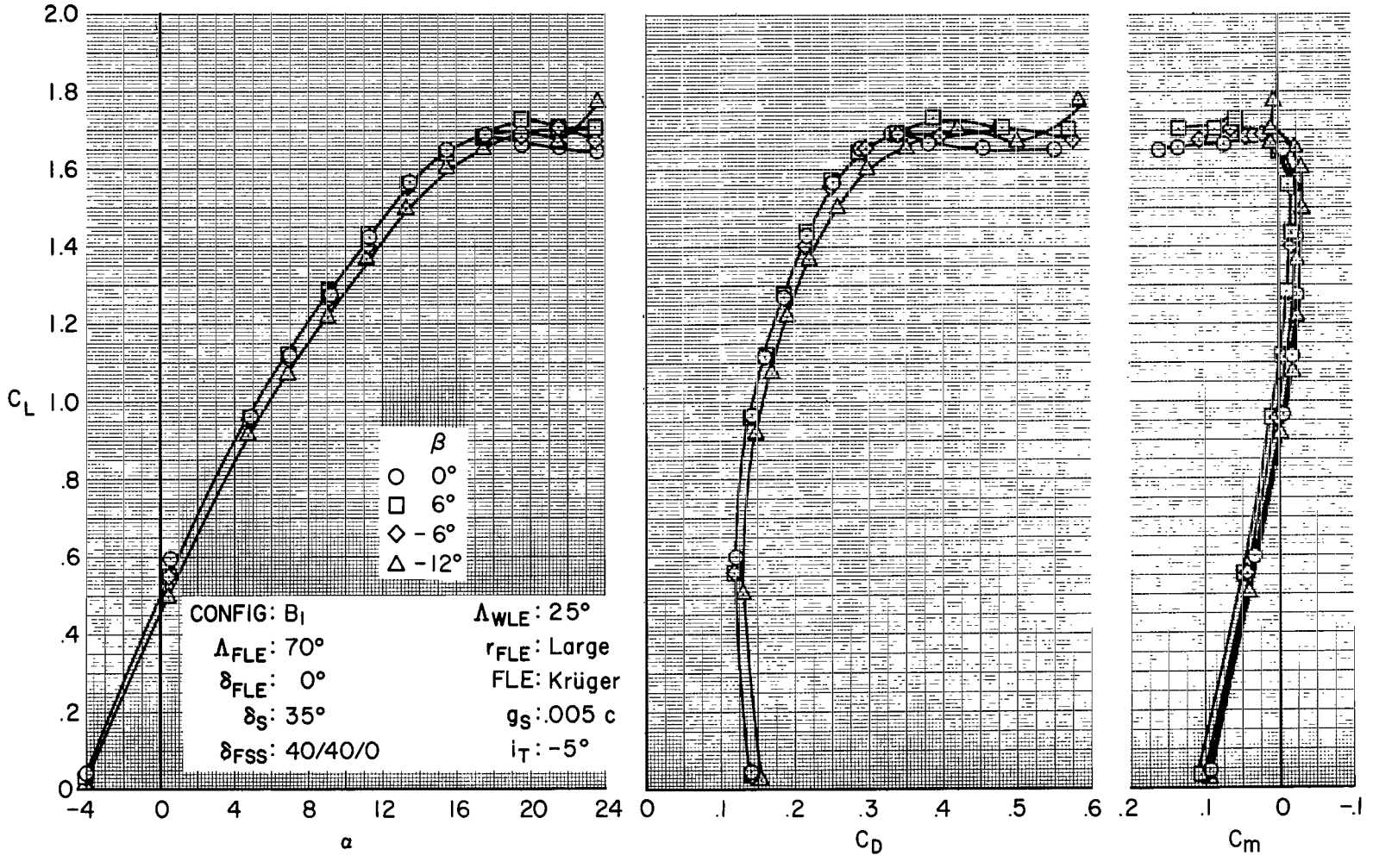

(b) Longitudinal characteristics in sideslip.

Figure 41.- Continued.

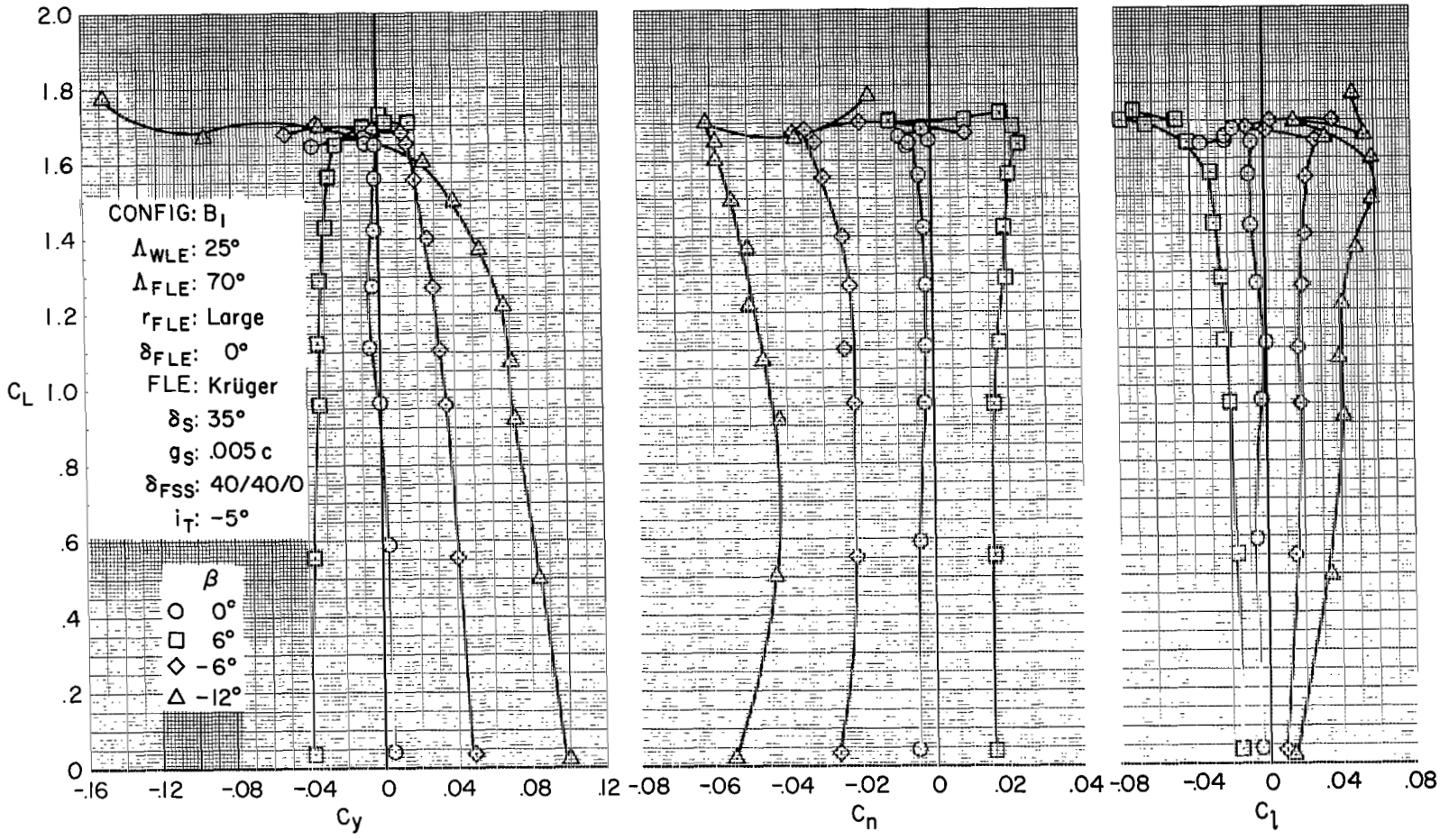

(c) Lateral characteristics in sideslip.

Figure 41.- Continued.

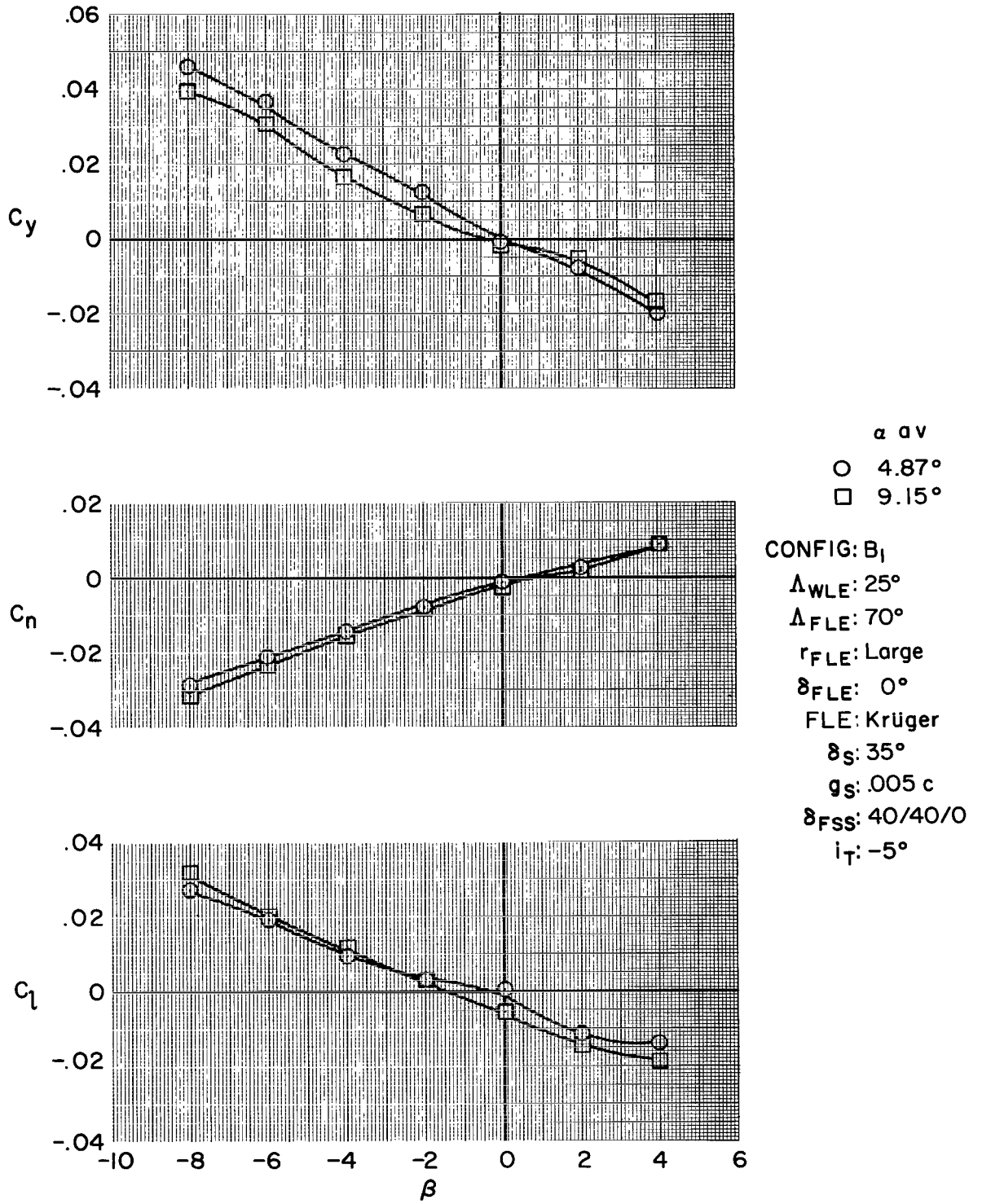

(d) Lateral characteristics at constant angle of attack.

Figure 41.- Concluded.

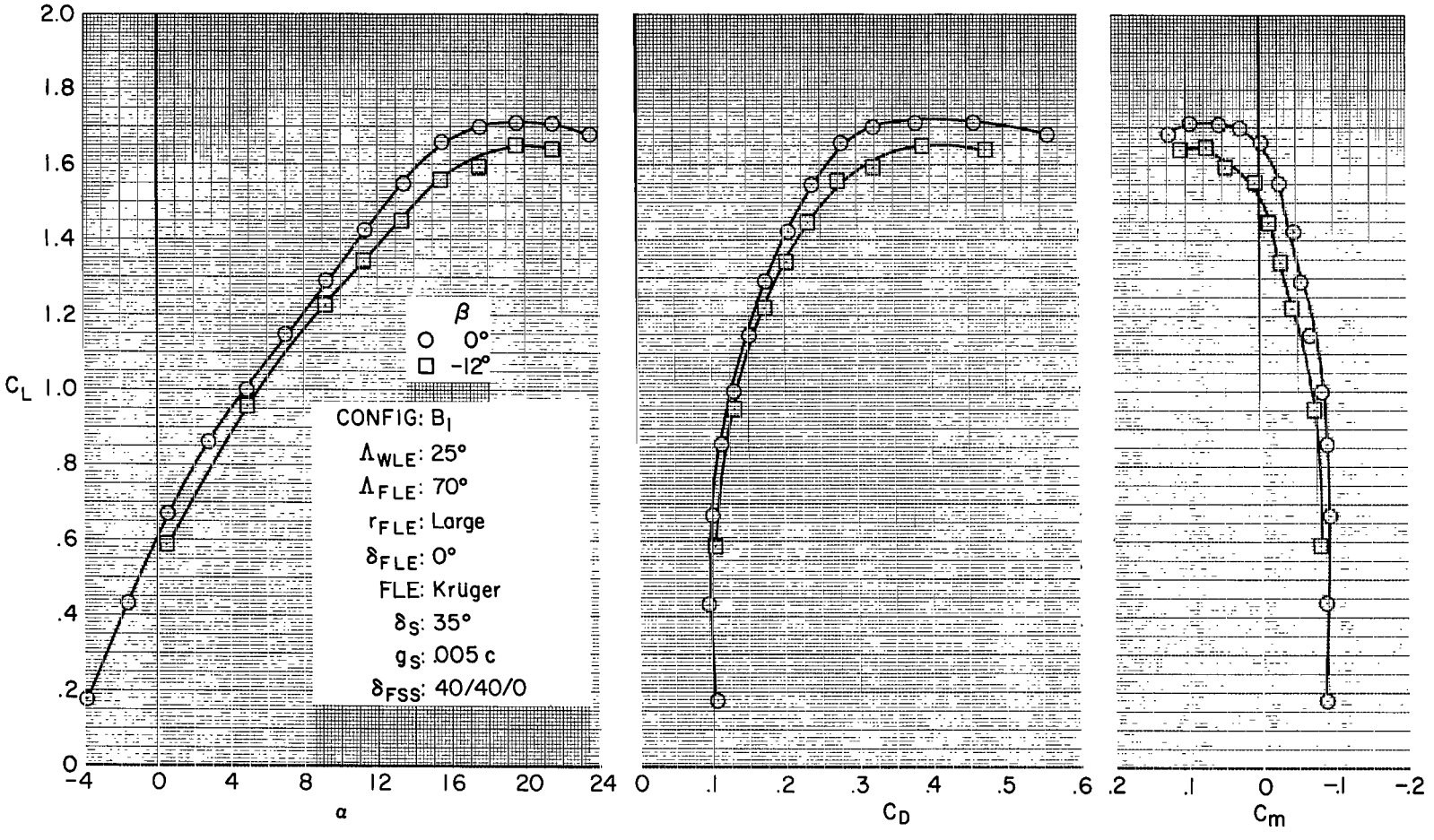

(a) Longitudinal characteristics in sideslip.

Figure 42.- Characteristics of low-aspect-ratio wing at 25° sweep, with large fixed-wing leading-edge radius and Krüger-type flap; tail off.

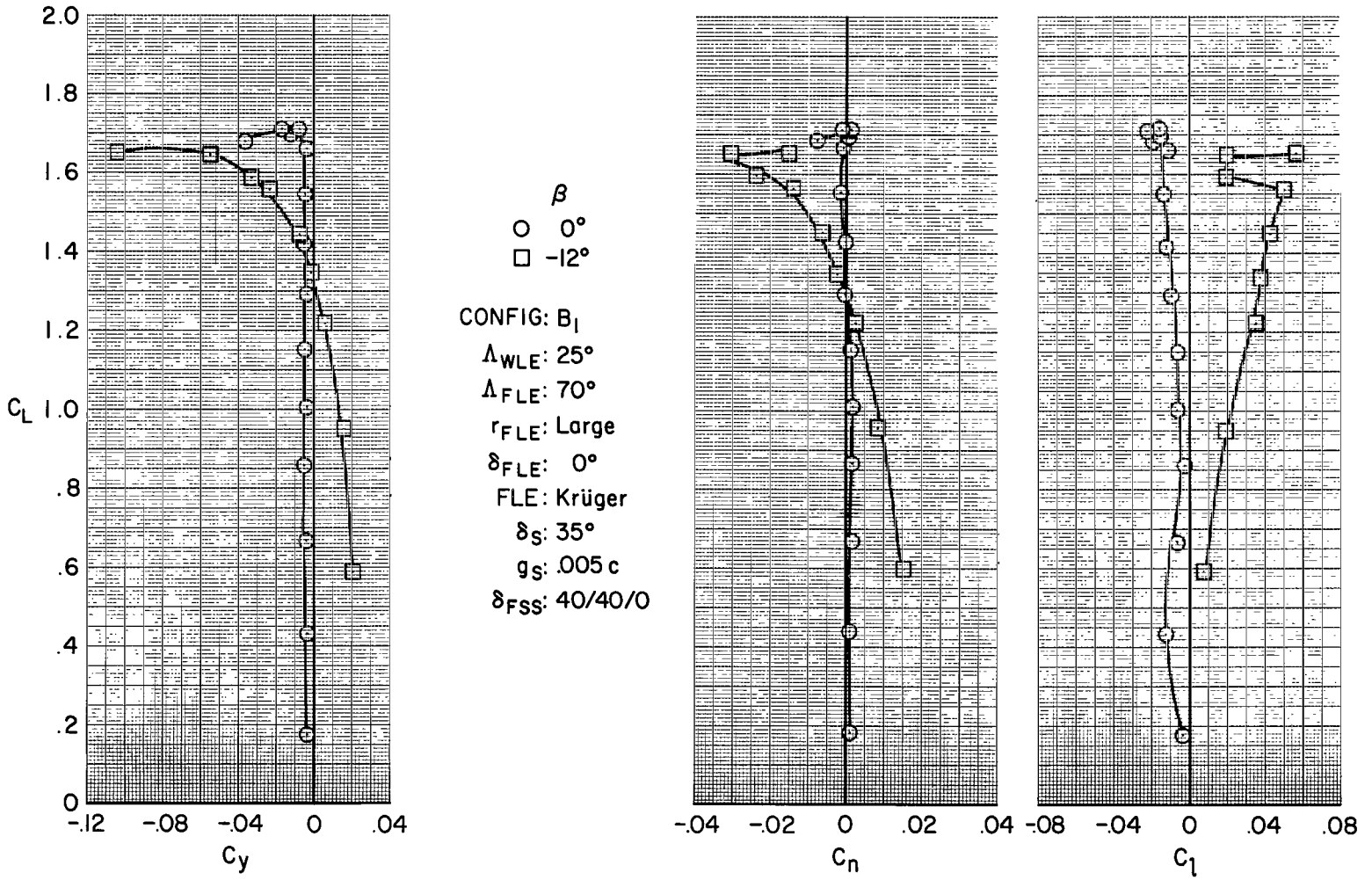

(b) Lateral characteristics in sideslip.

Figure 42.- Continued.

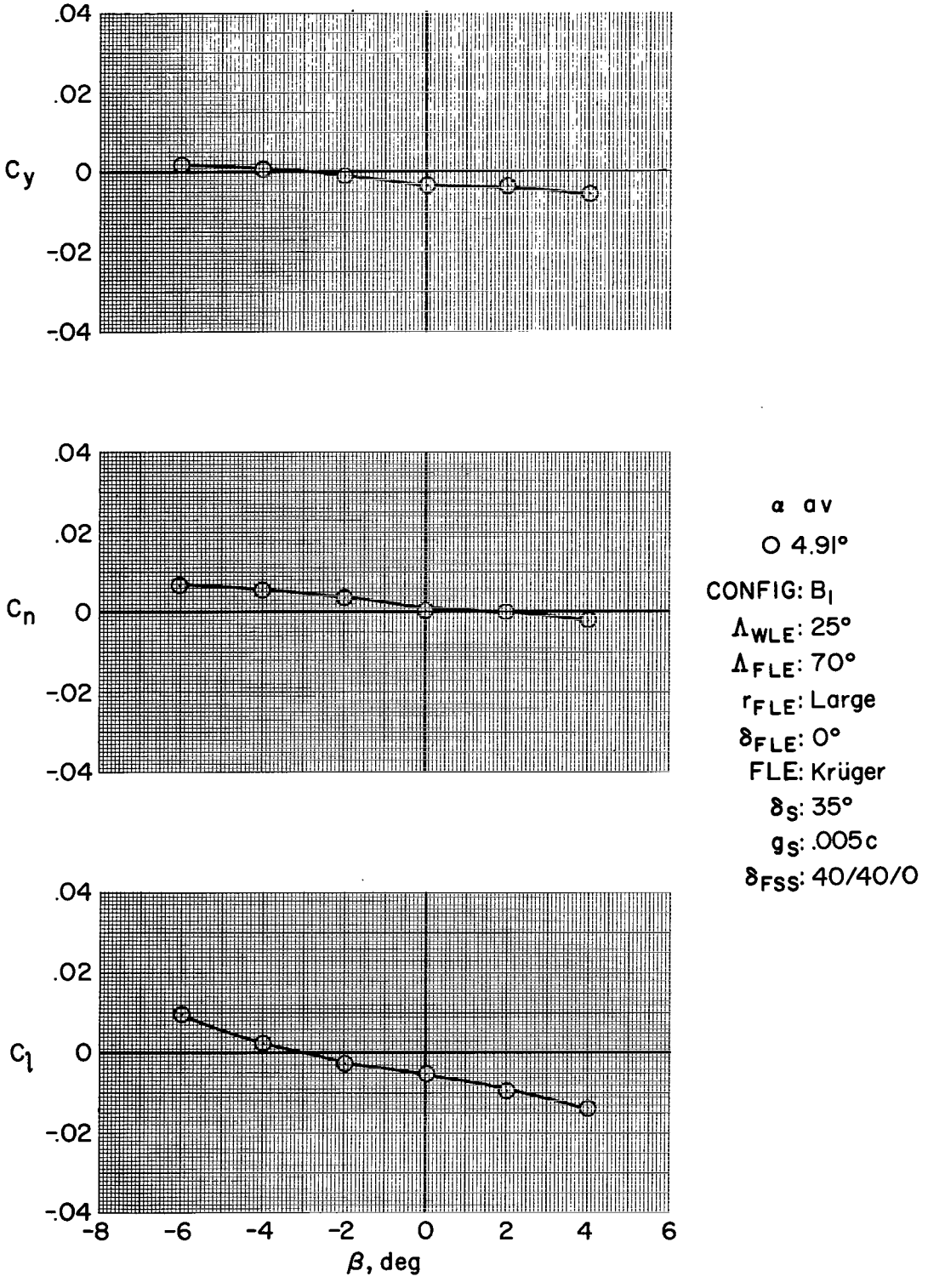

(c) Lateral characteristics at constant angle of attack.

Figure 42.- Concluded.

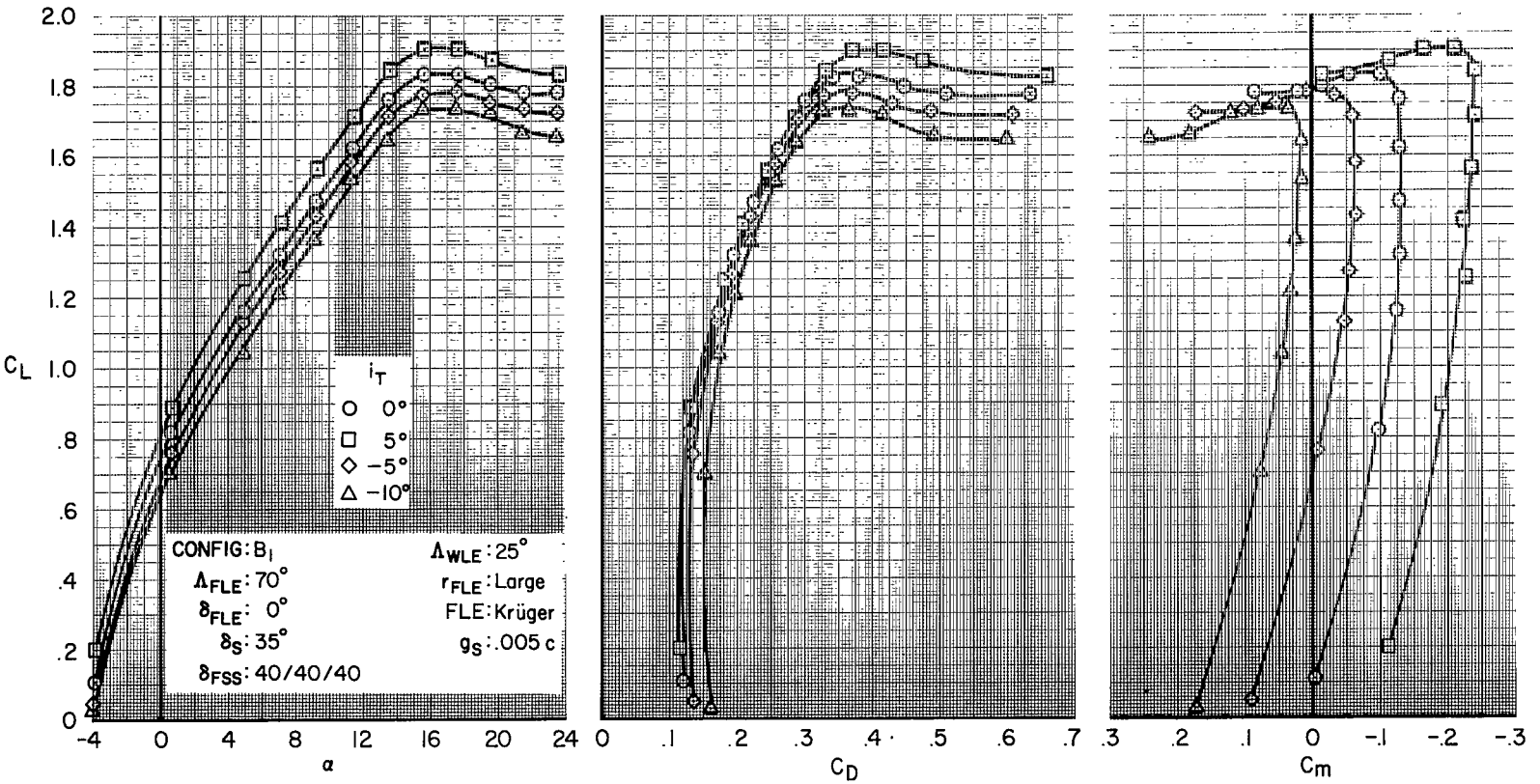

Figure 43.- Longitudinal characteristics, low-aspect-ratio wing at 25° sweep, 40° full-span flaps, large fixed-wing leading-edge radius and Krüger-type flap.

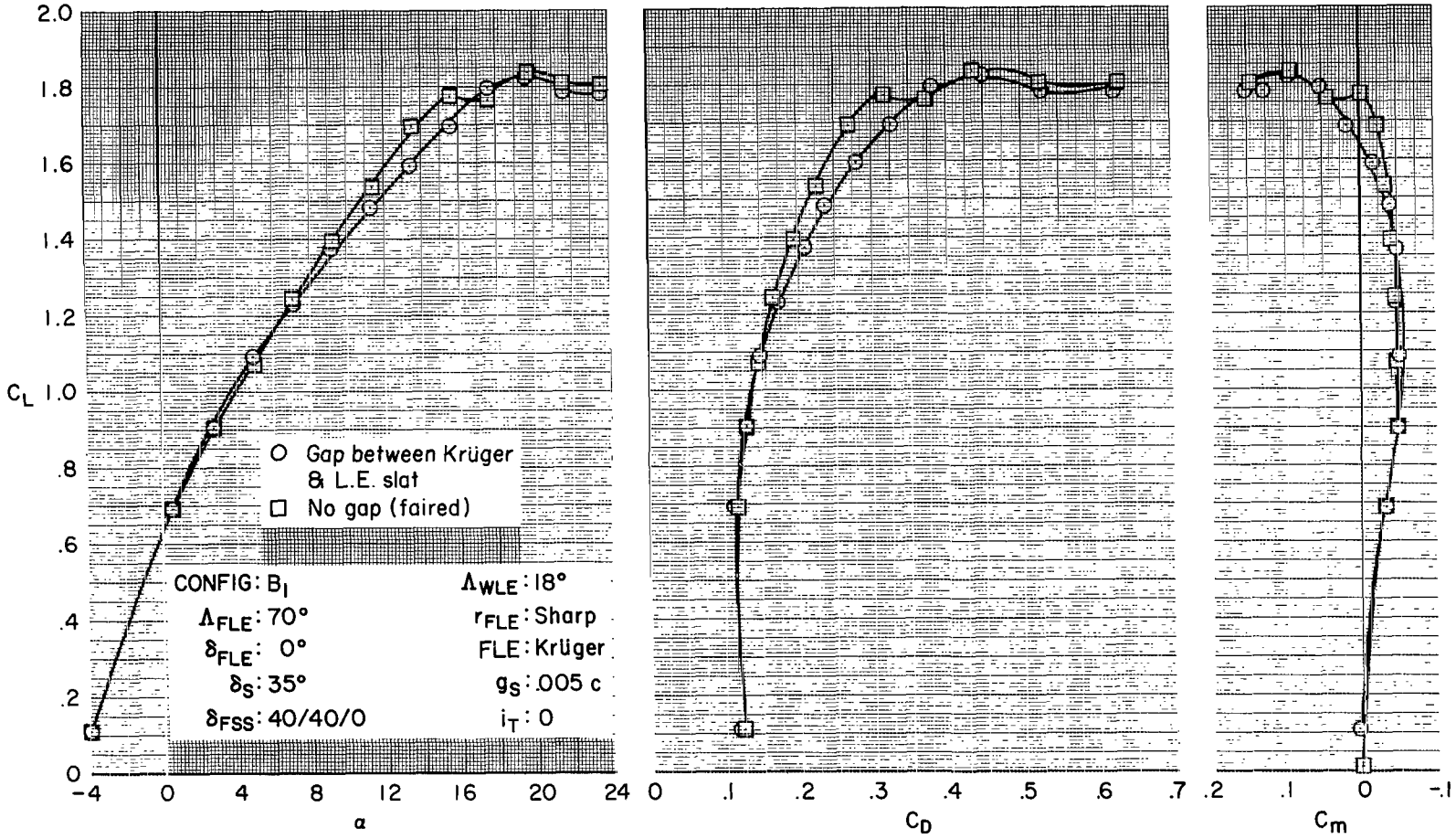

Figure 44.- Effect of gap between fixed-wing leading-edge Krüger flap and movable wing leading-edge slat at 18° wing sweep.

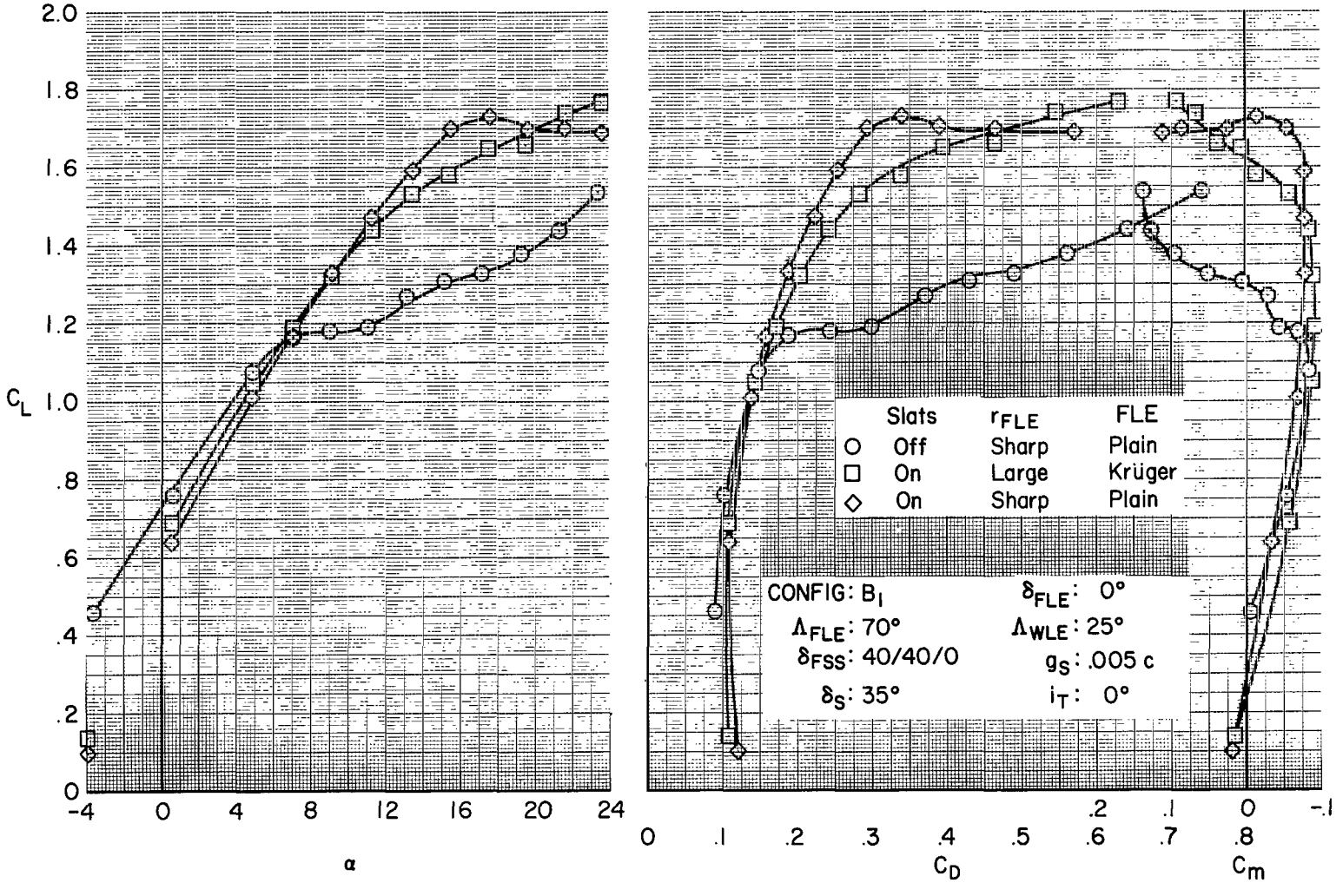

Figure 45.- Effect of movable wing leading-edge slats on low-aspect-ratio wing at 25° sweep.

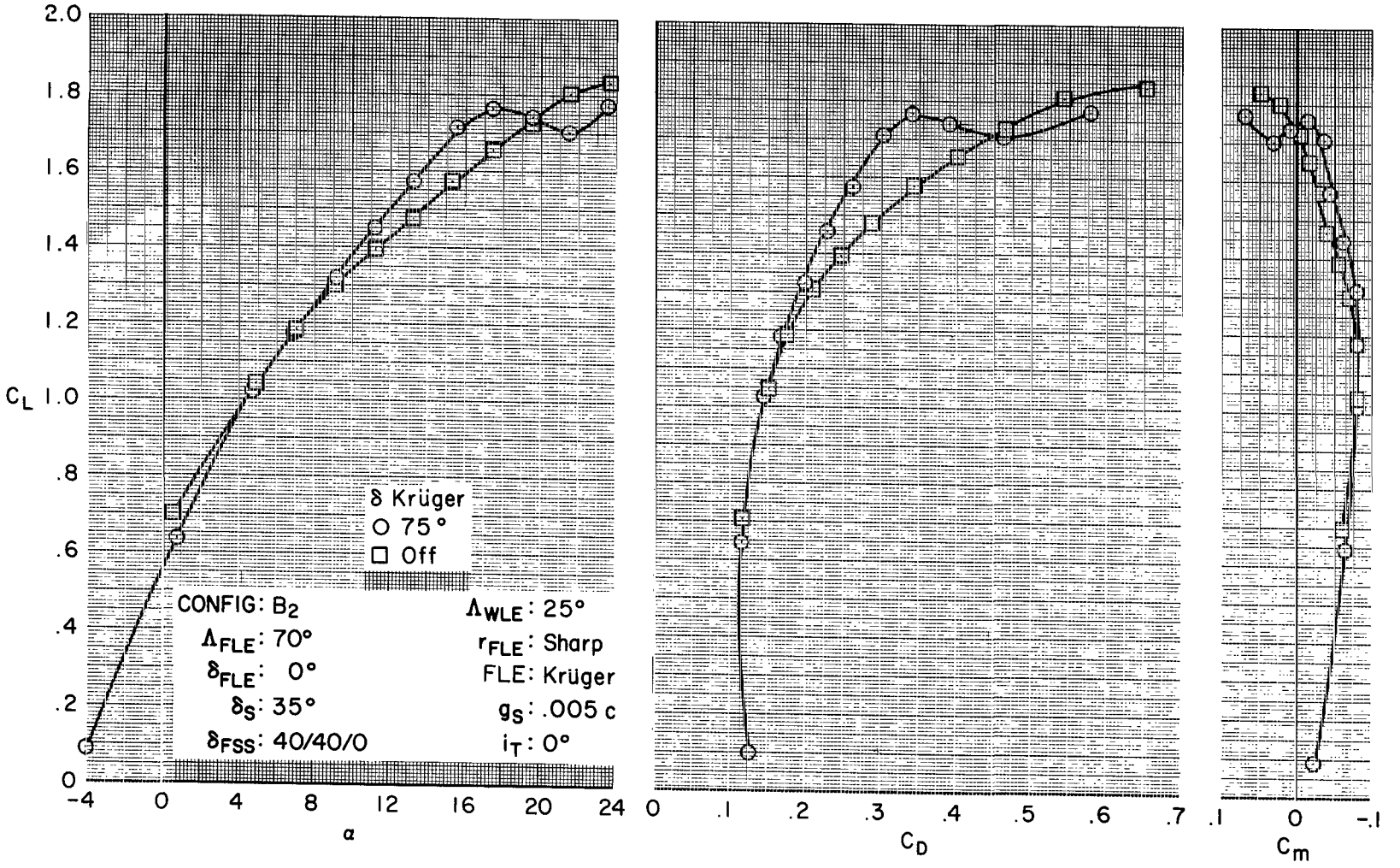

(a) Effect of Krüger flap with basic slat of 0.15c length.

Figure 46.- Effect of slat type and fixed-wing Krüger flap deflection on mid-tail configuration, B_2.

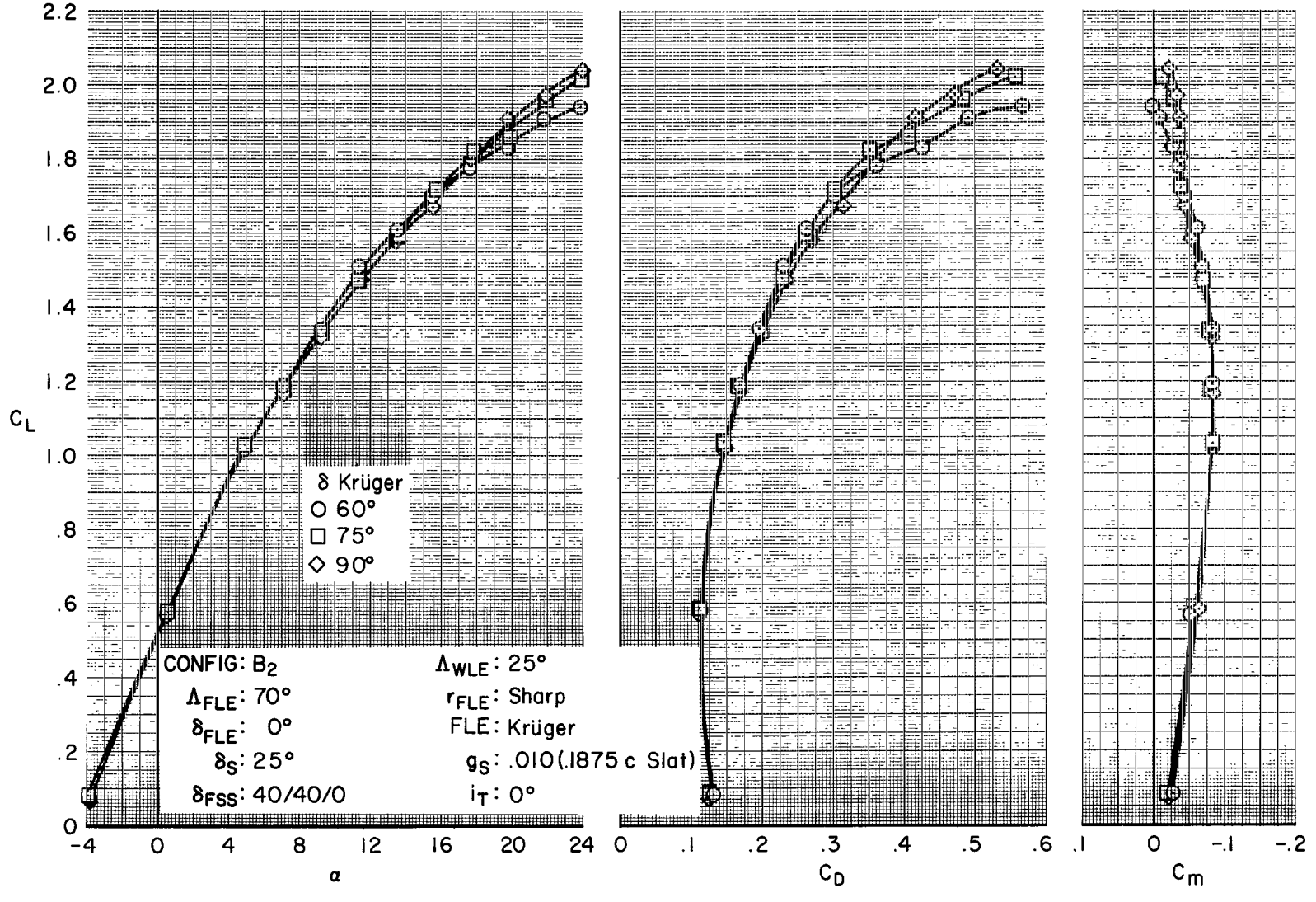

(b) Effect of Krüger flap with modified slat of 0.1875c length.

Figure 46.- Concluded.

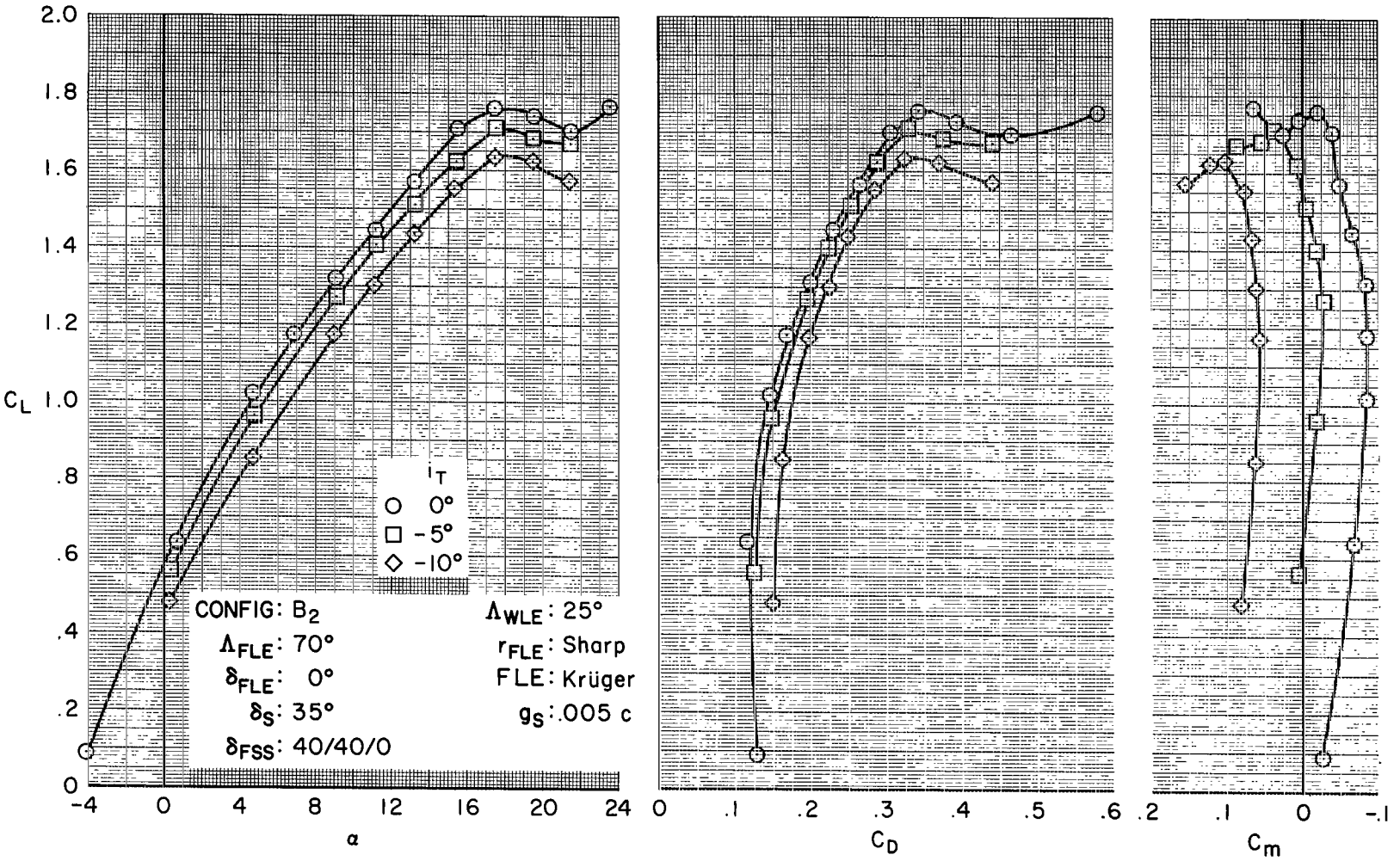

Figure 47.- Effect of fixed-wing Krüger flap deflection on longitudinal characteristics with basic (0.15c length) slat and 40° partial-span single-slotted flaps, mid-tail position, configuration B_2.

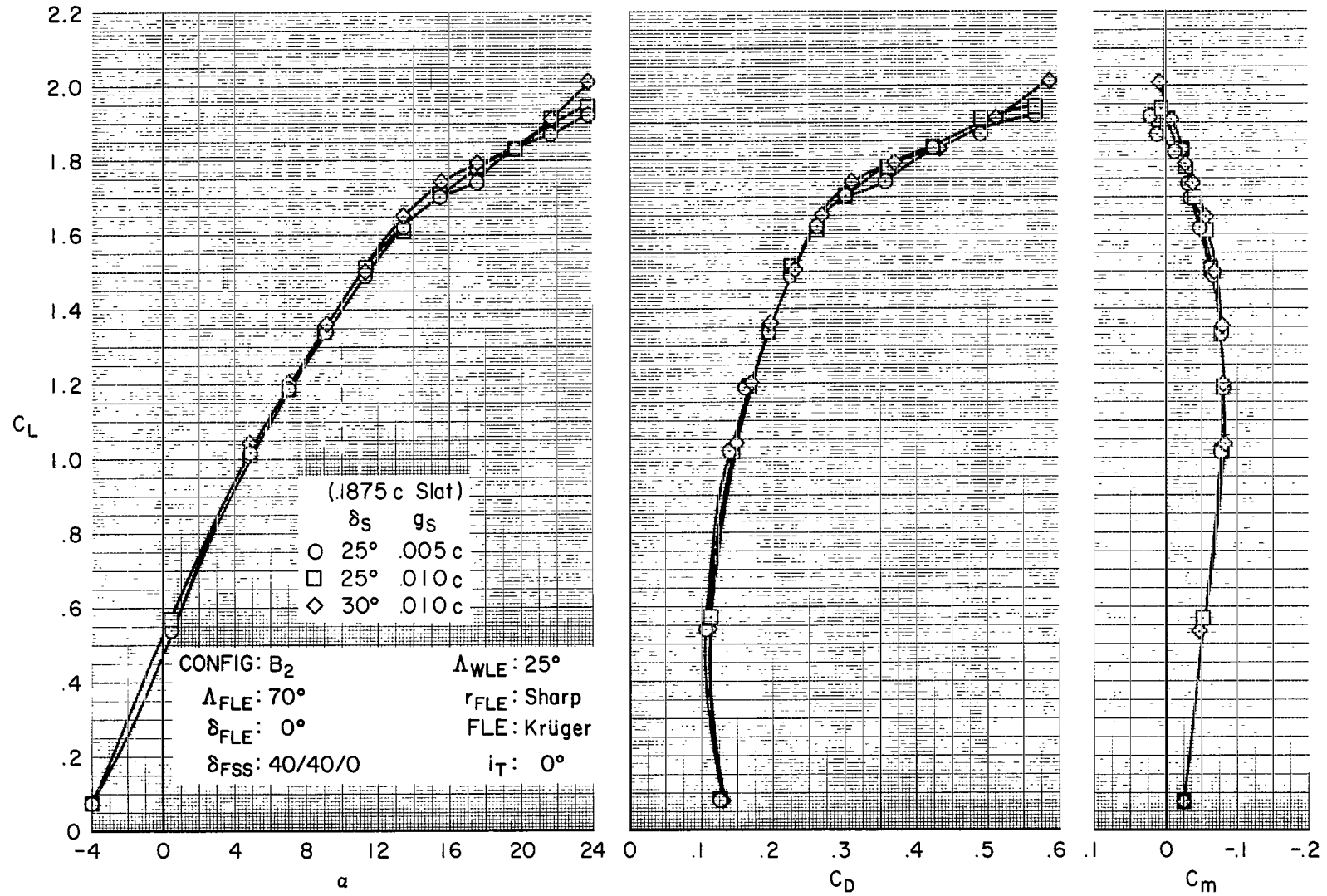

(a) 60° Krüger flap deflection.

Figure 48.- Effect of modified slat (0.1875c length) geometry and Krüger flap deflection on mid-tail configuration B_2.

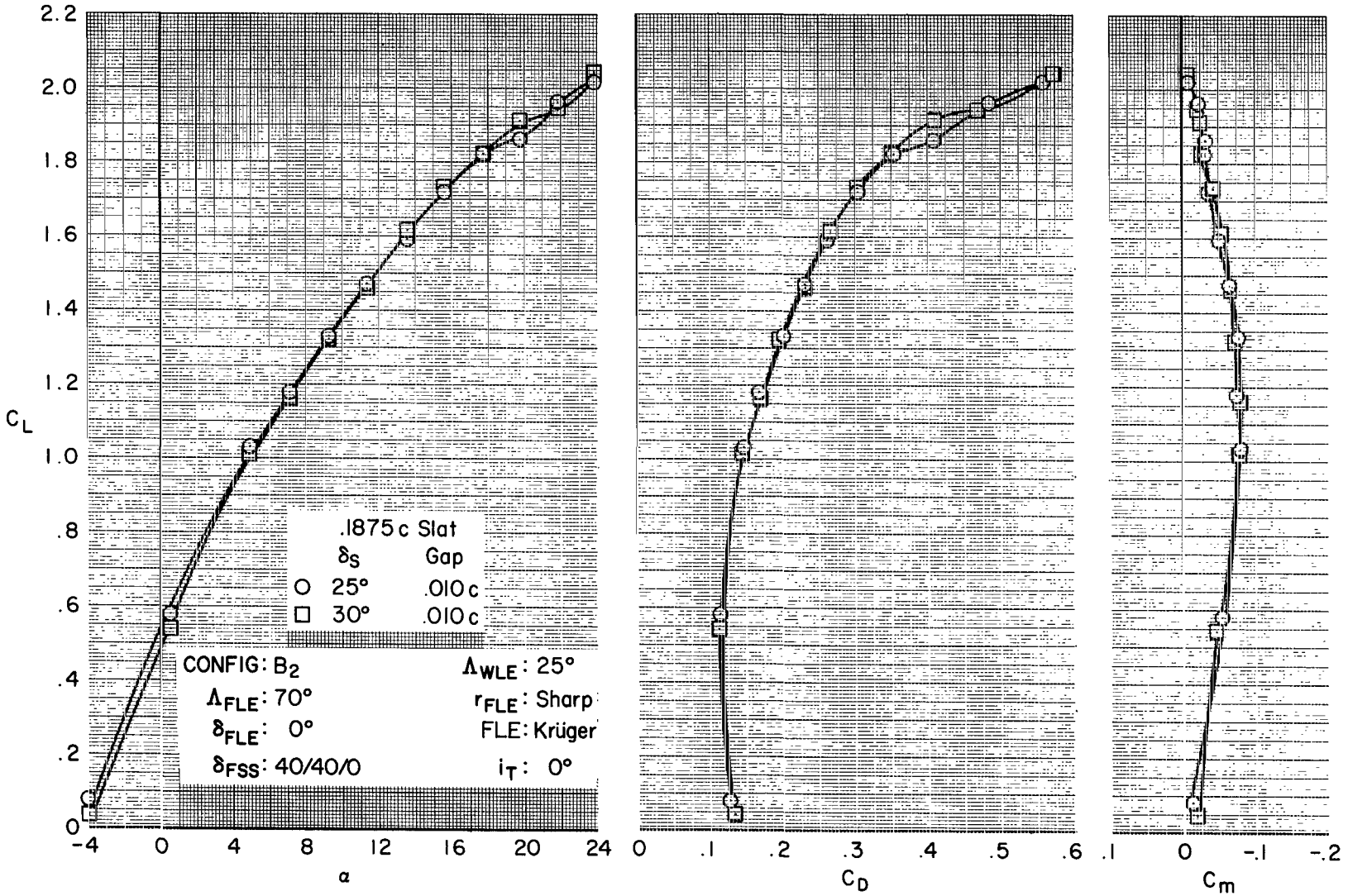

(b) 75° Krüger flap deflection.

Figure 48.- Concluded.

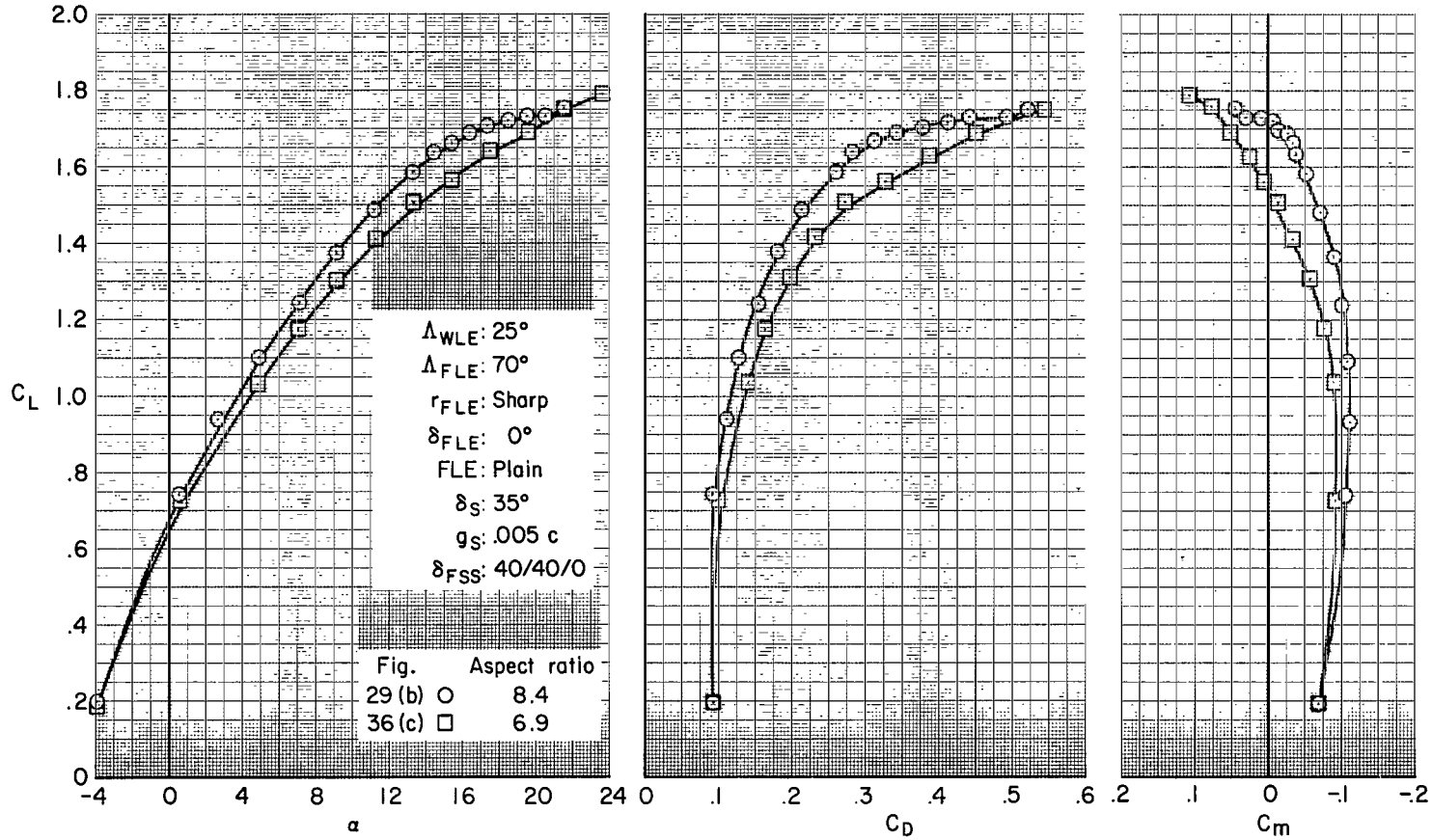

Figure 49.- Summary of the effects of aspect ratio on longitudinal characteristics with horizontal tail off.

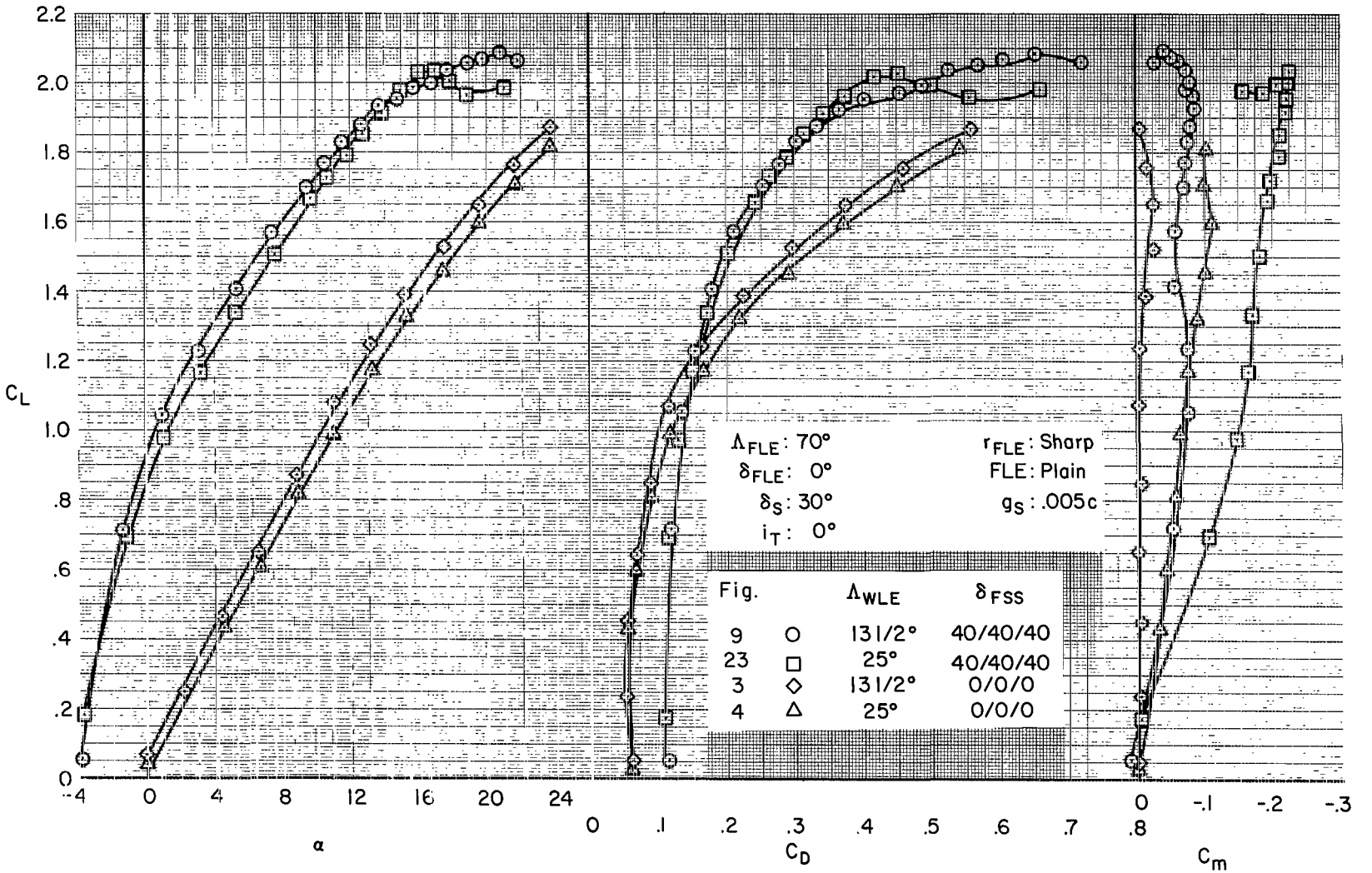

Figure 50.- Summary of the effects of wing leading-edge sweep on longitudinal characteristics, flaps both up and down.

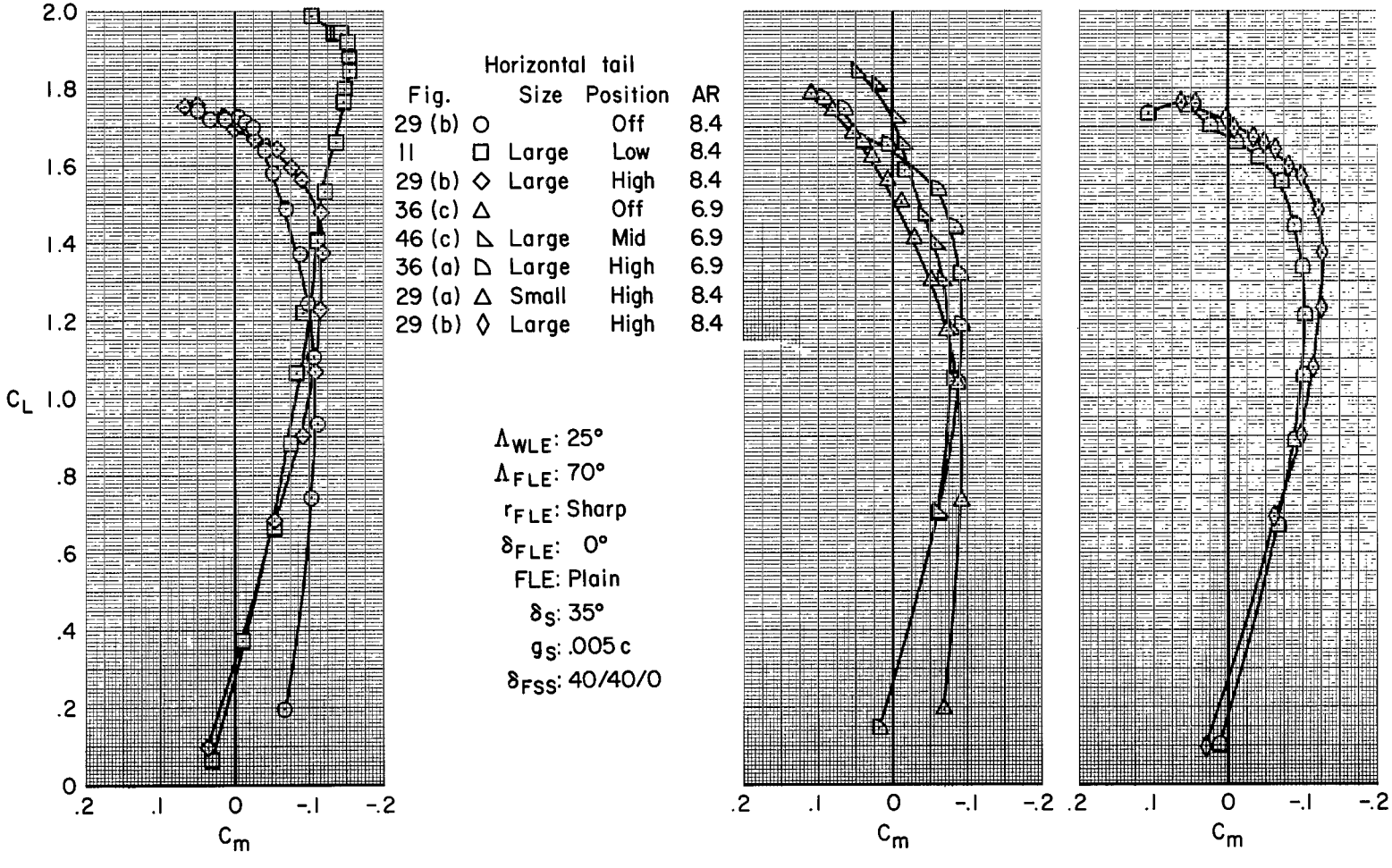

Figure 51.- Summary of the effects of horizontal-tail location and size on pitching-moment characteristics.

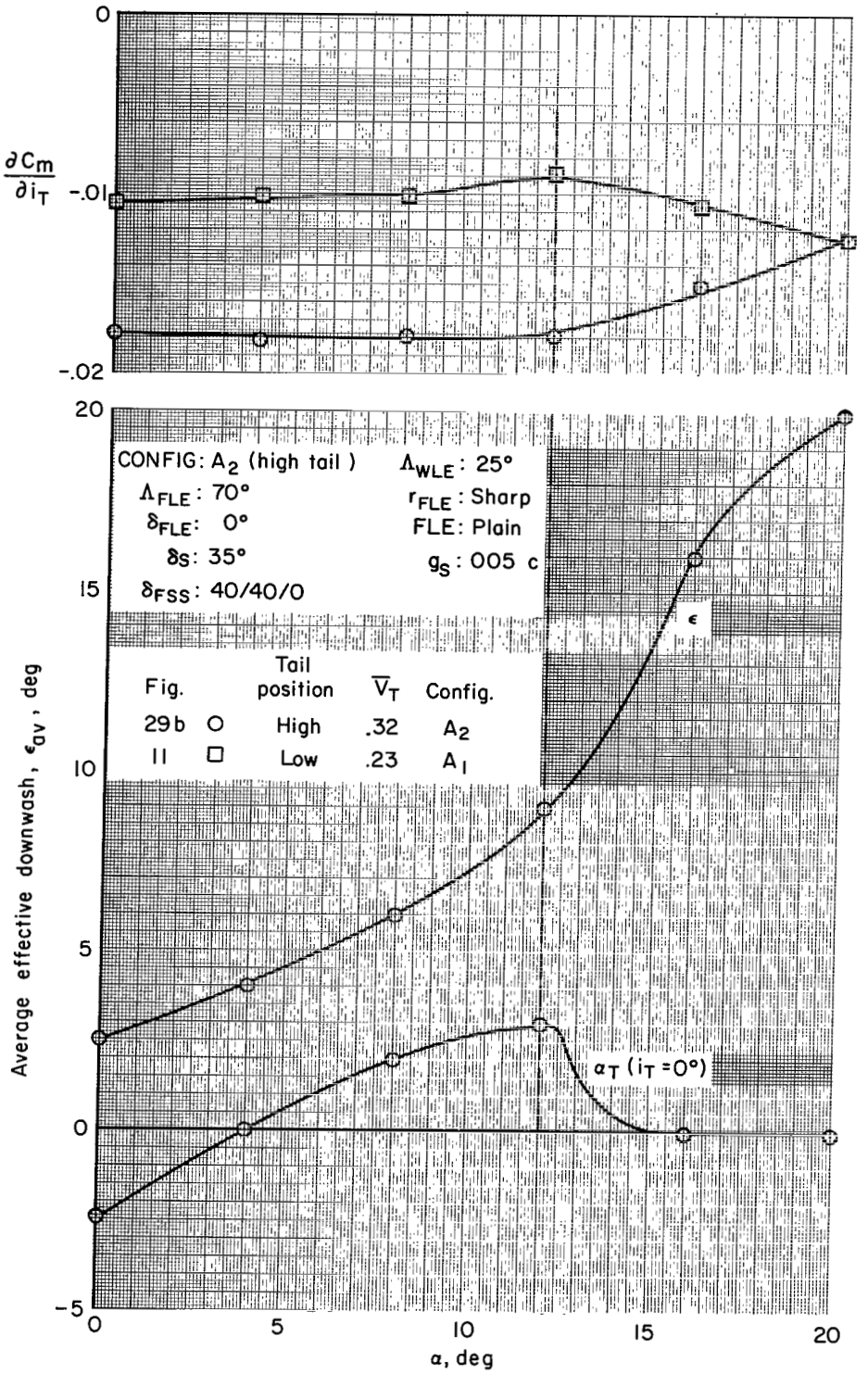

Figure 52.- Control effectiveness, average effective downwash angle, and tail angle of attack for horizontal-tail positions.

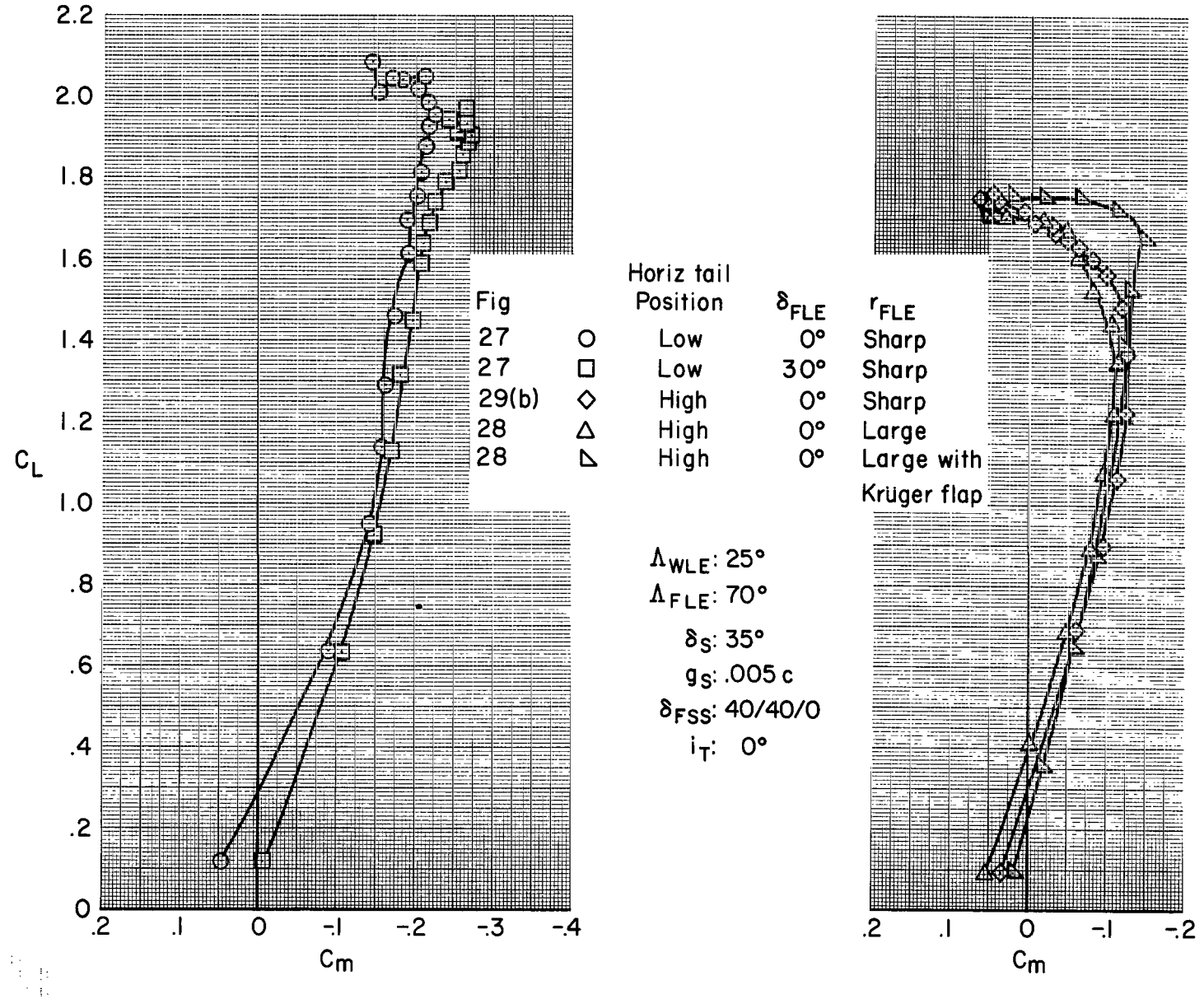

Figure 53.- Summary of the effects of fixed-wing leading-edge radius and Krüger flap deflection on pitching moment.

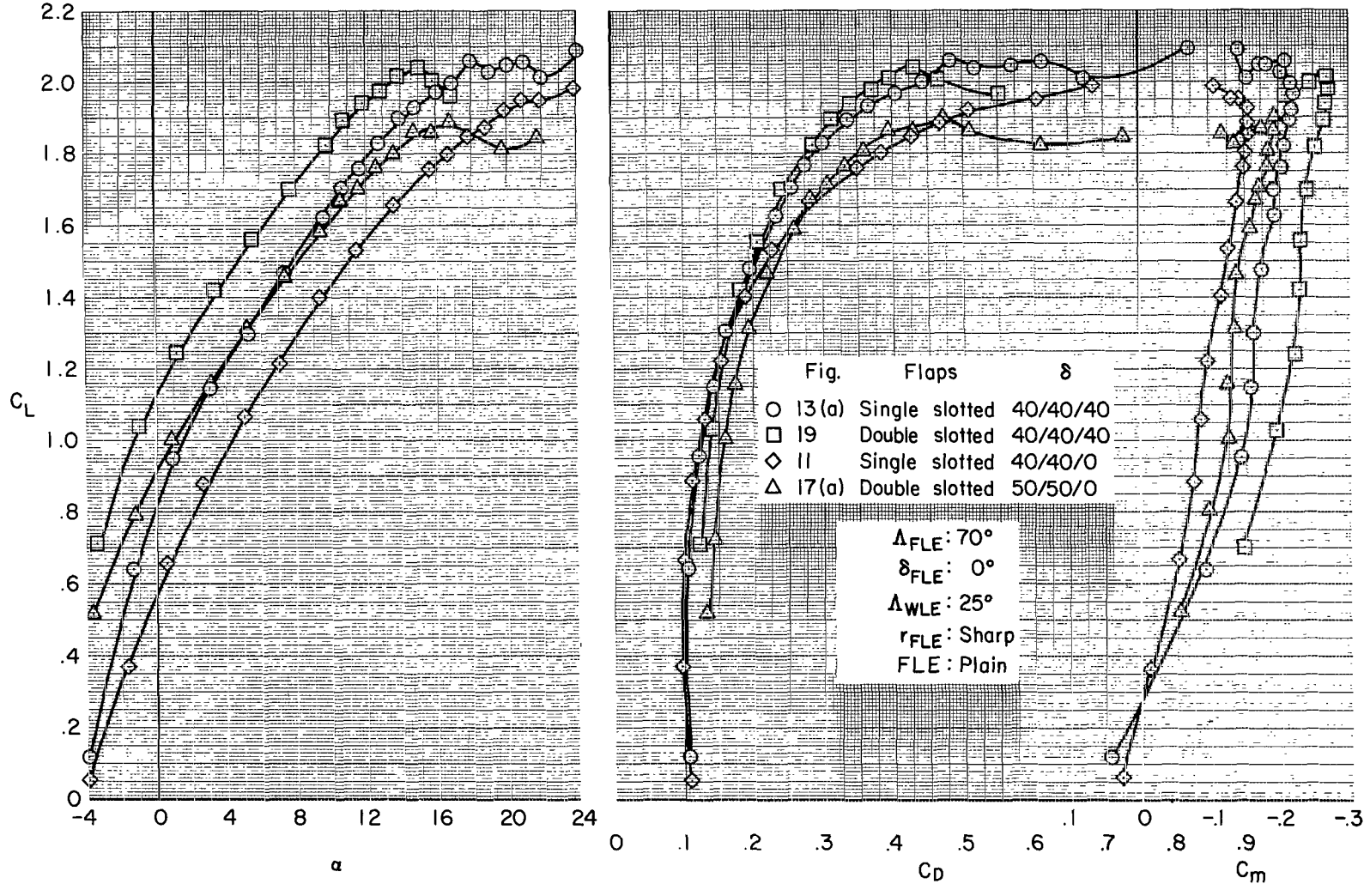

Figure 54.- Summary of the effects of single-slotted and double-slotted flap systems, configuration A_1, low tail, 25° wing sweep.

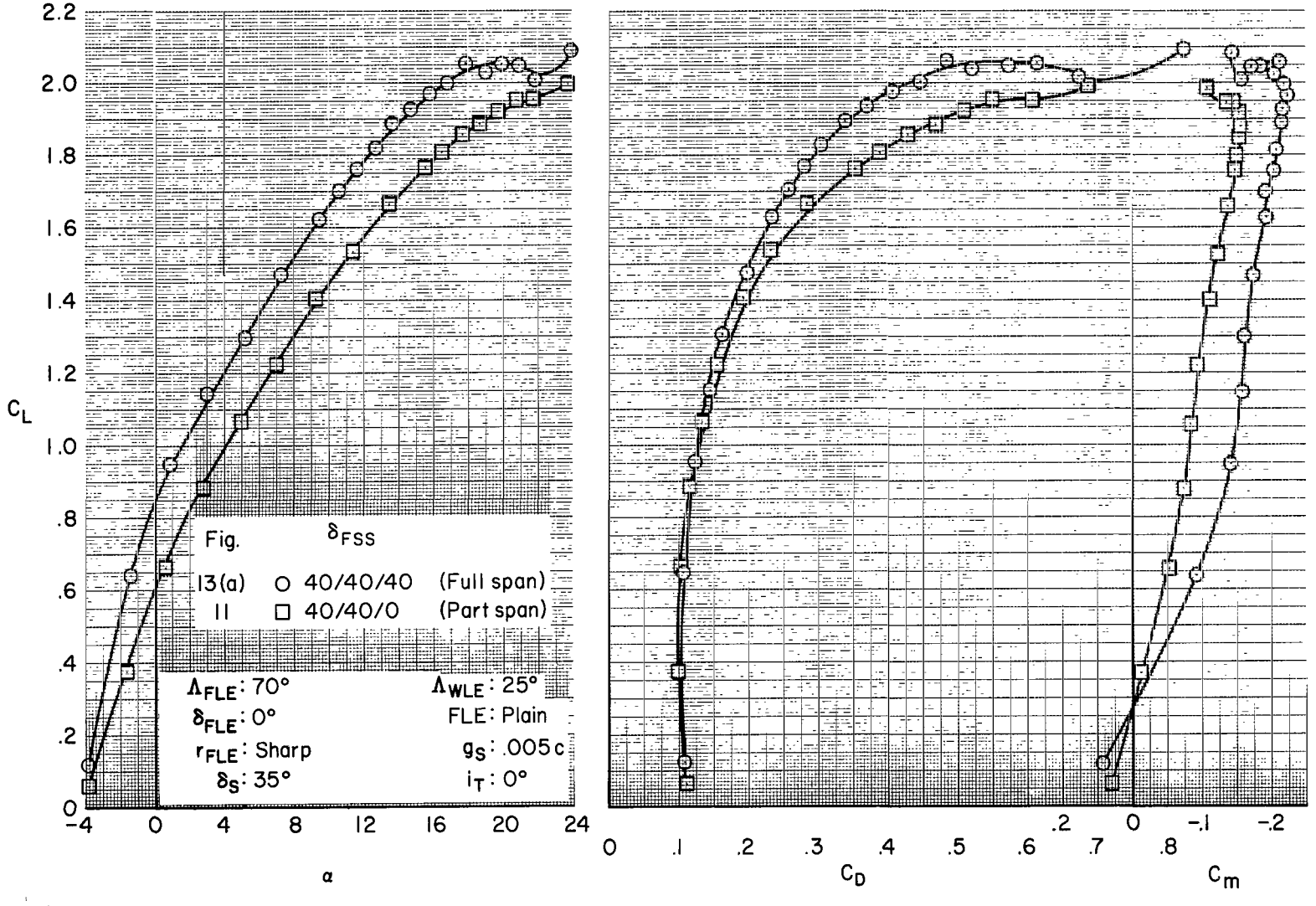

Figure 55.- Comparison of full- and partial-span flap deflection, configuration A_1, low tail, 25° wing sweep.

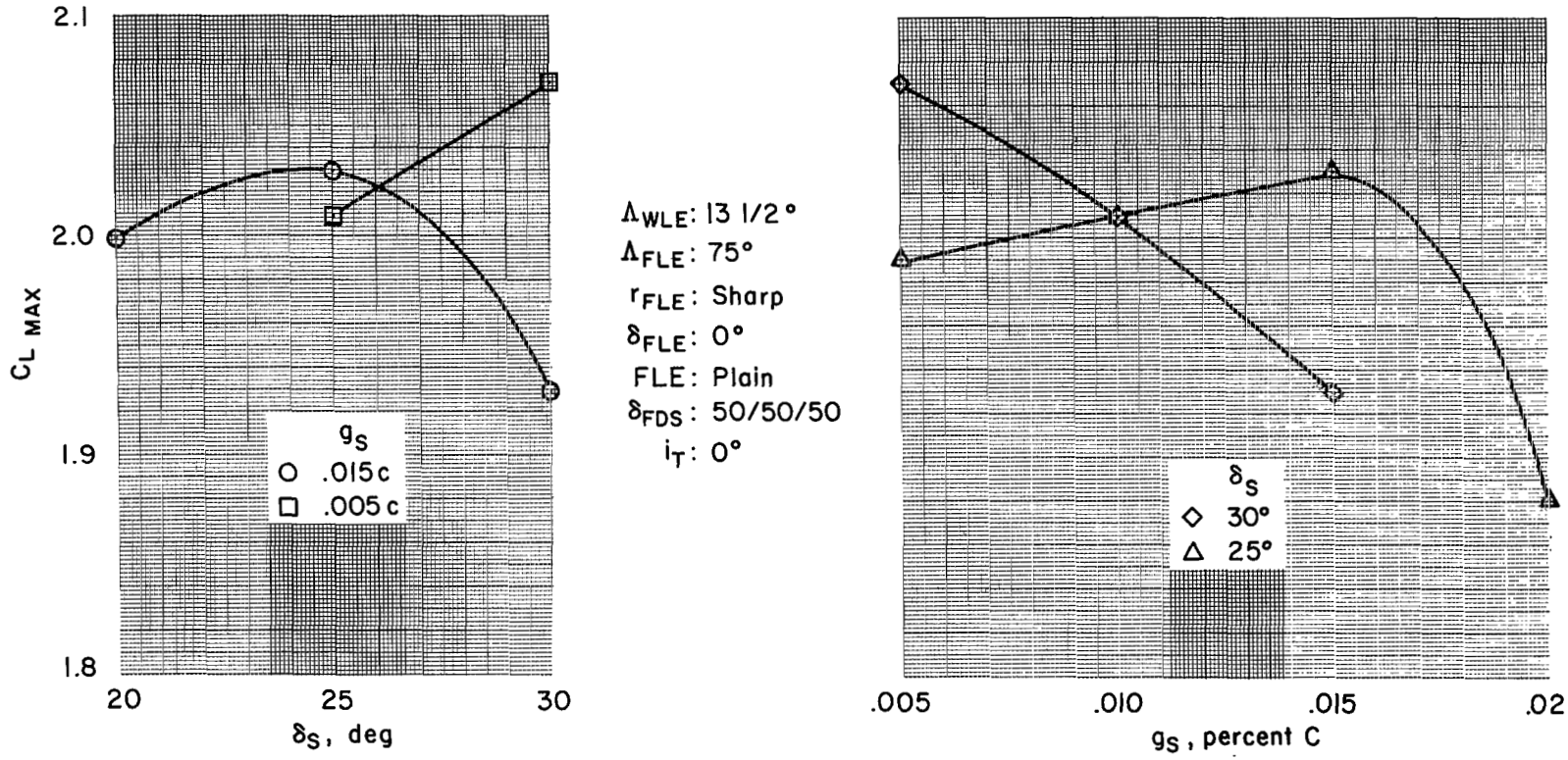

Figure 56.- Summary of effects of leading-edge slat geometry on maximum lift coefficient.

2/321 RT

"The aeronautical and space activities of the United States shall be conducted so as to contribute . . . to the expansion of human knowledge of phenomena in the atmosphere and space. The Administration shall provide for the widest practicable and appropriate dissemination of information concerning its activities and the results thereof."

—NATIONAL AERONAUTICS AND SPACE ACT OF 1958

NASA SCIENTIFIC AND TECHNICAL PUBLICATIONS

TECHNICAL REPORTS: Scientific and technical information considered important, complete, and a lasting contribution to existing knowledge.

TECHNICAL NOTES: Information less broad in scope but nevertheless of importance as a contribution to existing knowledge.

TECHNICAL MEMORANDUMS: Information receiving limited distribution because of preliminary data, security classification, or other reasons.

CONTRACTOR REPORTS: Technical information generated in connection with a NASA contract or grant and released under NASA auspices.

TECHNICAL TRANSLATIONS: Information published in a foreign language considered to merit NASA distribution in English.

TECHNICAL REPRINTS: Information derived from NASA activities and initially published in the form of journal articles.

SPECIAL PUBLICATIONS: Information derived from or of value to NASA activities but not necessarily reporting the results of individual NASA-programmed scientific efforts. Publications include conference proceedings, monographs, data compilations, handbooks, sourcebooks, and special bibliographies.

Details on the availability of these publications may be obtained from:

SCIENTIFIC AND TECHNICAL INFORMATION DIVISION

NATIONAL AERONAUTICS AND SPACE ADMINISTRATION

Washington, D.C. 20546